Marine Radiocarbon Reservoir Effects (MRE) in Archaeology: Temporal and Spatial Changes through the Holocene within the UK Coastal Environment

Nicola Russell (BSc Hons)

Submitted in fulfilment of the requirements for the Degree of Doctor of Philosophy

Scottish Universities Environmental Research Centre

College of Science and Engineering

University of Glasgow

July 2011

ABSTRACT

The purpose of this research was to investigate temporal and spatial trends in the Marine Radiocarbon Reservoir Effect (MRE) on the North Sea coast of Scotland throughout the Holocene. The MRE is a ^{14}C age offset between contemporaneous marine derived carbon and its terrestrial counterpart, owing to the extended residence time of ^{14}C in oceanic environments. This results in marine samples being depleted in ^{14}C relative to contemporaneous terrestrial samples and consequently, the production of ^{14}C ages that are erroneously old. The offset between contemporaneous marine and terrestrial entities varies through space and time on a global scale and so a single correction factor cannot be universally applied. In order to gain a coherent understanding of the MRE, its variability and its full impact on the radiocarbon dating of samples containing marine derived carbon, a brief background to the fundamental principles of radiocarbon dating is presented. This is followed by a global overview of variability in the MRE before focussing on the UK coastal environment, and in particular the North Sea coast of Scotland. Using contemporaneous multiple terrestrial and marine entities from secure archaeological contexts, this thesis investigates the MRE as represented by 13 contexts from 9 archaeological sites spanning a geographical range from Aberdeen in the north to Dunbar in the south. The sites are predominantly Medieval in age, owing to sample availability, and cover a calendar age range of c. 600 – 1500 AD. This thesis recommends the use of the multiple paired sample approach for ΔR calculations and the publication of ΔR using histograms alongside weighted mean values and the standard error for predicted values in order to provide a more accurate estimate of where ΔR values measured in the future for a similar site and location may lie. In so doing, a weighted mean for the sites studied in this thesis has produced a ΔR for the period described above of -19 ± 52 ^{14}C yrs. This thesis also compared ΔR values calculated using mollusc shell with those calculated from fish bone and found that although fish bone produces a slightly increased ΔR, this offset is not significant using the standard error for predicted values. When the fish bone results are included in the weighted mean for the study region; $\Delta R = -29 \pm 51$ ^{14}C years. This thesis highlights the variability inherent within the calculation of ΔR values and places caution on drawing definitive conclusions using ΔR as a proxy for large scale changes in oceanographic/climatic regimes. It also provides new methods of interpreting and presenting ΔR values and their associated errors for publication, alongside recommending best practice statistical treatment of the data used in ΔR calculations.

Previous MRE research in this geographic area is limited and therefore this thesis contributes significantly to the understanding of the temporal and spatial trends in the MRE on the North Sea coast of Scotland within the Medieval period.

TABLE OF CONTENTS

LIST OF TABLES

LIST OF FIGURES

ACKNOWLEDGEMENTS

It is with the deepest gratitude that I thank my supervisors Gordon Cook and Philippa Ascough of SUERC for their endless support and guidance throughout my entire course of study. I simply couldn't have done it without them. From helping me during the early days when it seemed that suitable samples would never be found, to providing academic support in the publication of the three papers deriving from this thesis, through to their dedicated and thorough evaluation of this thesis; their support and motivation has been unfaltering and I am so grateful to have enjoyed such a fantastic student-supervisor relationship. Grateful thanks are also due to my third supervisor, Andrew Dugmore at Edinburgh University, who always provided stimulating ideas.

Thanks must also be given to Philip Naysmith, Elaine Dunbar, Graham Muir, Kerry Sayle and Helen Hastie from the ^{14}C lab at SUERC for making my time in the lab as easy as possible and providing many opportunities to lighten the load with laughter when the going got tough.

It would have been impossible for me to produce the data in this thesis without the kind submission of samples from the following archaeology units: Aberdeen City Council, Addyman Archaeology, AOC Archaeology, Field Archaeology Specialists and SUAT. Special thanks go to Catherine Smith and Derek Hall, formerly of SUAT, who supplied material for over 50% of the sites and who were always available to answer any questions and provide a wealth of additional information for the sites which they had recommended.

Thanks are due to Marian Scott of the University of Glasgow for her infallible statistical advice, Terry Donnelly of SUERC for help with ^{18}O analysis and Fiona Naysmith for her formatting expertise. Gratitude is given to NERC for funding this studentship, Historic Scotland for their CASE support and in particular, Rod McCullagh for his personal and professional interest in the project and his help in the identification of suitable sites for study. I would also like to thank Ron and Paula Reimer for the provision of coding for the FORTRAN /UNIX ΔR program used to calculate ΔR values throughout this thesis.

Finally, on a more personal note I couldn't have done this without the overwhelming support I have received from my family and friends. Although my parents Andrew and Kay Russell cannot comprehend the content of this thesis, their pride and belief in me is more than I could ever have asked of them. I love you. My closest friends – Amy, Carol, Jo, Karen, Kim and Vicci have provided a constant circle of support, helping me forget about the tough times by providing 4 years of dedicated friendship to someone who is not always as available as she should be owing to the pressures of work. Sunshine respite provided by Jo, alongside the ability to make me laugh like no other, meant that my well-earned breaks from my thesis were always spent in the best way imaginable. Finally, Kim and Vicci – you have provided to the soundtrack to the completion of this thesis and championed the 'power of yes' and the positive attitude that anything is possible. Words cannot explain what this means to me and how integral you are to the successful completion of this thesis and my happiness in general. I would be lost without you.

"This is the opening night, for me and the rest of my life."

DECLARATION

I declare that, except where explicit reference is made to the contribution of others, that this dissertation is the result of my own work and has not been submitted for any other degree at the University of Glasgow or any other institution.

Signature _____

CHAPTER 1

SCIENTIFIC BACKGROUND

1.1 Fundamental radiocarbon dating principles

The process of radiocarbon dating relies on the principle that carbonaceous matter contains all three isotopic forms of the element carbon: the two stable isotopes; ^{12}C and ^{13}C, and the radioisotope ^{14}C (also known as radiocarbon). ^{12}C, the most abundant isotope, accounts for 98.89% of global atmospheric CO_2, ^{13}C for 1.11% and ^{14}C for 0.0000000001%. Atmospheric CO_2 is incorporated into the terrestrial biosphere via photosynthesis by the primary producers (green plants) (Equation 1.1). CO_2 enters the oceans across the air/ocean interface where it becomes part of the inorganic carbon pool of carbonic acid, bicarbonate ions, carbonate ions and CO_2 (Mills and Urey 1940, Mook et al., 1974). Biological uptake in the oceans is again via photosynthesis, this time by phytoplankton and algae.

$$6CO_2 + 12H_2O \xrightarrow{Light+chlorophyll} C_6H_{12}O_6 + 6O_2 + 6H_2O$$

Equation 1.1: Photosynthetic reaction showing the fixation of CO_2 to $C_6H_{12}O_6$ using chlorophyll in green plants to harness photons (light energy) and facilitate the conversion of carbon dioxide to carbohydrate.

The primary producers are consumed by higher trophic levels and so all living organisms therefore contain ^{14}C. The uptake of ^{14}C is offset by radioactive decay (Equation 1.2), resulting in an equilibrated concentration of ^{14}C in living organisms.

$$^{14}_{6}C \rightarrow ^{14}_{7}N + \beta^{-} + \bar{\nu}_e$$

Equation 1.2: Radioactive decay of ^{14}C to ^{14}N by emission of a beta particle and an electron neutrino.

Radiocarbon ceases to be exchanged with the surrounding environment upon final formation/death of a living organism, meaning that only decay of the radioisotope can affect the ^{14}C concentration of this material. Radioactive decay occurs at a known rate, known as the half-life, meaning that the time since final formation can be calculated using

Equation 1.3 which is a re-arrangement of the first order decay equation.

$$t = \frac{1}{\lambda} \ln\left(\frac{A_o}{A_t}\right)$$

Equation 1.3: Basic calculation of time since cessation of carbon exchange

Where: t = the time since the living sample ceased to exchange carbon
λ= decay constant = ln2/half-life of ^{14}C ($t_{1/2}$) where $t_{1/2}$ = 5568 years (Libby half-life)
A_o = activity at time of death/final formation
A_t = activity remaining in the sample "t" years after death

The Libby half-life of 5568 years was used for ^{14}C age determinations following early investigations into the use of radiocarbon as a dating technique (Libby et al., 1949). Subsequent re-investigation and refinement of the technique led to the correction of this half-life by Godwin (1962) to 5730 ± 40 years. In order to allow comparability with ages determined before 1962, the Libby half-life is still used in ^{14}C age calculations.

The ^{14}C activity of a sample can be measured by direct or indirect methods. The indirect method, known as radiometric measurement, involves counting beta (β^-) emissions in a set period of time, from a known sample weight, using gas proportional or liquid scintillation counting. The direct method of measurement involves ^{14}C atom counting relative to ^{13}C or ^{12}C atoms using accelerator mass spectrometry (AMS). Any ^{14}C measurement will have an uncertainty associated with it, published as a ± error term. This error is calculated based primarily upon the counting statistics of the measured events (β decays or ^{14}C counts), i.e: $\pm \sqrt{N}$ (where N = the number of measured events). However, the final reported error also incorporates statistical errors according to a range of other factors, which will be discussed further in the calibration and AMS sections, (Sections 1.8 and 3.3, respectively).

The concentration of ^{14}C in a sample to be dated is measured relative to ^{13}C or ^{12}C in order to account for chemical and physical processes throughout the atmosphere and biosphere that prevent a uniform abundance of ^{14}C from existing between different environments. In order to calculate accurate ^{14}C ages, the original concentration of ^{14}C needs to be

accurately quantified. If the original 'starting' concentration of ^{14}C is not the same for sample materials in different environments, then radiocarbon dates between different sample materials would not be comparable. In theory, calibration accounts for these different 'starting' concentrations of ^{14}C (see section 1.8) but in order to measure samples relative to an international standard, exactly the same mass of sample as standard would need to be weighed out in order to measure ^{14}C directly. Errors in weighing precision are not sufficient to account for this and so ^{14}C concentration is measured *relative* to ^{13}C or ^{12}C, normalised to an international standard. Accounting for natural (i.e. non-decay derived) variability in sample-to-sample $^{14}C/^{13}C$ ratios will be discussed in detail in Sections 1.6 and 1.8. Key factors which can result in this variability include changes in the global production of ^{14}C, the global distribution of ^{14}C and anthropogenic and/or natural factors, which can directly affect the atmospheric concentration of ^{14}C.

1.2 Mechanisms of ^{14}C Production

^{14}C is produced in the upper atmosphere by the bombardment of ^{14}N by thermal neutrons (Equation 1.4), mainly initiated by high energy galactic cosmic rays, although less energetic solar cosmic rays also contribute to the production of ^{14}C (Libby, 1946). These primary cosmic rays lose energy through ionization of molecules and interactions with atomic nuclei as they travel through the Earth's atmosphere, forming secondary particles: mainly neutrons, protons and muons (Tuniz et al., 1998; Muziker et al., 2003). A proportion of secondary particles, known as fast neutrons, lose further energy through nuclear collisions to form thermal neutrons, which are in vibrational equilibrium with atmospheric gases (Gosse and Phillips, 2001). ^{14}C production occurs when ^{14}N atoms absorb thermal neutrons, resulting in the formation of the radionuclide ^{14}C and a proton (Equation 1.4).

$$^{14}_{7}N + n \rightarrow ^{14}_{6}C + p$$

Equation 1.4: Formation of ^{14}C

^{14}C is then either rapidly oxidised to ^{14}CO and subsequently to $^{14}CO_2$ by interaction with hydroxyl radicals (Equation 1.5), or forms $^{14}CO_2$ directly in a minority of cases (Pandow et al., 1960).

$$^{14}C + 2OH \rightarrow {}^{14}CO_2 + H_2$$

Equation 1.5: Formation of $^{14}CO_2$ by interaction with hydroxyl radicals

Calculations of the modern production rate of radiocarbon give values of around 2-3 ^{14}C atoms cm^{-2} s^{-1} (Suess, 1965; Damon et al., 1978; Finkel and Suter, 1993), with the most recent publication by Masarik and Beer (1999) quantifying production at 2.02 ^{14}C atoms cm^{-2} s^{-1}. However, in order to use radiocarbon as a reliable dating technique, the production rate need not be accurately known provided that the global atmospheric concentration of ^{14}C can be quantified. Rapid circulation of atmospheric $^{14}CO_2$, on the order of 4-10 years (Craig, 1957a; Nydal and Lövseth, 1970), ensures an almost uniform global atmospheric ^{14}C concentration at any point in time, although certain factors can influence the rate of production of ^{14}C (and consequently $^{14}CO_2$) over time, including latitude, altitude and solar activity. Understanding these variations in ^{14}C concentration is fundamental to the calculation of accurate ^{14}C ages, and their subsequent interpretation.

1.3 Variations in ^{14}C production

1.3.1 Latitudinal and altitudinal variations

^{14}C production is greatest at high geomagnetic latitudes (i.e. the Polar Regions) as the Earth's magnetic field deflects incoming cosmic particles with low energy away from the Earth. This deflection occurs predominantly at low latitudes (where the magnetic field lines are perpendicular to the direction of incoming particles) (Muziker et al., 2003). Therefore, at higher latitudes, geomagnetic fields deflect less cosmic radiation, thereby enabling increased ^{14}C production (Stuiver et al., 1997). A production maximum is also observed at a height of approximately 15 km above the Earth's surface where collisions between thermal neutrons and ^{14}N atoms are most likely (Aitken, 1990).

1.3.2 Magnetic variation

Magnetic fields induced by solar activity also affect ^{14}C production, as high solar activity increases the flux of solar magnetic particles that deflect cosmic rays away from the Earth, thus decreasing ^{14}C production rates in the Earth's atmosphere (Stuiver et al., 1997). Changes in solar activity therefore correlate with ^{14}C activity, and the periodicity is evident throughout the solar cycles that affect irradiance on the Earth. Therefore, regular

variations in the flux of high energy galactic cosmic rays are evident in the ^{14}C record. 11 year Schwabe variations involve one cycle of increasing/decreasing sunspot activity and one reversal of the solar magnetic field, with ^{14}C production reaching a maximum of 1.15 times the normal production rate during periods of minimum solar activity (Masarik and Beer, 1999). 210 year Suess cycles (Masuda et al., 2009) and 2300 year Hallstatt cycles (Tobias et al., 2004; Clilverd et al., 2003, 2004) have similar effects, modulating ^{14}C production in inverse proportion to solar activity. Milankovitch cycles (Milankovitch, 1930; Imbrie and Imbrie, 1979; Bradley, 1985) are changes in the Earth's orbital parameters that also affect solar irradiance and can affect the geodynamo controlling the intensity of the Earth's dipole field, leading to modulated ^{14}C production rates (Yamazaki and Oda 2002).

1.4 Natural variation in ^{14}C concentration

The latitudinal production effects discussed above are generally minimised by the rapid mixing rate of $^{14}CO_2$ in the atmosphere. The atmospheric distribution is generally considered homogenous although slight variations do exist, regardless of the rapid atmospheric mixing rate. One such variation is the 56 ± 24 ^{14}C yr offset noted between the Northern and Southern Hemispheres (McCormac et al., 2004). This offset remains broadly constant, although some temporal variations do occur. Known as the North/South Hemisphere effect, it occurs because the Southern Hemisphere contains an area of ocean *c* 40% greater than that of the Northern (Aitken, 1990, Levin et al., 1987). This results in the Southern Hemisphere having a greater area of ocean / air interface available for exchange between atmospheric CO_2 and oceanic bicarbonate. Oceanic bicarbonate is depleted in ^{14}C relative to atmospheric CO_2 because of the extended residence time of ^{14}C in the marine environment known as the marine reservoir effect (MRE). The MRE will be discussed in detail in Chapter 1.7. Strong upwelling around Antarctica due to circumpolar winds increases this depletion, bringing old, ^{14}C depleted water from depth into contact with the atmosphere in the surface ocean. The Southern Hemisphere therefore has a larger return of depleted, oceanic ^{14}C to the atmosphere than the Northern Hemisphere, resulting in a lower ^{14}C activity. Atmospheric mixing between the hemispheres (as divided along the thermal equator rather than the geographical equator) (McCormac et al., 2004) is limited by the diverging direction of the equatorial trade winds and prevents homogenous hemispheric ^{14}C activity levels from being attained. This is accounted for during the calibration process

with separate calibration curves (IntCal09 for the Northern Hemisphere (Reimer et al., 2009), SHCal04 for the Southern Hemisphere (McCormac et al., 2004)).

Variations in ^{14}C concentration can also occur in areas with notable volcanic activity. Volcanic emissions release CO_2 which significantly depleted or devoid of ^{14}C, thus diluting the local ^{14}C concentration. The effect is not large enough to have a global influence, but consideration should be given to the ^{14}C content of flora and fauna in close proximity to volcanic sites (Sulerzhitkzy, 1971; Bruns et al., 1980; Aitken, 1990).

1.5 Anthropogenic effects on ^{14}C concentration

1.5.1 Suess effect

During the industrial revolution, and in particular from the 1850's onwards, combustion of fossil fuels occurred on an unprecedented scale. As these fuels are of geological age they have zero ^{14}C activity (i.e. activity indistinguishable from background levels). The CO_2 released into the atmosphere upon combustion, being ^{14}C-free, noticeably dilutes the atmospheric ^{14}C concentration. Tree ring studies from the last two centuries show that the radiocarbon activity in wood grown in AD 1950 (before nuclear weapons testing) is lower than in samples grown in AD 1850 (prior to the internationally accepted boom in fossil fuel combustion from the industrial revolution) despite the radioactive decay of ^{14}C that has occurred in the latter (Aitken, 1990). This was first reported by Suess (1955) and documents the uptake of '^{14}C-dead carbon' into the biosphere following increasing industrialisation and consequent release of fossil fuel CO_2 into the atmosphere. This 'Suess Effect' is visible in records of global atmospheric ^{14}C concentrations from AD 1890 onwards. These records show a marked decrease in atmospheric ^{14}C concentration from AD 1890, more so in large cities or industrial areas where fuel consumption is highest, leading to a ^{14}C depression in these areas. Specifically, more polluted areas such as Europe show a heightened Suess effect in comparison to the west coast of the United States (De Jong and Mook, 1982), especially in winter when fuel consumption is at its highest (Levin et al., 1989). Tree ring studies attempting to quantify the Suess effect have shown a strong offset for the period 1890 to 1950 of $\Delta^{14}C$ = -20‰ for the Pacific coast of the United States (oceanic air) (Levin and Hesshaimer, 2000) and a further c. 10‰ depression in $\Delta^{14}C$ observed in Dutch oak trees (De Jong and Mook, 1982). The Netherlands is surrounded by some of the most industrialized countries in Europe and

therefore shows a further localized dilution of the ^{14}C atmospheric concentration owing to intensive fossil fuel consumption at this time (De Jong and Mook, 1982).

1.5.2 Nuclear weapons testing

During the late 1950s and early 1960's, the nuclear weapons programme of many countries involved atmospheric testing, leading to a large rise in the production of ^{14}C (Levin and Hesshaimer, 2000) as the neutrons released from the fission and fusion explosions caused the formation of large quantities of ^{14}C (i.e. Equation 1.4). Atmospheric testing came to an end with the passing of the test ban treaty in 1963 (Rakowski et al., 2005) but significant amounts of ^{14}C, to the order of 630 $x10^{26}$ atoms or more (Hesshaimer et al., 1994), had been generated and released into the atmosphere within this short period. Effects were most noticeable within the Northern Hemisphere, reflecting the location of most of the atomic weapons tests, notably Novaya Zemyla in the former Soviet Union (Nydal and Lövseth, 1996). This 'spike' in atmospheric radiocarbon activity reached a maximum around 1963/4 of roughly double the level present in the Northern Hemisphere before nuclear testing began (Nydal and Lovseth, 1996). However, "bomb" ^{14}C has proven useful as a tracer in studies of atmospheric mixing rates (Nydal and Lovseth, 1996; Levin and Hesshaimer, 2000). Many studies have shown that the high ^{14}C levels induced by nuclear weapons testing are declining relatively rapidly, owing to the counteracting influence of the fossil fuel effect and the incorporation of atmospheric CO_2 into the biota and the oceans (Broeker et al., 1985; Levin and Hesshaimer, 2000; Otlet et al., 1992).

1.6 Variations within the terrestrial biosphere

Terrestrial fauna and flora within the biosphere are supported by atmospheric carbon, incorporated into the food chain via photosynthetic pathways as shown in Equation 1.1. The terrestrial biosphere represents a relatively homogenous reservoir of ^{14}C, provided that appropriate corrections are made for any isotopic fractionation that can occur during uptake and metabolic fixation of CO_2 by plants, and subsequent transport through the food chain (Figure 1.1).

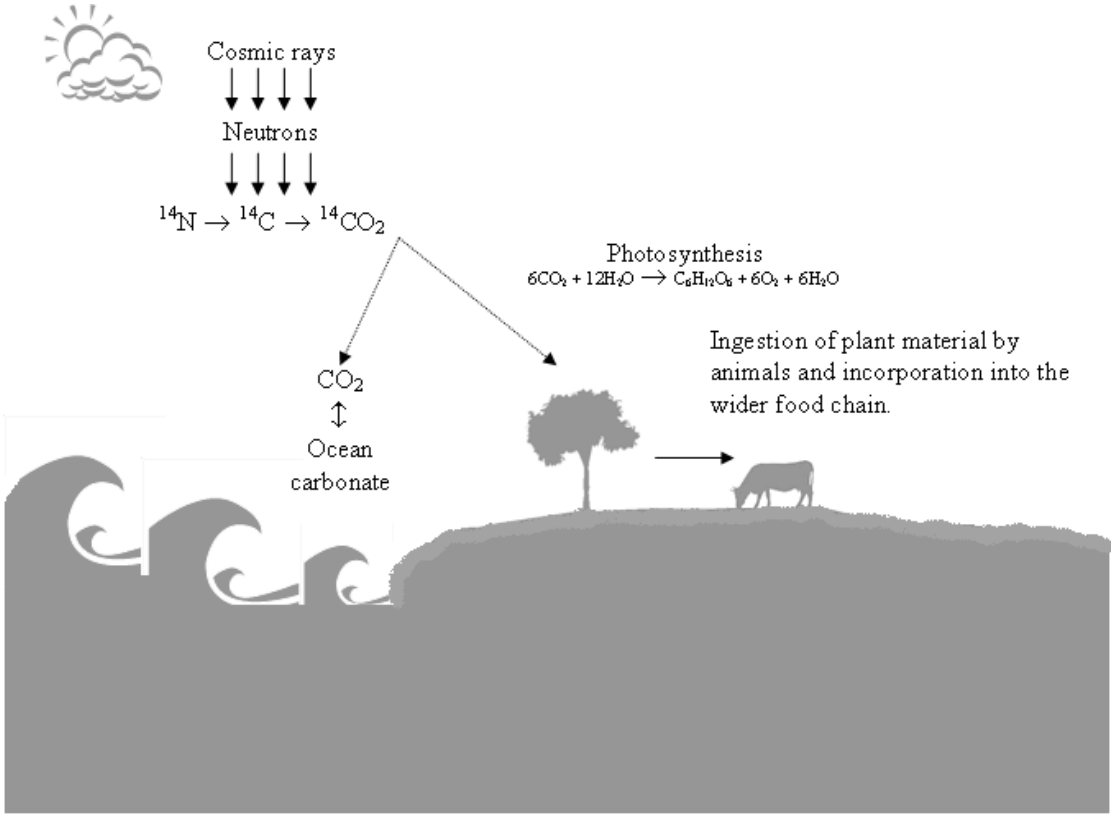

Figure 1.1: ^{14}C production and distribution into the food chain (after Aitken, 1990)

1.6.1 Kinetic isotopic fractionation

Isotopic fractionation involves enrichment of one isotope relative to another during chemical or physical processes. It was first proposed by Craig (1953) that biological systems could alter the isotopic equilibrium of ^{14}C, ^{13}C and ^{12}C through chemical processing, resulting in a non-homogenous ratio of ^{14}C to ^{13}C or ^{12}C throughout the biosphere. Terrestrial biosynthetic processes primarily incorporate carbon from the atmosphere via photosynthesis in green plants. In marine systems, phytoplankton and algae provide a similar base to the food chain. Plants preferentially take up ^{12}C in relation to ^{14}C during photosynthesis, thus lowering the ^{14}C activity in plant material compared to that of the atmosphere (Harkness, 1979). Plants also contain less ^{13}C than the atmosphere and this isotopic fractionation between the 3 isotopes occurs according to chemical and physical properties related to the differences in mass (O'Leary, 1981). The discrimination in relation to atomic mass means that the fractionation effects for ^{14}C relative to ^{12}C are double those for ^{13}C relative to ^{12}C. Photosynthetic pathways in plants can vary, discriminating against carbon isotopes according to their environment and metabolism but typically fall into two main categories; those that follow a C3 pathway (most terrestrial

plants e.g. trees, many grasses, wheat, barley, etc) and those that follow a C4 pathway (tropical zone plants, sedges, maize, millet, etc); C3 plants discriminate against ^{13}C more than C4 plants. As well as photosynthetic uptake of CO_2, a variety of other natural processes exist that result in different isotopic fractionation of carbon isotopes. The level of fractionation can then differ throughout the food chain during various metabolic processes. This means that the natural abundance of ^{14}C in different materials is different at a single point in time, due to the specific carbon isotopic fraction that has occurred during formation of these materials. The process of radiocarbon dating relies upon measuring the ratios of $^{14}C/^{12}C$ (or $^{14}C/^{13}C$) and so any sample formation processes that influence this ratio must be quantified. This problem can be rectified by normalising the ^{13}C content of samples to be dated, relative to an international standard. This is achieved by measuring the ratio of the stable carbon isotopes ($^{13}C/^{12}C$) in the sample. This is then compared with the $^{13}C/^{12}C$ in an international standard material. The depletion or enrichment of ^{13}C in the sample ($\delta^{13}C$) relative to the appropriate international standard can then be calculated (Equation 1.6). This $\delta^{13}C$ value can then be used to produce a fractionation factor to normalise ^{14}C activities (See section 3.4).

$$\delta^{13}C(‰) = \left[\frac{(^{13}C/^{12}C)\ \text{sample} - (^{13}C/^{12}C)\ \text{standard}}{(^{13}C/^{12}C)\ \text{standard}} \right] \times 1000$$

Equation 1.6: Calculation of $\delta^{13}C$ (per mille (‰)) to demonstrate depletion/enrichment of sample ^{13}C relative to the international standard (Craig, 1953)

The standard used for normalisation of ^{13}C is the Vienna Peedee Belemnite carbonate (VPDB) (Coplen, 1994). The isotopic composition of the sample being measured is expressed as $\delta^{13}C$, which represents the parts per thousand (‰) deviation of the sample ^{13}C content from the VPDB standard (Keith et al., 1964; Aitken, 1990). A more negative $\delta^{13}C$ means less ^{13}C relative to the standard and vice versa, a more positive $\delta^{13}C$ means more ^{13}C relative to the standard (O'Leary, 1988). Fractionation occurs to varying degrees throughout all biosynthetic processes, including the formation of animal tissues after green plant consumption. Table 1.1 shows some typical $\delta^{13}C$ values for a range of sample materials, showing the variation in deviation from the VPDB standard.

Sample material	**$\delta^{13}C$** (‰)
Wood, charcoal, peat, C3 plants	-25 ± 3
Bone collagen, amino acids	-20 ± 2
NBS Oxalic acid I	-19 ± 1
Freshwater plants	-16 ± 2
Arid zone grasses, sedges	-13 ± 2
Marine plants	-12 ± 2
C4 plants (eg. Maize, millet)	-10 ± 2
Bone apatite	-10 ± 2
Atmospheric CO_2	-9 ± 2
Non-marine carbonates	-5 ± 5
Marine carbonate	0 ± 3

Table 1.1: Average $\delta^{13}C$ values for commonly dated sample materials (Aitken, 1990 after Stuiver and Polach, 1977)

The ratio of carbon isotopes in different sample materials is therefore subject to variability according to metabolism and environment, resulting in a non-homogenous distribution of ^{14}C throughout the biosphere. Correction for fractionation through standardisation allows different sample materials to be comparably dated even though the natural abundance of the three carbon isotopes can vary widely according to sample material.

Not only does the isotopic ratio of carbon vary according to metabolism and environment, but the volume and flux capacity of total carbon can vary according to the carbon reservoir it occupies. Figure 1.2 shows the main carbon reservoirs of the natural environment and the mass of carbon present in each as well as the flux between each reservoir.

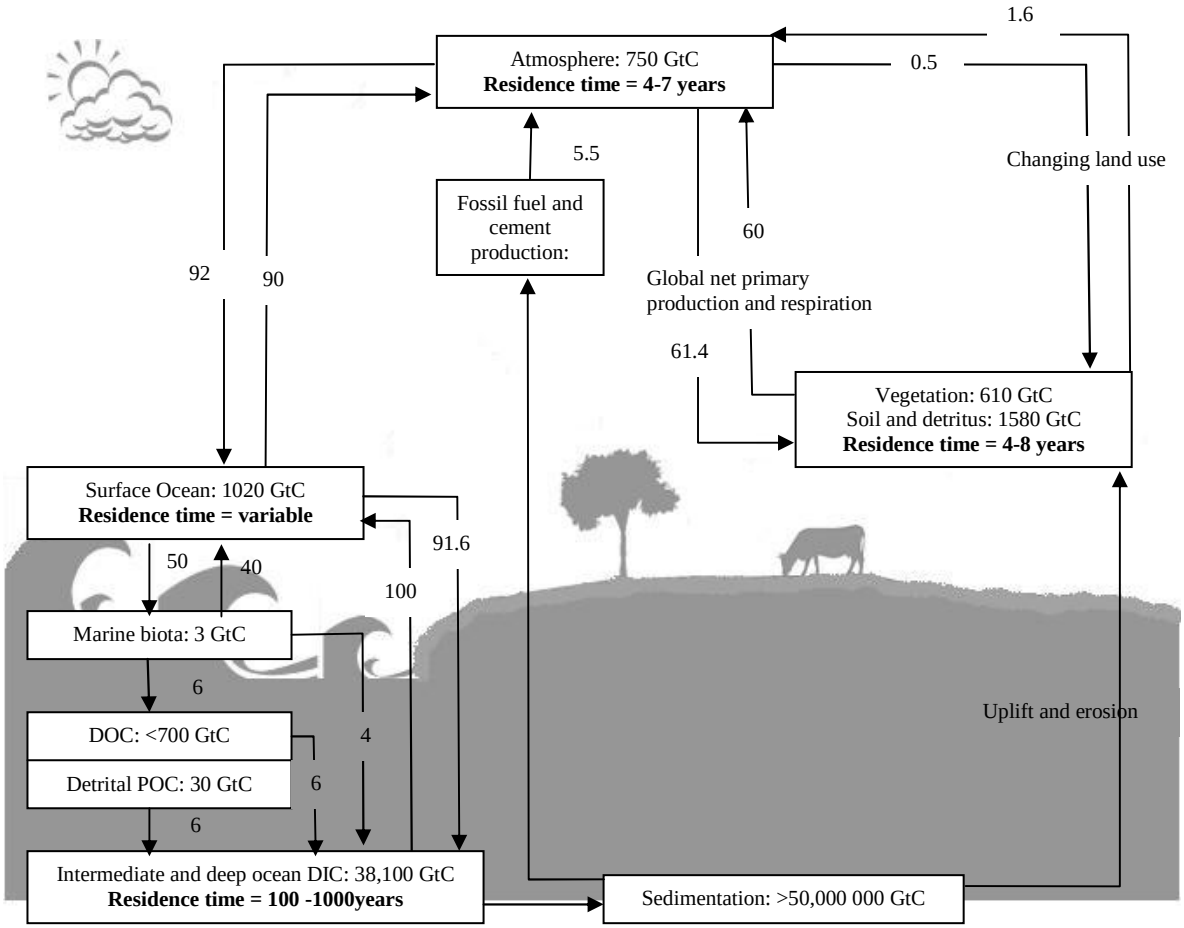

Figure 1.2: Reservoir volumes of carbon (GtC) and mean residence times for key stages in the biogeochemical carbon cycle

(Annual flux volumes (Schimel, 1995) are shown by arrows. Residence times (Craig, 1957a; Mangerud, 1972; Gaudinski et al., 2000) are in bold)

1.6.2 Residence times

Residence times for ^{14}C in the terrestrial biosphere are short; of the order of 4-8 years, including total soil respiration (Gaudinski et al., 2000). The marine environment contains about 50 times more carbon than the atmosphere and does not cycle carbon quickly, thus the rate of surface gaseous exchange with the atmosphere is not maintained throughout the entire oceanic reservoir. Exchange between carbon atoms in the surface ocean layers is much quicker than in the deep ocean, leading to varying residence times of carbon in the oceans, dependant on depth. Because of the large size of the reservoir and the varying rates of exchange, the marine system does not comprise a homogenous environment. Deep ocean residence times are subject to large variation owing to oceanic geography and circulation. Surface ocean residence times act as a function of the local deep ocean regime

and the air/sea exchange. The marine carbon system will be discussed in detail in Section 1.7.

Slow exchange with the atmosphere in certain reservoirs leads to carbon being removed from the point of atmospheric ^{14}C input. This leads to depleted levels of ^{14}C with respect to the contemporaneous atmospheric signal as ^{14}C is being removed from the system by radioactive decay, but is not being replaced by atmospheric input. This is known as a reservoir effect and will form the main body of work for this thesis, examining in particular the Marine Radiocarbon Reservoir Effect (MRE).

1.7 ^{14}C in the marine environment: Formation of the MRE

As previously discussed, the atmospheric reservoir is subject to rapid internal mixing which results in an almost homogenous distribution of ^{14}C throughout the atmosphere. The Northern Hemisphere represents a relatively homogenous reservoir although the Southern Hemisphere does show a gradient owing to strong upwelling of ^{14}C depleted water around Antarctica (Braziunas et al 1995). The oceanic reservoir however, is not homogenous, due to factors affecting the dissolution of atmospheric ^{14}C and circulation-induced variations in local ^{14}C activity.

^{14}C enters the oceans by CO_2 dissolution across the air-sea interface. This becomes part of the inorganic carbon equilibrium involving carbonic acid, bicarbonate ions, carbonate ions and CO_2 (Mills and Urey, 1940; Mook et al., 1974). The dissolution rate of CO_2 is temperature dependent, increasing with decreasing temperature and influenced by physical characteristics such as agitation by wave action and wind speed (Merlivat and Memery, 1983). The dissolution of CO_2 across the global ocean is therefore not uniform. The heterogeneity of the marine reservoir is further influenced by oceanic currents mixing bodies of water with variable ^{14}C activity.

As surface water currents travel towards the Polar Regions, the water begins to cool and in so doing becomes denser, sinking to depth within the water column (downwelling) (Broecker, 1987; Broecker et al., 1991). This process of thermohaline circulation removes water from the point of atmospheric ^{14}C input and allows it to sink to the intermediate and deep ocean layers (>100 m depth approx.). This water then travels slowly through the

deep oceans (during which time ^{14}C decay occurs) before upwelling and mixing with surface waters eventually occurs. Surface water ^{14}C activity is hence somewhat enriched relative to deep waters but depleted relative to the atmosphere and terrestrial biosphere (Broeker, 1987; Broecker et al., 1991; Gordon and Harkness, 1992). This depletion of the ocean ^{14}C content with respect to the atmosphere is known as the Marine Radiocarbon Reservoir Effect (MRE). Variations in local conditions and mixing rates prevent there from being a universal ^{14}C offset from the atmosphere for all oceanic environments (Jones et al., 2007; Gomez et al., 2008; Harkness, 1983). Conditions such as the stratification of water masses, upwelling and residence time all affect the ^{14}C content of water bodies, resulting in a non-uniform ^{14}C concentration (Gordon and Harkness, 1992). On average, the MRE age offset between contemporary marine and terrestrial material is to the order of 400 years for the global surface oceans in the Northern Hemisphere (Stuiver and Braziunas, 1993). However, because of the inherently variable nature of this offset, accurate calibration of radiocarbon ages determined from samples containing marine derived carbon can be problematic (Ascough et al., 2004).

1.8 Accounting for global variation in ^{14}C concentration: Producing ^{14}C ages and the need for calibration

Variations in the global ^{14}C concentration for both the terrestrial and marine reservoirs occur through time in a non-linear fashion. Variations occur on spatial and temporal scales that must be accounted for in order to establish accurate ^{14}C concentrations at the time of final formation for any sample to be dated. The initial 'starting' ^{14}C concentration of the sample at the time of final formation/death must be known in order to quantify any depletion, and therefore allow the calculation of the time since final formation (t) as per Equation 1.3. Using the decay equation (Equation 1.3) produces a conventional radiocarbon age (CRA) or time since final formation in radiocarbon years before present (^{14}C years BP). Present is defined as 1950AD and although radiocarbon dating has been carried out since 1950, as long as both standards and samples are reported relative to 1950, there is no need to decay correct ages as both the samples and the standards have been decaying at the same rate since this time. The calculation of results in ^{14}C years BP does not allow the results to be interpreted within a calendrical timescale as the concentration of ^{14}C in the atmosphere and oceans varies through time in a non-linear way. This means the initial $^{14}C/^{13}C$ ratio of the atmosphere or ocean and hence 'starting' $^{14}C/^{13}C$ ratio of the

sample depends upon the calendar time period in which the sample was formed. The ^{14}C 'age' depends not only upon the (calendar) time since death or final formation of the sample, but also upon the $^{14}C/^{13}C$ concentration of the atmosphere at the time of death/final formation. The ^{14}C ages must therefore be calibrated in order to account for these variations in atmospheric ^{14}C concentrations and to allow conversion of the sample ^{14}C 'age' to calendar years.

Converting ^{14}C ages to calendar years allows the sample age to be interpreted in relation to samples dated by other techniques and calendar events published using year notations BC or AD. Calibration of ^{14}C ages is achieved using a calibration curve of ^{14}C age versus calendar age. The calibration curve is produced by ^{14}C dating a time series of samples for which the exact calendar date is known or can be calculated (Pearson and Stuiver, 1993; Stuiver and Braziunas, 1993; Stuiver et al., 1998a; Stuiver et al., 1998b; Reimer et al., 2004; Reimer et al., 2009). Separate calibration curves have been constructed for the atmospheric (terrestrial) environment (INTCAL09 (Reimer et al., 2009)) and the marine environment (MARINE 09 (Reimer et al., 2009)) to account for the large offset in ^{14}C concentration between the two reservoirs caused by the MRE.

1.8.1 Terrestrial Calibration

Calibration using dendrochronologically dated, continuously overlapping tree-ring sequences has proven to be the most successful method since the production of the first calibration curves (Stuiver and Suess 1966, Suess 1979). Dendrochronological (calendar) dates can be matched with ^{14}C dates, using ^{14}C age measurements made on annually ringed tree samples to construct a calibration curve for atmospheric/terrestrial biospheric ^{14}C dates. Use of this curve allows calibration of ^{14}C ages to calendar years. Beyond the limit of the absolutely dated tree ring sequence, calibration becomes more problematic (Reimer et al., 2009; Bronk Ramsey et al., 2006; Mellars, 2006a; Mellars, 2006b; Turney at al., 2006; Blockley and Housley, 2009). The most recent publication of the atmospheric calibration curve is INTCAL09 (Reimer et al., 2009) which superceded the previous dataset, INTCAL04 (Reimer et al., 2004).

At present, a continuous dataset of tree-rings linked to present day only extends for the past 12.59 cal kBP (Friedrich et al., 2004b), but the possibility remains to tie in the floating European tree-ring record and extend this limit to the past 14 cal kBP (Friederich et al.,

2004a; Schaub et al., 2008a; Schaub et al., 2008b; Reimer et al., 2009).

Since atmospheric calibration using the tree ring record is currently possible only for the past 12.59 cal kBP, other materials have to be used to extend the curve beyond this point. From 12.59 cal kBP onward, a variety of marine based samples are used to construct the rest of the calibration curve, including foraminifera from varved sediments (Hughen et al., 2004) and U-Th dated corals (Bard et al., 1998, 2004; Fairbanks et al., 2005). The marine samples used for calibration beyond 12.59 cal kBP are ^{14}C dated and the ^{14}C dates are modelled to produce an equivalent atmospheric age using a specific reservoir correction to account for the MRE age offset.

The INTCAL09 dataset updates the INTCAL04 dataset from 12 – 26 cal kBP and extends the calibration range to 50 cal kBP. No change was made to the calibration data from 0-12 cal kBP (Reimer et al., 2009), the period of focus for this thesis. At the time of publication for INTCAL04 and MARINE 04, the discrepancies between the various datasets after 26 cal kBP had been deemed too large by the INTCAL Working Group to provide confident calibration beyond this limit (Reimer et al., 2009). However, developments in the construction of INTCAL09 have resolved many of these discrepancies and pushed the publication of calibration data to 50 cal kBP. This extension acknowledges that anomalously large variations in the datasets are evident, that may be due to changes in oceanic circulation or magnetic field intensity. The shape of the curve may therefore be subject to further change in the future, when more calibration data become available (Reimer et al., 2009).

The curves are constructed using a Markov Chain Monte Carlo (MCMC) random walk model (Reimer et al., 2009; Buck and Blackwell, 2004). The model generates the calibration curve at 5 year intervals from 0 - 11.2 cal kBP, 10 year intervals from 11.2 –15 cal kBP, 20 year intervals from 15 – 25 cal kBP, 50 year intervals from 25 – 40 cal kBP and 100 year intervals from 40 – 50 cal kBP (Reimer et al., 2009).

The calibration curves (INTCAL09 and MARINE 09) plot ^{14}C ages BP on the vertical axis versus calendar years on the horizontal axis and allow the calculated age in years BP to be determined on the curve as a corresponding date BC or AD age (Figure 1.3). The entire probability distribution of the ^{14}C age and its associated error is translated through the

curve, resulting in a calibrated age range in years BC or AD. Because the curve is non-linear, there may be multiple points of intercept, depending upon the shape of the curve, all equally valid (Pearson, 1987).

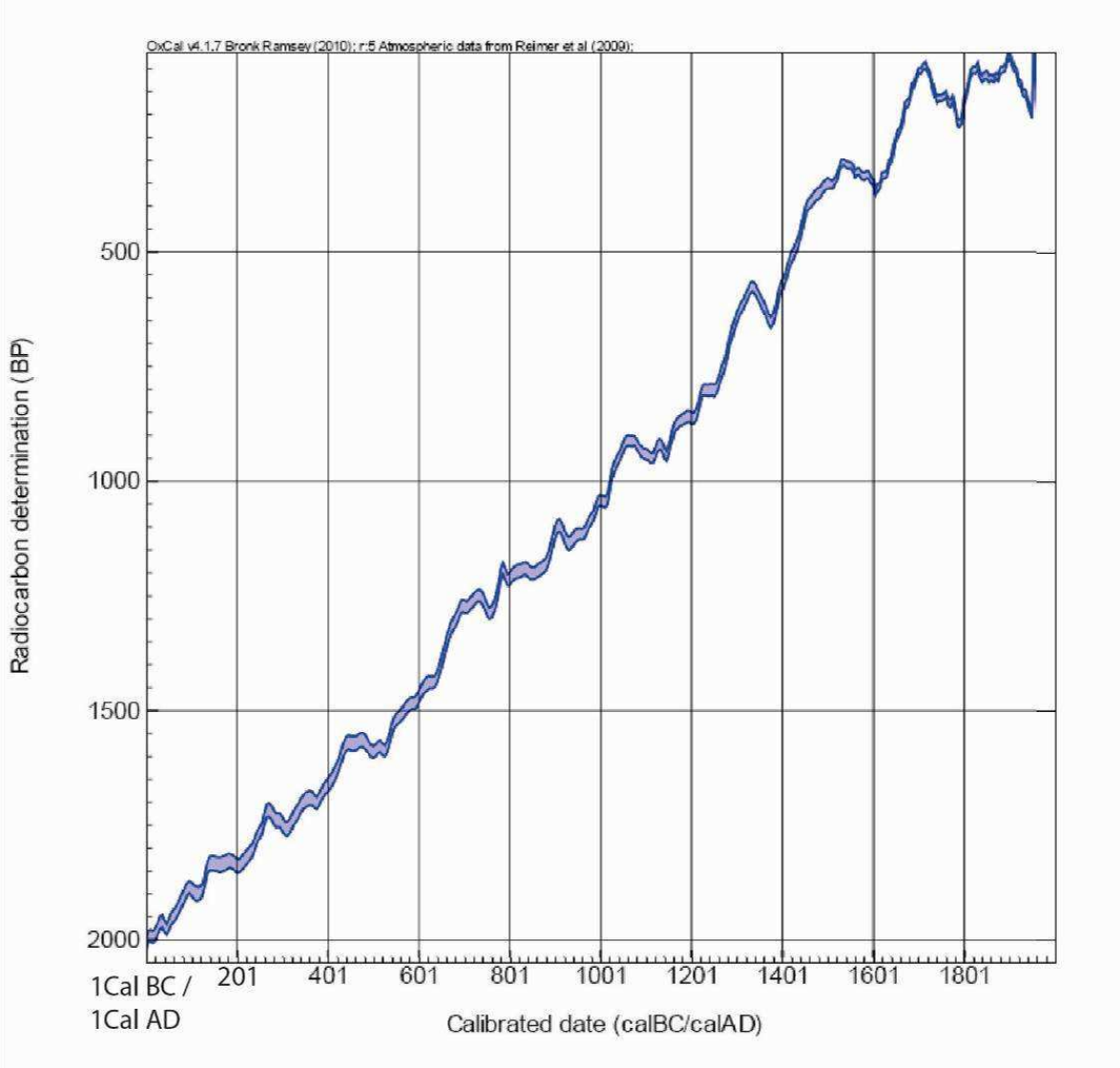

Figure 1.3: A section of the atmospheric calibration curve (OxCal version 4.17 (Bronk Ramsey, 2009))

(Atmospheric data from Reimer et al., 2009)

The width of the translated age limits for each point of intercept will be dependant upon the steepness of the curve at that particular point, resulting in a non-Gaussian distribution for the calibrated age range and therefore preventing the production of a single midpoint with an associated error term. A ^{14}C age falling on a plateau on the calibration curve will result in a large calendar age range whereas steep sections of the curve will provide short calendar age ranges (Figure 1.4). All valid age ranges at 68 and 95% confidence (1 and 2σ) are published alongside their relative probability using, Calib or OxCal (the most

widely used calibration programs).

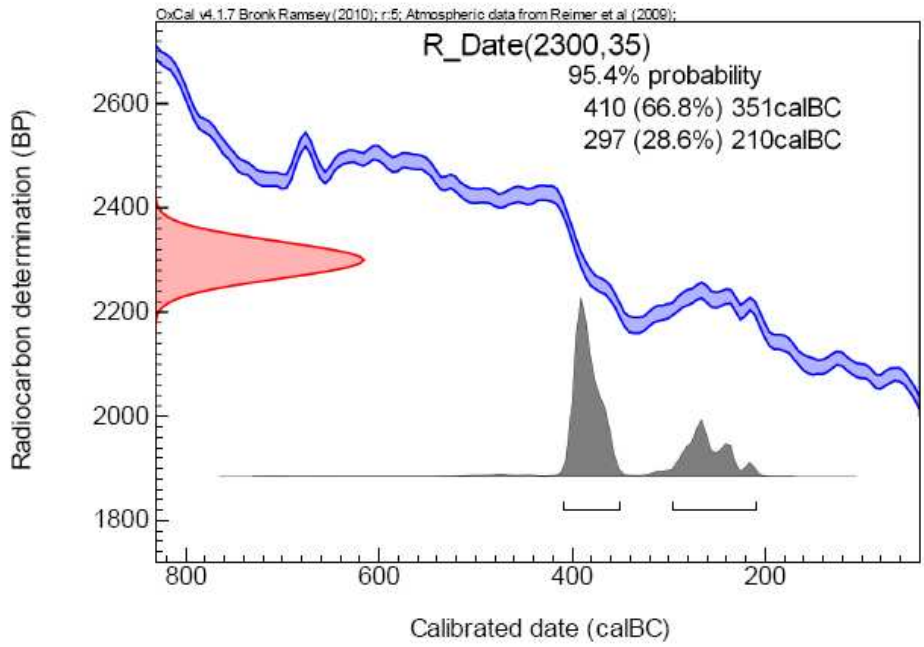

a) Calibration of a radiocarbon date of 2300 ± 35 BP which falls on a steep part of the calibration curve, giving a tight range of probable dates

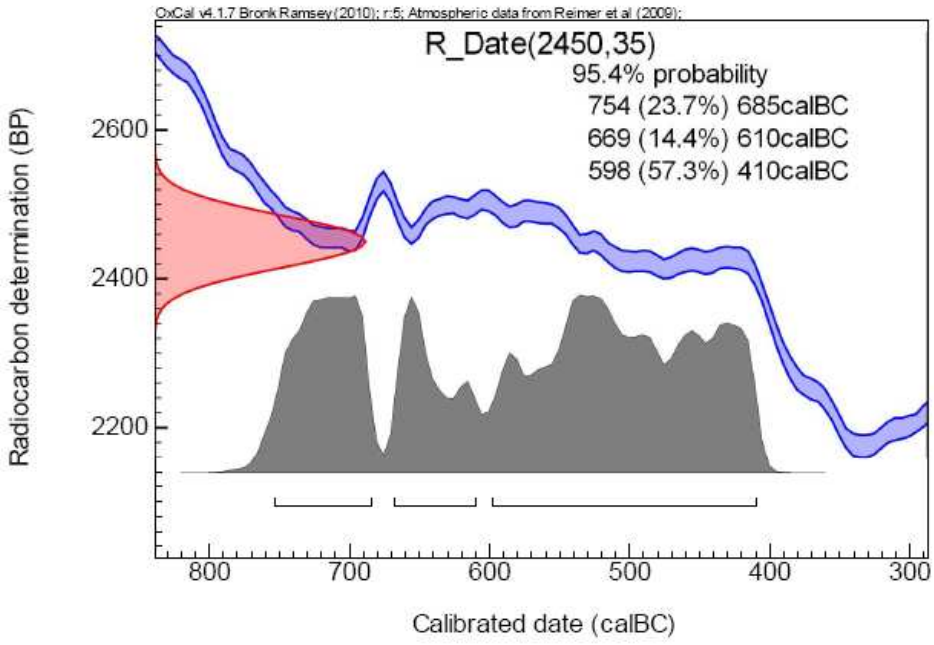

b) Calibration of a radiocarbon date of 2450 ± 35 BP which falls on a plateau within the calibration curve, giving a wide range of probable dates

Figure 1.4: Plots of radiocarbon age vs calendar date showing the difference in the range of dates produced from radiocarbon measurements that fall on a) a steep part of the

calibration curve and b) a plateau on the calibration curve
(Calibrations performed using OxCal 4.17 (Bronk Ramsey, 2009); Atmospheric data from Reimer et al., 2009)

Radiocarbon ages are almost always converted to calendar age ranges using calibration software programs such as CALIB (Stuiver and Reimer, 1993; Stuiver et al., 2005) or OxCal (Bronk Ramsey, 1994, 1995, 2005, 2009). The calibration program used throughout this study is OxCal version 4.17 (Bronk Ramsey, 2009).

The calibration of atmospheric/terrestrial ages uses the INTCAL09 dataset, however, the calibration of ages based on marine derived carbon must use a separate curve (MARINE09), in order to account for the MRE.

1.8.2 Marine Calibration

Marine ages are calibrated using a modelled marine curve based on the atmospheric data. The current calibration curve (MARINE09) (Reimer et al., 2009) takes the data from 0-12.5 cal kBP directly from the preceding calibration curve MARINE04 (Hughen et al., 2004), which uses the ocean- atmosphere box diffusion model (Oeschger et al., 1975; Stuiver and Braziunas, 1993). The modelled marine calibration curve accounts for the global average offset of oceanic ^{14}C with respect to the atmosphere, producing an present day average surface water reservoir offset of 405 ± 22 ^{14}C yr (Hughen et al., 2004), however, temporal and spatial deviations from this offset, known as ΔR, are evident (Stuiver and Braziunas, 1993; Ascough et al., 2006). The offset, as well as the deviations, are visible in Figure 1.5, which illustrates both the atmospheric and marine calibration curves.

From 12.5 – 50 cal kBP Marine 09 is simply INTCAL09 (which is derived directly from marine records) plus the reservoir age of 405 yr (Reimer et al., 2009).

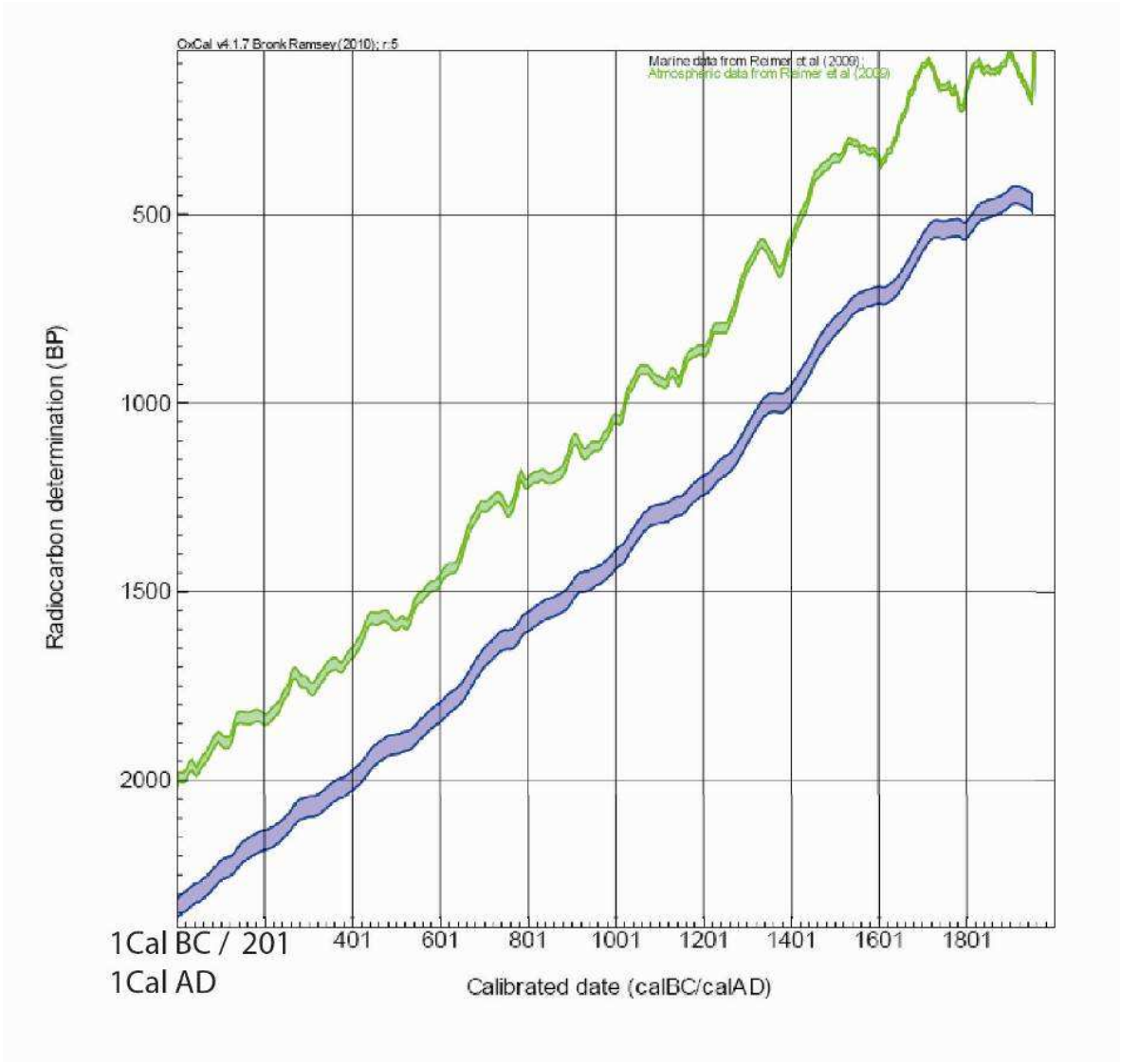

Figure 1.5: A section of the atmospheric (green) and marine (blue) calibration curves using OxCal 4.17 (Bronk Ramsey, 2009)

The offset between the marine and atmospheric calibration curves varies in magnitude according to the degree of oceanic buffering of sharp changes in atmospheric ^{14}C concentration. The buffering capacity of the ocean smoothes out any sharp changes in atmospheric ^{14}C concentration as the large volume of carbon in the oceanic reservoir, coupled with slow mixing rates and exchange with the atmosphere induce a delayed and diluted response to atmospheric fluctuations. Marine and atmospheric data from Reimer et al., (2009).

Variability in the parameters of the modelled marine curve itself must also be considered as the model can only reflect fixed modes of oceanic circulation and so large deviations from the model output may be evident in areas where such parameters vary greatly. The

uncertainties given in the ocean-atmosphere box model results for Marine 09 were calculated by varying eddy diffusity and air-sea gas exchange rate within 'reasonable' ranges (Hughen et al., 2004). Variation in the MRE as a direct consequence of uncertainties in the parameters of the model itself is of great importance when considering the significance of any deviations (ΔR) from this modelled output.

Current methods of determining temporal and spatial variations in the MRE include the quantification of ΔR values for geographical locations worldwide. ΔR is factored into the calibration process by subtracting ΔR from the conventional radiocarbon age (CRA) then calibrating with the marine curve. A positive ΔR will therefore increase the MRE whilst a negative ΔR will decrease the offset. Globally, ΔR values can show significant variation (Figure 1.6) as shown by the data held on the 14 CHRONO Marine Reservoir database at http://intcal.qub.ac.uk/marine/. Currently, the largest global ΔR value is recorded at +2482 ± 46 ^{14}C yrs BP from Punta Mogotes in Argentina (Gomez, 2008), whilst the lowest value of -280 ^{14}C yrs BP is recorded from the St Catherine Isles, off the coast of Georgia, USA (Thomas, 2008). However, it is important to note that extreme ΔR values such as +2482 ± 46 ^{14}C yrs BP from Punta Mogotes are influenced by old dissolved terrestrial carbonate entering the ocean from rivers and groundwater and so are not true marine reservoir effects *per se*. Nevertheless, in the absence of suitable terrestrial material, accurate and precise quantification of ΔR is imperative for accurate calculation of calendar age ranges based on samples containing marine-derived carbon.

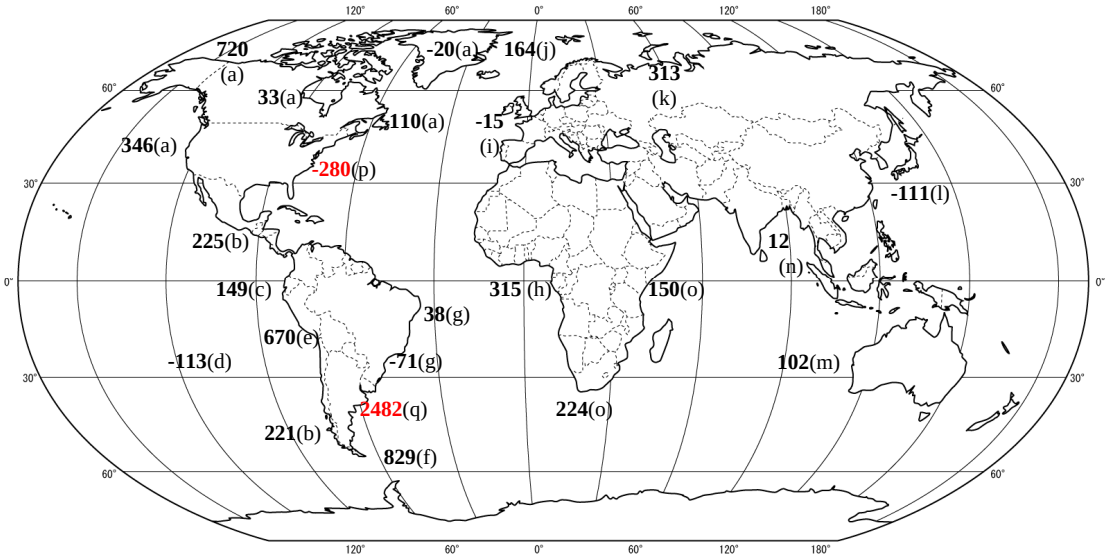

Figure 1.6: Global variations in ΔR (^{14}C yrs BP). Maximum and minimum global values are shown in red

(All values are taken from the online 14 CHRONO Marine Reservoir database. References for each value are: a) - McNeeley et al., 2006, b) - Ingram and Southon, 1996, c) – Jones et al., 2007, d) - Beck et al., 2003, e) - Taylor and Berger, 1967, f) - Bjork et al., 1991, g) - Nadal de Masi, 1999, h) - Lewis et al., 2008, i) – Harkness, 1983, j) – Funder, 1982, k) - Forman and Polyak, 1997, l) - Kong and Lee, 2005, m) - Bowman and Harvey, 1983, n) - Dutta et al., 2001, o) - Southon et al., 2002, p) – Thomas, 2008, q) - Gomez, 2008)

To demonstrate the effect of changing ΔR values on radiocarbon calibrations, a hypothetical radiocarbon date of 900 ± 35 BP was calibrated using OxCal 4.1 with a ΔR of 0 ^{14}C yrs BP, a ΔR of +100 ^{14}C yrs BP and a ΔR of -100 ^{14}C yrs BP using the Marine09 curve. This produced the variable calendar age ranges shown in Figure 1.7, showing the pronounced effect that ΔR can have on the accurate calibration of marine derived material.

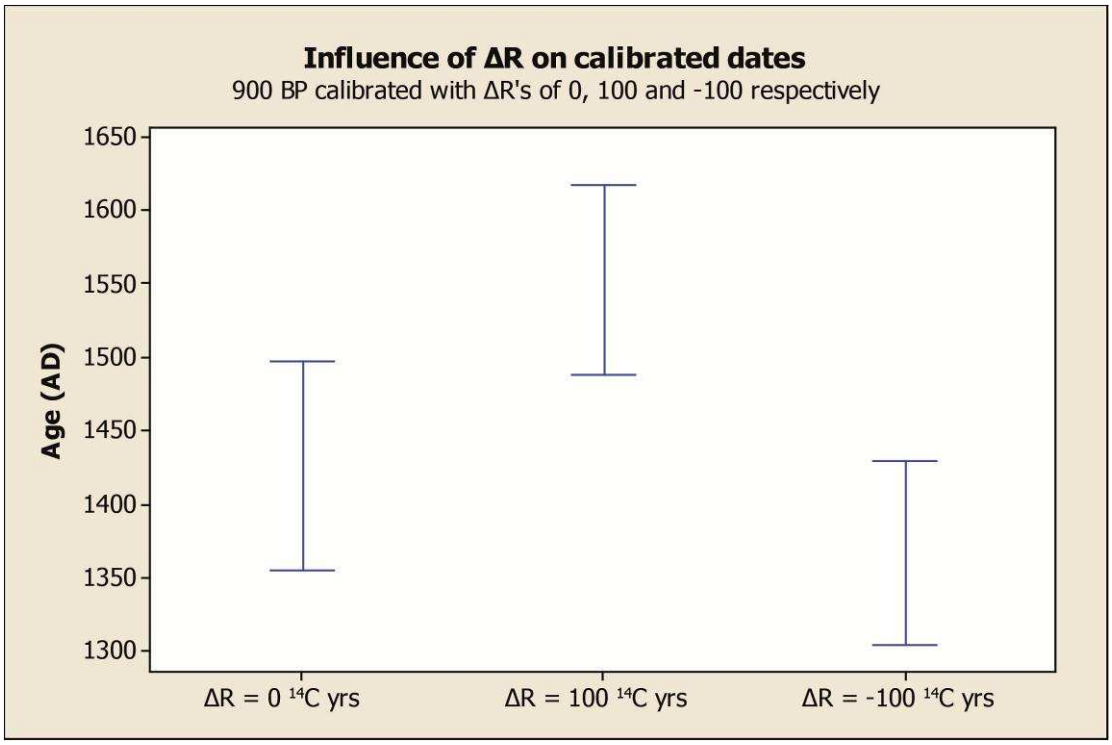

Figure 1.7: Calibrated age ranges of a 900 ± 35 BP age measurement showing the difference in resultant calendar age range depending upon the specific ΔR value used in the calibration (calibrated using OxCal4.1 (Reimer et al., 2009; Bronk Ramsey, 2009))

1.9 Understanding variability in ΔR: global values in relation to oceanic regimes

As previously mentioned, the MRE is subject to temporal and spatial deviations. Currently, the global average reservoir age for surface waters, R(t), is around 400 years and deviations from this average are termed ΔR where ΔR = 0 ^{14}C yrs BP for the global average. The spread of ΔR values shown in Figure 1.6 demonstrates the global variability in ΔR. This range in ΔR reflects differences in local water ^{14}C content, influenced by a variety of factors including oceanic circulation and the movement of water bodies with varying levels of ^{14}C activity. ΔR is variable through time and place, owing to the dynamic nature of water movement in the world oceans. In order to produce accurate ^{14}C ages on marine derived carbon, a temporally and spatially specific MRE (by means of ΔR derivation) must be calculated.

The variations in ΔR are predominantly influenced by factors such as the rate of atmosphere-ocean gas exchange, oceanic circulation variability and upwelling. Brief

acknowledgement (Section 1.7) has already been given to the fact that temperature, and agitation by wind speed/wave action can influence the rate of dissolution of CO_2 across the air-ocean interface. This results in geographically distinct areas of the surface ocean in terms of CO_2 dissolution, which inherently affects the local water ^{14}C activity. The transport of water bodies due to ocean circulation and current movement induce further variability to the heterogeneous oceanic carbon reservoir.

Wind strength and direction influence oceanic currents; a prime example being the opposing trade winds in the Northern and Southern Hemispheres which are generated by the Coriolis force, producing clockwise gyres in the Northern oceans and counter clockwise gyres in the Southern oceans (Jarumayan and Sadili, 2003). On a smaller scale, wind driven circulation can influence surface ocean water to a depth of c.100 m as energy is transferred vertically (Ekman transport) (Thurman, 1990). Where surface water is moved horizontally by wind action away from a certain point, deeper water is upwelled to conserve volume. Major upwelling of deep water occurs at continental margins as shown in Figure 1.8 (Broecker, 1991). Upwelling brings deeper, older water into contact with surface water, depleting the ^{14}C content and therefore increasing the offset from the atmosphere and therefore the MRE. Areas affected by upwelling therefore tend to display very positive ΔR values, showing the presence of very old, ^{14}C depleted water.

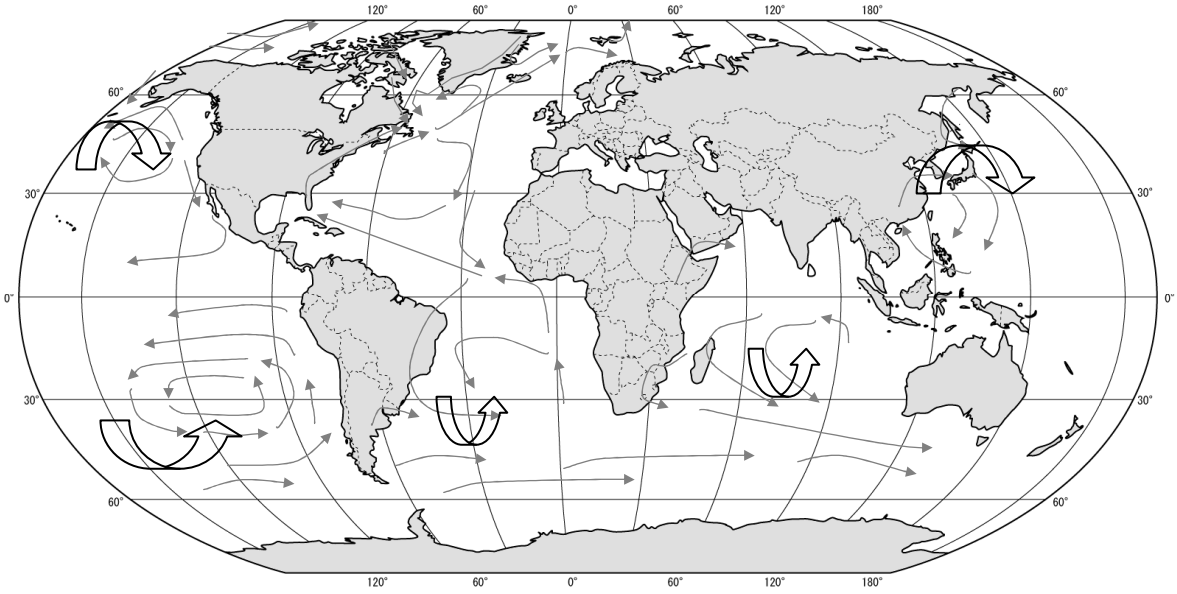

Figure 1.8: Main oceanic patterns of circulation (grey solid arrows) after Hoyt (1973) and major zones of deep water upwelling (transparent block arrows) after Broecker (1991)

This mass movement of water bodies and upwelling is induced by the process of thermohaline circulation. The principles of thermohaline circulation are well defined by Wüst (1935) and Wüst and Defant (1936) and essentially involve the evaporative cooling of surface waters as they move closer to the poles and the subsequent increase in salinity and therefore density, the sinking of these cooler and denser waters which then spread towards the equator and the eventual ascent of deep water through the thermocline into the surface layer (Wyrtki, 1961).

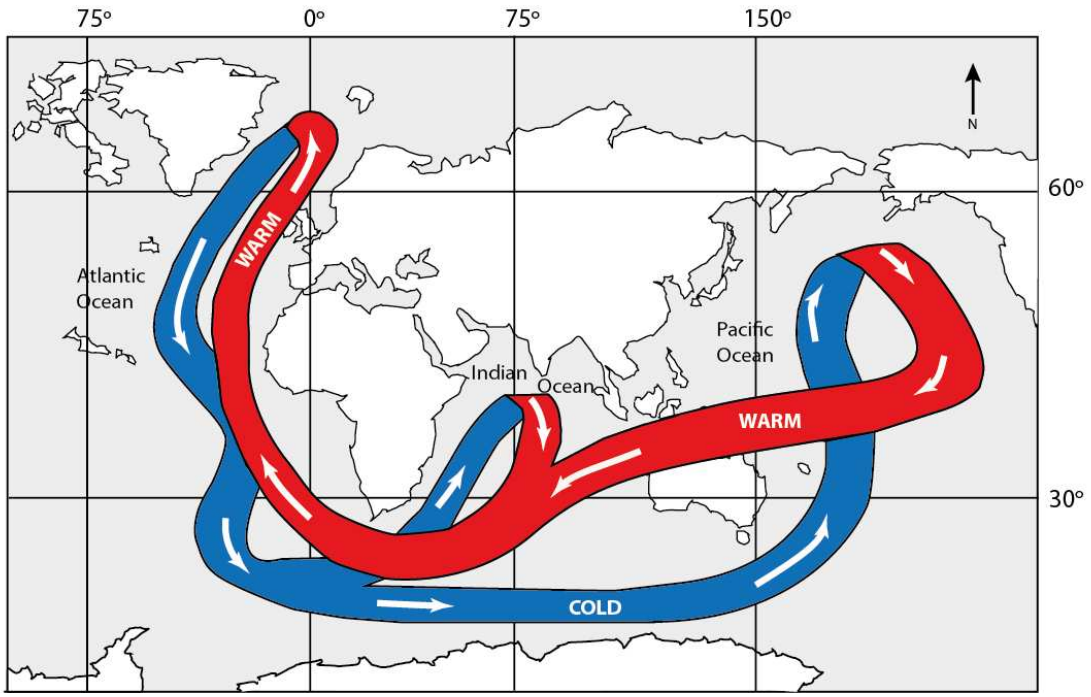

Figure 1.9: 'The great ocean conveyor' - an overview of global thermohaline circulation

(After Broecker et al., (1991) and http://planetforlife.com/gwarm/globclimate.html)

Depictions of 'the great ocean conveyor' (Figure 1.9) (Broecker, 1991) summarise the global circulation, starting with saline Icelandic waters cooling and sinking upon contact with the Canadian Arctic air masses. This water, known as North Atlantic Deep Water (NADW), then sinks and flows southward through the deep Atlantic towards the southern tip of Africa. This water mass is underlain by Antarctic Bottom Water (AABW), which intrudes into the NADW, increasing transport of the southward flowing water mass. The water mass here diverges into two main limbs, the lower limb joining a fast moving deep current that encircles the Antarctic, mixing the NADW with deep water generated from the Antarctic continent and also with old deep water from the deep Pacific and Indian Oceans. This water is then upwelled in the Pacific Ocean as it becomes warmer and fresher, being brought into contact with surface waters on its journey through the Northern Pacific and Indian Oceans. The upper limb moves northward from the tip of Africa, upwelling in the northern Indian Ocean, before cycling back towards the Atlantic alongside the lower limb.

This general ocean model, summarised in Figure 1.9 and detailed in Figure 1.8, correlates with key variations in ΔR values visible in Figure 1.6. Strongly positive ΔR values are

located in areas with active upwelling of older, deeper waters and lower values that are closer to the global average are observed in areas where upwelling is absent. The rationale for this thesis involved investigating variations in ΔR for the North Sea coast of Scotland, a semi enclosed basin of North Atlantic origin and therefore the North Atlantic circulatory pattern must be examined in more detail.

1.9.1 The North Atlantic marine environment

The North Atlantic plays an important part in the global thermohaline circulation system as discussed in section 1.9 and therefore must be examined in greater detail in order to examine any relationship between oceanic circulation and changes in ΔR. A brief overview of circulatory patterns in the North Atlantic region is shown in Figure 1.10.

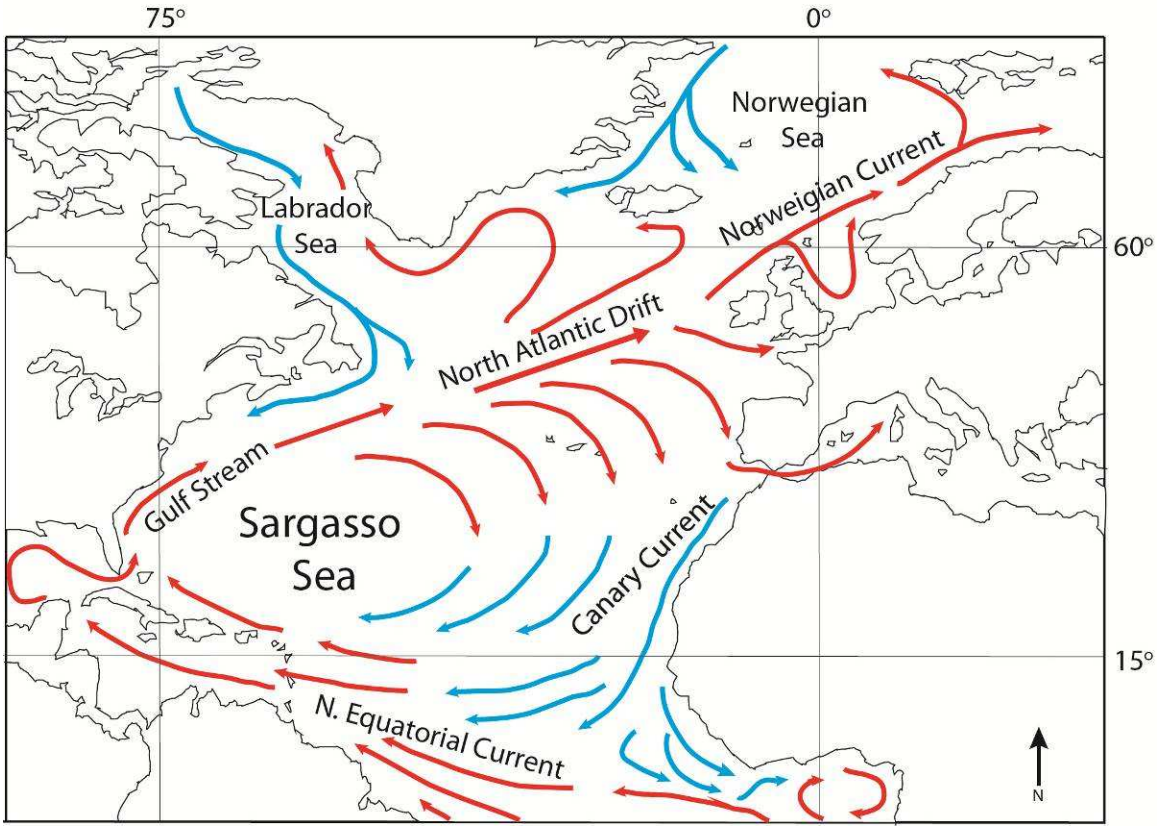

Figure 1.10: Ocean surface circulation of the North Atlantic in its wider context. Northward flowing warm water masses are shown in red, with cooler southward bound masses shown in blue

(After http://outreach.eurosites.info/outreach/DeepOceans/station.php?id=1, OSPAR 2000)

Figure 1.10 shows the equatorial waters that comprise the Gulf Stream form the major water mass flowing north-east into the North Atlantic. This body of water becomes the

North Atlantic Current (NAC) around 40ºN and 45ºW. The NAC continues on its north-east trajectory, branching off north and south around the European continent with some branches returning southward to form the anti-cyclonic circulation around the Sargasso Sea. The northward branches navigate the Northern North Atlantic, one branch following the UK coastline and becoming the Norwegian Current (NC) upon entering the Norwegian Sea, and the other branching off towards the Denmark Strait, known as the Iceland Current (IC), which is destined towards the Labrador Sea. The northward flowing water masses are relatively warm and saline, maintaining relatively rapid atmospheric CO_2 exchange, resulting in a relatively high ^{14}C activity (Campin et al., 1999).

The returning southward flow from the cold Arctic water masses is composed of fresher, less saline NADW. The evaoporative cooling from the Arctic air masses increases the density of the NADW, causing it so sink to depths below the northward moving water. This sinking results in the removal of NADW from the point of atmospheric exchange and the consequent depletion in ^{14}C activity. This water mass is dominated by the East Greenland Current (EGC) which skirts the east, then west coast of Greenland, (becoming the West Greenland Current (WGC)) before joining southward flowing water from the Labrador Sea. The zone of contact between the northern and southern flowing water masses is known as the Polar Front and is presently located to the north of Iceland.

The location of the Polar Front and the convergence of the warm and cold waters is strongly correlated with oceanographic changes and climatic variation over time (Ruddiman and McIntyre, 1981; Dansgaard et al., 1993; Haflidason et al., 1995). The North Atlantic is consequently a very climatically sensitive area and it has been suggested that these climatic and oceanographic changes can be seen in the ^{14}C record. ΔR values are often used as proxy indicators for specific ocean ^{14}C activity and therefore any shifts in oceanic regimes that may have forced such a change (e.g. Kennett et al., 1997; Kovanen and Easterbrook, 2002, Fontugne et al., 2004; Burr et al., 2009).

ΔR values across the North Atlantic show considerable variation, as shown in Figure 1.11, often interpreted in relation to oceanographic variables such as temperature and salinity (Mangerud, 1972; Mangerud and Guliksen, 1975; Eiríksson et al., 2004). Polar waters from the Arctic tend to display higher MRE values and therefore higher ΔR values due to the lower ^{14}C content of the depleted deep water. Sea ice cover in the polar regions also

affects the MRE by providing a physical barrier between sea-air exchange, thus preventing atmospheric 'reinvigoration' and thus keeping the surface waters depleted in ^{14}C. The opposite is true for the warmer, more saline currents associated with the NAC, giving lower MRE and ΔR values. Maximum ΔR values in the North Atlantic region are unsurprisingly associated with the EGC such as values of 260 ± 40 ^{14}C yrs BP in Disko in Greenland (McNeeley et al., 2006). Larger values in the area can be attributed to a distinct hard water effect in areas with specific geology i.e. Randers Fjord in Denmark, which has a ΔR value of 559 ± 58 ^{14}C yrs BP (Heier-Nielsen et al., 1995). Minimum values in the area such as -155 ± 37 ^{14}C yrs BP around the Isle of Man (Butler, 2009) are clearly associated with the northward flow of the NAC.

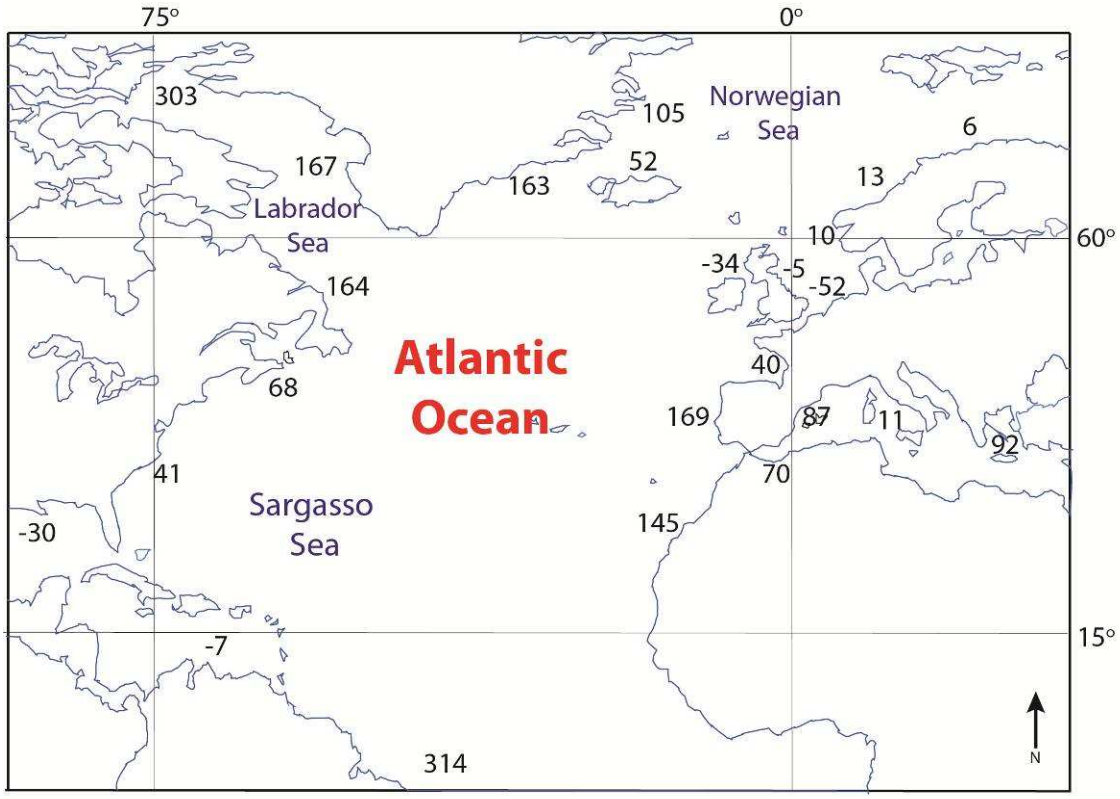

Figure 1.11: Variability in ΔR values (^{14}C yrs BP) across the North Atlantic showing average values for geographical locations

(Data from the online 14 CHRONO Marine Reservoir database)

Correlation of ΔR values with ocean water ^{14}C activity in relation to characteristics such as temperature and salinity has led to ΔR being used as a proxy for past oceanographic changes in a number of studies. Large environmental studies have focused on cores taken

from the Greenland ice sheet (GRIP and GISP) and provide data on oxygen isotope ($^{18}O/^{16}O$) fluctuations for the past 200,000 years (Mayewski and White, 2002). $^{18}O/^{16}O$ variations can provide proxy records of temperature fluctuations as relationships exist between temperature, salinity and oxygen isotope ratios. Variations in $^{18}O/^{16}O$ are calculated relative to an international standard (VSMOW) and expressed as $\delta^{18}O$ (‰). Low $\delta^{18}O$ values correlate with colder periods, whilst higher values are linked with warmer conditions. By examining the ice core data in Figure 1.12, significant drops in $\delta^{18}O$ can be correlated with significant climatic events, showing very low $\delta^{18}O$ values during the Younger Dryas and 8.2 kyr event. The Younger Dryas period predominated c13,000 – 11,500 years ago (Ruddiman et al., 1977) and involved the advancement of the Polar Front and a return to glacial conditions for the North Atlantic. The 8.2 kyr event involved a period of rapid cooling 8400-8000 years ago, linked to a final, rapid melt-water pulse from the Laurentide ice sheet (Barber et al., 1999; Alley et al., 1997; Klitgaard-Kristensen et al., 1998; Birks and Koç, 2002). The GISP2 data translates to falls in temperature of 15 ºC at the summit of Greenland (Alley et al., 1993) during the Younger Dryas and 4-8ºC in central Greenland (Alley et al., 1997) during the 8.2 kyr event.

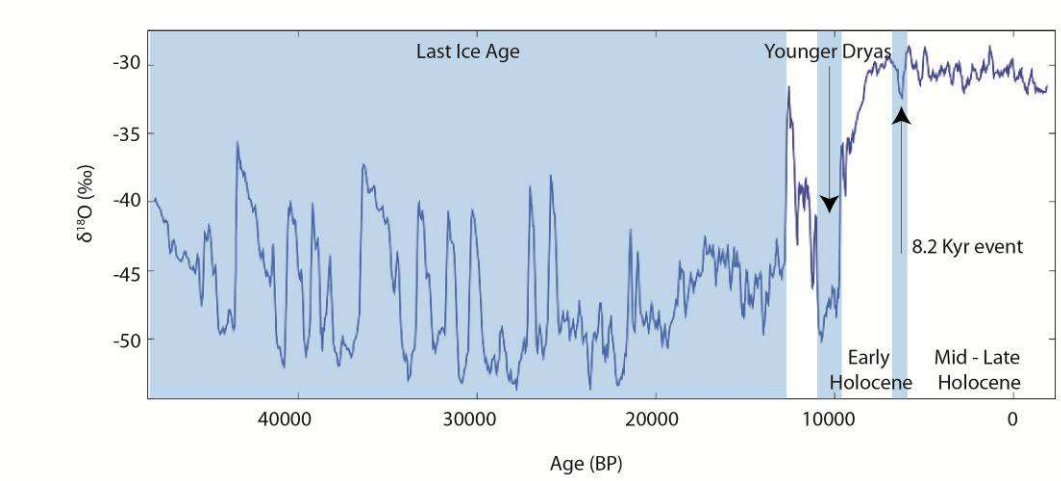

Figure 1.12: GISP2 data showing fluctuations in $\delta^{18}O$ through time and correlations with key climatic events

(After Alley, 2004; Alley, 2000)

These key climatic events such as major periods of warming and cooling can be seen in the ^{14}C record of both the atmosphere and oceans and correlate with the $\delta^{18}O$ data (Waelbroeck et al., 2001; Bjorck et al., 2003). Paleoclimatic variations that affect the amount of time that water is in contact with the atmosphere will invariably affect the MRE. Colder conditions such as the extension of the Arctic ice sheet would increase sea ice

cover, leading to less area available for ocean/atmosphere CO_2 exchange. Deep waters would become increasingly depleted in ^{14}C as they are further removed from contact with the atmosphere. Conditions which induce a higher rate of return from deep, older waters will increase the MRE and vice versa any conditions which allow the waters to stay near the surface, in contact with the atmosphere, will reduce the MRE. Changes in the formation of NADW have been suggested as mechanisms for such changes in the residence times of water bodies (Stocker and Wright, 1996). If NADW production slowed, this would at first reduce the sinking of surface water masses, leading to the deep water bodies spending longer away from the surface and becoming further depleted. When production rates recovered, the depleted waters would then be brought back into contact with surface water, leading to a sharp increase in the MRE until 'normal' exchange rates between the deep and surface waters were resumed.

1.9.2 The North Sea marine environment

Previous research in the SUERC radiocarbon laboratory investigated the MRE for the Atlantic seaboard from the west coast of Ireland, through to the Faroe Isles. This facilitated a comprehensive investigation of temporal ^{14}C variations for this region during the Holocene and produced revised ΔR values for the west coast of Scotland, Northern Iceland and the Faroes (Ascough et al., 2004; 2006; 2007a; 2007b; 2009). Significant re-evaluation and re-interpretation of Scottish archaeological sites followed, where conclusions had been drawn, based on dates from marine derived carbon. The research for this thesis extends the investigation to the east coast of Scotland, where a more complicated topographical estuarine system exists, draining into the semi-enclosed North Sea basin.

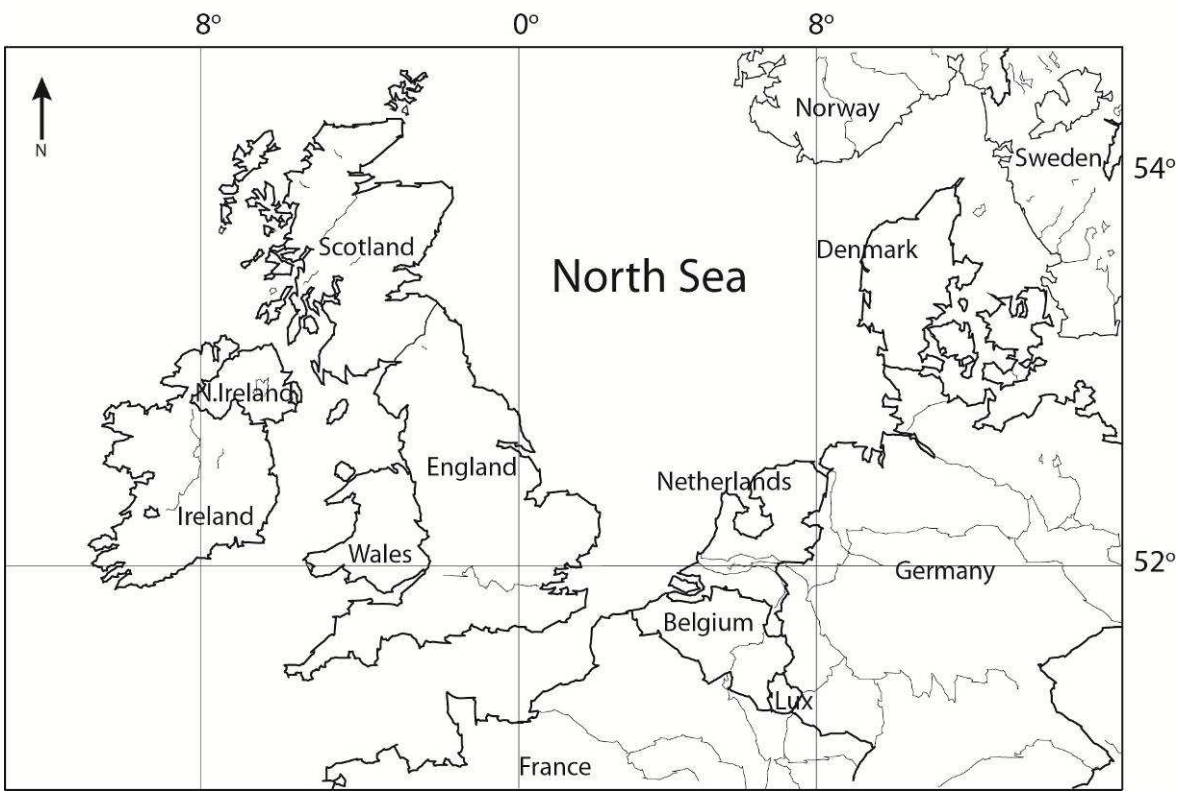

Figure 1.13: Geographical location of the North Sea

The North Sea is a marginal, shallow, shelf sea that lies between the British Isles, Norway and the European continent (Figure 1.13), not exceeding depths of 100 m for most of its extent, excepting the Norwegian Trench which reaches up to 700 m in depth (Winther and Johannessen, 2006). Nearly all of the North Sea water mass is Atlantic in origin. Figure 1.14 shows the input of water masses to the North Sea with Scottish Coastal Water from the west (SCW (W)) following the northern Scottish coast, before turning south to enter the North Sea system (Turrell et al., 1992).

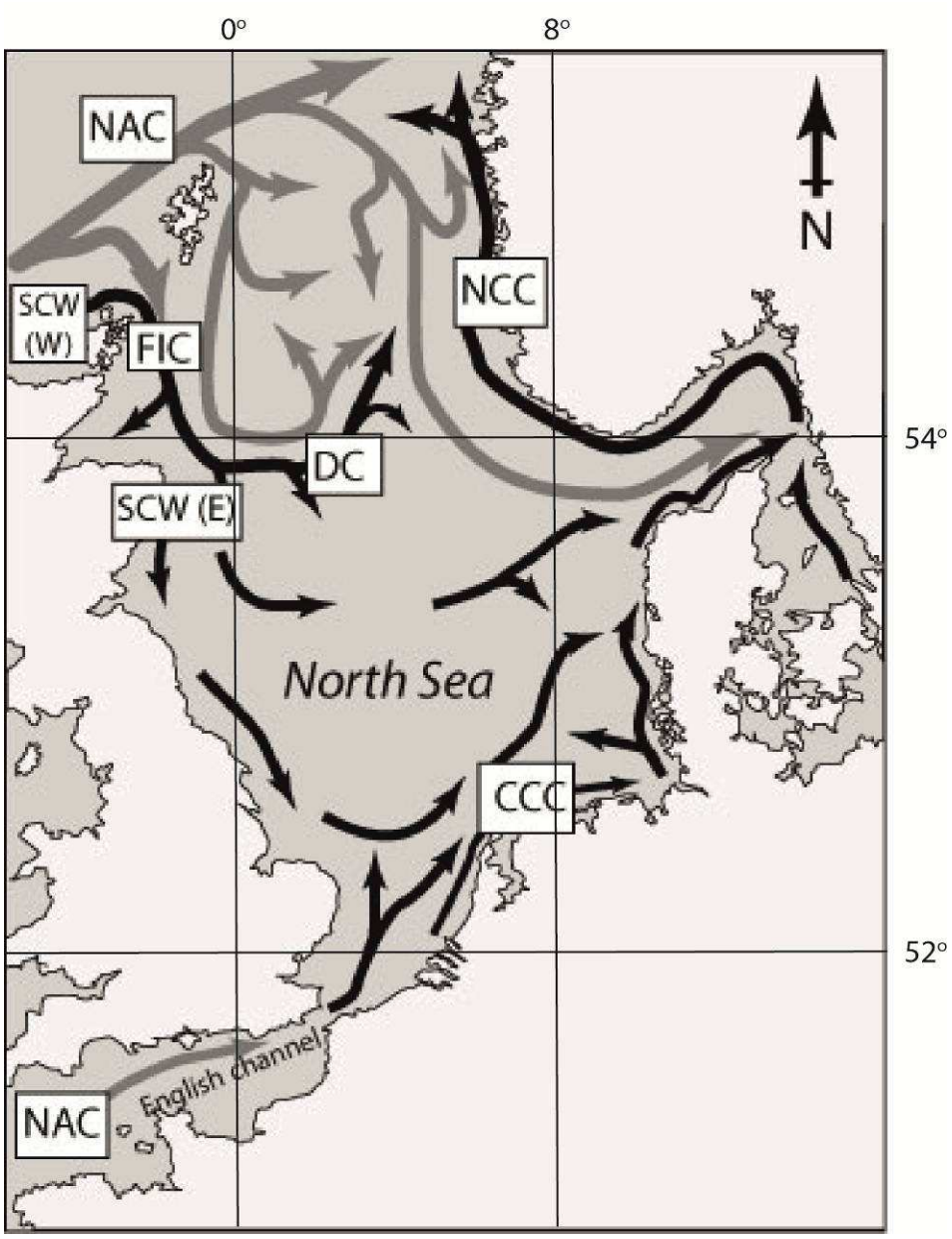

Figure 1.14: Flow of major currents in the North Sea (Russell et al., 2010)

(Grey arrows show Atlantic-derived waters, and black arrows show coastal currents and interior North Sea circulation. NAC: North Atlantic Current; SCW (W): Scottish Coastal Water (West); SCW (E): Scottish Coastal Water (East); FIC (Fair Isle Current); DC: Dooley Current; CCC: Continental Coastal Current; NCC: Norwegian Coastal Current (after Turrell et al., 1992; OSPAR, 2000))

The North Sea is fed with Atlantic water (AW) via the English Channel to the south and via the northern boundary, which is subdivided into various input sites including; the Orkney-Shetland section (known as the Fair Isle Current (FIC)), the Shetland shelf and the western part of the Norwegian trench (Winther and Johannessen, 2006). A zone of strong tidal mixing occurs around the Orkney Isles, mixing AW and SCW (W), resulting in a fairly homogenous, well-mixed FIC flowing towards the Scottish mainland (Turrell, 1992). Scottish Coastal Water in the east (SCW (E)) is therefore a composite of SCW (W) and well-mixed FIC, deduced by Turrell et al., (1992) to be of the following proportions;

- SCW (E) 85% SCW (w) + 15% FIC
- SCW (W) 55% AW + 45% IS/C (Irish /Clyde Seas)
- FIC 66% AW + 34% SCW (w)

Circulation of North Sea water is mainly cyclonic, flowing south along the British Isles with a divergence along the Norwegian Trench from the North East of Scotland towards Norway, known as the Dooley Current (Svendsen et al., 1991).

Previous to this study, very few estimates of ΔR were available for the North Sea coast of Scotland, or indeed any coastal region of the North Sea, according to the 14 CHRONO Marine Reservoir database at http://intcal.qub.ac.uk/marine/. Details of the data previously available are shown in Figure 1.11. By adding more ΔR values from the North Sea coast to the database, this study aims to increase confidence in the calibration of radiocarbon dates derived from marine material in this region. Also, the production of new North Sea values is of crucial importance in order to build a dataset large enough to assess the sychroneity (or lack) of North Sea values with those previously calculated for the west (Atlantic) coast of Scotland. Ascough et al. (2004, 2005b, 2006, 2007a, 2007b, 2009), Butler et al., (2009), Cage et al., 2006, Harkness (1983), Reimer et al., 2002 and Russell et al., (2010) have all conducted studies around the U.K. coastline and produced varying ΔR values from -172 to +93 ^{14}C yrs BP. The east coast is subject to a much more complicated estuarine system than the west, with most of the major Scottish rivers draining into the North Sea and so the addition of freshwater must be considered as a possible source of variation in this range of values. The addition of freshwater into the marine system can cause large variations in local ^{14}C content if the freshwater is depleted in ^{14}C due to the hard water effect.

1.9.3 Hard water effects

The hard water effect occurs in areas with significant carbonate strata where the underlying bedrock is very depleted or devoid of ^{14}C. The hard water effect was first described by Godwin (1951), investigating dissolution in hard water environments but subsequent investigations by Deevey et al., (1954) have concentrated on the dissolution of ^{14}C depleted bicarbonate in both soft and hard water environments. Dissolution by groundwater incorporates the 'old', depleted carbon from the surrounding geology, thus depleting the freshwater ^{14}C activity and creating a considerable reservoir offset. Aquatic plants or indeed any sample material that incorporates carbon from freshwater influenced in such a manner will therefore display a depleted ^{14}C signal. A freshwater reservoir effect may manifest itself in any non-marine aquatic environments such as rivers and freshwater lakes and may complicate the MRE in estuarine environments with a significant freshwater input. Even in areas where calcareous strata is absent and groundwater ^{14}C activity is comparable to that of the terrestrial biosphere, the addition of this runoff to the marine environment will significantly affect the local marine ^{14}C signal. The marine signal is depleted compared to that of the terrestrial biosphere and so a considerable freshwater input in estuarine environments can result in a reduction of this depletion. Studies by Cook et al., (2001) and Culleton (2006) have shown the significance of a freshwater reservoir effect (of 300 - 500 ^{14}C years) when dealing with samples such as riverine fish and freshwater shellfish, and any higher trophic levels (including humans), which may incorporate these samples into the food chain.

1.9.4 Fresh water effects in Scotland

The majority of the east coast of Scotland displays sandstone rich strata, devoid of any major outcrops of calcareous rocks that could produce a significant hard water effect, although some small seams may be present in Aberdeenshire (Geological Map Data © NERC). Freshwater dilution of the MRE must however be considered owing to the proliferation of estuarine environments, created by the majority of Scottish rivers discharging into the North Sea. Many of the minor rivers discharge directly into the sea although the major rivers have a tendency to form estuarine environments, known as firths, shown in Figure 1.15. The mean annual freshwater input to the Scottish North Sea Coastal Zone (SNSCZ) from the major Scottish rivers is shown in Table 1.2 to demonstrate the

relative importance of local freshwater fluxes (Lyons et al., 1993; Scottish Environment Protection Agency (http://www.sepa.org.uk)). The total maximum discharge to the North Sea in winter was calculated at around 1380 $m^3 s^{-1}$ (Lyons et al., 1993).

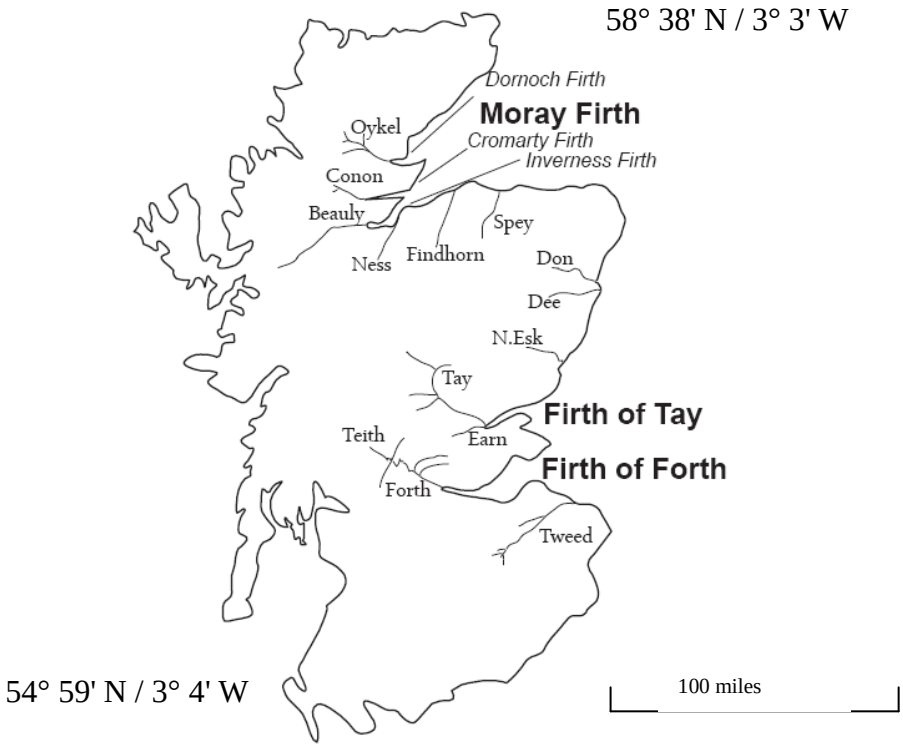

Figure 1.15: Major Scottish mainland rivers draining into the North Sea with mean freshwater discharges over 15 $m^3 s^{-1}$ (after Lyons et al., 1993)

River	Mean freshwater discharge (m^3s^{-1})
Tay	183.3
Ness	97.7
Tweed	77.0
Spey	64.5
Conon	57.2
Beauly	54.4
Dee	42.3
Teith	33.5
Earn	29.3
Findhorn	20.3
Forth	16.8
Don	16.5
N.Esk	16.3
Oykel	15.6

Table 1.2: Mean freshwater discharge rates of major Scottish rivers (1987– 91) with outputs over 15 m^3s^{-1} (Lyons et al., 1993)

Studies by Lyons et al., (1993) regarding the importance of riverine input to the SNSCZ proposed that 45% of the mean freshwater discharge to the North Sea originated from the Moray Firth via the Inverness Firth, Cromarty Firth and River Spey. However, it is notable that current meters from the same study have indicated that water from the Moray Firth does not follow the along-shore route south, but is directed east towards the tidal mixing zone of the Buchanan front in the central North Sea (Figure 1.14). This results in a much reduced input from the North to the rest of the coastal waters on the east of Scotland. A further 25% of the total freshwater input to the SNSCZ was contributed by the Firth of Tay, showing the dominance of 2 specific environments on the freshwater flux to the SNSCZ. These two inputs are therefore responsible for the major addition of freshwater masses to the coastal water in the east, which itself is derived from coastal water from the west, and a small contribution from the FIC (Figure 1.14)

The potential remains for significant freshwater input at specific sites throughout the east

coast of Scotland. Any values calculated from such environments may not represent a true MRE *per se*, instead demonstrating a local MRE, diluted by freshwater input. The location of sample sites and their proximity to freshwater input is therefore crucial in assessing the contribution of any freshwater effects to the variability in the MRE.

CHAPTER 2

METHODOLOGY: SITES AND CONTEXT

2.1 Methods of calculating ΔR

A ΔR value is calculated using a sample of marine carbon for which the terrestrial/atmospheric ^{14}C age is known, or can be established with a high degree of confidence. A modelled marine ^{14}C age is then derived for this sample, by converting the terrestrial/atmospheric ^{14}C age ± 1 sigma to a modelled marine age via interpolation between the INTCAL09 atmospheric curve and the MARINE09 curve (Reimer et al., 2009). ΔR is the difference between this modelled marine ^{14}C age and the measured ^{14}C age of the marine carbon sample (Figure 2.1). The 1σ error on the ΔR values is calculated by the propagation of errors as shown in Equation 2.1.

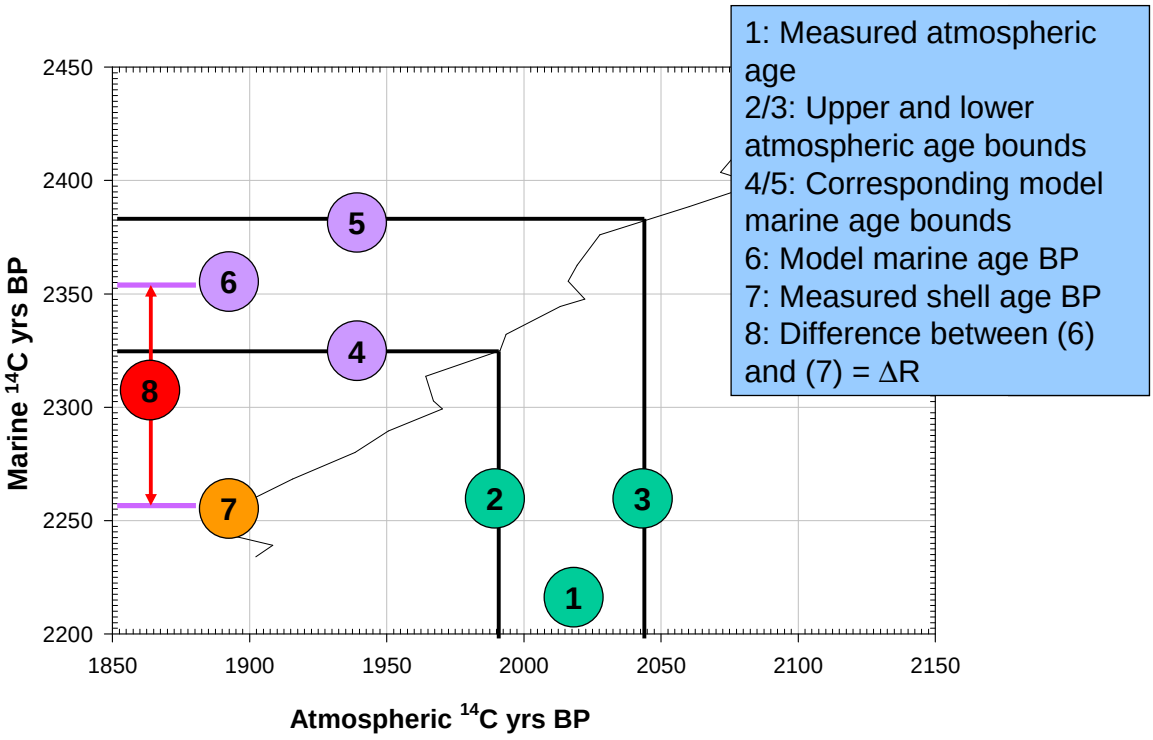

Figure 2.1: Graphical representation of the determination of a ΔR value showing interpolation of atmospheric and marine ages

$$\sigma_{\Delta R} = \sqrt{(\sigma_w + \sigma_m)^2}$$

Where ($\sigma_{\Delta R}$) = the 1σ error for the ΔR determination

(σ_w) = the error on the measured marine age

(σ_m) = the error on the modelled marine age.

Equation 2.1: Propagation of ΔR errors:

A variety of methodological approaches are used to obtain suitable ^{14}C ages for calculation of ΔR values and these are well discussed by Ascough et al. (2005a). They include measurement of: 1. known age marine shell samples from museum collections; 2. samples associated with onshore/offshore tephra isochrones and 3 paired samples from secure archaeological contexts. Recently, Butler et al. (2009) have used samples of *Arctica islandica* from their "annually resolved multi-centennial (489-year), absolutely aged" master chronology. While Butler's technique is potentially extremely useful in providing a continuous record of ΔR values it is currently limited in time to a 489 year period (late- and Post-Medieval periods) and in the future will be limited to locations where *Arctica islandica* shells will be found in numbers sufficient to duplicate the chronological work. Ascough et al. (2005a) supported an approach involving multiple paired samples, where the terrestrial and marine ^{14}C age used to calculate ΔR is based upon multiple samples of both material types, using short-lived species from secure archaeological contexts (i.e. where there is a high degree of confidence that all organisms within the deposit have the same time of death). Again, this technique is temporally limited, only providing snapshots in time of ΔR values, but these snapshots are available for time periods of importance in archaeology. A multiple paired sample approach was employed within this thesis to ensure contemporeity between groups of marine and terrestrial materials that can be statistically evaluated by the χ^2 test. This approach gives a high degree of confidence that the samples used to calculate ΔR are from secure contexts and that the terrestrial and marine samples are therefore contemporary in age.

2.1.1 Multiple paired sample approach

Using the multiple paired sample approach, secure archaeological contexts are selected through close consultations with site excavators and excavation reports to identify contexts containing suitable marine and terrestrial entities which have been relatively unaffected by post-depositional disturbance (e.g. Ascough et al., 2007a; 2009). The importance of selecting single entities for dating ensures that mixed sample material of potentially different individual ^{14}C ages is not combined to provide a 'bulk-date' and that consequently the ^{14}C ages used in the ΔR calculation are as accurate and precise as possible. Ashmore (1999) championed the protocol of single entity dating, defined as 'any thing, being demonstrably a single part of an organism, in which the absolute chronological relationship between all components forming that part can be established to the nearest calendar year'. Single entity dating is always enforced by Historic Scotland, CASE partners in this studentship. The methodology developed for this study advocated the collection of at least 4 suitable marine and 4 suitable terrestrial entities per archaeological context in order to allow meaningful interpretation of the χ^2 test results (discussed in detail in Section 3.5).

2.1.2 Suitable marine material

Molluscs are most frequently selected as the marine material of choice for ΔR calculations as they are relatively sedentary organisms that precipitate their shell carbonate in equilibrium with the ambient seawater (Epstein et al., 1953). Archaeological research has also shown that most mollusc shells are processed by human communities close to the place of collection, as a result of the large weight of the shell relative to that of the edible soft tissue (Meehan, 1982; Waselkov, 1987). Therefore, mollusc shells, particularly where they are present in significant numbers in a deposit, can be taken as a reliable indicator of local coastal conditions around the site from which they were collected. The possibility exists for fish bone to be considered as marine sample material, although fish are much more mobile, increasing the possibility of carbon uptake from a wider geographical area. Fish bone is therefore not necessarily representative of the immediate coastline conditions around the area of collection.

2.1.3 Suitable terrestrial material

Suitable terrestrial material for ΔR calculations can include carbonised cereal grains, roundwood charcoal and herbivore bones. Carbonised grains represent a single year's growth of the plant and are ideal sample material as they typically have high carbon content (>60%) and are relatively resistant to post-depositional chemical and physical processes that could affect the ^{14}C content. Roundwood charcoal represents short-lived species (<5yr) and use of this material therefore avoids any uncertainties incorporated by the 'old-wood effect' (Schiffer, 1986). The 'old-wood effect' presents itself where wood from long-lived species does not represent the date of deposition, but instead, the date of wood formation, which can lack association with the context to be dated. Herbivore bones provide suitable sample material if they represent a truly terrestrial ^{14}C signal. Grazing mammals such as cattle and sheep/goats (ovicaprids) are selected in preference to animals with more diverse feeding habits such as scavengers which have a greater likelihood of incorporating a marine signal into their diet through consumption of seafood such as fish remains or even seabirds. However, studies have shown that even grazing herbivores can incorporate a significant marine signal by grazing on seaweed (Ambers, 1987). $\delta^{13}C$ analysis can help identify marine contributions to diet as the values for a purely terrestrial diet in herbivore collagen should be around -22‰ (Van der Merwe, 1989) whereas a significant marine contribution would result in significantly heavier values (Ambers, 1987). Bones used in this study were only approved for inclusion in ΔR calculations when $\delta^{13}C$ values were within a suitable range around -19 to -23‰.

Once contexts are identified that contain suitable sample material, it is imperative that the contexts also contain a high volume of sample material and have well defined boundaries to ensure the samples were deposited at the same time. The protocol for selection of material from which ΔR is calculated in this thesis sets a minimum of 4 terrestrial and 4 marine entities per context, although larger quantities are advantageous. Selecting several entities of each sample type helps reinforce context security by producing ^{14}C ages that can be subjected to chi-squared (χ^2) testing to demonstrate that they are statistically indistinguishable from each other. The statistical treatment of the data, including χ^2 testing, will be discussed in detail in Section 3.5.

The strict site selection criteria of suitable sample materials, abundance of suitable sample materials and context security obviously limit the number of suitable sites available for this

study. The following section details the sites and contexts which met the site selection criteria.

2.2 The selected sites

Using a multiple paired sample approach places strict conditions upon the sites and sample materials that can be used for accurate and precise ΔR calculation. Sites must produce multiple (>4) samples of both terrestrial and marine entities from secure archaeological contexts unaffected by post-depositional disturbance. It was intended that this study would be an investigation of the MRE within the North Sea coast of Scotland throughout the Holocene, as a number of excavators had indicated that sites from various periods contained suitable samples. However, owing to the strict selection criteria, sites from several time periods failed to produce suitable samples and the dataset for this thesis has a distinct Medieval focus. Three sites selected for study did not produce suitable material, owing to archaeological misidentification of the samples as contemporary marine and terrestrial entities. These sites were excluded from this study and are discussed in Appendix A.

The chosen sites span a geographical range from Orkney in the north to East Lothian in the south as illustrated in Figure 2.2. The majority of the samples were supplied from developer-funded urban excavations from major archaeological units including:- Scottish Urban Archaeological Trust (SUAT), Aberdeen City Council Archaeological Unit, AOC Archaeology, Field Archaeology Specialists (FAS), Addyman Archaeology and the MacDonald Institute for Archaeological Research.

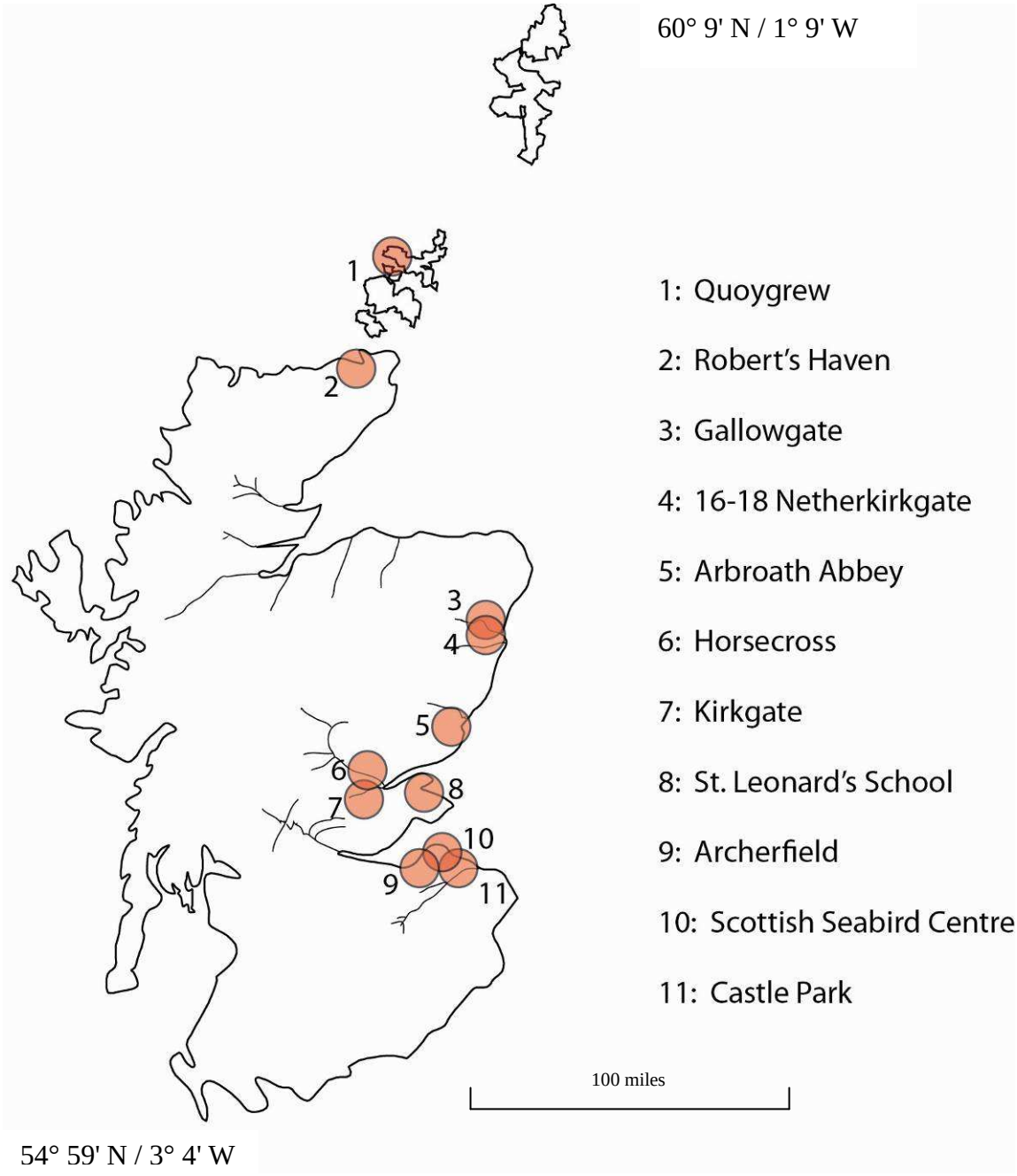

Figure 2.2: Geographical location of the study sites throughout the North Sea Coastal Zone

(Proximity to the major rivers of Scotland and estuarine environments can be identified. Sites are assigned identification codes in Table 2.1 and detailed location maps are shown in Section 2.3)

Site code	Site name	Geographical Location
QG	Quoygrew	Westray, Orkney
RH	Robert's Haven	Caithness
GG	Gallowgate Middle School	Aberdeen
NG	16-18 Netherkirkgate	Aberdeen
AA	Arbroath Abbey	Arbroath, Angus
HC	Horse Cross	Perth, Perth and Kinross
KG	Kirkgate	Perth, Perth and Kinross
StL	St Leonard's School	St Andrews, Fife
AR	Archerfield	Dirleton, East Lothian
SSC	Scottish Seabird Centre	North Berwick, East Lothian
CP	Castle Park	Dunbar, East Lothian

Table 2.1: Summary information for the selected sites shown in Figure 2.2, showing side code, site name and geographical location from north to south

2.3 Site details and the chosen contexts

2.3.1 Gallowgate Middle School, Aberdeen (NJ 9421 0659)

Lat: 57.150154N Long: 2.097331W

Figure 2.3: Location map showing the site of Gallowgate Middle School within Aberdeen City
(Site location marked by the red dot)

The demolition of Gallowgate Middle School (Figure 2.3) for housing development led to the discovery of Medieval industrial activity by Aberdeen City Council Archaeological Unit. The site of Gallowgate Middle School produced notable archaeological finds including 12th/early 13th century shoemaking material, suggesting waste from a cobbling area (Cameron and Stones, 1991), giving a great insight into the medieval industrial activity in the area.

Suitable sample material was identified in context 84, a discrete layer slumping into a clearly defined pit which was overlain by the undisturbed stratigraphic units above (Alison Cameron, pers.comm). The context was secure, free from post-depositional disturbance and contained multiple terrestrial and marine entities. Four individual (MNI) terrestrial mammal bones were selected for analysis. These comprised three ovicaprid lower right hand side (RHS) mandibles and a bone from a red deer. The 4 marine samples selected for analysis were all winkle shells (*Littorina littorea*).

2.3.2 16 – 18 Netherkirkgate, Aberdeen (NJ 9428 0637)

Lat: 57.148179N Long: 2.096168W

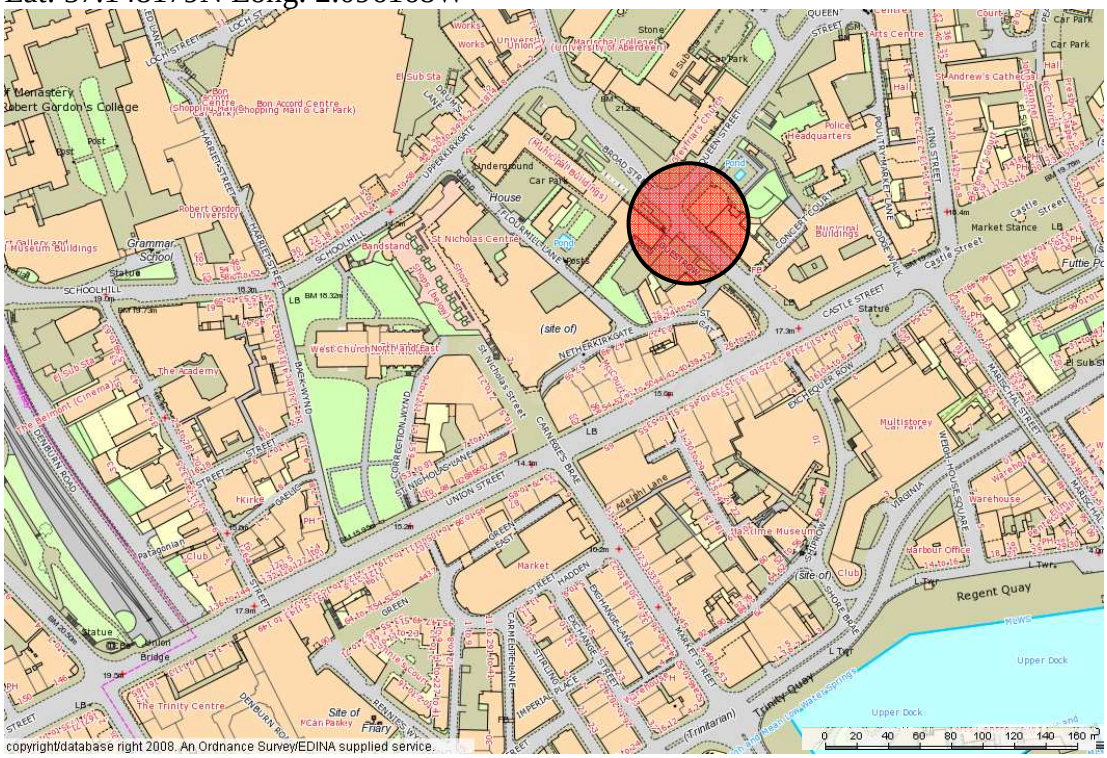

Figure 2.4: Location map showing the site of 16-18 Netherkirkgate within Aberdeen city centre
(Site location marked by the red dot)

The site of 16-18 Netherkirkgate (Figure 2.4) was excavated by Aberdeen City Council in preparation for the construction of a beer cellar and car parking. Evidence of medieval buildings was found, as well as portions of probable post-medieval stone buildings. Under the medieval deposits was a widespread and uniform clay and stone layer containing several hundred worked flints (Cameron, 1992).

Sample material was selected from context 442, feature KQ, a 1 m x 1 m square pit, well defined and lined with clay. This context was deemed free from any intrusive action or post-depositional interference by the presence of the undisturbed stratigraphical units directly above. Four individual limpet (*Patella vulgata*) shells were selected as the marine samples while the 4 terrestrial samples comprised a cattle bone, a bone from a hare and 2 lower LHS ovicaprid mandibles.

2.3.3 Arbroath Abbey, Arbroath (NO 642 413)

Lat: 56.562291N Long: 2.584092W

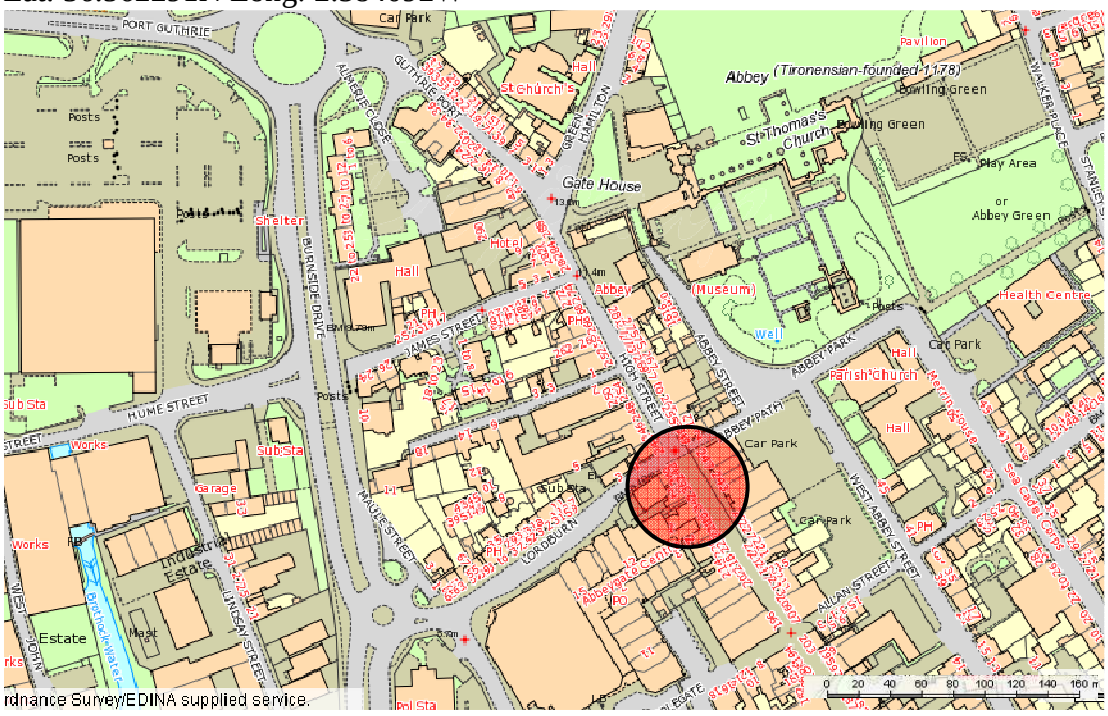

Figure 2.5: Location map showing the site of excavations around Arbroath Abbey within Arbroath town centre
(Site location marked by the red dot)

Excavations were undertaken around Arbroath Abbey (Figure 2.5) by SUAT in 2000 before the construction of a new Arbroath Abbey visitor centre. The excavation

discovered part of the original wall around the medieval Abbey as well as part of a gateway and part of a track that led into the Abbey precinct. Four human skeletons were also found during the excavation which may have been the remains of medieval monks buried in the vicinity. Carved stones were also uncovered, some of which showed evidence of simple stone carving (Cachart, 2000). Waste material from metal-working was also found, suggesting this may have been the site of craftworking areas. Other finds from the excavation include pottery fragments, coins, window glass, personal possessions and clothing items such as buckles.

Context 212 was selected as it contained a high volume of suitable sample material. The samples chosen for analysis were 4 oyster (*Ostreidae*) shells, 8 winkle (*Littorina littorea*) shells, 4 carbonised cereal grains, 2 cattle tibias, 2 ovicaprid humeri (both distal ends, right hand side) and 3 ovicaprid humeri (all left hand side).

2.3.4 Horse Cross, Perth (NO 1187 2388)

Lat: 56.398924N Long: 3.429424W

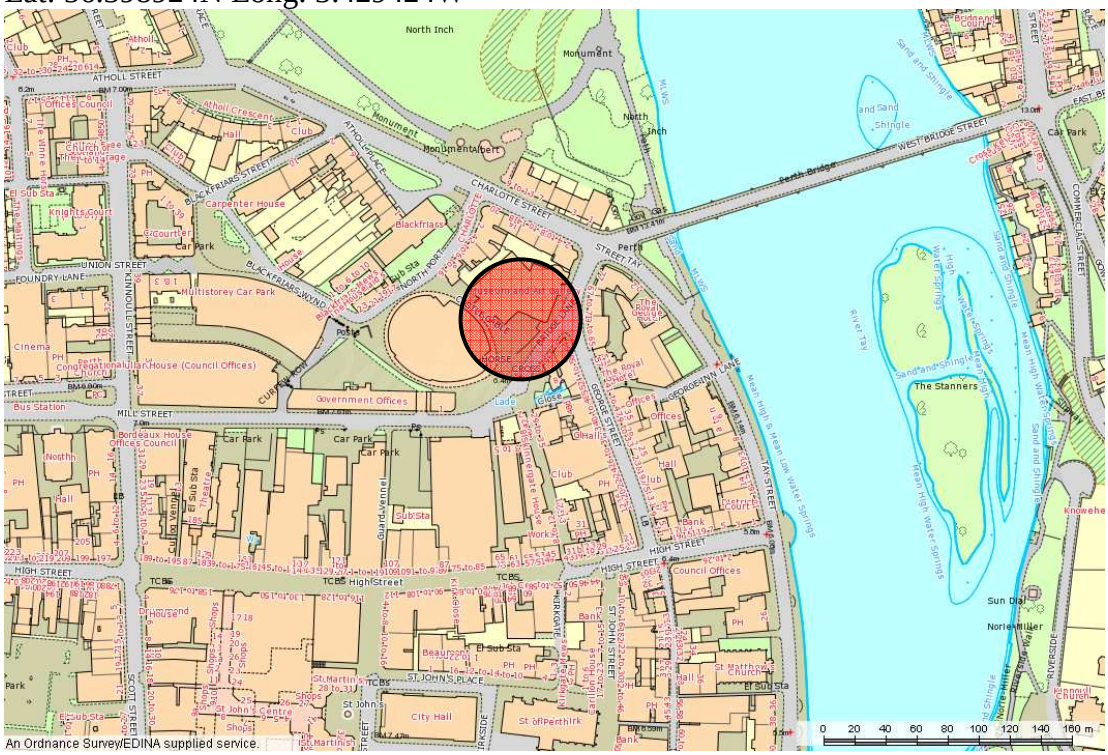

Figure 2.6: Location map showing the site of the Horse Cross in Perth town centre
(Site location marked by the red dot)

The archaeological site of Horse Cross in Perth (Figure 2.6) is located beneath the current Perth Concert Hall and was excavated by SUAT in advance of its construction. The

excavations were designed to determine the location of the medieval castle and the chapel of St Laurence and in doing so, produced vital social information on the medieval and later development of the suburb (Cox et al., 2007). Anomalously early radiocarbon dates had already been produced from secure contexts within this site on human bone and this had been attributed to the (unlikely) possibility of contamination from a surface oil spill, or a pronounced MRE effect owing to a largely marine diet. It was decided therefore that it would be beneficial to investigate contexts which had produced other datable material, i.e. pottery, in order to provide independent chronological information for the dated contexts.

Context 595 was chosen as it was part of a gravel trackway that appeared to be free from any post-depositional disturbance and had already produced pottery that was typologically dated to the 13th Century. The trackway may have been part of a Medieval street surface known as Castle Gable (Catherine Smith, pers. comm.), sealed by the deposition of the overlying midden material. Context 595 produced ample shell for dating although the bone content was not as plentiful. The marine material consisted of 4 oyster (*Ostreidae*) shells and 2 mussel (*Mytilus edulis*) shells. A maximum of 4 MNI could be assured for the terrestrial material which included 2 unidentified charred grains, 2 cattle distal metacarpals, 1 cattle upper molar, 1 cattle 1st phalange and one cattle pubic bone

2.3.5 Kirkgate, Perth (NO 1196 2360)

Lat: 56.396426N Long: 3.427872W

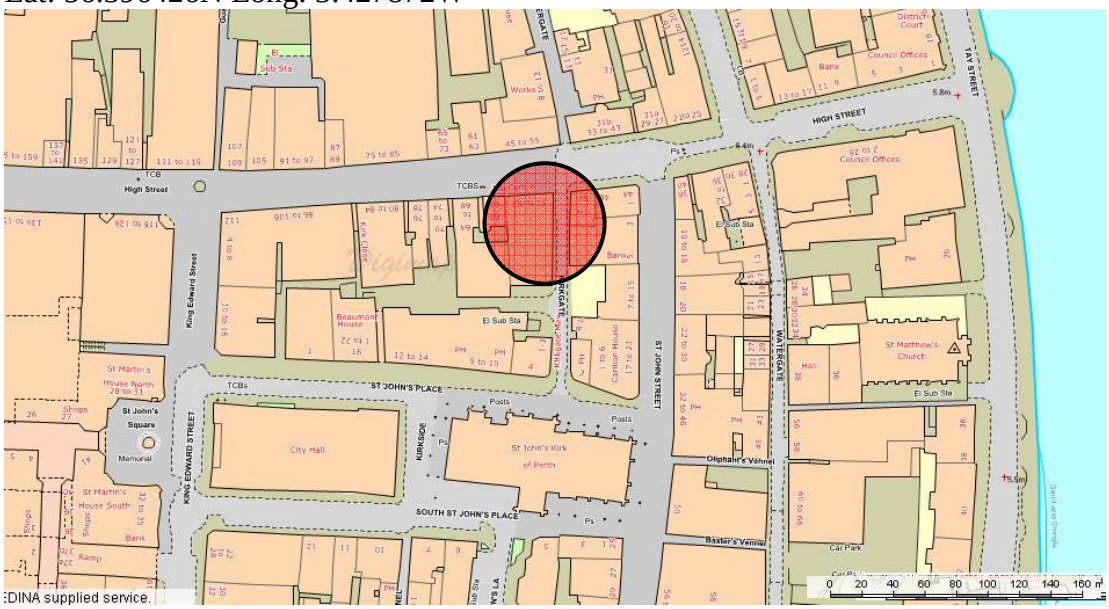

Figure 2.7: Location map showing the site of Kirkgate, in Perth town centre
(Site location marked by the red dot)

Work was undertaken at Kirkgate, Perth in January 2008 by SUAT under the direction of Scottish Water during the excavation of a sewage pipe trench centered on NO 1196 2360 (Figure 2.7). Well preserved midden material was revealed, including leather, bone and pottery dating from the 12th-15th centuries. The west facing sections showed the midden to be stratified with layers of gravel deposits, thought to be resurfacing layers of the street or the forelands associated with the buildings lining the street at the time (Barton, 2008). This stratigraphical information instilled confidence that there was little evidence of disturbance since deposition and therefore that the material from this context would be suitable for dating.

Two contexts from the midden (400 and 413) were selected for dating as they both contained a quantity of bone and oyster shell, as well as pottery for independent dating by typological analysis. Shell material was abundant within the contexts but no more than 2 MNI could be identified within the bone assemblage for each context. In a similar situation to the Horse Cross site, 4 bones were dated for both context 400 and 413, but this may not be indicative of 4 separate entities. Context 400 provided 4 oyster (*Ostreidae)* shells, 1 ovicaprid maxilla, 1 cattle metatarsal, 1 cattle pelvis and 1 cattle first phalange. Context 413 also provided 4 oyster (*Ostreidae)* shells, as well as 1 ovicaprid metatarsal, 1 cattle maxilla, 1 cattle tibia and 1 cattle radius.

2.3.6 St Leonard's School, St Andrews (NO 51266 16634)

Lat: 56.339545N Long: 2.789904W

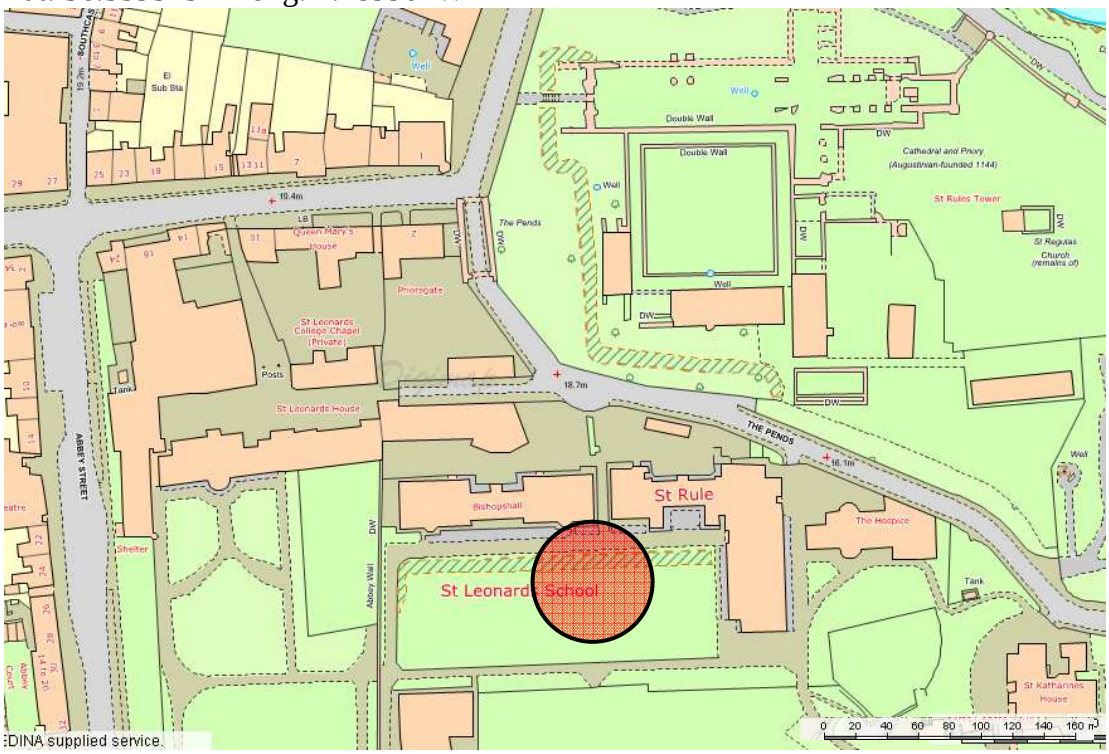

Figure 2.8: Location map showing the site of St Leonard's School in St Andrews
(Site location marked by the red dot)

Excavations were undertaken at the site of St Leonard's School in St Andrews by SUAT (Figure 2.8). The site appears to have 7th century connections with the early religious centre and later medieval connections with the abbey.

Material was chosen from context 0131 which again provided ample shell material in the form of 4 winkle (*Littorina littorea*) shells, but only 2 separate terrestrial entities could be guaranteed out of the 4 bones provided. These bone samples were; 1 ovicaprid metacarpal, 1 cattle mandible, 1 cattle humerus and 1 ovicaprid tibia.

2.3.7 Archerfield, East Lothian (NT 509 841)

Lat: 56.047237N Long: 2.789794W

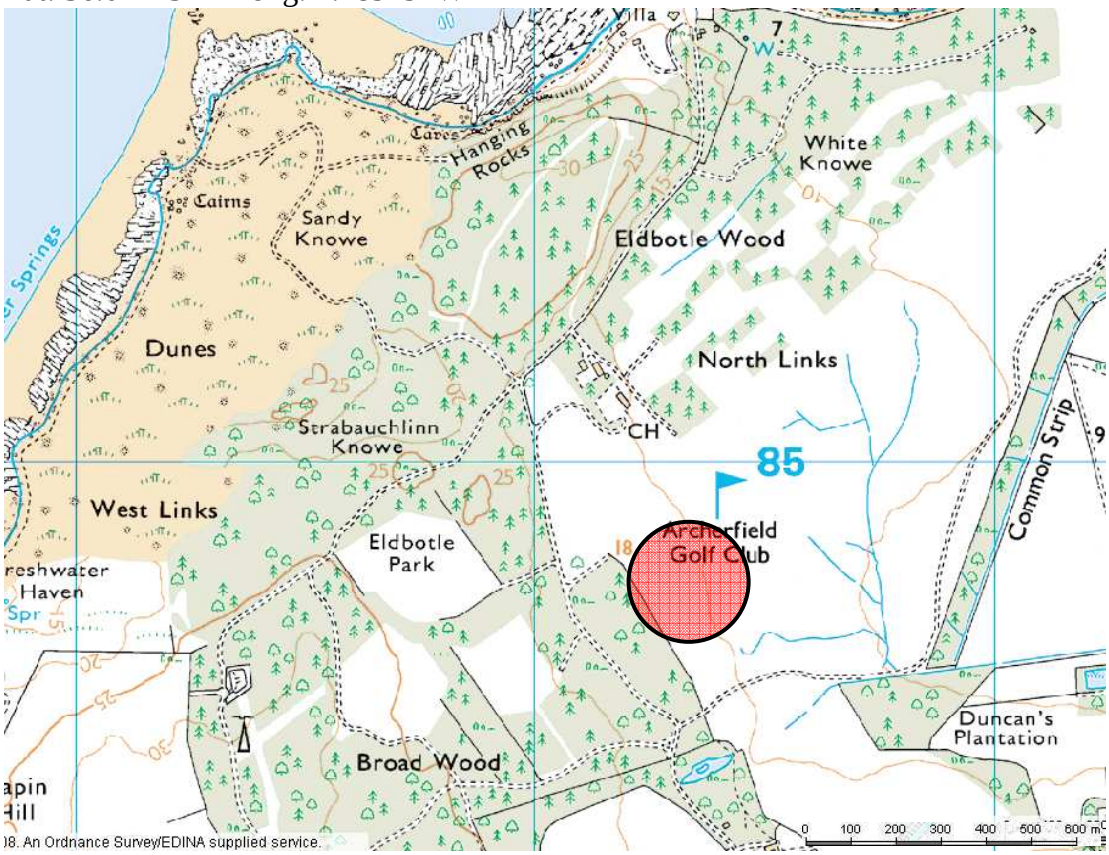

Figure 2.9: Location map showing the site of Archerfield, Dirleton, East Lothian
(Site location marked by the red dot)

The excavations of the Medieval village of Archerfield (Figure 2.9), East Lothian, were undertaken by AOC, under the direction of Erlend Hindmarch, AOC Archaeology Group Project Officer. The site is located in Archerfield Estate, Dirleton, and was discovered during the planning of the golf course, which has now been redesigned to preserve the remains of the site under the 16th and 17th holes. An excavation and evaluation were carried out as part of an ongoing programme of archaeological investigation within the Archerfield Estate. The site was of considerable archaeological importance owing to its rural location, as the majority of information on Medieval Scotland is obtained from urban excavations. (Hindmarch pers comm., 2008).

The site provided 2 secure contexts (contexts 90 and 142) with an abundance of suitable sample material from similar periods in time. Context 90 was a discrete dump of material within domestic structure 6 and provided 8 terrestrial samples and 8 marine shells. The

terrestrial material for context 90 consisted of 4 barley (*Hordeum* sp.) grains and 4 oat (*Avena* sp.) grains whilst the marine material was 4 limpet (*Patella vulgata*) shells and 4 winkle (*Littorina littorea*) shells. Context 142 was a short-lived occupation deposit within the floor levels of structure 8 and provided 5 terrestrial grain samples (2 oat and 3 barley) and a total of 3 marine shells (2 winkles and 1 limpet)

2.3.8 Scottish Seabird Centre, North Berwick (NT 55422 85627)

Lat: 56.061399N Long: 2.717463W

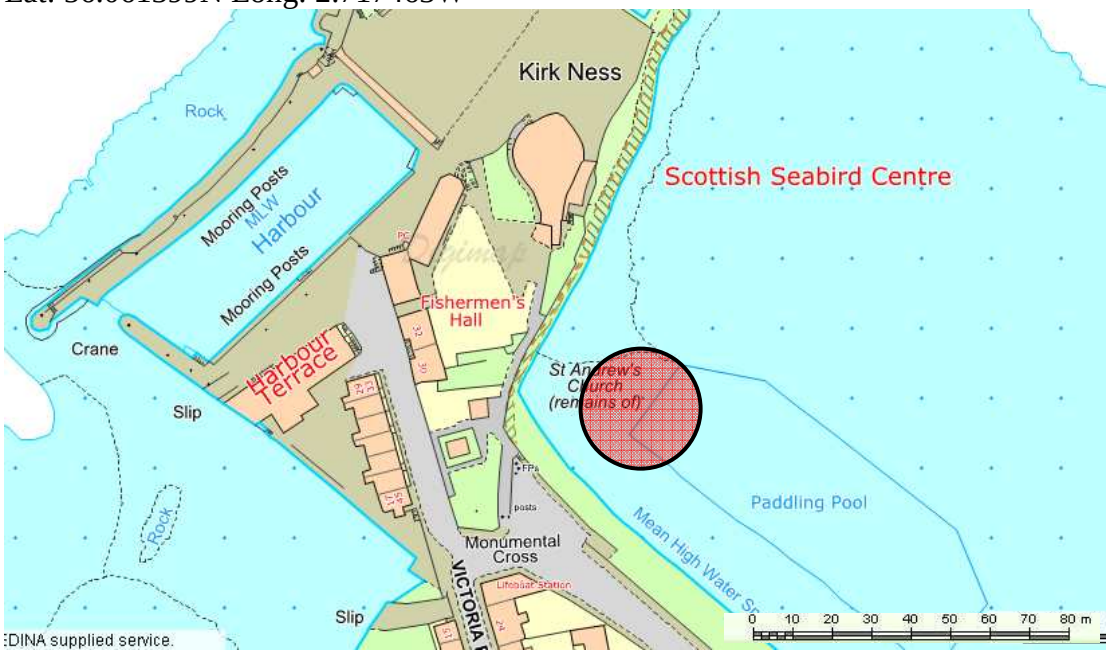

Figure 2.10: Location map showing the site of the excavations at the Scottish Seabird Centre in North Berwick
(Site location marked by the red dot)

Excavations were undertaken by Addyman Associates at Anchor Green, North Berwick in 2004 (Figure 2.10), prior to the construction of an underground tunnel between the basement of the Scottish Seabird Centre and the basement chambers below the existing Centre administration building. During the excavations it was discovered that beneath a complex series of recent deposits and features, a medieval occupation surface was present alongside associated deposits that overlay remains likely to be considerably earlier. The possibility that these earlier deposits were of an early Christian or even prehistoric age was suggested, in support of results from previous excavations at Anchor Green, by Addyman Associates in 1999-2002 (Addyman Associates, 2007 unpub. data).

Two contexts from the site provided suitable dating material. Context 1226 was associated

with a nearby kiln, thus producing multiple carbonised barley (*Hordeum* sp.) grains as well as ample winkle (*Littorina littorea*) shells for dating. Four grains and 4 shells were selected. Context 1287 represented probable floor deposits containing marine material in the form of 4 winkle shells and terrestrial entities in the form of 1 barley grain and 3 herbivore bones (1 cattle tooth and 2 RHS ovicaprid mandibles).

2.3.9 Castle Park, Dunbar (NT 6776 7917)

Lat: 56.004381N Long: 2.518558W

Figure 2.11: Location map showing the site of Castle Park, Dunbar, East Lothian
(Site location marked by the red dot)

Castle Park is a multi-phased occupation site located on the coastal promontory at Dunbar (Figure 2.11), excavated by SUAT from 1987 – 1983. The excavations were necessitated by the redevelopment of the barracks site and the construction of a leisure pool opposite the ruins of the castle (Perry, 2000). The earliest occupation on site appears to have been the Iron Age promontory fort with discontinuous occupation ranging through to the post-medieval period, creating a palimpsest of archaeology and offering vital information about the occupation of the area over time.

Two contexts were chosen from this site, to give further confidence in the results produced. Contexts 0341 and 3017 were from slightly different periods in time, approximately 300 ^{14}C years apart. This was used to investigate any relatively short lived changes in the ΔR value over time at the same location. Context 0341 provided 4 winkle (*Littorina littorea*) shells and 4 terrestrial herbivore bones. These bones represented 4 individuals and comprised 1 ovicaprid mandible and single bones from a horse, hare and cow. Context 3017 also provided 4 winkle shells as well as 4 terrestrial entities represented by an ovicaprid mandible, a cattle maxilla, a bone from a horse and a bone from a red deer.

2.3.10 Quoygrew, Orkney (HY 443 506)

Lat: 59.338063N Long: 2.980865W

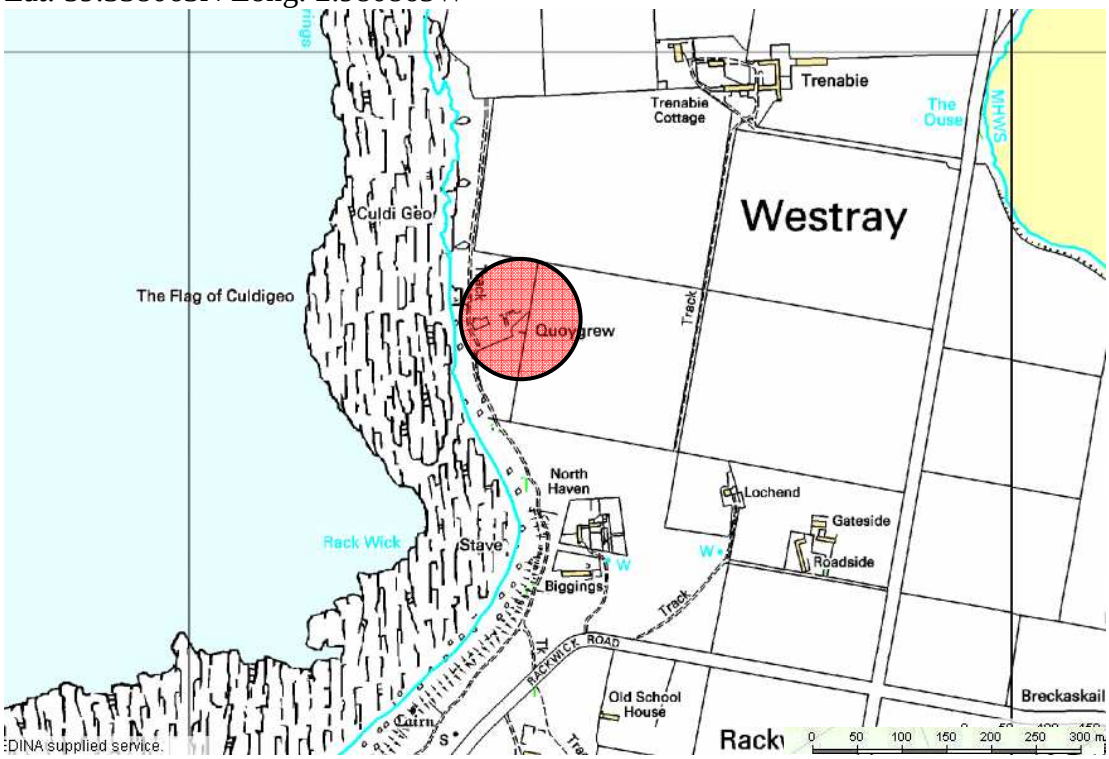

Figure 2.12: Location map showing the site of Quoygrew, Orkney
(Site location marked by the red dot)

The site of Quoygrew (Figure 2.12) is a late Viking Age/ Medieval settlement on the island of Westray, Orkney, facing north-west towards the Atlantic Seaboard, with midden material dating to the 10th–13th centuries AD (Milner et al., 2007). Quoygrew was selected for this study to compare ΔR values calculated from dates on fish bone with those following the usual convention of using mollusc shell. ΔR calculations on shell had already been carried out by Ascough et al., (2009); meaning that these shell values could

be directly compared with new values calculated using fish bone. Comparison of ΔR values between fish and shell allowed investigation of whether fish bone could be considered as reliable an indicator of local ΔR values as shell. The previously published terrestrial dates (Ascough et al., 2009) were used alongside new fish bone data to produce new ΔR values.

Contexts QG A004 and QG A023 were selected as they had already provided suitable terrestrial and mollusc material for ΔR calculations (Ascough et al., 2009) and had an abundance of fish bone present. The previous ΔR values had been calculated from barley (*Hordeum* sp) grain and limpet (*Patella vulgata*) shell. The new ΔR values were calculated using the previous dates from the barley grain and new dates on North Sea cod, a non migratory stock of Atlantic cod (*Gadus morhua*).

2.3.11 Robert's Haven, Caithness (ND 3903 7353)

Lat: 58.645334N Long: 3.052158W

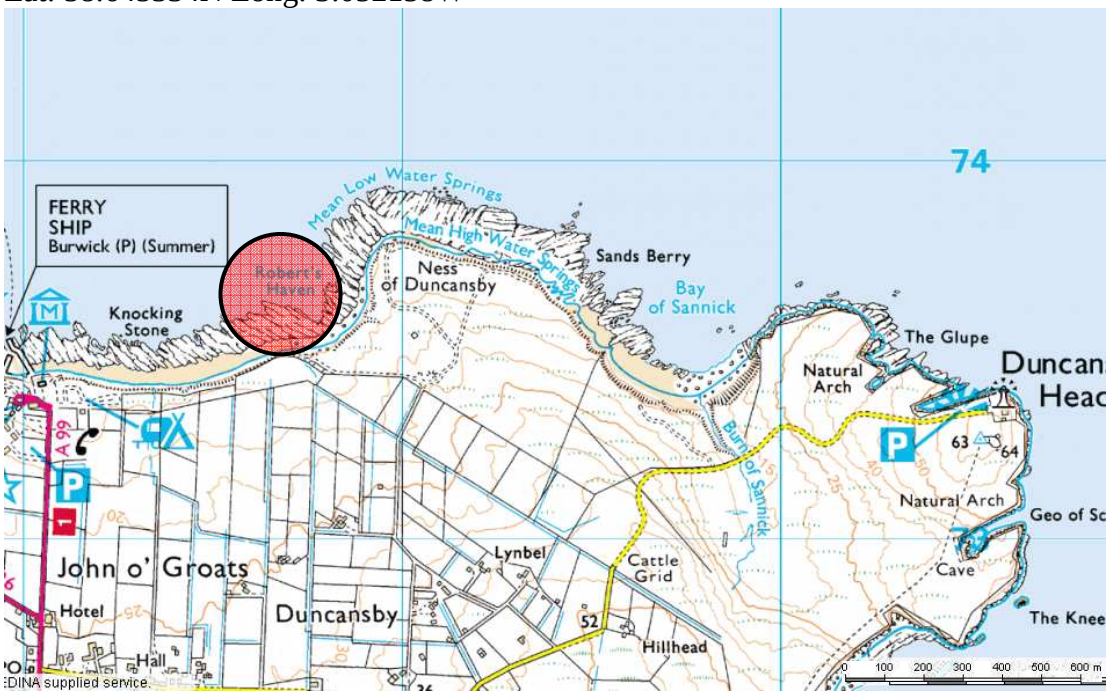

Figure 2.13: Location map showing the site of Robert's Haven, Caithness
(Site location marked by the red dot)

The site of Robert's Haven (Figure 2.13) lies within a small bay in Caithness facing north-west into the Pentland Firth on the North Sea coast of the Scottish mainland. The midden deposits at this site are dated to the 12th–17th centuries AD and the dominant material within many of the stratigraphic units is fish bone (Simpson and Barrett, 1996).

Contexts RH 3004 and RH 3019 were selected as they had already provided suitable terrestrial and mollusc material for ΔR calculations (Ascough et al., 2009). The previous ΔR values had been calculated from barley (*Hordeum* sp) grain and limpet (*Patella vulgata*) shell. The new ΔR values were calculated using the previous dates from the barley grain and new dates on North Sea cod (*Gadus morhua*).

CHAPTER 3

SCIENTIFIC METHODOLOGY: LABORATORY TECHNIQUES AND GENERAL STATISTICAL TREATMENT OF THE DATA

3.1 Sample pre-treatment

Sample pre-treatment is employed to ensure that the sample carbon is free from any non-sample carbon contamination. Different pre-treatment methods are employed for different sample types, although many are based around treatment with acid and alkali. The treatments applicable to the samples for this study are detailed below.

3.1.1 Grain

Carbonised cereal grains were subjected to standard acid-base-acid (ABA) pre-treatment in order to remove contaminants soluble in each of these reagents (de Vries and Barendsen 1952). Grains were heated at 80ºC for 2 hours in 0.5M HCl in order to remove carbonates and acid soluble contaminants such as fulvic acids. The samples were then decanted, removing the excess acid, and rinsed with water purified by reverse osmosis. The samples were then warmed in dilute NaOH (c. 0.25%) for an hour to remove any contaminants such as humic acids, which are alkali soluble. This process was not carried out in a nitrogen environment and so absorption of atmospheric CO_2 can occur. This was counteracted by a final acid wash, involving a repeat of the first stage of pre-treatment. Samples were then thoroughly rinsed using reverse osmosis water and dried, ready for combustion.

3.1.2 Bone

Bones were sub-sampled to provide a piece of bone (approx. 1-2 g) suitable for collagen extraction, which was carried out by a variation of the Longin method (Longin, 1971). Bone collagen was selected for dating as it is more resistant to post depositional changes than carbon within bone hydroxyapatite (Yoneda et al., 2002). Subsamples of bone were cleaned using a Dremel™ drill and sanding bit before immersion in 1M HCl at room temperature for roughly 20 hours, or until the dissolution of bone phosphate had allowed the sample to become soft and pliable. The acid solution containing the phosphate and any impurities was then decanted without rinsing, and the remnant bone material immersed in

reverse osmosis water, resulting in a mildly acidic solution. Upon gentle heating, the bone collagen became fully soluble and was then filtered, reduced in volume by evaporation and freeze dried prior to combustion and ^{14}C analysis.

3.1.3 Shell

Shell carbonate was pre-treated by removing any adhering detritus from the depositional environment by physical abrasion before sonication in an ultrasonic bath to remove any further debris. 20% by mass of the outer surface was then removed by etching in 1M HCl solution. After rinsing and drying, a 0.1 g cross section of the shell, from umbo to shell margin, was selected for acid hydrolysis to integrate the entire lifespan of the organism. The fragments received a further 20% surface removal, *in situ*, immediately before hydrolysis, in order to remove any adsorbed CO_2 that may have accumulated in the storage period between pre-treatment and hydrolysis. The sample CO_2 was released by complete acid hydrolysis of the pre-treated sample, under vacuum, using an excess of 1M HCl.

3.2 Sample preparation - graphitisation

After pre-treatment, sample carbon was prepared for measurement by combustion or hydrolysis to CO_2 before graphitisation and AMS analysis.

Carbon dioxide was obtained from the organic samples (grain and bone collagen) by combustion in pre-cleaned, sealed quartz tubes (Vandeputte et al., 1996). The combustion tubes contained quartz wool, supporting 0.5g of copper oxide (CuO) and a small length of silver wire. The tubes were evacuated, sealed and combusted at 850°C, converting the sample carbon to CO_2, using the CuO as the oxidant and the silver wire to absorb any contaminants that were produced, such as halides and oxides of nitrogen (Buchanan and Corcoran, 1959).

All CO_2 samples were then cryogenically purified using a mixture of ethanol and solid CO_2 to freeze down any water vapour, and liquid nitrogen to freeze down the CO_2, allowing the removal of non-condensing gases. The vacuum line system employed permitted the sub-sampling of accurate quantities of CO_2 via a calibrated finger to allow a controlled volume (3 ml) to be collected for graphitisation and AMS measurement, a second sample for $\delta^{13}C$

analysis, and an archive sample for future assay (Figure 3.1).

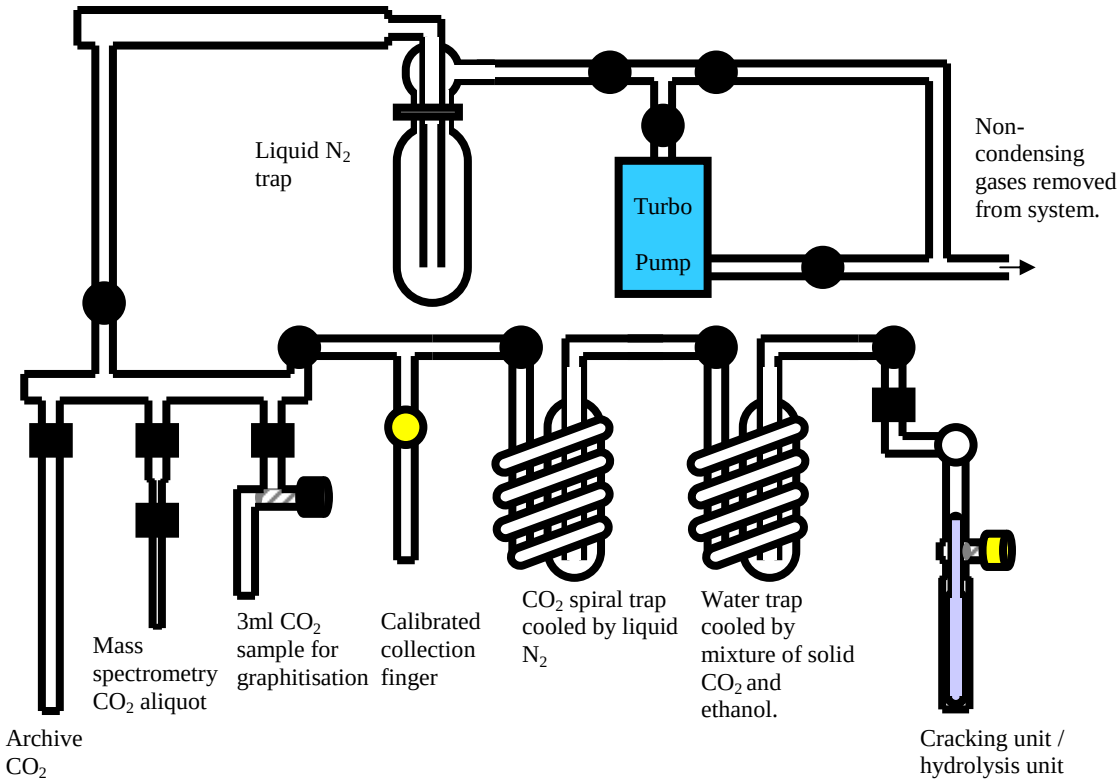

Figure 3.1: Schematic diagram of the vacuum system used for cryogenic purification of sample CO_2

Sample CO_2 was released into the system via the cracking of the quartz combustion tube for grain and bone samples or via *in situ* hydrolysis of shell carbonates. The 3mls of sample CO_2 were converted to graphite using zinc (Zn) and iron (Fe) catalysts under vacuum as shown in Figure 3.2. Reduction to CO was achieved using c. 70 mg Zn at 450ºC, followed by further reduction to C using 3 mg Fe powder at 550ºC (Vogel et al., 1987; Lowe and Judd, 1987).

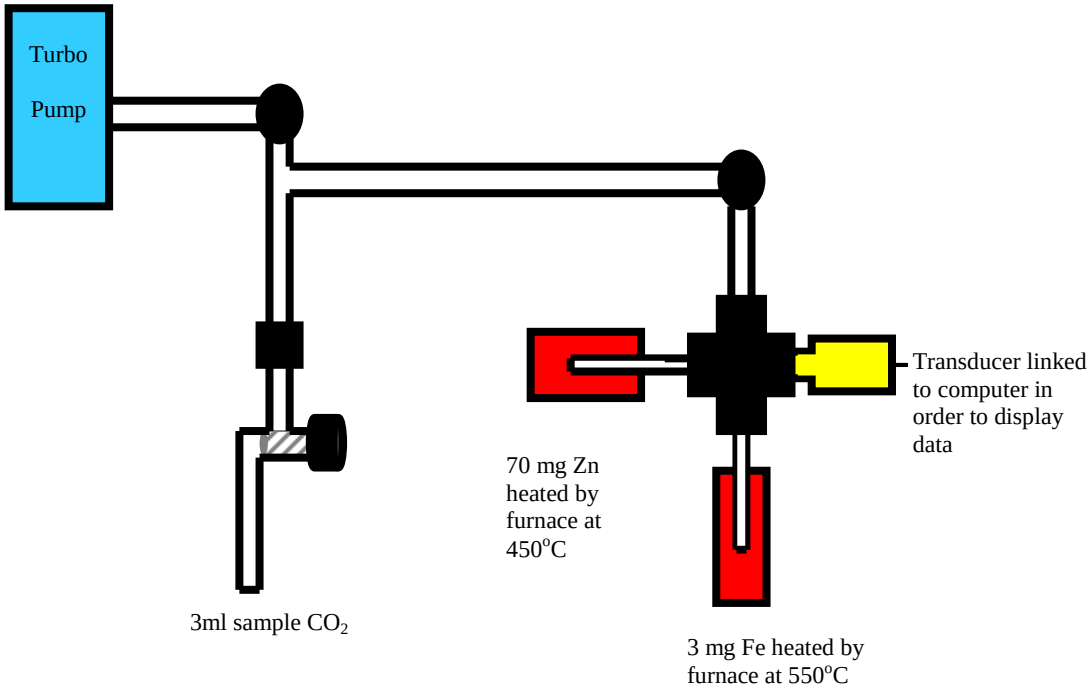

Figure 3.2: Schematic diagram of the graphitisation system

The pressure within the graphitisation unit was monitored using pressure transducers linked to a computer where the pressure input could be plotted relative to the time elapsed since the reaction began. The reaction took roughly 20 hours to run to completion, upon which a calculation of percentage graphite yield could be employed to evaluate the success of the graphitisation process. Any samples with less than 95% graphite were repeated from the archived CO_2 in order to avoid the potential for fractionation to have occurred during the reaction, which could compromise the accuracy of the measured sample ^{14}C age. The graphite was then pressed into an aluminium cathode, ready for AMS analysis.

Sample $\delta^{13}C$ was measured off-line using a VG SIRA 10 isotope ratio mass spectrometer, comparing sample values with those of a working standard reference gas of known isotopic composition. The internal reference gas was pre-calibrated using sample gases of known isotopic composition produced from International Reference Materials such as NBS 19 and IAEA-CO-1. The measurement results were expressed using the δ-notation (Craig, 1957) as per mille deviations from the VPDB standard. $\delta^{13}C$ values are calculated as per equation 1.6 and used to produce a fractionation factor to normalise ^{14}C activities.
The $^{14}C/^{13}C$ ratios of the graphitised samples were measured on the SUERC 250kV

SSAMS (Freeman et al., 2008, 2010). All samples from each site were measured as a group within the same wheel to reduce any uncertainties attributed to random error. Results were then calculated using the background subtraction method on the $^{14}C/^{13}C$ ratio data (Section 3.4).

Oxygen ($^{18}O/^{16}O$) and carbon ($^{13}C/^{12}C$) isotopic ratios of shell carbonate were measured using a VG Isogas Prism II dual inlet stable isotope mass spectrometer incorporating a VG Isocarb common acid bath automated carbonate dissolution system, hydrolysing the samples in 103% phosphoric acid. Again, the measurement results were expressed using the δ-notation (Craig, 1957) as per mille deviations from the VPDB standard, calibrated using the IAEA CO1 (Carrara marble) international standard. The internal analytical precision of the standards was 0.04‰ for $\delta^{13}C$ and 0.08‰ for $\delta^{18}O$.

3.3 AMS measurement

3.3.1 AMS ^{14}C measurement

The AMS technique requires much less sample material than radiometric methods to achieve comparable precision, and reduces the measurement time required for a particular level of precision significantly, allowing precise measurement of ^{14}C activity to be gained quickly from milligram quantities of carbon. This is because, for example, in order to obtain 0.5% statistical precision using radiometric methods on 1g modern carbon, it would be necessary to count for 48 hours as 1 g of modern carbon contains 6×10^{10} atoms of ^{14}C, of which only approximately 14 decay per minute. Using AMS, the same precision can be achieved in 10 minutes as the counting rate of ^{14}C atoms is of the order of 100 s^{-1}, and therefore mg sample quantities are all that are required (Fifield, 1999).

The AMS capability to measure low isotopic abundances (c. 10^4 atoms) and ratios of radioactive to stable isotopes as low as to the order of 10^{-15} (Elmore and Philips, 1987; Fifield, 1999; Muzikar et al., 2003) has revolutionised the application of the ^{14}C dating technique, especially in archaeological studies. Smaller, single entity samples such as individual cereal grains can now be considered as suitable samples for dating, removing the uncertainties previously associated with bulk dating of mixed samples in order to produce gram quantities of carbon necessary for radiometric analysis.

All samples in this study were measured using the NEC 250kV single stage accelerator mass spectrometer (SSAMS) at SUERC, which is dedicated to radiocarbon measurement (Freeman et al., 2008). The graphite sample targets were loaded into the ion source (see Figure 3.3) where Cs vapour is ionised to generate Cs^+ ions (Muzikar et al., 2003). The positively charged Cs beam is then accelerated towards the negatively charged sample holder, focusing on the cathode of the sample to be measured. This sputtering with Cs^+ ions generates C^- ions by collision (Middleton et al., 1983) and ^{14}N ions are lost from the system at this point as nitrogen does not form stable negative ions. The C^- ions are then repelled from the negatively charged sample holder and accelerated along the beam line towards the high voltage terminal of the accelerator. At this stage, the injection magnet (Figure 3.3) is used to preferentially select ions of atomic mass 12, 13 and14 (McNichol et al., 2001). The heavier the ions, the less the curvature and so the isotopes are separated into three separate beams by atomic mass. Molecular ions with similar mass such as $^{12}CH_2$ and ^{13}CH ions are incorporated along with C^- ions. These molecular ions are dissociated upon collision with the gas molecules in the stripper canal (Figure 3.3), converting negative ions to positive ions. The analyser magnet then selects ions with the appropriate momentum for ^{14}C ions and discriminates against molecular fragments of the correct mass-energy and unwanted charge states using electrostatic analysers. The ^{12}C, ^{13}C and ^{14}C isotopes are again directed by curvature, the stable isotopes, ^{12}C and ^{13}C to Faraday cups and finally, the filtered ^{14}C ions impinge on a passivated implanted planar silicon (PIPS) detector where the number of ^{14}C ions are counted (Figure 3.3).

Ratios of $^{14}C/^{12}C$ or $^{14}C/^{13}C$ can then be generated in order to calculate ages. At present, measurement precision at SUERC favours calculations based upon the $^{14}C/^{13}C$ ratio with the $\delta^{13}C$ values measured and calculated off-line by a VG Sira 10 isotope ratio mass spectrometer to allow the AMS to run with greater ion beams (Naysmith et al., 2010; Freeman et al., 2010).

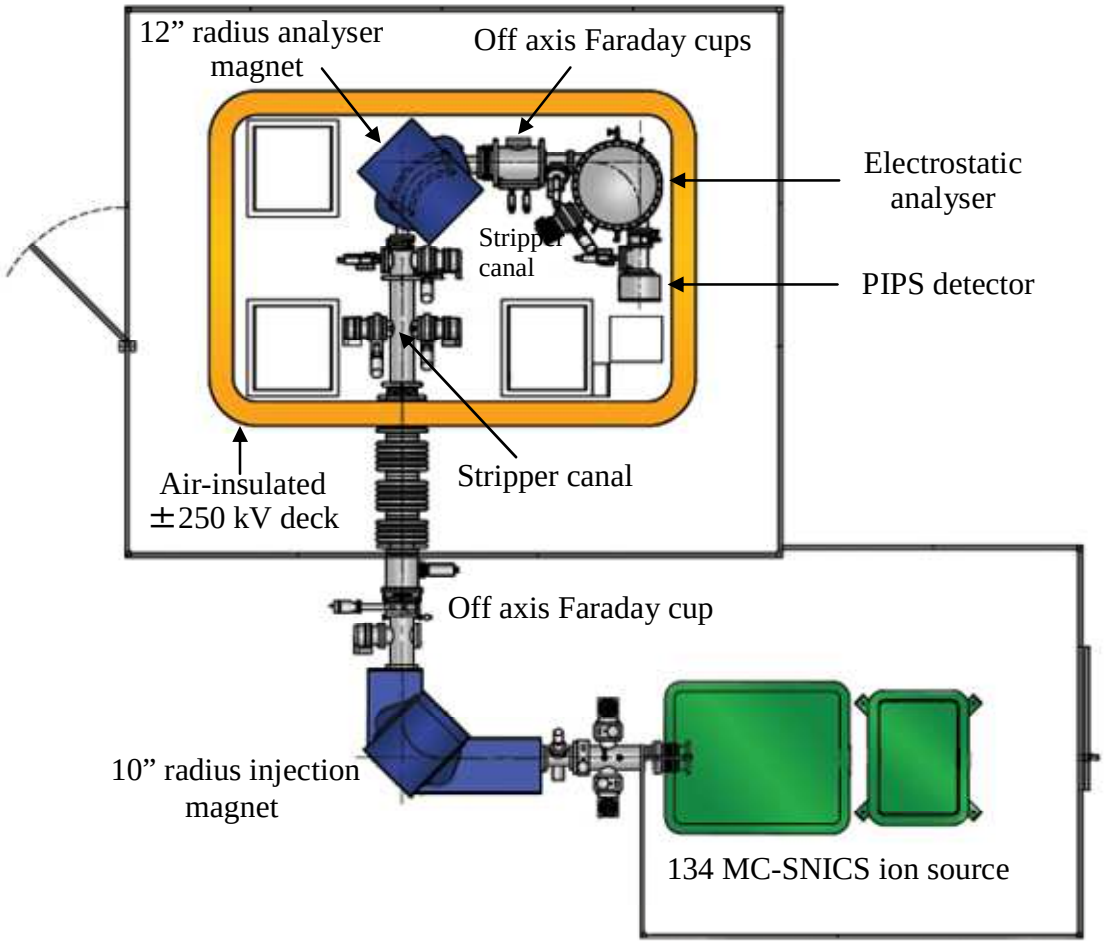

Figure 3.3: Layout of the SUERC SSAMS (Freeman et al., 2008 courtesy of NEC)

3.3.2 Quality assurance and quality control of results

Measurement precision is limited by 3 main factors, the total number of ^{14}C ions detected by the AMS, the background measurement, and the actual amount of ^{14}C that the sample contains. These factors are monitored by an in-house QA programme involving a variety of primary and known age standards. Many of the standards employed at SUERC have been used in intercomparison studies between AMS laboratories worldwide in order to produce consensus values and greater quality assurance through quantitative assessment of comparability of results between laboratories. Intercomparison studies in the radiocarbon community are considered the best tool to determine the current level of laboratory comparability (Scott, 2003) and SUERC plays an active part in each study in order to maintain high user confidence in the ^{14}C results reported. The studies carry acronyms

according to the order of study i.e. TIRI (Third International Radiocarbon Intercomparison) (Gulliksen and Scott, 1995; Scott, 2003), FIRI (Fourth International Radiocarbon Intercomparison) (Scott, 2003), VIRI (Fifth International Radiocarbon Intercomparison) (Scott et al., 2007, 2010a, 2010b), and employ a variety of sample types allowing a comparison of all possible sources of error in the ^{14}C dating process. In the publication of each study, a new set of reference materials are created, giving further possibilities for materials to be used as in–house standards at each individual laboratory.

All reputable laboratories should reference their results directly to the oxalic acid standard (OXII) (SRM-4990C) or a related standard for control of results. This standard is produced and sold by the National Institute of Standards and Technology and is in the form of oxalic acid formed from a 1977 harvest of beet molasses. Its activity is normalized to the theoretical activity of 1890 wood (pre Suess and bomb effects) corrected to 1950AD to provide an atmospheric value of ^{14}C activity in 1950AD. 1950 is the year that all radiocarbon dates are reported relative to, using the terminology 'before present' (BP), with present being taken as 1950AD. The internationally recognised radiocarbon reference value (A_{on}) is 0.7459 times the specific activity of OXII, normalised to $\delta^{13}C$ = -25‰ (per mil) with respect to the VPDB standard (Olsson 1970; Stuiver and Polach, 1977; Stuiver, 1983; Donahue et al., 1990). The OXII primary standard is labelled in-house with the prefix 'M' (modern) (Naysmith et al., 2010).

The background standard (in house code BK) is interglacial Heidelberg wood used in the VIRI intercomparison study (Scott et al., 2007, 2010a, 2010b) (code VIRI K). This standard was prepared from bulk wood subject to ABA pre-treatment (see methodology section), then reduced to the structural cellulose fraction by bleaching with $NaOCl_2$, followed by a final ABA wash. When unknown carbonate samples are included within a batch, geological carbonate backgrounds (Icelandic doublespar) are prepared in order to replicate the laboratory process undertaken on these samples. Each batch of samples on the 132 position wheel will typically contain 6 or 7 BK samples which are analysed together to produce a mean background value for the batch. This represents the background value for the entire process, including laboratory pre-treatment, graphitization and measurement, giving a reliable indication of the lower age limit achievable. Currently, background measurement is limited to around 55 kyr owing to sample chemistry (Naysmith et al., 2010).

The secondary wood standard (in house code BC) is prepared from Scots Pine collected from the Garry Bog in Northern Ireland, which is just under one ^{14}C half-life in age. Again, this wood is reduced to the cellulose fraction and was the subject of an inter-comparison study (sample FIRI I), which produced a consensus value of 4485 ± 5 BP (Scott, 2003). This value is in accordance with dendrochronological dating on the sample material, which ranged from 3299-3257BC giving an average ^{14}C age of 4471 y BP (Scott, 2003). Each AMS batch contains 13 BC samples; these are again averaged to give a mean age for the group. The standard deviation on BC values is used as the determining factor on the error reported on unknown samples from each batch (Naysmith et al., 2010).

The modern secondary standard (denoted as BBM) is generated from a single year's growth of barley mash from the Glengoyne Distillery. The BBM is prepared by combusting a sufficient quantity of barley mash to generate 2 litres of CO_2 that are stored in a glass bulb. Aliquots of gas are then taken and converted to graphite and as all samples come from the same bulk gas, measurement of the BBM gives an accurate check of the performance of the graphitisation and AMS processes (Naysmith et al., 2010). The BBM standard was used in the TIRI intercomparison study (TIRI A) (Scott, 2003) and produced a consensus value of 116.35 ± 0.41 pMC (percent modern carbon).

If large quantities of bone are measured within a batch, a known age bone (KAB) in-house standard is also measured to promote confidence in the laboratory procedures involved in the preparation of bone samples. This KAB was supplied by English Heritage and has produced a mean age of 2132 ^{14}C y BP since its first analysis in 2003.

Each full batch of 132 samples measured by the SUERC SSAMS is broken up notionally into smaller groups of 10 cathodes, including standards, in order to measure any variation or drift in the measurement throughout each run. Each group of 10 includes one OXII primary standard, one secondary wood standard (BC), and either the modern standard material (BBM) or the background standard (BK) as well as 7 unknown samples. All samples, including both standards and unknowns, are automatically repeatedly measured in intra-group rotation until the counting statistics on each sample and the scatter on the $^{14}C/^{13}C$ ratio achieves a quality of 3‰ or better.

3.4 Background subtraction calculation of ^{14}C ages

Although previous results at SUERC had been calculated using other methods such as that of Donahue et al., (1990), all measurements within this study were carried out using the background subtraction method (Equation 3.1). Using this method, an average background ratio for the batch is determined from the mean of the BK values generated. This ratio is then subtracted from all the standards and unknowns in the wheel to produce fraction modern (Fm) values. Fractionation correction is then applied to all unknowns and standards using the fractionation factor determined from the off-line $\delta^{13}C$ to calculate F. F is the fraction modern corrected for background. BBM and BK standards are reported using F whereas BC standards and all unknowns are calculated to Age BP (before present) as per Equation 3.2.

$$F = \frac{\left[\left(^{14}C/^{13}C\right)_s - \left(^{14}C/^{13}C\right)_{bk}\right] * \left[975/1000 + \delta^{13}C_s\right]}{0.7459 * \left[\left(^{14}C/^{13}C\right)_{OXII} - \left(^{14}C/^{13}C\right)_{bk}\right] * \left[975/1000 + \delta^{13}C_{OxII}\right]}$$

Equation 3.1: Background subtraction calculation of ^{14}C ages

Where: F = Fm corrected for background and fractionation, s = sample; bk = the mean background measurement; OXII = the mean measurement from the multiple OXII data in each batch.

The radiocarbon age of the sample is the calculated as shown:

$$Radiocarbon\ Age = \frac{1}{\lambda} \ln \frac{1}{F} = 8033 \ln \frac{1}{F}$$

Equation 3.2: Radiocarbon age calculation

Where λ= decay constant = ln2/5568 and F = Fm corrected for background and fractionation as per equation 3.1.

3.5 General statistical data treatment – chi-squared testing and subsequent ΔR calculations

Following measurement, the calculated radiocarbon ages for each site (Chapter 4) were then subject to chi-squared (χ^2) statistical testing to determine whether each sample within

a group was statistically indistinguishable from the remainder at 95% confidence (and therefore could be considered to be contemporaneous). This statistical treatment of the data must take place before the samples can be considered suitable for ΔR calculations. Ages that passed the chi-squared test were then considered suitable for calculation of ΔR. In cases where samples did not pass the χ^2 test, a judgement call had to be made on whether the remaining samples from this context that do pass the χ^2 test were in fact suitable for determining a ΔR value. The ΔR values were calculated for every possible remaining pairing of marine/terrestrial samples within a context following χ^2 testing, using a Fortran/Unix ΔR calculation program, with coding provided by Ron and Paula Reimer. This program calculates ΔR values by converting the terrestrial ^{14}C ages to modelled marine ^{14}C ages, allowing direct comparison with the measured marine ^{14}C ages from the contemporaneous marine samples as described in Chapter 2.1.

The statistical treatment of the data was evaluated throughout the course of this study and revised in the final year, leading to the production of revised ΔR values and subsequent re-interpretations. The original data handling method is presented in Chapter 5 and the revised method in Chapter 6.

CHAPTER 4

RESULTS

This chapter presents a series of tables detailing the sample codes, AMS results and $\delta^{13}C$ results for each site. The AMS results are presented in both a rounded and unrounded format. Convention normally sees results published by rounding to the nearest 5 years and the error rounded up to the nearest 5 years. The standard deviation on the in-house QA (Belfast Cellulose for this study) is used as the limiting factor for the error reported on the measurement, conventionally rounding the largest value between the 1σ error and the standard deviation on the QA up to the nearest 5 years and publishing this as the error on the measurement. The results are interpreted according to convention in Chapter 5, but the development of the new methodology, detailed in Chapter 6, addresses sources of uncertainty incorporated into ΔR calculations, including those introduced by rounding and suggests a best practice for future calculations. All of the data are therefore presented for interpretation by the relevant data handling techniques employed in Chapters 5 and 6 respectively. The data from the Quoygrew and Robert's Haven concerning the comparison of ΔR calculations made on fish bone with that of mollusc shell will be discussed separately in Chapter 7.

4.1 Gallowgate Middle School, Aberdeen

Context: 84

Standard deviation on batch QA: 15 ^{14}C yr.

	Sample lab code	Sample type	δ^{13}C (± 0.1‰)	Age BP (Unrounded)	Error 1σ (Unrounded)	Unrounded error (Batch limited)	Age BP (Rounded)	Error 1σ (Rounded)
Terrestrial	SUERC - 17031	Sheep/Goat Lower mandible LHS (*Ovis aries*/*Capra aegagrus hircus*)	-21.0	894	35	35	895	35
	SUERC - 17035	Sheep/Goat Lower mandible LHS (*Ovis aries/Capra aegagrus hircus*)	-21.1	898	34	34	900	35
	SUERC - 17036	Sheep/Goat Lower mandible LHS (*Ovis aries*/*Capra aegagrus hircus*)	-19.7	937	34	34	935	35
	SUERC - 17037	Red Deer bone (*Cervus elaphus*)	-21.7	838	34	34	840	35
Marine	SUERC - 17027	Winkle (*Littorina littorea*)	1.9	1237	35	35	1235	35
	SUERC - 17028	Winkle (*Littorina littorea*)	1.7	1195	34	34	1195	35
	SUERC - 17029	Winkle (*Littorina littorea*)	2.3	1195	34	34	1195	35
	SUERC - 17030	Winkle (*Littorina littorea*)	2.0	1206	34	34	1205	35

Table 4.1: Results of ^{14}C and δ^{13}C measurements on samples from Gallowgate Middle School, Aberdeen

4.2 16 -18 Netherkirkgate, Aberdeen.

Context: 442 **Standard deviation on batch QA:** 26 ^{14}C yr.								
	Sample lab code	**Sample Type**	**δ^{13}C (± 0.1‰)**	**Age BP (Unrounded)**	**Error 1σ (Unrounded)**	**Unrounded error (Batch limited)**	**Age BP (Rounded)**	**Error 1σ (Rounded)**
Terrestrial	SUERC - 17252	Sheep/Goat Lower mandible RHS (*Ovis aries/Capra aegagrus hircus*	-21.6	920	34	34	920	35
	SUERC - 17253	Sheep/Goat Lower mandible RHS (*Ovis aries/Capra aegagrus hircus*)	-21.2	901	34	34	900	35
	SUERC - 17254	Cattle bone (*Bos primigenius)*	-21.1	936	32	32	935	35
	SUERC - 17258	Hare bone (*Lepus europaeus*)	-22.4	997	34	34	995	35
Marine	SUERC - 17248	Limpet (*Patella vulgata*)	1.7	1235	32	32	1235	35
	SUERC - 17249	Limpet (*Patella vulgata*)	1.4	1272	32	32	1270	35
	SUERC - 17250	Limpet (*Patella vulgata*)	-0.4	1226	34	34	1225	35
	SUERC - 17251	Limpet (*Patella vulgata*)	1.5	1272	34	34	1270	35

Table 4.2: Results of ^{14}C and δ^{13}C measurements on samples from 16 – 18 Netherkirkgate, Aberdeen

4.3 Arbroath Abbey, Arbroath

Context: 212 **Standard deviation on batch QA:** 32 ^{14}C yr								
	Sample lab code	**Sample Type**	**δ^{13}C (± 0.1‰)**	**Age BP (Unrounded)**	**Error 1σ (Unrounded)**	**Unrounded error (Batch limited)**	**Age BP (Rounded)**	**Error 1σ (Rounded)**
Terrestrial	SUERC-17041 (SUERC-16283)$^{+}$	Unidentified grain	-22.2	689	35	35	690	35
	SUERC - 16284	Unidentified grain	-22.8	695	35	35	695	35
	SUERC-17045 (SUERC-16285)$^{+}$	Unidentified grain	-21.6	643	35	35	645	35
	SUERC - 16286	Unidentified grain	-22.1	668	35	35	670	35
	SUERC - 16290	Cattle tibia (*Bos primigenius)*	-22.0	937	35	35	935	35
	SUERC - 16291	Cattle tibia (*Bos primigenius)*	-22.0	687	35	35	685	35
	SUERC - 16292	Sheep/Goat humerus (RHS) (*Ovis aries/Capra aegagrus hircus*	-19.4	731	35	35	730	35
	SUERC - 16293	Sheep/Goat humerus (RHS) (*Ovis aries/Capra aegagrus hircus*)	-21.8	784	35	35	785	35
	SUERC - 19709	Rabbit tibia with knife cut (*Oryctolagus cuniculus)*	-20.8	600	29	32	600	35
	SUERC - 19710	Sheep/Goat Humerus (LHS) (*Ovis aries/Capra aegagrus hircus*)	-21.2	634	29	32	635	35
	SUERC - 19711	Sheep/Goat Humerus (LHS) (*Ovis aries/Capra aegagrus hircus*)	-20.6	606	29	32	605	35
	SUERC - 19715	Sheep/Goat Humerus (LHS) (*Ovis aries/Capra aegagrus hircus*)	-21.1	578	29	32	580	35

Table 4.3: Results of ^{14}C and δ^{13}C measurements on samples from Arbroath Abbey, Arbroath

Context: 212 **Standard deviation on batch QA:** 32 ^{14}C yr.								
	Sample lab code	**Sample Type**	**δ^{13}C (± 0.1‰)**	**Age BP (Unrounded)**	**Error 1σ (Unrounded)**	**Unrounded error (Batch limited)**	**Age BP (Rounded)**	**Error 1σ (Rounded)**
Marine	SUERC - 16295	Winkle (*Littorina littorea*)	2.2	1093	35	35	1095	35
	SUERC - 16296	Winkle (*Littorina littorea*)	2.7	1109	35	35	1110	35
	SUERC - 16300	Winkle (*Littorina littorea*)	2.6	1079	35	35	1080	35
	SUERC - 16301	Oyster (*Ostreidae*)	2.7	1123	35	35	1125	35
	SUERC - 16302	Oyster (*Ostreidae*)	2.3	1097	35	35	1095	35
	SUERC - 16303	Oyster (*Ostreidae*)	3.0	1191	36	36	1190	40
	SUERC - 16304	Oyster (*Ostreidae*)	2.9	1223	35	35	1225	35
	SUERC - 19705	Winkle (*Littorina littorea*)	2.1	1027	29	32	1025	35
	SUERC - 19706	Winkle (*Littorina littorea*)	1.2	1052	30	32	1050	35
	SUERC - 19707	Winkle (*Littorina littorea*)	1.3	983	29	32	985	35
	SUERC - 19708	Winkle (*Littorina littorea*)	2.3	1047	29	32	1045	35

Table 4.3 (contd): Results of ^{14}C and δ^{13}C measurements on samples from Arbroath Abbey, Arbroath
$^{+}$ Symbol denotes grain samples that were repeated owing to the original grain failing to produce enough CO_2 for measurement.

4.4 Horse Cross, Perth

Context: 595 **Standard deviation on batch QA:** 15 ^{14}C yr								
	Sample lab code	**Sample Type**	**δ^{13}C (± 0.1‰)**	**Age BP (Unrounded)**	**Error 1σ (Unrounded)**	**Unrounded error (Batch limited)**	**Age BP (Rounded)**	**Error 1σ (Rounded)**
Terrestrial	SUERC - 16276	Cattle; distal metacarpal (*Bos primigenius)*	-22.5	638	35	35	640	35
	SUERC - 16280	Cattle; distal metacarpal (*Bos primigenius)*	-22.1	937	35	35	935	35
	SUERC - 16281	Cattle; 1st phalange (*Bos primigenius)*	-21.6	914	35	35	915	35
	SUERC - 16282	Cattle; upper molar (*Bos primigenius)*	-22.3	663	35	35	665	35
	SUERC - 20276	Unidentified grain	-24.9	642	29	29	640	30
	SUERC - 20277	Unidentified grain	-25.3	557	29	29	555	30
	SUERC - 20278	Cattle pubic bone (*Bos primigenius)*	-21.8	579	29	29	580	30
Marine	SUERC - 16270	Oyster (*Ostreidae*)	2.4	1042	33	33	1040	35
	SUERC - 16271	Oyster (*Ostreidae*)	2.4	1043	35	35	1045	35
	SUERC - 16272	Oyster (*Ostreidae*)	2.3	1032	35	35	1030	35
	SUERC - 16273	Oyster (*Ostreidae*)	2.5	1065	35	35	1065	35
	SUERC - 16274	Mussel (*Mytilus edulis*)	0.6	1052	35	35	1050	35
	SUERC-17038 (SUERC-16275)	Mussel (*Mytilus edulis*)	1.0	1026	33	33	1025	35

Table 4.4: Results of ^{14}C and δ^{13}C measurements on samples from Horse Cross, Perth

4.5 Kirkgate, Perth (Context 400)

Context: 400 **Standard deviation on batch QA:** 21 ^{14}C yr								
	Sample lab code	**Sample Type**	**δ^{13}C (± 0.1‰)**	**Age BP (Unrounded)**	**Error 1σ (Unrounded)**	**Unrounded error (Batch limited)**	**Age BP (Rounded)**	**Error 1σ (Rounded)**
Terrestrial	SUERC - 18883	Sheep/Goat maxilla LHS (*Ovis aries/Capra aegagrus hircus*)	-21.6	801	32	32	800	35
	SUERC - 18884	Cattle metatarsal, distal end RHS (*Bos primigenius)*	-22.2	697	34	34	695	35
	SUERC - 19717	Cattle pelvis (*Bos primigenius)*	-20.5	848	24	24	850	25
	SUERC - 19718	Cattle 1st phalange (*Bos primigenius)*	-21.4	721	29	29	720	30
Marine	SUERC - 18876	Oyster (*Ostreidae*)	1.0	1111	32	32	1110	35
	SUERC - 18880	Oyster (*Ostreidae*)	0.5	1137	34	34	1135	35
	SUERC - 18881	Oyster (*Ostreidae*)	0.9	1168	34	34	1170	35
	SUERC - 18882	Oyster (*Ostreidae*)	1.8	1109	34	34	1110	35

Table 4.5: Results of ^{14}C and δ^{13}C measurements on samples from Kirkgate, Perth (Context 400)

4.6 Kirkgate, Perth (Context 413)

Context: 413 **Standard deviation on batch QA:** 21 ^{14}C yr								
	Sample lab code	**Sample Type**	**δ^{13}C (± 0.1‰)**	**Age BP (Unrounded)**	**Error 1σ (Unrounded)**	**Unrounded error (Batch limited)**	**Age BP (Rounded)**	**Error 1σ (Rounded)**
Terrestrial	SUERC - 18892	Sheep/Goat metatarsal, proximal end LHS (*Ovis aries*/*apra aegagrus hircus*)	-23.2	598	34	34	600	35
	SUERC - 18893	Cattle maxilla LHS (*Bos primigenius)*	-21.6	645	32	32	645	35
	SUERC - 19719	Cattle R. Tibia (*Bos primigenius)*	-20.9	642	29	29	640	30
	SUERC - 19720	Cattle L. Radius (*Bos primigenius)*	-21.2	670	29	29	670	30
Marine	SUERC - 18885	Oyster (*Ostreidae*)	2.6	1039	34	34	1040	35
	SUERC - 18886	Oyster (*Ostreidae*)	0.7	1112	34	34	1110	35
	SUERC - 18890	Oyster (*Ostreidae*)	2.2	992	32	32	990	35
	SUERC - 18891	Oyster (*Ostreidae*)	0.2	1073	31	31	1075	35

Table 4.6: Results of ^{14}C and δ^{13}C measurements on samples from Kirkgate, Perth (Context 413)

4.7 St Leonard's School, St Andrews

Context: 0131 **Standard deviation on batch QA:** 32 ^{14}C yr								
	Sample lab code	**Sample Type**	**δ^{13}C (± 0.1‰)**	**Age BP (Unrounded)**	**Error 1σ (Unrounded)**	**Unrounded error (Batch limited)**	**Age BP (Rounded)**	**Error 1σ (Rounded)**
Terrestrial	SUERC - 19109	Sheep/Goat metacarpal RHS (*Ovis aries/Capra aegagrus hircus*)	-21.4	1234	34	34	1235	35
	SUERC - 19110	Cattle mandible LHS (*Bos primigenius)*	-21.2	1278	34	34	1280	35
	SUERC - 21117	Cattle L. humerus, distal end (*Bos primigenius)*	-21.3	685	27	32	685	35
	SUERC - 21121	Sheep/Goat R. tibia, distal epiphyses (*Ovis aries/Capra aegagrus hircus*)	-23.1	1225	27	32	1225	35
Marine	SUERC - 19665	Winkle (*Littorina littorea*)	-2.1	1476	29	32	1475	35
	SUERC - 19666	Winkle (*Littorina littorea*)	-1.1	1466	29	32	1465	35
	SUERC - 19667	Winkle (*Littorina littorea*)	-1.5	1457	29	32	1455	35
	SUERC - 19668	Winkle (*Littorina littorea*)	-1.8	1418	23	32	1420	35

Table 4.7: Results of ^{14}C and δ^{13}C measurements on samples from St Leonard's School, St Andrews

4.8 Archerfield, East Lothian (Context 90)

Context: 90 **Standard deviation on batch QA:** 32 ^{14}C yr								
	Sample lab code	**Sample Type**	**δ^{13}C (± 0.1‰)**	**Age BP (Unrounded)**	**Error 1σ (Unrounded)**	**Unrounded error (Batch limited)**	**Age BP (Rounded)**	**Error 1σ (Rounded)**
Terrestrial	SUERC - 19680	Barley (*Hordeum* sp.)	-22.4	497	29	32	495	35
	SUERC - 19681	Barley (*Hordeum* sp.)	-23.1	471	29	32	470	35
	SUERC - 19685	Barley (*Hordeum* sp.)	-24.0	502	29	32	500	35
	SUERC - 19686	Barley (*Hordeum* sp.)	-24.1	493	29	32	495	35
	SUERC - 19687	Oat (*Avena* sp.)	-25.3	485	29	32	485	35
	SUERC - 19688	Oat (*Avena* sp.)	-24.9	502	29	32	500	35
	SUERC - 19689	Oat (*Avena* sp.)	-25.0	455	29	32	455	35
	SUERC - 19690	Oat (*Avena* sp.)	-24.1	527	29	32	525	35
Marine	SUERC - 19669	Limpet (*Patella vulgata*)	0.1	823	29	32	825	35
	SUERC - 19670	Limpet (*Patella vulgata*)	-2.4	830	29	32	830	35
	SUERC - 19671	Limpet (*Patella vulgata*)	0.7	912	30	32	910	35
	SUERC - 19675	Limpet (*Patella vulgata*)	-1.8	897	29	32	895	35
	SUERC - 19676	Winkle (*Littorina littorea*)	1.9	910	29	32	910	35
	SUERC - 19677	Winkle (*Littorina littorea*)	1.2	840	29	32	840	35
	SUERC - 19678	Winkle (*Littorina littorea*)	0.5	932	29	32	930	35
	SUERC - 19679	Winkle (*Littorina littorea*)	1.0	940	29	32	940	35

Table 4.8: Results of ^{14}C and δ^{13}C measurements on samples from Archerfield, East Lothian (Context 90)

4.9 Archerfield, East Lothian (Context 142)

Context: 142 **Standard deviation on batch QA:** 34 ^{14}C yr								
	Sample lab code	**Sample Type**	**δ^{13}C (± 0.1‰)**	**Age BP (Unrounded)**	**Error 1σ (Unrounded)**	**Unrounded error (Batch limited)**	**Age BP (Rounded)**	**Error 1σ (Rounded)**
Terrestrial	SUERC - 19760	Barley (*Hordeum* sp.)	-22.5	502	28	34	500	35
	SUERC - 19761	Barley (*Hordeum* sp.)	-22.5	504	25	34	505	35
	SUERC - 19762	Barley (*Hordeum* sp.)	-23.1	584	25	34	585	35
	SUERC - 19763	Oat (*Avena* sp.)	-23.6	493	29	34	495	35
	SUERC - 19767	Oat (*Avena* sp.)	-22.7	639	25	34	640	35
Marine	SUERC - 19757	Winkle (*Littorina littorea*)	1.4	817	29	34	815	35
	SUERC - 19758	Winkle (*Littorina littorea*)	0.9	844	26	34	845	35
	SUERC - 19759	Limpet (*Patella vulgata*)	1.2	781	29	34	780	35

Table 4.9: Results of ^{14}C and δ^{13}C measurements on samples from Archerfield, East Lothian (Context 142)

4.10 Scottish Seabird Centre, North Berwick (Context 1226)

Context: 1226

Standard deviation on batch QA: 39 ^{14}C yr

	Sample lab code	Sample Type	δ^{13}C (± 0.1‰)	Age BP (Unrounded)	Error 1σ (Unrounded)	Unrounded error (Batch limited)	Age BP (Rounded)	Error 1σ (Rounded)
Terrestrial	SUERC - 29353	Barley (*Hordeum* sp.)	-23.3	1276	34	39	1275	40
	SUERC - 29357	Barley (*Hordeum* sp.)	-21.9	1334	34	39	1335	40
	SUERC - 29358	Barley (*Hordeum* sp.)	-23.1	1356	34	39	1355	40
	SUERC - 29359	Barley (*Hordeum* sp.)	-22.0	1462	34	39	1460	40
Marine	SUERC - 29349	Winkle (*Littorina littorea*)	1.4	1717	32	39	1715	40
	SUERC - 29350	Winkle (*Littorina littorea*)	1.1	1787	32	39	1785	40
	SUERC - 29351	Winkle (*Littorina littorea*)	0.6	1789	34	39	1790	40
	SUERC - 29352	Winkle (*Littorina littorea*)	1.1	1764	34	39	1765	40

Table 4.10: Results of ^{14}C and δ^{13}C measurements on samples from the Scottish Seabird Centre, North Berwick (Context 1226)

4.11 Scottish Seabird Centre, North Berwick (Context 1287)

Context: 1287 **Standard deviation on batch QA:** 39 ^{14}C yr								
	Sample lab code	**Sample Type**	**δ^{13}C (± 0.1‰)**	**Age BP (Unrounded)**	**Error 1σ (Unrounded)**	**Unrounded error (Batch limited)**	**Age BP (Rounded)**	**Error 1σ (Rounded)**
Terrestrial	SUERC - 29367	Cattle mandible (*Bos primigenius)*	-22.8	1515	32	39	1515	40
	SUERC - 29368	Sheep/ Goat mandible RHS (*Ovis aries/Capra aegagrus hircus*)	-21.8	1487	31	39	1485	40
	SUERC - 29369	Sheep/ Goat mandible RHS (*Ovis aries/Capra aegagrus hircus*)	-21.3	1461	34	39	1460	40
	SUERC - 29370	Barley (*Hordeum* sp.)	-22.5	1413	34	39	1415	40
Marine	SUERC - 29360	Winkle (*Littorina littorea*)	2.3	1793	32	39	1795	40
	SUERC - 29361	Winkle (*Littorina littorea*)	1.2	1827	34	39	1825	40
	SUERC - 29362	Winkle (*Littorina littorea*)	1.3	1677	31	39	1675	40
	SUERC - 29363	Winkle (*Littorina littorea*)	0.4	1784	34	39	1875	40

Table 4.11: Results of ^{14}C and δ^{13}C measurements on samples from the Scottish Seabird Centre, North Berwick (Context 1287)

4.12 Castle Park, Dunbar (Context 0341)

Context: 0341

Standard deviation on batch QA: 14 ^{14}C yr

	Sample lab code	Sample Type	δ^{13}C (± 0.1‰)	Age BP (Unrounded)	Error 1σ (Unrounded)	Unrounded error (Batch limited)	Age BP (Rounded)	Error 1σ (Rounded)
Terrestrial	SUERC - 19098	Horse bone (*Equus ferus caballus*)	-22.7	1382	34	34	1380	35
	SUERC - 19099	Cattle bone (*Bos primigenius)*	-20.7	1290	34	34	1290	35
	SUERC - 19100	Sheep/Goat mandible LHS (*Ovis aries/Capra aegagrus hircus*)	-21.1	1318	32	32	1320	35
	SUERC - 19104	Hare bone (*Lepus europaeus*)	-22.2	1314	34	34	1315	35
Marine	SUERC - 19094	Winkle (*Littorina littorea*)	1.8	1757	34	34	1755	35
	SUERC - 19095	Winkle (*Littorina littorea*)	-0.1	1745	34	34	1745	35
	SUERC - 19096	Winkle (*Littorina littorea*)	-0.9	1698	34	34	1700	35
	SUERC - 19097	Winkle (*Littorina littorea*)	0.7	1710	34	34	1710	35

Table 4.12: Results of ^{14}C and δ^{13}C measurements on samples from Castle Park, Dunbar (Context 0341)

4.13 Castle Park, Dunbar (Context 3017)

Context: 3017 **Standard deviation on batch QA:** 32 ^{14}C yr								
	Sample lab code	**Sample Type**	**δ^{13}C (± 0.1‰)**	**Age BP (Unrounded)**	**Error 1σ (Unrounded)**	**Unrounded error (Batch limited)**	**Age BP (Rounded)**	**Error 1σ (Rounded)**
Terrestrial	SUERC - 19105	Red deer bone (*Cervus elaphus*)	-21.2	925	29	32	925	35
	SUERC - 19106	Cattle maxilla LHS (*Bos primigenius)*	-21.4	1048	34	34	1050	35
	SUERC - 19107	Sheep / goat mandible LHS (*Ovis aries*) or (*Capra aegagrus hircus*)	-21.5	1123	34	34	1125	35
	SUERC - 19108	Horse bone (*Equus ferus caballus*)	-21.4	1110	34	34	1110	35
Marine	SUERC - 19658	Winkle (*Littorina littorea*)	1.5	1450	29	32	1450	35
	SUERC - 19659	Winkle (*Littorina littorea*)	1.6	1433	27	32	1435	35
	SUERC - 19660	Winkle (*Littorina littorea*)	1.0	1445	28	32	1445	35
	SUERC - 19661	Winkle (*Littorina littorea*)	1.4	1487	26	32	1485	35

Table 4.13: Results of ^{14}C and δ^{13}C measurements on samples from Castle Park, Dunbar (Context 3017)

4.14 Quoygrew, Orkney

Context: A004 **Standard deviation on batch QA:** 36 ^{14}C yr								
	Sample lab code	**Sample Type**	**δ^{13}C (± 0.1‰)**	**Age BP (Unrounded)**	**Error 1σ (Unrounded)**	**Unrounded error (Batch limited)**	**Age BP (Rounded)**	**Error 1σ (Rounded)**
Marine	SUERC - 24564	Atlantic Cod bone (*Gadus morhua)*	-12.6	1251	29	36	1250	40
	SUERC - 24565	Atlantic Cod bone (*Gadus morhua)*	-14.0	1230	29	36	1230	40
	SUERC - 24566	Atlantic Cod bone (*Gadus morhua)*	-13.9	1181	30	36	1180	40
	SUERC - 24570	Atlantic Cod bone (*Gadus morhua)*	-13.3	1210	29	36	1210	40
Context: A023 **Standard deviation on batch QA:** 36 ^{14}C yr								
	Sample lab code	**Sample Type**	**δ^{13}C (± 0.1‰).**	**Age BP (Unrounded)**	**Error 1σ (Unrounded)**	**Unrounded error (Batch limited)**	**Age BP (Rounded)**	**Error 1σ (Rounded)**
Marine	SUERC - 24571	Atlantic Cod bone (*Gadus morhua)*	-12.0	1287	29	36	1285	40
	SUERC - 24572	Atlantic Cod bone (*Gadus morhua)*	-12.7	1283	29	36	1285	40
	SUERC - 24573	Atlantic Cod bone (*Gadus morhua)*	-13.0	1246	29	36	1245	40
	SUERC - 24574	Atlantic Cod bone (*Gadus morhua)*	-13.8	1256	29	36	1255	40

Table 4.14: Results of ^{14}C and δ^{13}C measurements on samples from Quoygrew, Orkney

4.15 Robert's Haven, Caithness

Context: 3004 **Standard deviation on batch QA:** 36 ^{14}C yr								
	Sample lab code	**Sample Type**	**δ^{13}C (± 0.1‰)**	**Age BP (Unrounded)**	**Error 1σ (Unrounded)**	**Unrounded error (Batch limited)**	**Age BP (Rounded)**	**Error 1σ (Rounded)**
Marine	SUERC - 24553	Atlantic Cod bone (*Gadus morhua)*	-14.4	1187	29	36	1185	40
	SUERC - 24554	Atlantic Cod bone (*Gadus morhua)*	-13.8	1115	29	36	1115	40
	SUERC - 24555	Atlantic Cod bone (*Gadus morhua)*	-13.6	1157	29	36	1155	40
	SUERC - 24556	Atlantic Cod bone (*Gadus morhua)*	-13.4	1167	29	36	1165	40
Context: 3019 **Standard deviation on batch QA:** 36 ^{14}C yr								
	Sample lab code	**Sample Type**	**δ^{13}C (± 0.1‰)**	**Age BP (Unrounded)**	**Error 1σ (Unrounded)**	**Unrounded error (Batch limited)**	**Age BP (Rounded)**	**Error 1σ (Rounded)**
Marine	SUERC - 24560	Atlantic Cod bone (*Gadus morhua)*	-14.3	1229	27	36	1230	40
	SUERC - 24561	Atlantic Cod bone (*Gadus morhua)*	-12.4	1280	29	36	1280	40
	SUERC - 24562	Atlantic Cod bone (*Gadus morhua)*	-13.2	1270	27	36	1270	40
	SUERC - 24563	Atlantic Cod bone (*Gadus morhua)*	-13.1	1315	29	36	1315	40

Table 4.15: Results of ^{14}C and δ^{13}C measurements on samples from Robert's Haven, Caithness

CHAPTER 5

ORIGINAL METHODS OF DATA HANDLING, CALCULATING RESULTS AND INTERPRETATIONS

The results presented in Chapter 4 were originally published using the statistical treatment detailed in section 5.1 (Russell et al., 2010). As the study progressed, this statistical treatment was re-evaluated and revised, leading to the development of a new method of data handling (Russell et al., 2011b) and subsequent re-interpretations: These are discussed in Chapter 6. Chapter 5 will deal with the original methods of data handling, the ΔR results produced and the original interpretations.

5.1 Statistical analysis and calculation of ΔR

The calculated radiocarbon ages for each site (Chapter 4, Tables 4.1 – 4.15) were subjected to chi-squared (χ^2) statistical testing to determine whether each sample within a group of terrestrial or marine material was statistically indistinguishable at 95% confidence from the remainder and therefore considered to be contemporary. It is commonplace in publication for radiocarbon dates to be rounded to the nearest 5 years for ease of interpretation and the errors are commonly rounded up to the nearest 5 years. The χ^2 test was performed using unrounded ages with rounded errors for each sample group. It was imperative that each sample within a group was determined to be contemporaneous with the remainder of the terrestrial or marine samples from that context (at 95% confidence). This would ensure that any age offset between the terrestrial and marine samples had an acceptable probability of being representative of a true MRE value for these samples, and did not represent the result of intrusive material. The critical value for the χ^2 test differs according to the number of measurements within a group of samples and this value is compared to the T- statistic for each group to determine whether the samples are statistically indistinguishable (Ward and Wilson, 1978). The calculation of the T-statistic is shown in Equation 5.1.

$$T = \sum \frac{(t_i - t)^2}{\sigma_i^2}$$

Where: t = the weighted mean of the ^{14}C age group (weighted by σ_i^2)

t_i = the individual ^{14}C measurement

σ_i = the error on the individual measurement

Equation 5.1: T-statistic calculation.

Where the T-statistic for the group was less than the critical value, the samples were considered to be contemporaneous, whereas where the T-statistic was greater than the critical value, the samples were not considered to be internally coherent and so the ages were subject to more intense scrutiny (see Ascough et al., 2007a). The method of calculating the T-statistic means that samples contributing significantly to the T-statistic can be identified as outliers, with a higher likelihood than the remainder of the samples to relate to contextual mixing/extended deposition. The results of the χ^2 test are shown in Table 5.1. Any results which had to be excluded in order for the remaining ages to pass the χ^2 test are identified in Table 5.2.

Ages that passed the χ^2 test, as described above, were then used to calculate ΔR. The ΔR value was calculated by converting the terrestrial ^{14}C age $\pm$ 1σ error to modelled marine age bounds using an interpolation between the INTCAL09 atmospheric curve and the MARINE09 curve (Reimer et al., 2009). The difference between the modelled and the measured marine age (from the measurement of the mollusc shells) is the ΔR value. The 1σ error on the ΔR values is calculated by a propagation of errors as shown in Equation 5.2 (assuming no covariance between the measured and modeled marine age).

$$\sigma_{\Delta R} = \sqrt{(\sigma_w + \sigma_m)^2}$$

Where ($\sigma_{\Delta R}$) = the 1σ error for the ΔR determination

(σ_w) = the error on the measured marine age

(σ_m) = the error on the modelled marine age.

Equation 5.2: Propagation of ΔR errors.

By using every possible pairing, typically 16 estimates of ΔR were calculated for each context. A weighted mean ΔR was then calculated to give a single representative value for each context, placing more weight on the values with lower associated errors, as is commonplace in statistical manipulations. The results for each site / context are shown in Table 5.3. A weighted mean terrestrial age for each context was also determined and then calibrated to produce a calendar age range for the context using OxCal 4.1 (Table 5.4).

5.2 Results

Results of all ^{14}C and $\delta^{13}C$ measurements are given in Chapter 4. The measured $\delta^{13}C$ values of the terrestrial mammal bones used within this study (-19.4‰ to -23.2‰), fall within the typical range for animals existing on purely terrestrial dietary resources in C3-dominated environments (e.g. DeNiro and Epstein, 1978; Chisholm et al., 1982; Post, 2002; Petersen and Fry, 1987; Schoeninger and DeNiro, 1984). Had there been a significant marine signal within the mammal's diet, this would have been reflected in a heavier $\delta^{13}C$ signal, which would have led to its rejection on the basis of it being unrepresentative of a wholly terrestrial sample. An example of the visible shift in $\delta^{13}C$ caused by marine contribution to diet can be seen in the values from seaweed eating sheep on Orkney. The bioapatite of these samples display considerably heavier $\delta^{13}C$ values by at least 8‰ compared to those expected for terrestrial herbivores, suggesting a significant marine contribution to diet (Balasse et al., 2005). The measured $\delta^{13}C$ values of the carbonized cereal grains ranged from -21.6‰ to -25.3‰, representative of a C3 photosynthetic pathway (Craig, 1953; O'Leary, 1981). The $\delta^{13}C$ values for the shells ranged from -2.1 to 2.9, within the accepted range for marine carbonate (Rounick and Winterbourn, 1986).

5.2.1 Chi-squared test results

Site	Terrestrial χ^2 T-statistic	Critical 95% acceptance value	Marine χ^2 T-statistic	Critical 95% acceptance value
Gallowgate middle school	4.04	7.81	0.98	7.81
16 - 18 Netherkirkgate	4.23	7.81	1.44	7.81
Arbroath Abbey	12.16	15.5	13.00	16.9
Horse Cross	8.25	9.49	0.81	11.07
Kirkgate 400	4.95	5.99	1.87	7.81
Kirkgate, 413	2.43	7.81	6.36	7.81
St Leonard's School	1.31	5.99	1.58	7.81
Archerfield, 90	2.67	14.07	12.82	14.07
Archerfield, 142	4.45	7.81	1.66	5.99
Scottish Seabird Centre 1226	2.14	5.99	2.10	7.81
Scottish Seabird Centre 1287	3.53	7.81	0.64	5.99
Castle Park 0341	3.79	7.81	1.92	7.81
Castle Park 3017	2.62	5.99	1.33	7.81

Table 5.1: Chi-squared test results for each context showing the critical value needed to pass the test at 95% confidence and the T-statistic for each group of terrestrial and material samples after exclusion of samples contributing highly to the T-statistic and therefore failing the test

(Where the T-statistic is less than the critical value, samples pass the χ^2 test. Samples which were excluded in order for the contexts to pass the test are shown in Table 5.2)

Site	Marine samples excluded from the group on the basis of the 95% χ^2 test.	Terrestrial samples excluded from the group on the basis of the 95% χ^2 test.
Arbroath abbey	SUERC – 16303	SUERC – 16290 SUERC – 16292 SUERC – 16293
Horse Cross		SUERC – 16280 SUERC – 16281
Kirkgate 400		SUERC – 19717
St Leonard's School		SUERC – 21117
Archerfield 142		SUERC – 19767
Scottish Seabird Centre 1226		SUERC – 29359
Scottish Seabird Centre 1287	SUERC – 29362	
Castle Park 3017		SUERC – 19105

Table 5.2: Samples that failed to pass the χ^2 test and had to be excluded on the basis of their large contribution to the T-statistic

Each context that produced ages that were excluded from the χ^2-test was scrutinized to ensure the data had not been subject to excessive rejection in order to pass the statistical analysis. If a context contained a large proportion of samples that were not considered contemporary, the likelihood of post-depositional disturbance increased, reducing confidence in the security of the context and therefore the validity of any ΔR that was calculated. Arbroath Abbey and Horse Cross were the only sites that produced multiple samples that had to be excluded as a result of their high contribution to the T statistic. It was deemed acceptable to exclude 1 sample from each group of 4 in order for the remainder to pass the χ^2-test and still avoid the risk of calculating a ΔR based on non-contemporaneous samples. 3 samples from the group of 12 terrestrial entities from Arbroath Abbey were excluded and although 2 samples were excluded from the group of 7 terrestrial samples from Horse Cross, it was considered acceptable for the remaining

material at both sites to be used in the study as representative of contemporaneous material from secure archaeological contexts. Thirteen contexts from 9 archaeological sites produced χ^2 test results that ensured confidence in the contemporeity of the samples, and were therefore used to calculate ΔR values (Table 5.3). 3 sites that did not produce suitable results were excluded from the study, owing to archaeological misidentification of the samples as contemporary marine and terrestrial entities and these sites are discussed in Appendix A.

5.2.2 ΔR results

Site	Weighted mean ΔR (^{14}C yrs BP)	Uncertainty on the weighted mean ± 2σ
Gallowgate middle school	-57	34
16 - 18 Netherkirkgate	-95	28
Arbroath Abbey	7	14
Horse Cross	15	24
Kirkgate 400	-2	24
Kirkgate, 413	8	34
St Leonard's School	-172	40
Archerfield, 90	-42	10
Archerfield, 142	-130	26
Scottish Seabird Centre 1226	39	30
Scottish Seabird Centre 1287	-21	38
Castle Park 3017	1	28
Castle Park 0341	4	28

Table 5.3: Weighted mean ΔR values calculated from the ^{14}C ages that passed the χ^2 test

(The error on the mean is shown at 2 σ)

The weighted mean ΔR value was calculated from the multiple ΔR values produced from the pairing of all suitable terrestrial and marine ages from each context. The mean values produced from all of the sites and contexts in this study range from -172 ± 40 to 39 ± 30 ^{14}C yrs BP (see Table 5.3). The samples provided for this study show a Medieval focus, from the Early Middle Ages (EMA) through the High Middle Ages (HMA) to the Late Middle Ages (LMA); this is due solely to the availability of suitable archaeological material. The definition of Scottish archaeological periods varies according to geographical location and so a general division of the Medieval period into High, Middle and Early Middle Ages was determined as the most representative definition of the time

period investigated for this thesis. The EMA ranged from the end of the Roman occupation in Southern Britain c. 400AD until the formation of the kingdom of Alba c. 900AD (Bell and Ogilvie, 1978). The HMA lasted from c. 900AD until the death of Alexander III and the Scottish Wars of independence in the 14th Century (Bartlett, 1993) and the Late Middle Ages define the period of independence from Britain until the beginning of the 16th Century (Nicholson, 1974).

Site	Weighted mean terrestrial age (BP)	Cal age range 2σ (AD)	General time period
Gallowgate Middle School	892 ± 41	1033 - 1220	(HMA)
16 - 18 Netherkirkgate	938 ± 41	1020 - 1185	(HMA)
Arbroath Abbey	644 ± 43	1280 -1400	(LMA)
Horse Cross	616 ± 45	1286 - 1410	(LMA)
Kirkgate 400	740 ± 55	1173 - 1389	(LMA)
Kirkgate, 413	639 ± 30	1283 - 1396	(LMA)
St Leonard's school	1246 ± 28	681 - 870	(EMA)
Archerfield, 90	492 ± 22	1410 - 1445	(LMA)
Archerfield, 142	520 ± 43	1310 - 1449	(LMA)
Scottish Seabird Centre 1226	1322 ± 41	645 - 776	(EMA)
Scottish Seabird Centre 1287	1469 ± 43	443 - 657	(EMA)
Castle Park 3017	1094 ± 40	870 - 1023	(HMA)
Castle Park 0341	1326 ± 39	646 - 773	(EMA)

Table 5.4: Weighted mean terrestrial ages for each context (with errors of 1 standard deviation) and their respective calendar age ranges calibrated using OxCal 4.1 (Bronk Ramsey 2009; Reimer, 2009)

(The corresponding time periods are shown to aid archaeological interpretation.)

5.3 Interpretations

The sites span most of the east coast of Scotland from the most northerly in Aberdeen to the most southerly in East Lothian. Many of the ΔR values are consistent around 0 ^{14}C yrs BP (the global average), but there are occasional excursions to negative values (for example the mean ΔR value from Archerfield 142 of -130 ^{14}C yrs BP), indicating the presence of water that is less depleted in ^{14}C. These variations in ΔR are often attributed to spatial or temporal relationships owing to local geology or topography influencing the carbon content of the surrounding waters or events influencing ocean regimes at certain times (Kennett et al., 1997; Kovanen and Easterbrook, 2002; Ascough et al., 2006). It can be observed in Figure 5.1 that although apparent spatial groupings of similar ΔR values are broadly evident, closer investigation does not reveal significant positive correlation with

topographical or geological features such as estuarine environments or limestone-rich areas that could influence the ^{14}C content of local waters. The majority of the east coast of Scotland displays a sandstone-rich geology, with no major outcrops of calcareous rocks, although some small seams are present in Aberdeenshire (Geological Map Data © NERC 2010). However, this does not sufficiently explain the significant deviations visible in the ΔR values, as significant shifts in ΔR values occur between individual sites even in areas with very similar geology, i.e. Archerfield and Dunbar.

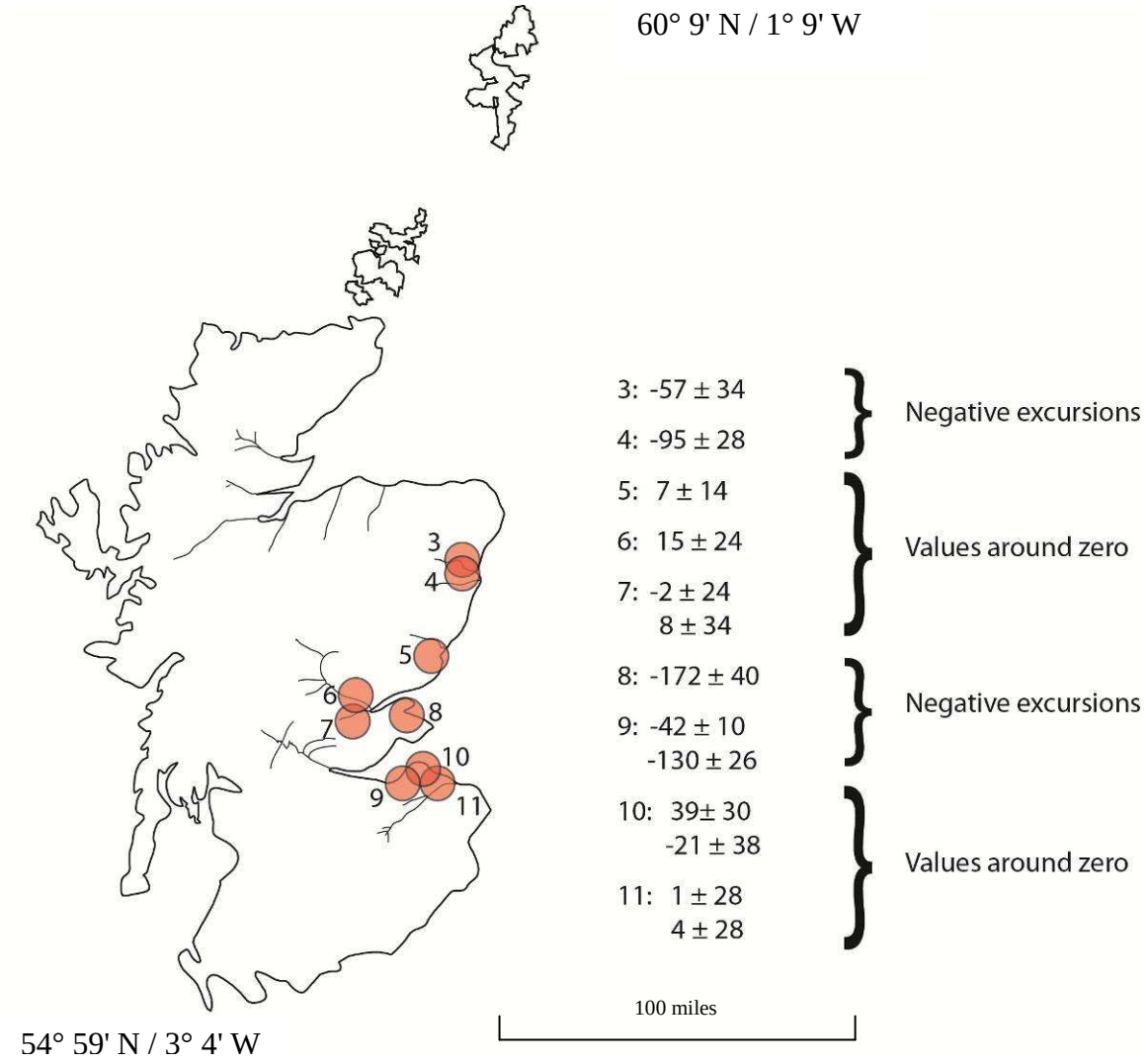

Figure 5.1: Spatial distribution of ΔR values after Russell et al., (2010)

(ΔR values displayed in ^{14}C yrs BP. Site numbers correspond to those in Figure 2.2)

One source of variability in the ΔR values may be differences in freshwater input, given the extensive run-off to the North Sea from the east coast of Scotland. It is assumed that shells precipitate their carbonate in equilibrium with the surrounding water and so can provide isotopic data for the ambient seawater (Epstein et al., 1953). Therefore, $\delta^{18}O$ shell

data were used to investigate whether the variation in ΔR values was a function of freshwater input to the environment in which the shells had grown.

In order to determine whether the variability in ΔR values (i.e. from within error of zero, to significant negative excursions) could be attributed to freshwater input alone, the mean $\delta^{18}O$ values of the shells were examined to see if any direct correlation could be drawn. The method for measurement of the stable carbon and oxygen isotope ratios of shell carbonate is described in section 3.2. The shells were crushed and homogenised prior to measurement, and so the samples measured were assumed to be representative of the mean $\delta^{18}O$ signal of the shell.

It is well known that shells have seasonality of growth and with this comes variability in $\delta^{18}O$ values (Shackleton, 1973; Jones and Quitmyer, 1996), but the purpose of this experiment was merely to determine whether groups of shells that were showing significant negative ΔR values also showed evidence for a freshwater input. Such a result would support the interpretation that these shells grew in water with a lower ^{14}C activity throughout the annual cycle (due to a freshwater input) than shells from sites with less negative ΔR values. ^{14}C levels can vary in the coastal zone due to the mixing of freshwater containing modern carbon with the ambient seawater, or mixing of freshwater containing "old carbon" components from the terrestrial environment with the ambient seawater (Dutta, 2008). The first of these possibilities would result in a net increase in local seawater ^{14}C, while the second would result in a net decrease in local seawater ^{14}C. Either of these factors (or a combination of both) has the potential to lead to varying levels of ^{14}C in specific locales, therefore driving the localised changes visible in the ΔR determinations. A representative value for the $\delta^{18}O$ of the surrounding water was calculated based upon the measured shell carbonate $\delta^{18}O$ using equation 5.3:

$$\delta^{18}O_w = \delta^{18}O_C\text{-}((16.9\text{-}T)/4.38))$$

Where $(\delta^{18}O_w)$ = Derived water $\delta^{18}O$

$(\delta^{18}O_C)$ = measured shell carbonate $\delta^{18}O$

(T) = Average water temperature

Equation 5.3: Calculation of $\delta^{18}O$ for water in which sampled shells were formed. (Epstein et al., 1953)

Mean values of $\delta^{18}O_C$ were calculated for each context before converting to $\delta^{18}O_w$ values. The derived value of $\delta^{18}O_w$ was converted to the SMOW scale using the relationship: $\delta^{18}O_w$ (VPDB) = $\delta^{18}O_w$ (SMOW) – 0.27 (Hut, 1987; Bemis et al., 1998) and is shown for all 13 contexts in Table 5.5. An average temperature of 8.5°C was chosen on the basis of CEFAS (http://www.cefas.co.uk/) data for surface waters in the North Sea. It is acknowledged that temperature can vary in the coastal waters investigated, but as most of the shells are from a similar time period and with the lack of precise climatic information for this period, it was felt that using this mean temperature was justifiable. Any large temporal shifts in sea surface temperature (SST) between the sample groups could have influenced the $\delta^{18}O_C$ results without reflecting changes in $\delta^{18}O_{w.}$ Acknowledgement must be given to this factor although there is nothing in the literature or proxy records from the time to suggest such short, sharp changes in the SST of the North Sea at this time. These shifts in SST would have to be specific to the individual site as any shifts in mean temperature across the dataset would have forced the results in the same direction. Essentially, the purpose of the investigation was to identify any large $\delta^{18}O$ differences within the dataset that were not related to changes in temperature and were obviously attributable to significant freshwater input and could therefore potentially be causing the changes in ΔR.

Ocean water salinity and $\delta^{18}O$ are proportionally related for the study region as shown in Figure 5.2, using the mixing line for the North Sea region as generated by Austin et al., (2006) using $\delta^{18}O_w = 0.18*S\text{-}6.0$. The calculated sample $^{18}O_w$ SMOW values are shown in Table 5.5 and were plotted on the salinity mixing line in Figure 5.2 to determine whether

values were representative of open coastal/marine water with high salinity or freshwater with low salinity.

Site	$\delta^{18}O_w$ SMOW (ppt) (±0.08‰)	Salinity (PSU)
Gallowgate Middle School	0.4	33.7
16 - 18 Netherkirkgate	0.9	34.3
Arbroath Abbey	0.4	33.7
Horse Cross	-0.5	32.8
Kirkgate 400	-0.7	32.6
Kirkgate, 413	-0.7	32.7
St Leonard's School	0.5	33.8
Archerfield, 90	0.5	33.8
Archerfield, 142	0.5	33.9
Scottish Seabird Centre 1226	0.8	34.1
Scottish Seabird Centre 1287	0.6	33.9
Castle Park 0341	0.4	33.8
Castle Park 3017	0.7	34.1

Table 5.5: $\delta^{18}O$ results for the 13 contexts and the derived salinity using $\delta^{18}O_w = 0.18*S-6.0$ (Austin et al., 2006)

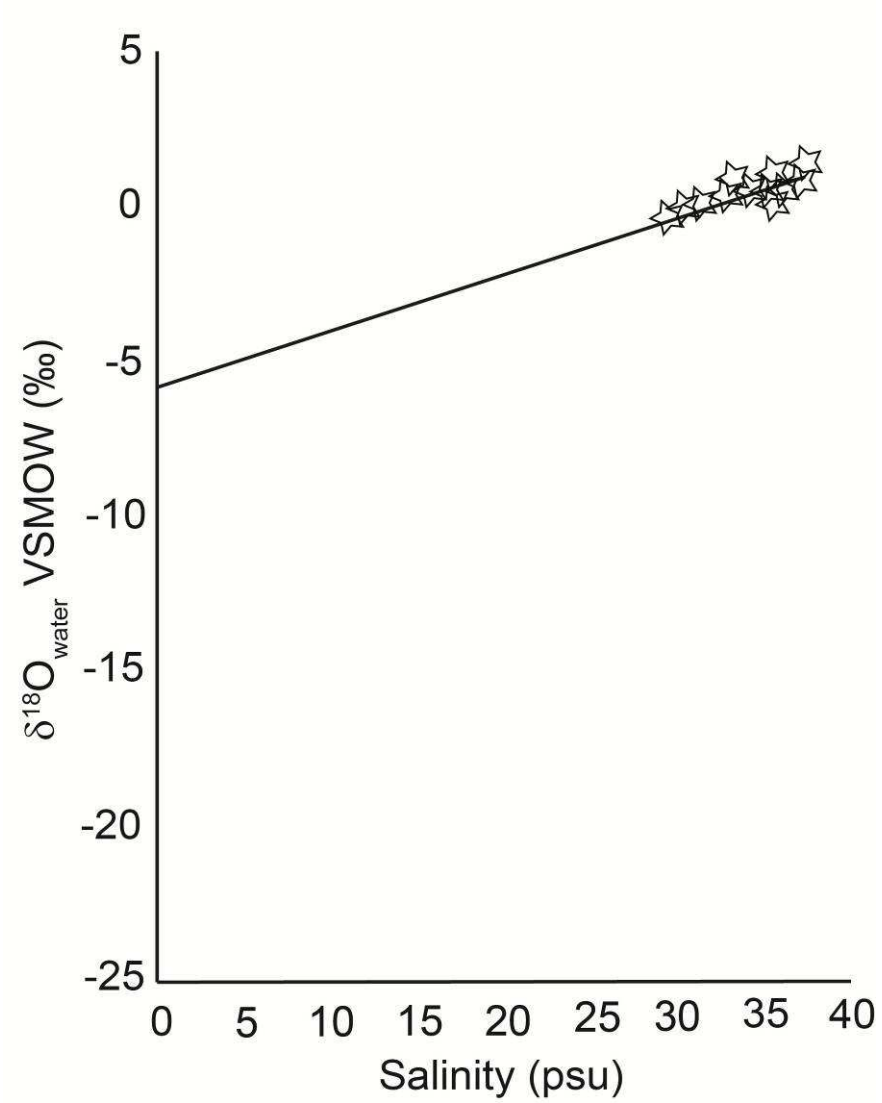

Figure 5.2: Relationship between $\delta^{18}O_w$ and salinity, (after Austin et al., 2006), showing the calculated values for $\delta^{18}O_w$ derived from measured $\delta^{18}O_c$ for the sample shells after Russell et al., 2010

It can be observed from Figure 5.2 that all of the shell $\delta^{18}O$ values for the 9 sites are located in the high salinity position on the mixing line. It would appear from these data that none of the shells within the sample set grew in water with a significant freshwater input and therefore freshwater input is unlikely to be an underlying cause of the variability in ΔR values. As no positive correlation could be observed between the ΔR values and the geographical distribution of the sites and proximity to freshwater input, the possibility of a temporal relationship seemed the next logical step of investigation.

Knowing that proxy data and climatic records show peak British temperatures towards the end of the 12th century AD followed by a general cooling towards the Little Ice Age of the Late Medieval/Early Modern period (1564 – 1730's) (Reiter, 2000), it was hypothesised

that these climatic changes could be allied with oceanic circulation shifts resulting in variation in the composition of water entering the North Sea. Such variation would be a potential cause of changes in ΔR. However, the results from the plotted data in Figure 5.3 show that no directly proportional relationship exists between ΔR and terrestrial age.

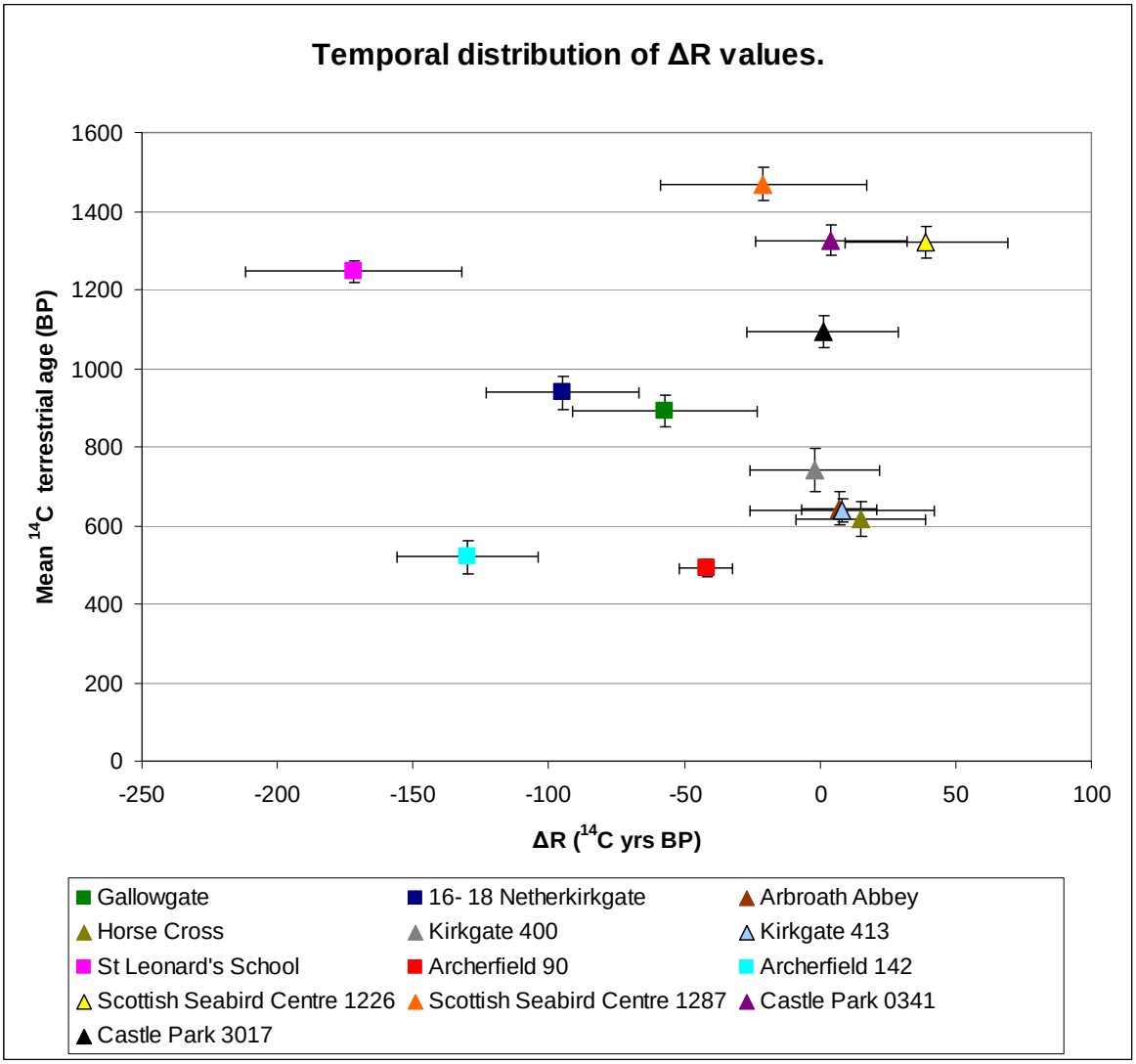

Figure 5.3: Temporal relationships in ΔR values ± 2σ showing little correlation of ΔR with time (R^2 = 0.0017)

As North Sea coastal water originates from west coast Atlantic waters with a small Atlantic input via the FIC, the possibility exists that the shifts in ΔR may act as a proxy for shifts in Atlantic values at the same time and therefore indicate shifts in circulatory patterns and/or sources of Atlantic water as shown in previous studies where oceanic circulatory changes are marked by variations in ΔR values (Bersch et al., 2007; Hakkinen and Rhines, 2009). The North Sea data presented here show greater variability than the consistently negative

data produced by Ascough et al., (2004) for the Atlantic Middle Iron Age in Scotland where the average $\Delta R = -79 \pm 17$ ^{14}C yrs BP. It is acknowledged that Ascough's study and the data presented in this thesis consider different time periods throughout the Holocene, but the complication of east coast estuarine mixing processes compared to the open marine conditions on the west coast may have provided an explanation for the additional variability in the east coast ΔR values. Preliminary oxygen isotope data suggest that major freshwater contributions are not evident in the shells and therefore freshwater input is not an obvious cause of the variations in ΔR.

The remaining possibility is therefore that Atlantic water entering the North Sea has experienced changes in composition or perhaps magnitude throughout the periods investigated in this study, leading to varying levels of ^{14}C in North Sea surface waters. The small direct Atlantic contribution to the SNSCZ provided by the FIC is coupled with SCW (W), also Atlantic derived, which provides the major constituent of SCW (E) and so short, sharp shifts in AW may be readily apparent in the North Sea water. The possibilities remain that either the ΔR for the region is around zero, with excursions to negative values caused by incursions of less depleted water or that the ΔR value for the region is indeed negative and therefore more similar to the west coast values published by Ascough et al., (2004), with incursions of more depleted water. The consistency in the data for ΔR values around zero in the present dataset when compared to the more variable negative values (e.g. Archerfield), plus the results of shell sample $\delta^{18}O$ measurements suggests that the changes in ΔR represented on the east coast of Scotland are being driven by incursions of less depleted water of marine origin.

Previous large-scale changes in the composition of North Sea water have been documented, such as the Great Salinity Anomaly, which involved a decrease in North Sea salinities during the mid to late 1970's. This was explained by Dickson et al., (1988) as alteration of the mean pressure over the European Arctic resulting in an increase of Arctic water flowing to the south, thus reducing the temperature and salinity of the waters to the east of Greenland (Turrell, 1992). This hypothesis was challenged by Turrell et al., (1992) who proposed that the anomaly was the result of a drop in production of 18º mode water (water with homogenous salinity, density, and temperature of around 18°C) in the Sargasso Sea, coupled with predominantly northerly winds over the Greenland sea forcing a decline in the Gulf Stream and therefore the supply to the North Sea. These water bodies, reduced

in temperature and salinity then followed the circulatory system of the North Atlantic, and into the North Sea. This relatively recent shift in the composition of North Sea water may support our hypothesis of previous changes in Atlantic water composition causing shifts in ΔR values.

5.4 Conclusions

The variable values of ΔR obtained for the North Sea within the period from c. 600 to 1500AD, ranging from -172 to +39 ^{14}C years, show little correlation with time (R^2= 0.0017). The spatial pattern of the ΔR values at first appears to show faint groupings of values within error of zero, and values that are significantly negative. These spatial groupings do not appear attributable to any obvious topographic or geological features that could affect the ^{14}C content of local waters. The possibility of the changes in ΔR manifesting themselves as a direct result of proximity to an estuarine location was investigated via ^{18}O analysis of the shell samples, however, there was no variation in the results that could explain the range in ΔR values as being directly related to a significant freshwater input. This leaves two possible reasons for the shift in ΔR; firstly, that the ΔR for the region is close to zero, with the excursions to negative values being driven by the incursion of younger, less depleted Atlantic water during relatively rapid, local events or secondly, that the ΔR for the region is negative, although exceedingly variable, with the excursions to zero values being driven by the incursion of older, more depleted Atlantic water. The apparent stability in the data for ΔR values around zero supports the first statement. The second hypothesis is supported by observations that previous incursions of older water to the area have been documented i.e. the Great Salinity Anomaly, however, it is not supported by the fact that the excursions to negative ΔR values are very variable, suggesting that these incursions of older water vary greatly in their intensity and/or specific ^{14}C activity. Therefore, the most likely mechanism for the ΔR values observed in this study is that the underlying ΔR value for the region during the Medieval period is around zero with occasional episodes of less depleted water of marine origin entering the North Sea system, resulting in negative values. The source of these events driving the changes in Atlantic source water to the North Sea is as yet unknown, but provides the focus for further study in this region alongside further investigation of estuarine processes in order to understand the variability in ΔR for the region. Finally, this study demonstrates the care required when dealing with marine based carbon from this region and the consequent

calibration of ^{14}C ages using assumed ΔR values for the North Sea.

CHAPTER 6

NEW METHODS OF DATA HANDLING, CALCULATING RESULTS AND INTERPRETATIONS

In order to investigate the variability in ΔR values shown in Chapter 5, this study focused on defining whether the values from the 13 contexts ranging from -172 to +39 ^{14}C yrs BP were truly significantly different from one another. This involved challenging the convention of publishing mean ΔR values and the associated error on that mean. It became apparent that the spread of ΔR values produced during the multiple paired sample calculations for each context was being under-represented by publishing a single mean value and the associated error on the mean. A revised method of data handling was employed to ensure future ΔR calculations addressed any possible sources of variation within the ΔR derivation itself and published a more representative error for mean values.

To summarise from previous discussion (chapters 1,2 and 3), the potential uncertainties inherent in deriving ΔR values fall into four main categories which are discussed by Russell et al., (2011b):

1) the samples used to generate the ^{14}C ages from which the ΔR values will be calculated,
2) the generation of the sample ^{14}C ages and their associated errors,
3) the modelled marine ^{14}C ages used in ΔR calculation (see Figure 2.1) and the uncertainty arising from the use of a relatively simple marine model to generate these, and
4) the actual calculation of the ΔR value, and the number of ^{14}C ages used in its calculation.

This chapter assesses the degree to which apparent shifts in ΔR values can be explained by examining the degree of variability inherent in the production of single (mean) ΔR values, even when based upon multiple paired samples. In so doing, this work challenges the reproducibility of ΔR values that are derived using single pairs of terrestrial and marine ^{14}C ages in other methodological approaches. An important point is that the marine model uncertainties (point 3 above) are not further considered in this present study. These model

uncertainties are likely to be considerable and will add in quadrature to the 3 main variability points discussed below; however, consideration of this uncertainty is outside the scope of this study but is recommended for future investigation in Chapter 8. New data handling and publication methods are discussed here and lead to the proposition of a best-practice method of publishing ΔR determinations and associated errors, in order to incorporate the sources of variability discussed above.

6.1 Data analysis and calculation of ΔR

In order to address the issues in the production of an appropriate error term for ΔR calculations, sources of error and uncertainty associated with the determination of a ΔR value have been identified as follows:

1) Underpinning the ΔR calculation lies a marine (box diffusion) model and the uncertainty on this has not been considered here. As discussed above, to quantify the model uncertainty is beyond the scope of this study; nevertheless, it is clear that the effect of this uncertainty would be to increase the variability in the ΔR values.
2) Uncertainty regarding the contemporaneity of terrestrial and marine ^{14}C ages used to generate ΔR values. These uncertainties and recommendations for sample selection criteria that minimize such uncertainties are discussed in Chapter 2.1 and in detail by Ascough et al., (2005a). Any uncertainties associated with sample selection and identification for this thesis have been minimized by adhering to the strict selection policy outlined in Chapter 2.1 and by maintaining excellent communication with sample submitters.
3) Errors associated with the ^{14}C analysis procedures: These include: (i) Contamination - this is an unquantifiable error that can derive from contamination at any stage throughout the entire laboratory process and incorporates any human error in the sample preparation. As far as possible, this can be identified by reference to known age standards measured in the same batch as the unknown samples, although 100% elimination of contamination can never be guaranteed; (ii) Inappropriate errors placed on the age measurements - this estimate of the error has to be realistic and should not be based solely on counting statistics. At SUERC, the counting error is based on overall statistics of approximately 3‰ or better but the final quoted error associated with a measurement is limited by the standard

deviation on a series of standards of known activity, of which there are typically 13 in a batch (Naysmith et al., 2010). An in-depth discussion of SUERC's in-house secondary standards is presented in Chapter 3.3.

In order to prevent the introduction of any unnecessary variability into the ΔR calculation, the results from Chapter 4 were handled according to the new methodology developed here in Chapter 6, using unrounded age measurements and unrounded errors, the latter limited by the standard deviation on the batch standards. The convention at SUERC and generally in the ^{14}C community has been to round errors up to the next multiple of 5 years. It is conceivable that some ΔR values could be calculated with ^{14}C errors that are unrounded, or rounded differently than to the nearest 5 years. This has the potential to introduce a source of uncertainty in ΔR calculation, as the number of individual sample ^{14}C ages in a group identified as contemporaneous by the χ^2 test is affected by the size of the error on each ^{14}C age. Underestimation of the sample ^{14}C errors can lead to fewer ^{14}C ages passing the χ^2 test for contemporaneity. Conversely, overestimation of sample ^{14}C errors may lead to a larger number of the tested ^{14}C ages passing the χ^2 test. Examples of the possible differences in ΔR values calculated using rounded versus unrounded errors are discussed by Russell et al., (2011a) and detailed in section 6.2.1. It is possible that under some circumstances, statistically different values could arise from the use of unrounded versus rounded data, meaning this consideration is not a trivial one for ΔR calculations. Acknowledgement must be given to the fact that unrounded ages may not be available to all researchers carrying out ΔR investigations, and while the use of unrounded dates is recommended as best practice, this may be applicable only under ideal circumstances.

6.2 Results - New methods

The χ^2 testing of the ^{14}C ages was carried out as per Chapter 5, with the main difference being that unrounded age measurements were used alongside unrounded errors. The results are shown in Table 6.1. Table 6.2 shows samples that had to be excluded in order to pass the χ^2-test. The same rationale was applied to excluding samples as described in Chapter 5, resulting in the calculation of ΔR values for 13 contexts from 9 sites.

6.2.1 χ^2 test results

Site	Terrestrial χ^2 T statistic	Critical value	Marine χ^2 T statistic	Critical value
Gallowgate Middle School	4.28	7.81	1.00	7.81
16 - 18 Netherkirkgate	4.48	7.81	1.60	7.81
Arbroath Abbey	13.36	15.50	14.47	16.90
Horse Cross	8.64	9.49	0.84	11.07
Kirkgate 400	2.02	5.99	5.68	7.81
Kirkgate, 413	2.59	7.81	7.23	7.81
St Andrews	1.44	5.99	1.89	7.81
Archerfield, 90	3.20	14.07	10.96	12.60
Archerfield, 142	4.71	7.81	1.76	5.99
Scottish Seabird Centre 1226	2.25	5.99	2.21	7.81
Scottish Seabird Centre 1287	3.71	7.81	0.68	5.99
Castle Park 0341	4.02	7.81	2.04	7.81
Castle Park 3017	2.62	5.99	1.41	7.81

Table 6.1: χ^2 test results for each context showing the critical value needed to pass the test and the T statistic for each group of terrestrial and material samples after exclusion of samples contributing highly to the T statistic and therefore failing the χ^2 test

(Where the T statistic is less than the critical value, samples pass the test. Samples which were excluded in order for the contexts to pass the test are shown in Table 6.2)

Site	Excluded marine samples	Excluded terrestrial samples
Arbroath Abbey	SUERC – 16303	SUERC – 16290 SUERC – 16292 SUERC – 16293
Horse Cross		SUERC – 16280 SUERC – 16281
Kirkgate 400		SUERC – 19717
St Andrews		SUERC – 21117
Archerfield 90	SUERC-19669	
Archerfield 142		SUERC – 19767
Scottish Seabird Centre 1226		SUERC – 29359
Scottish Seabird Centre 1287	SUERC – 29362	
Castle Park 3017		SUERC – 19105

Table 6.2: Samples that failed to pass the χ^2 test and had to be excluded on the basis of their large contribution to the T statistic

It can be observed from a comparison of Table 6.2 with Table 5.2 that using the unrounded ages and errors leads to the additional exclusion of one marine ^{14}C age (SUERC-19669) from the sample group from Archerfield 90, in order to pass the χ^2 test. In Table 5.2 SUERC-19669 passed the χ^2 test using rounded values. In Table 6.2, using unrounded values, SUERC-19669 does not pass the χ^2 test. The use of unrounded ages for these samples therefore results in the use of a different set of samples (i.e. excluding SUERC-19669) for ΔR calculation compared to the use of rounded ages (as in Chapter 5) (when all

samples would pass the χ^2 test and SUERC-19669 would be included).

In order to introduce as little unnecessary additional uncertainty as possible, the decision was made to use unrounded ^{14}C ages from this point forth in the study. The error on a measurement is limited in accordance with the variability on a set of standards (shown for each batch of samples in Chapter 4). For some contexts, the standard deviation on the ^{14}C ages within each sample group is larger than either the unrounded errors on the individual samples or the standard deviation on the standards for the batch in which they were measured. Therefore, there is additional variability associated with these groups of samples that is either associated with the age of the samples or the integrity of the context. A conservative approach is therefore proposed of using the standard deviation on the individual sample groups after χ^2-testing as the limiting factor on the error on the ages for ΔR calculations. To define this approach, an example from Archerfield (Context 90) is shown in Table 6.3 using the data from Table 4.8. The errors on each individual measurement are limited by the standard deviation on the batch standards to ± 32 ^{14}C years. For the terrestrial dataset, the standard deviation for the sample group is 22 ^{14}C years which is less than the error on the individual measurements and the standard deviation on the known age standards. However, for the marine data, the standard deviation within the sample group of 43 ^{14}C years is considerably larger than either term discussed above. The error of ± 32 ^{14}C yrs BP would be used to test the samples for contemporeity using the χ^2-test and samples that then passed the χ^2-test would then be used to calculate ΔR with an error of 32 ^{14}C yrs BP for the terrestrial samples and 43 ^{14}C years for the marine samples.

All of the results from Chapter 4 were recalculated using unrounded ages and errors for the χ^2-test. Ages that passed the chi test were then used to calculate ΔR. ΔR's were calculated using unrounded ages and unrounded errors unless the standard deviation on a sample group was larger than the error on the measurement, in which case the standard deviation would be used as the error on the age of samples from that group. The recalculated results are shown in Table 6.4.

	Sample lab code	^{14}C age (BP) ± 1σ (no rounding)
Terrestrial	SUERC - 19680	497 ± 32
	SUERC - 19681	471 ± 32
	SUERC - 19685	502 ± 32
	SUERC - 19686	493 ± 32
	SUERC - 19687	485 ± 32
	SUERC - 19688	502 ± 32
	SUERC - 19689	455 ± 32
	SUERC - 19690	527 ± 32
	Mean ± 1 std dev	**492 ±22**
Marine	SUERC - 19670	830 ± 32
	SUERC - 19671	912 ± 32
	SUERC - 19675	897 ± 32
	SUERC - 19676	910 ± 32
	SUERC - 19677	840 ± 32
	SUERC - 19678	932 ± 32
	SUERC - 19679	940 ± 32
	Mean ± 1 std dev	**886 ± 43**

Table 6.3: ^{14}C results for marine and terrestrial samples from Archerfield 90 (data from Russell et al., 2010)

6.2.2 ΔR results

Publishing the mean value from ΔR calculations for each context is commonplace (Ascough et al., 2004, 2005a, 2005b, 2006, 2007a, 2007b, 2009; Reimer et al., 2002; Russell et al., 2010; Soares and Martins, 2010; Weisler et al., 2009) and provides a concise method of presenting the values. By employing a multiple paired sample approach, there is the possibility for multiple values of ΔR to be produced using a matrix-type approach of individual pairings. These multiple values are combined and a weighted mean value published to avoid the complication of large datasets as shown in Table 6.4. Other approaches can involve calculating a mean value for the multiple terrestrial and/or marine ages and then performing a single ΔR determination e.g. Soares and Alveirinho, (2006, 2007). No matter which variant of the multiple paired sample approach is employed, the dataset showing every possible ΔR value from the individual pairings is rarely published. In order to understand the true spread of ΔR values from a multiple paired sample approach as a more appropriate measure of variability, a useful method is to employ a histogram to display these derived multiple ΔR values (e.g. in most instances for this study, the range of 16 ΔR values calculated from individual pairings of 4 terrestrial and 4

marine sample ^{14}C ages). The histogram should be illustrated alongside the mean value (Figures 6.1-6.13). For the purposes of this study, histograms were constructed using Minitab® 16. The spread of values as displayed in Table 6.4 are plotted in the histograms in Figures 6.1 – 6.13.

	Sample pairing (SUERC no)		ΔR (^{14}C yrs BP)	Error	Sample pairing (SUERC no)		ΔR (^{14}C yrs BP)	Error
Gallowgate	17031	17027	-43	77	17035	17027	-45	77
		17028	-85	76		17028	-87	77
		17029	-85	76		17029	-87	77
		17030	-74	77		17030	-76	77
	17036	17027	-86	70	17037	17027	28	59
		17028	-128	69		17028	-14	58
		17029	-128	69		17029	-14	58
		17030	-117	70		17030	-3	59
Weighted mean ΔR = -59. Standard deviation = 46 (both ^{14}C yrs BP)								

Table 6.4(a): All possible pairings of ΔR for Gallowgate showing the weighted mean value for ΔR alongside one standard deviation on the spread of values

	Sample pairing (SUERC no)		ΔR (^{14}C yrs BP)	Error	Sample pairing (SUERC no)		ΔR (^{14}C yrs BP)	Error
16-18 Netherkirkgate	17252	17248	-77	62	17253	17248	-57	65
		17249	-40	62		17249	-20	65
		17250	-86	62		17250	-66	66
		17251	-40	62		17251	-20	66
	17254	17248	-87	64	17258	17248	-150	36
		17249	-50	64		17249	-113	36
		17250	-96	65		17250	-159	35
		17251	-50	65		17251	-113	35
Weighted mean ΔR = -98. Standard deviation = 42 (both ^{14}C yrs BP)								

Table 6.4(b): All possible pairings of ΔR for 16-18 Netherkirkgate showing the weighted mean value for ΔR alongside one standard deviation on the spread of values

	Sample pairing (SUERC no)		ΔR (^{14}C yrs BP)	Error	Sample pairing (SUERC no)		ΔR (^{14}C yrs BP)	Error
Arbroath Abbey	16284	16294	3	81	16286	16294	10	78
		16295	24	81		16295	31	78
		16296	40	81		16296	47	78
		16300	10	81		16300	17	78
		16301	54	81		16301	61	78
		16302	28	81		16302	35	78
		19705	-42	81		19705	-35	78
		19706	17	81		19706	-10	78
		19707	-86	81		19707	-79	78
		19708	-22	81		19708	-15	78
	16291	16294	5	80	17041	16294	5	80
		16295	26	80		16295	26	80
		16296	42	80		16296	42	80
		16300	12	80		16300	12	80
		16301	56	80		16301	56	80
		16302	30	80		16302	30	80
		19705	-40	80		19705	-40	80
		19706	-15	80		19706	-15	80
		19707	-84	80		19707	-84	80
		19708	-20	80		19708	-20	80
	17045	16294	19	75	19709	16294	45	72
		16295	40	75		16295	66	72
		16296	56	75		16296	82	72
		16300	26	75		16300	52	72
		16301	70	75		16301	96	72
		16302	44	75		16302	70	72
		19705	-26	75		19705	0	72
		19706	-1	75		19706	25	72
		19707	-70	75		19707	-44	72
		19708	-6	75		19708	20	72
	19710	16294	23	74	19711	16294	42	74
		16295	44	74		16295	63	74
		16296	60	74		16296	79	74
		16300	30	74		16300	49	74
		16301	74	74		16301	93	74
		16302	48	74		16302	67	74
		19705	-22	74		19705	-3	74
		19706	3	74		19706	22	74
		19707	-66	74		19707	-47	74
		19708	-2	74		19708	17	74
	19715	16294	61	69				
		16295	82	69				
		16296	98	69				
		16300	68	69				
		16301	112	69				
		16302	86	69				
		19705	16	69				
		19706	41	69				
		19707	-28	69				
		19708	36	69				
Weighted mean ΔR = 22. Standard deviation = 45 (both ^{14}C yrs BP)								

Table 6.4(c): All possible pairings of ΔR for Arbroath Abbey showing the weighted mean value for ΔR alongside one standard deviation on the spread of values

	Sample pairing (SUERC no)		ΔR (^{14}C yrs BP)	Error	Sample pairing (SUERC no)		ΔR (^{14}C yrs BP)	Error
Horse Cross	16276	16270	-9	71	16282	16270	-19	73
		16271	-8	72		16271	-18	74
		16272	-19	72		16272	-29	74
		16273	14	72		16273	4	74
		16274	1	72		16274	-9	74
		17038	-25	71		17038	-35	73
	20276	16270	-11	71	20277	16270	48	62
		16271	-10	72		16271	49	64
		16272	-21	72		16272	38	64
		16273	12	72		16273	71	64
		16274	-1	72		16274	58	64
		17038	-27	71		17038	32	62
	20278	16270	30	66				
		16271	31	67				
		16272	20	67				
		16273	53	67				
		16274	40	67				
		17038	14	66				
Weighted mean ΔR = 12. Standard deviation = 30 (both ^{14}C yrs BP)								

Table 6.4(d): All possible pairings of ΔR for Horse Cross showing the weighted mean value for ΔR alongside one standard deviation on the spread of values

	Sample pairing (SUERC no)		ΔR (^{14}C yrs BP)	Error	Sample pairing (SUERC no)		ΔR (^{14}C yrs BP)	Error
Kirkgate 400	18883	18876	-66	49	18884	18876	39	80
		18880	-40	50		18880	65	81
		18881	-9	50		18881	96	81
		18882	-68	50		18882	37	81
	19718	18876	-18	43				
		18880	8	44				
		18881	39	44				
		18882	-20	44				
Weighted mean ΔR = -8. Standard deviation = 52 (both ^{14}C yrs BP)								

Table 6.4(e): All possible pairings of ΔR for Kirkgate 400 showing the weighted mean value for ΔR alongside one standard deviation on the spread of values

	Sample pairing (SUERC no)		ΔR (^{14}C yrs BP)	Error	Sample pairing (SUERC no)		ΔR (^{14}C yrs BP)	Error
Kirkgate 413	18892	18885	15	74	18893	18885	-13	77
		18886	88	74		18886	60	77
		18890	-32	74		18890	-60	77
		18891	49	74		18891	21	77
	19719	18885	-11	76	19720	18885	-21	80
		18886	62	76		18886	52	80
		18890	-58	76		18890	-68	80
		18891	23	76		18891	13	80
Weighted mean ΔR = 8. Standard deviation = 48 (both ^{14}C yrs BP)								

Table 6.4(f): All possible pairings of ΔR for Kirkgate 413 showing the weighted mean value for ΔR alongside one standard deviation on the spread of values

	Sample pairing (SUERC no)		ΔR (^{14}C yrs BP)	Error	Sample pairing (SUERC no)		ΔR (^{14}C yrs BP)	Error
St Leonard's School	19109	19665	-126	69	19110	19665	-194	62
		19666	-136	69		19666	-204	62
		19667	-145	69		19667	-213	62
		19668	-184	69		19668	-252	62
	21121	19665	-118	68				
		19666	-128	68				
		19667	-137	68				
		19668	-176	68				
Weighted mean ΔR = -172. Standard deviation = 42 (both ^{14}C yrs BP)								

Table 6.4(g): All possible pairings of ΔR for St Leonard's School showing the weighted mean value for ΔR alongside one standard deviation on the spread of values

	Sample pairing (SUERC no)		ΔR (^{14}C yrs BP)	Error	Sample pairing (SUERC no)		ΔR (^{14}C yrs BP)	Error
Archerfield 90	19680	19670	-101	49	19681	19670	-86	48
		19671	-19	49		19671	-4	48
		19675	-34	49		19675	-19	48
		19676	-21	49		19676	-6	48
		19677	-91	49		19677	-76	48
		19678	1	49		19678	16	48
		19679	9	49		19679	24	48
	19685	19670	-104	49	19686	19670	-99	49
		19671	-22	49		19671	-17	49
		19675	-37	49		19675	-32	49
		19676	-24	49		19676	-19	49
		19677	-94	49		19677	-89	49
		19678	-2	49		19678	3	49
		19679	6	49		19679	11	49
	19687	19670	-95	49	19688	19670	-104	49
		19671	-13	49		19671	-22	49
		19675	-28	49		19675	-37	49
		19676	-15	49		19676	-24	49
		19677	-85	49		19677	-94	49
		19678	7	49		19678	-2	49
		19679	15	49		19679	6	49
	19689	19670	-75	47	19690	19670	-118	48
		19671	7	47		19671	-36	48
		19675	-8	47		19675	-51	48
		19676	5	47		19676	-38	48
		19677	-65	47		19677	-108	48
		19678	27	47		19678	-16	48
		19679	35	47		19679	-8	48
Weighted mean ΔR = -33. Standard error for predicted values = 42 (both ^{14}C yrs BP)								

Table 6.4(h): All possible pairings of ΔR for Archerfield 90 showing the weighted mean value for ΔR alongside one standard deviation on the spread of values

	Sample pairing (SUERC no)		ΔR (^{14}C yrs BP)	Error	Sample pairing (SUERC no)		ΔR (^{14}C yrs BP)	Error
Archerfield 142	19760	19757	-117	45	19761	19757	-118	45
		19758	-90	45		19758	-91	45
		19759	-153	45		19759	-154	45
	19762	19757	-199	66	19763	19757	-113	44
		19758	-172	66		19758	-86	44
		19759	-235	66		19759	-149	44
Weighted mean ΔR = -130. Standard deviation = 46 (both ^{14}C yrs BP)								

Table 6.4(i): All possible pairings of ΔR for Archerfield 142 showing the weighted mean value for ΔR alongside one standard deviation on the spread of values

	Sample pairing (SUERC no)		ΔR (^{14}C yrs BP)	Error	Sample pairing (SUERC no)		ΔR (^{14}C yrs BP)	Error
Scottish Seabird Centre 1226	29353	29349	46	68	29357	29349	-13	49
		29350	116	68		29350	57	49
		29351	118	68		29351	59	49
		29352	93	68		29352	34	49
	29358	29349	-28	46				
		29350	42	46				
		29351	44	46				
		29352	19	46				
Weighted mean ΔR = 39. Standard deviation = 45 (both ^{14}C yrs BP)								

Table 6.4(j): All possible pairings of ΔR for Scottish Seabird Centre 1226 showing the weighted mean value for ΔR alongside one standard deviation on the spread of values

	Sample pairing (SUERC no)		ΔR (^{14}C yrs BP)	Error	Sample pairing (SUERC no)		ΔR (^{14}C yrs BP)	Error
Scottish Seabird Centre 1287	29367	29360	-62	52	29368	29360	-48	56
		29361	-28	52		29361	-14	56
		29363	-71	52		29363	-57	56
	29369	29360	-23	56	29370	29360	8	49
		29361	11	56		29361	42	49
		29363	-32	56		29363	-1	49
Weighted mean ΔR = -21. Standard deviation = 34 (both ^{14}C yrs BP)								

Table 6.4(k): All possible pairings of ΔR for Scottish Seabird Centre 1287 showing the weighted mean value for ΔR alongside one standard deviation on the spread of values

	Sample pairing (SUERC no)		ΔR (^{14}C yrs BP)	Error	Sample pairing (SUERC no)		ΔR (^{14}C yrs BP)	Error
Castle Park 0341	19098	19094	-3	38	19099	19094	80	68
		19095	-15	38		19095	68	68
		19096	-62	38		19096	21	68
		19097	-50	38		19097	33	68
	19100	19094	68	72	19104	19094	70	71
		19095	56	72		19095	58	71
		19096	9	72		19096	11	71
		19097	21	72		19097	23	71
Weighted mean ΔR = 4. Standard deviation = 42 (both ^{14}C yrs BP)								

Table 6.4(l): All possible pairings of ΔR for Castle Park 0341 showing the weighted mean value for ΔR alongside one standard deviation on the spread of values

	Sample pairing (SUERC no)		ΔR (^{14}C yrs BP)	Error	Sample pairing (SUERC no)		ΔR (^{14}C yrs BP)	Error
Castle Park 3017	19106	19658	30	41	19107	19658	-31	52
		19659	13	43		19659	-48	54
		19660	25	43		19660	-36	54
		19661	67	43		19661	6	54
	19108	19658	-26	53				
		19659	-43	55				
		19660	-31	55				
		19661	11	55				
Weighted mean ΔR = 1. Standard deviation = 36 (both ^{14}C yrs BP)								

Table 6.4(m): All possible pairings of ΔR for Castle Park 3017 showing the weighted mean value for ΔR alongside one standard deviation on the spread of values

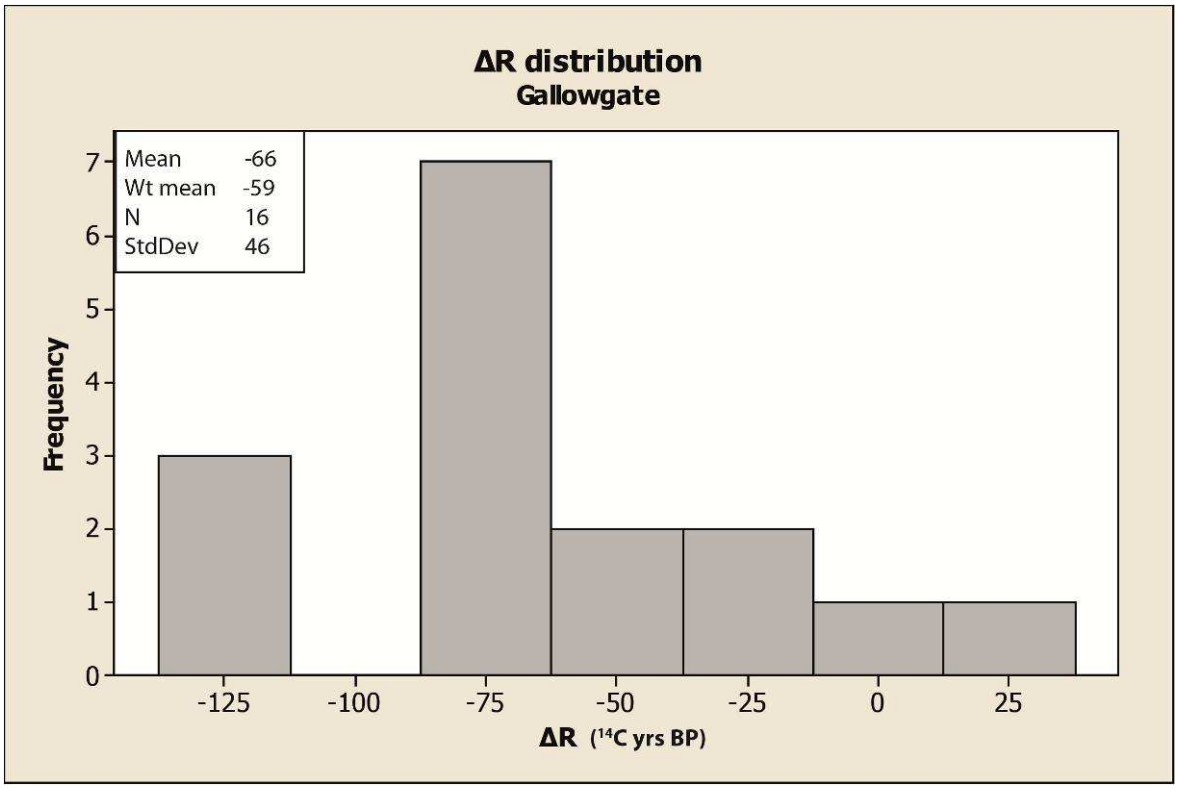

Figure 6.1: Histogram showing the distribution of ΔR values for Gallowgate as per Table 6.4(a)

(The mean and weighted mean ΔR values are shown alongside the standard deviation and the number of ΔR measurements per context (N))

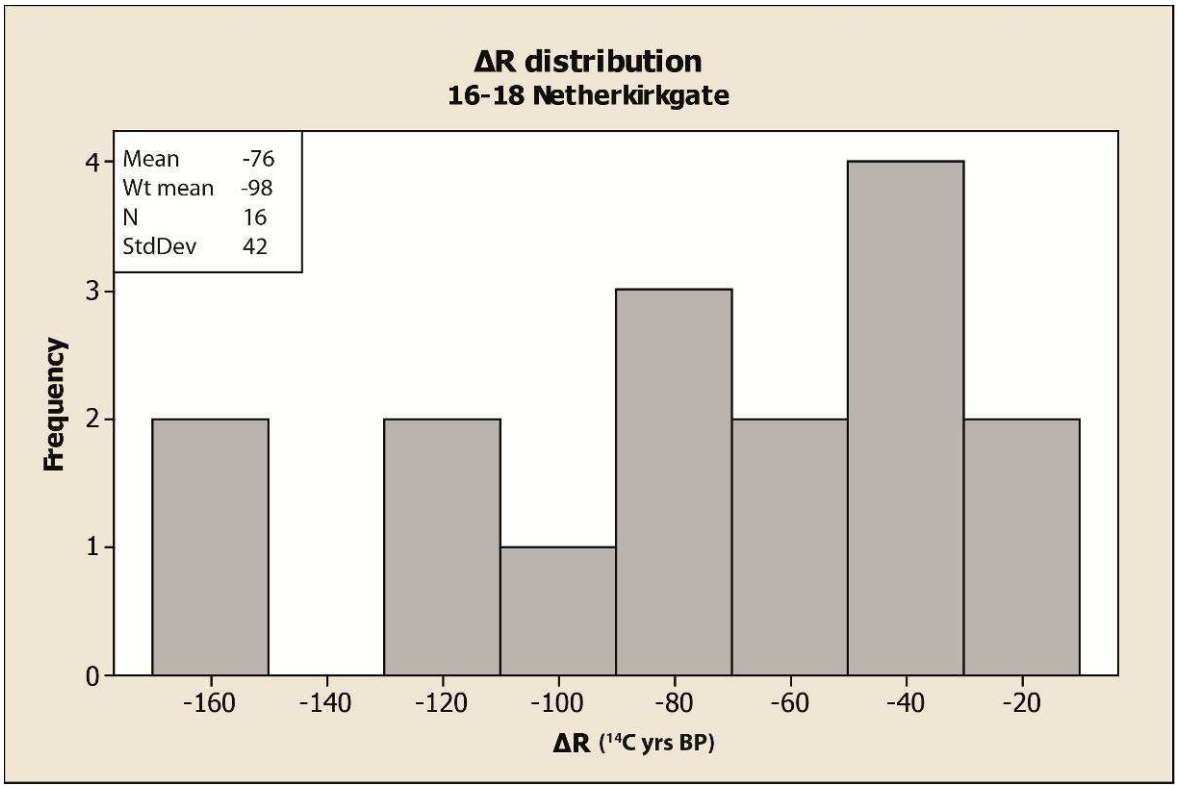

Figure 6.2: Histogram showing the distribution of ΔR values for 16-18 Netherkirkgate as per Table 6.4(b)

(The mean and weighted mean ΔR values are shown alongside the standard deviation and the number of ΔR measurements per context (N))

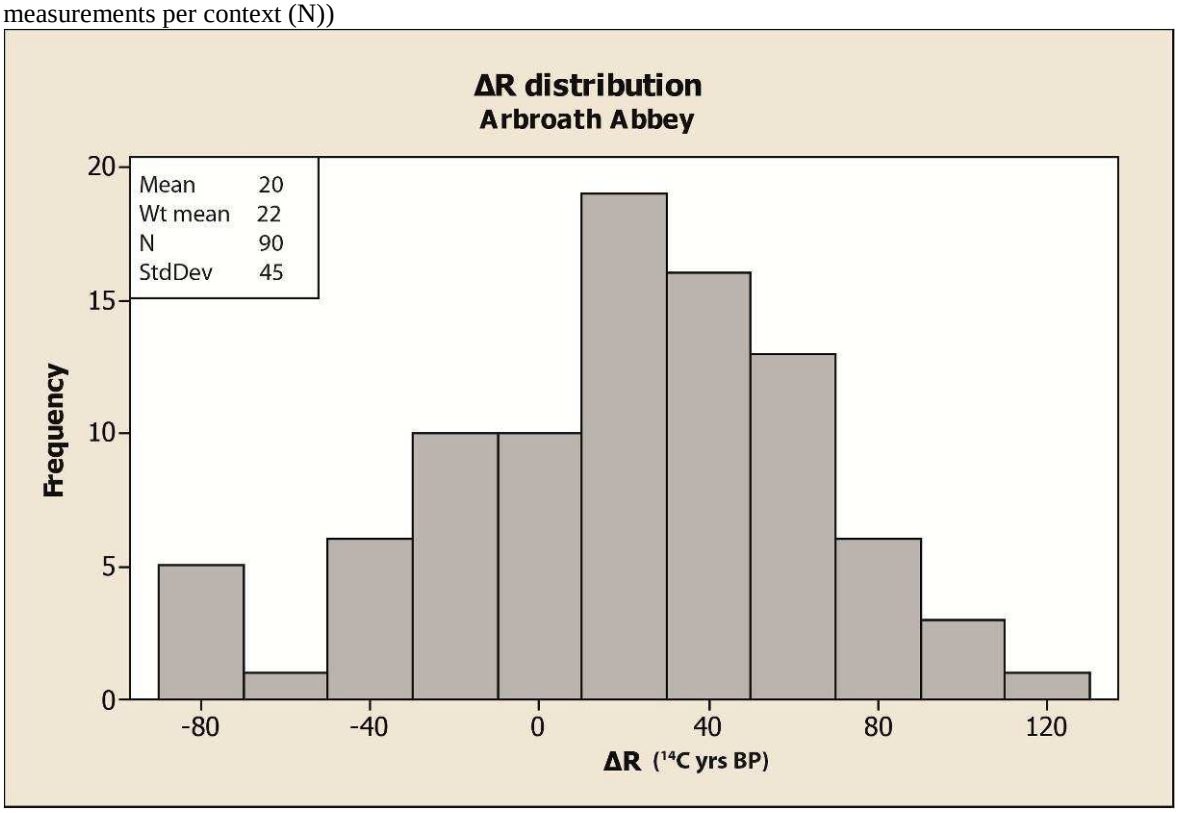

Figure 6.3: Histogram showing the distribution of ΔR values for Arbroath Abbey as per Table 6.4(c)

(The mean and weighted mean ΔR values are shown alongside the standard deviation and the number of ΔR measurements per context (N))

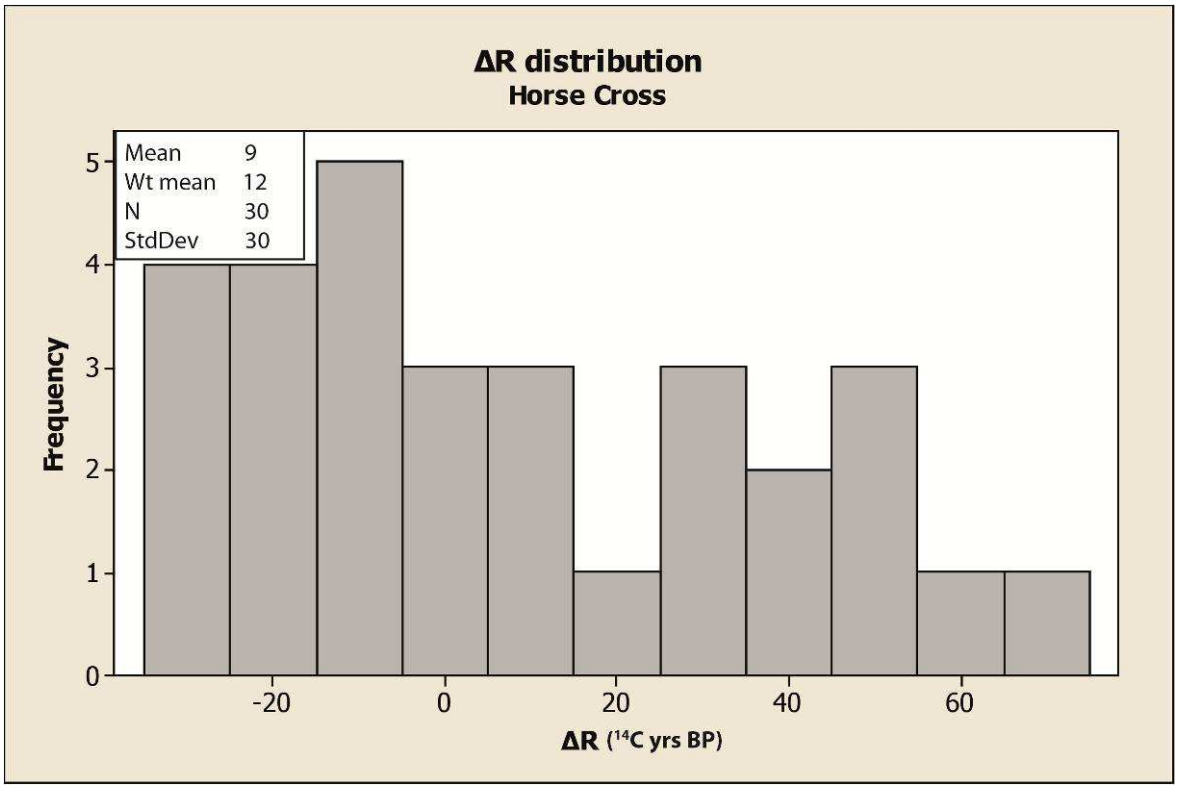

Figure 6.4: Histogram showing the distribution of ΔR values for Horse Cross as per Table 6.4(d)
(The mean and weighted mean ΔR values are shown alongside the standard deviation and the number of ΔR measurements per context (N))

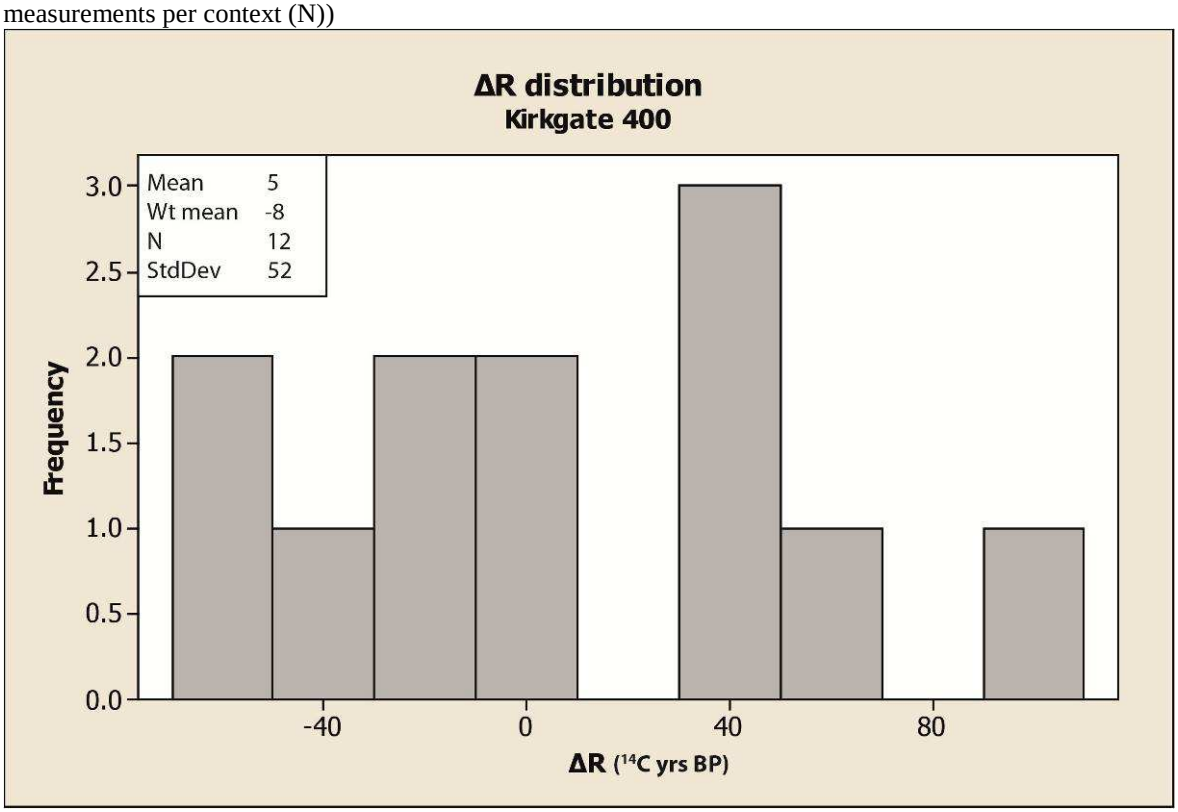

Figure 6.5: Histogram showing the distribution of ΔR values for Kirkgate 400 as per Table 6.4(e)
(The mean and weighted mean ΔR values are shown alongside the standard deviation and the number of ΔR measurements per context (N))

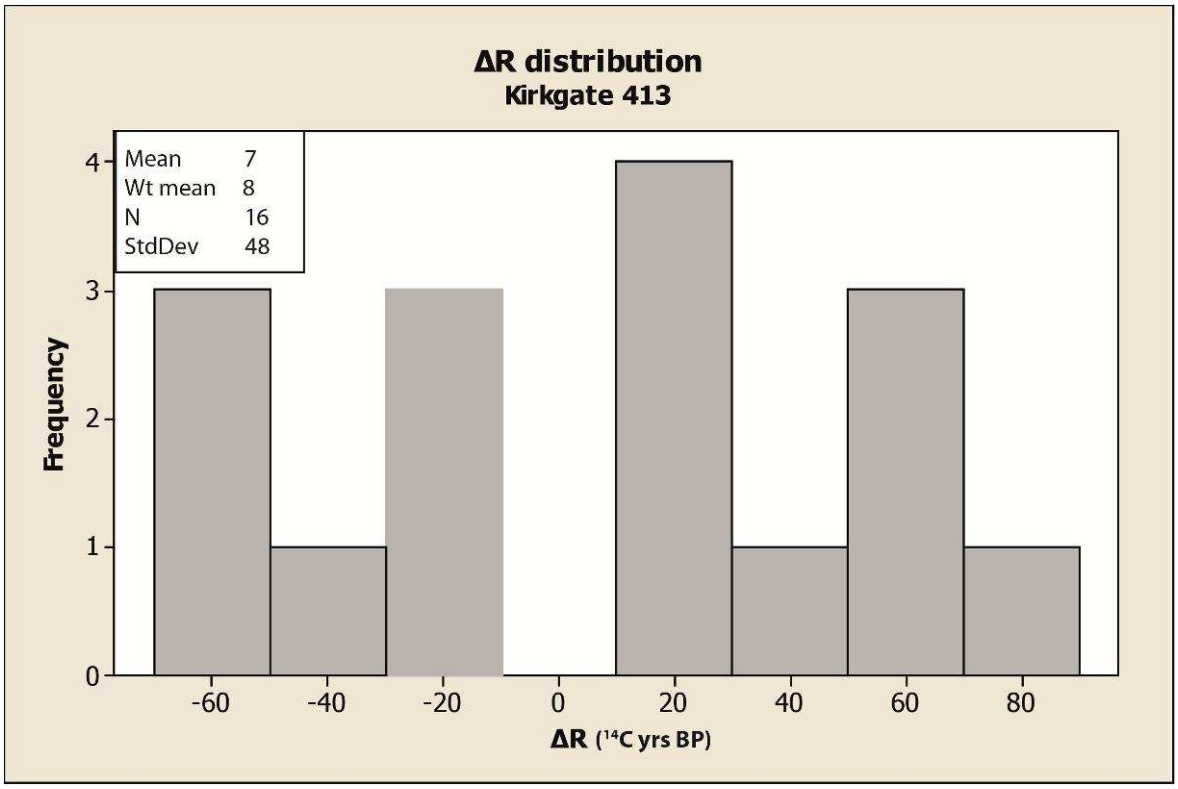

Figure 6.6: Histogram showing the distribution of ΔR values for Kirkgate 413 as per Table 6.4(f)
(The mean and weighted mean ΔR values are shown alongside the standard deviation and the number of ΔR measurements per context (N))

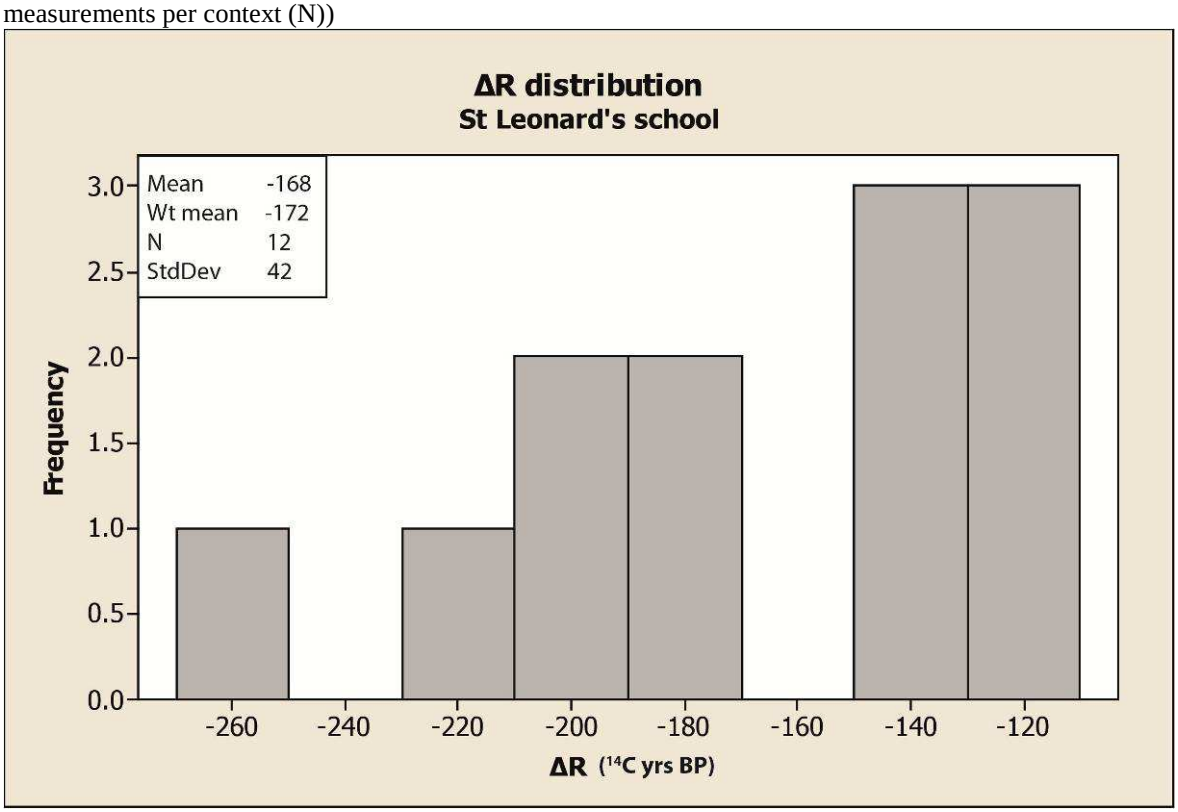

Figure 6.7: Histogram showing the distribution of ΔR values for St Leonard's School as per Table 6.4(g)
(The mean and weighted mean ΔR values are shown alongside the standard deviation and the number of ΔR measurements per context (N))

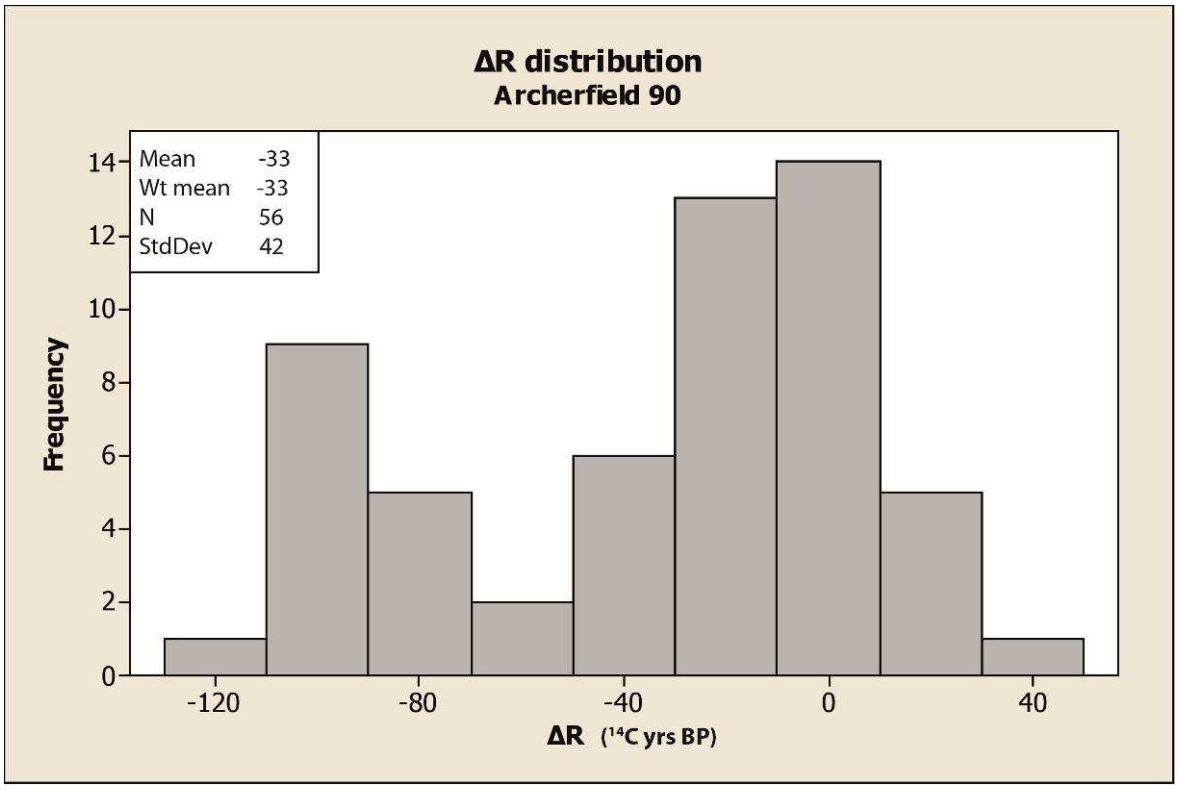

Figure 6.8: Histogram showing the distribution of ΔR values for Archerfield 90 as per Table 6.4(h)
(The mean and weighted mean ΔR values are shown alongside the standard deviation and the number of ΔR measurements per context (N))

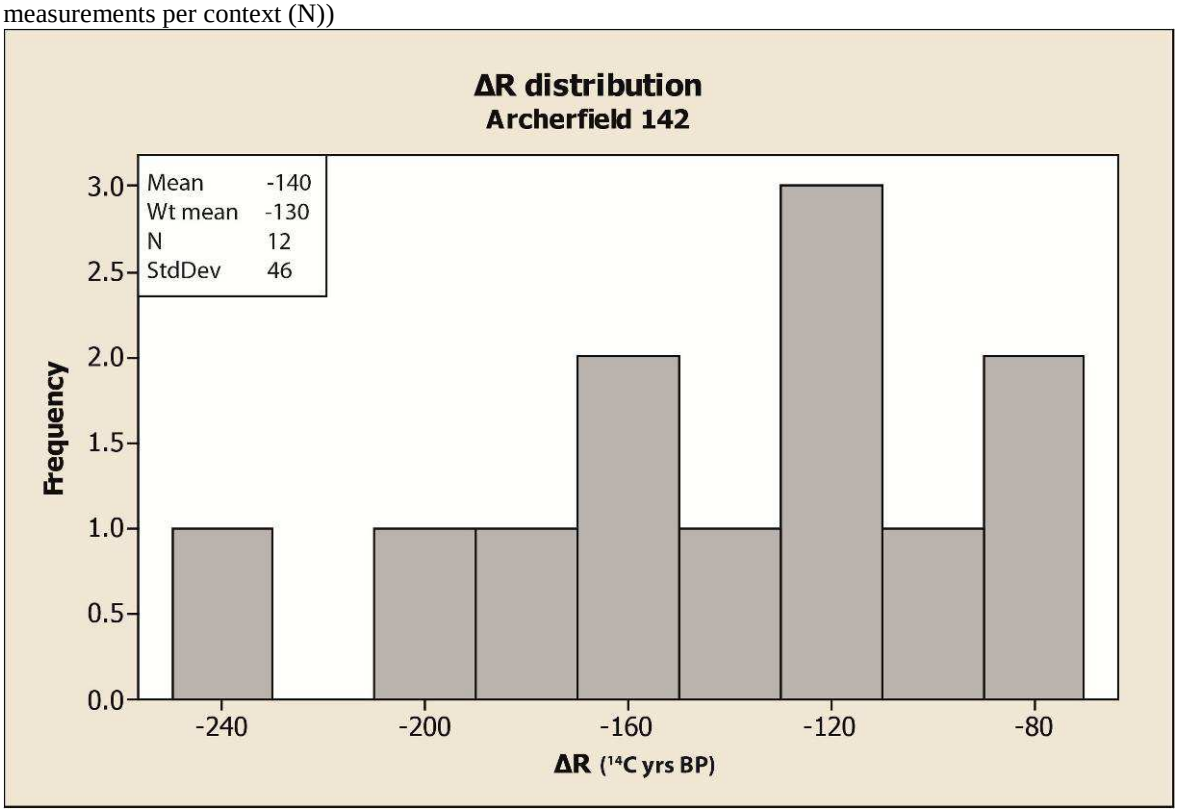

Figure 6.9: Histogram showing the distribution of ΔR values for Archerfield 142 as per Table 6.4(i)
(The mean and weighted mean ΔR values are shown alongside the standard deviation and the number of ΔR measurements per context (N))

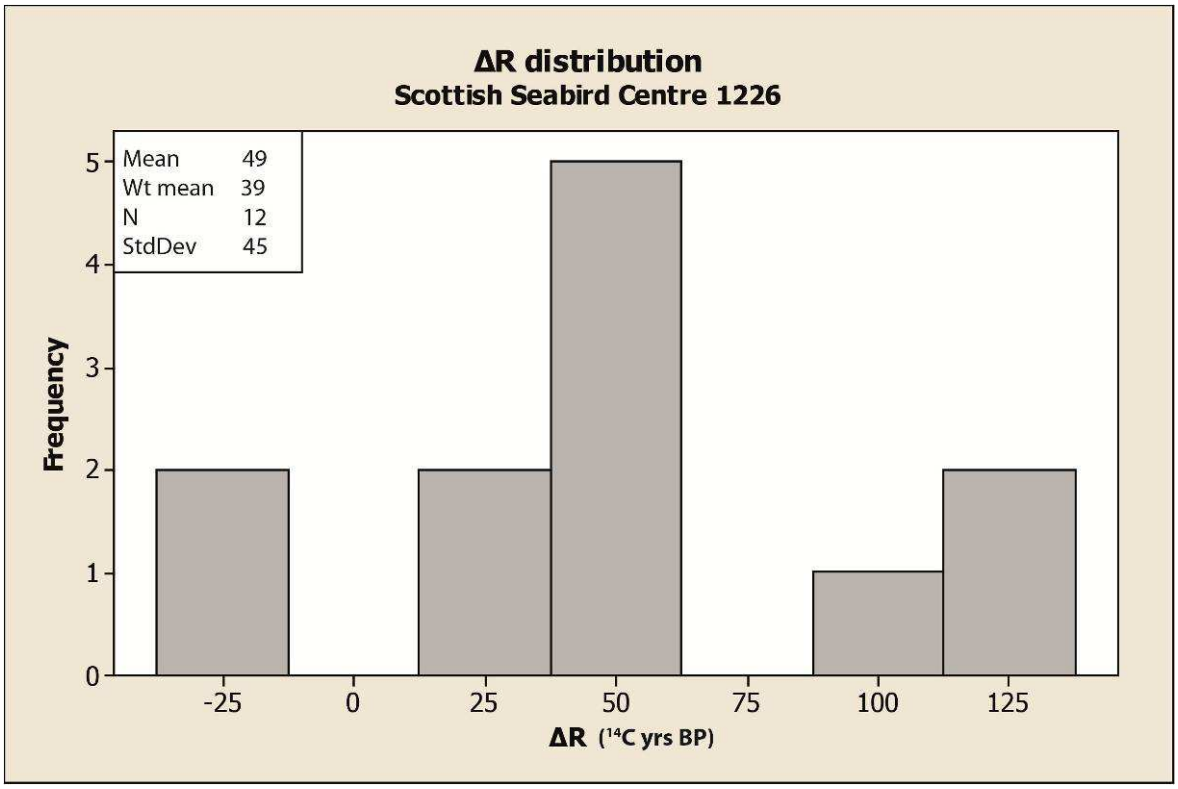

Figure 6.10: Histogram showing the distribution of ΔR values for Scottish Seabird Centre 1226 as per Table 6.4(j)
(The mean and weighted mean ΔR values are shown alongside the standard deviation and the number of ΔR measurements per context (N))

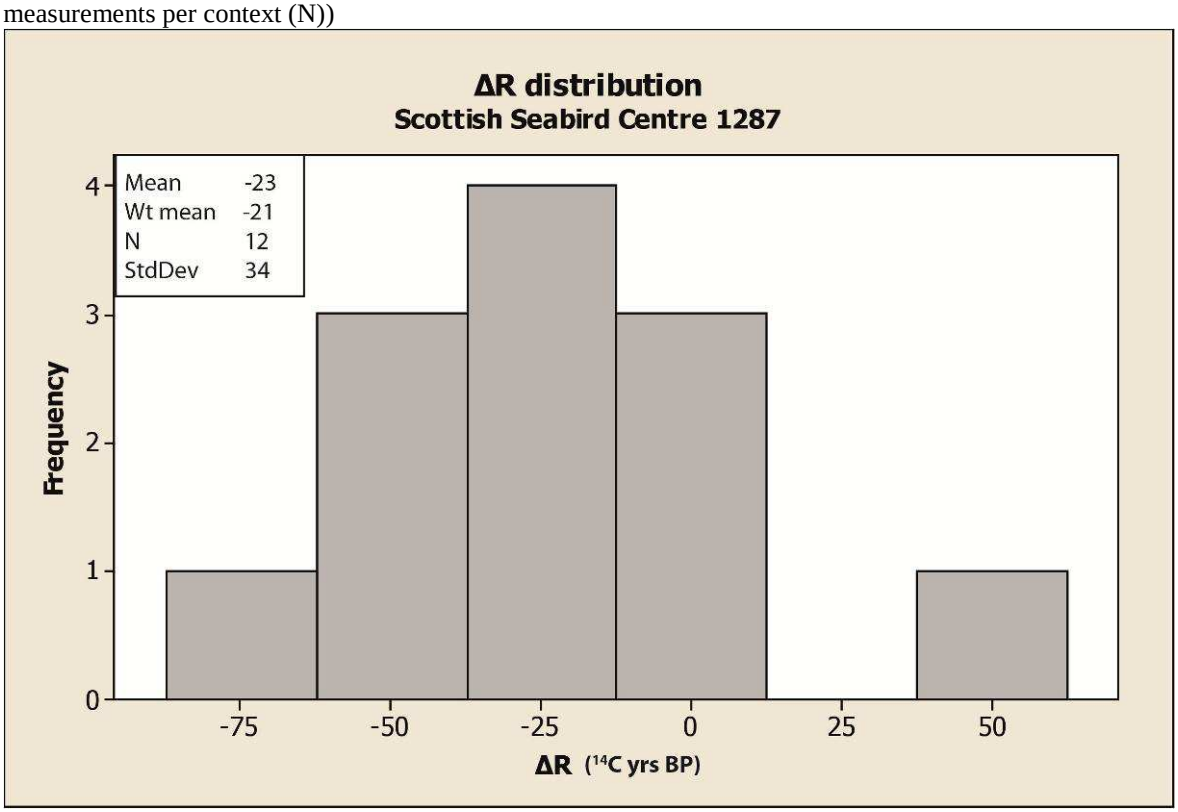

Figure 6.11: Histogram showing the distribution of ΔR values for Scottish Seabird Centre 1287 as per Table 6.4(k)
(The mean and weighted mean ΔR values are shown alongside the standard deviation and the number of ΔR measurements per context (N))

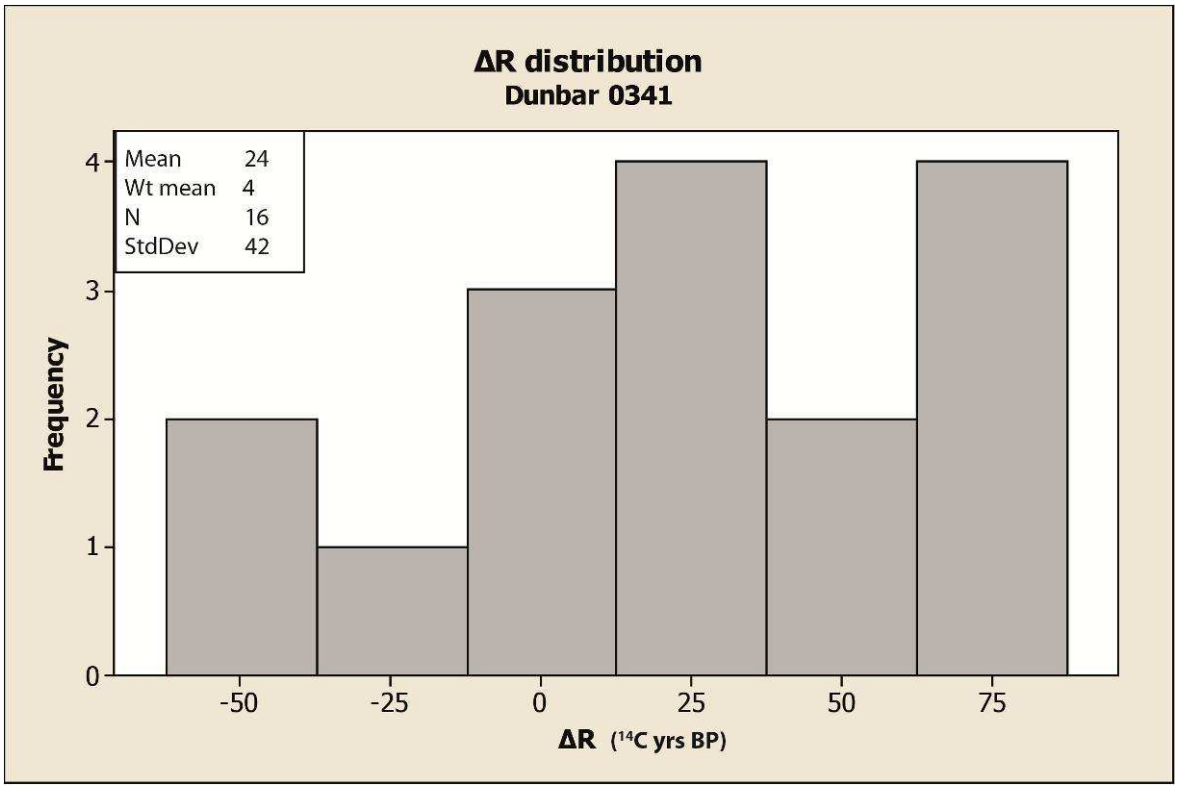

Figure 6.12: Histogram showing the distribution of ΔR values for Castle Park 0341 as per Table 6.4(l)
(The mean and weighted mean ΔR values are shown alongside the standard deviation and the number of ΔR measurements per context (N))

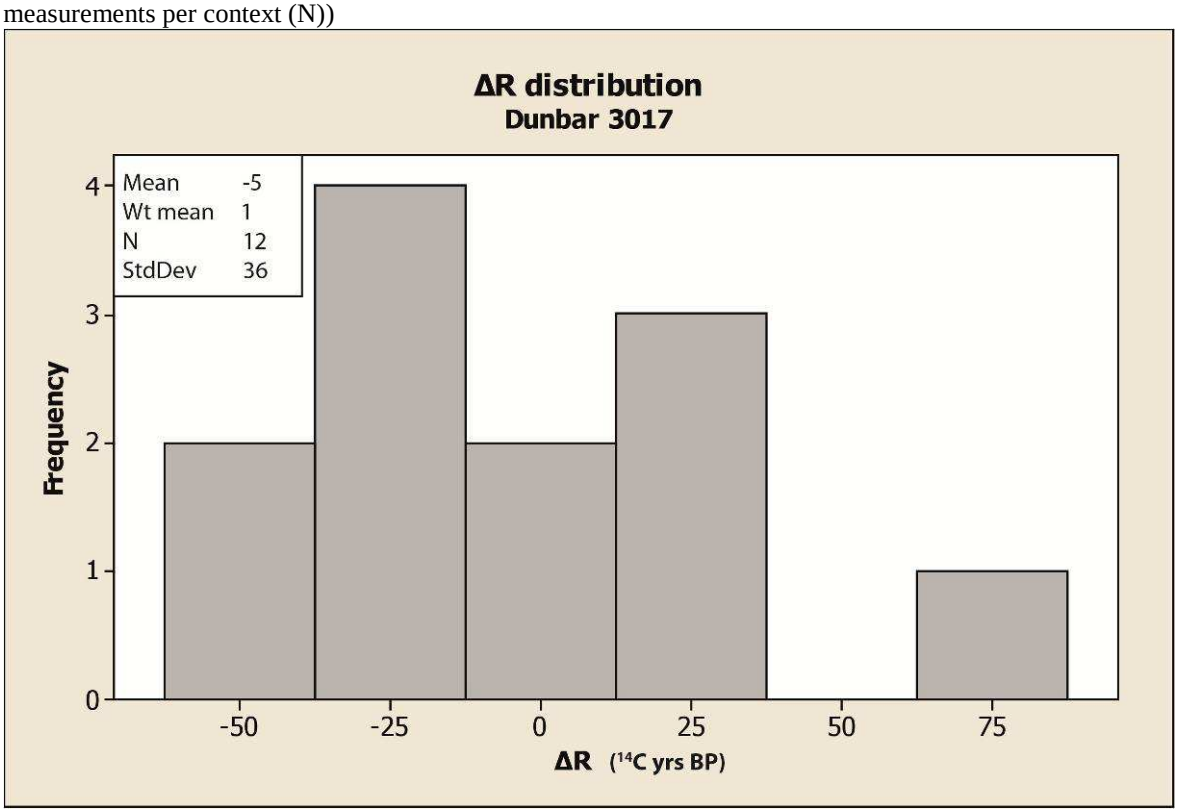

Figure 6.13: Histogram showing the distribution of ΔR values for Castle Park 3017 as per Table 6.4(m)
(The mean and weighted mean ΔR values are shown alongside the standard deviation and the number of ΔR measurements per context (N))

6.3 Interpretations

Publishing ΔR values using histograms allows for a better understanding of the population to which the mean value relates, and the possible variability in the ΔR value. This method allows all of the data from the multiple calculations in a multiple paired sample approach to be displayed and interpreted with appropriate caution. It can be seen that the distribution of ΔR values for many of the sites is relatively widespread with standard deviations of up to 52 ^{14}C yr within a single context. By publishing the ΔR values using histograms, this spread in values becomes more apparent and challenges the convention of publishing the error on the mean. Gaussian distributions are not evident in every histogram but this may be as a result of low quantities of measurements (generally N<16) and so there is no need to identify any of the distributions as significantly skewed from normal (Marian Scott pers. comm.) Figure 6.14 shows that although the weighted mean values for the sites vary from ΔR = +39 ^{14}C yrs BP to ΔR = -172 ^{14}C yrs BP, the populations of ΔR values calculated from different contexts/sites are not as distinguishable as the previous method (Chapter 5) may have suggested.

It can be observed from Chapter 5 and previous publication (Russell et al., 2010) that if these values were published using the method of the weighted mean ΔR value and the associated error on the mean, the data from the study sites could be interpreted as representing water bodies of differing ^{14}C specific activities. For example, the conclusions drawn from Russell et al., (2010) interpret mean ΔR values ranging from -172 ^{14}C yrs BP to +39 ^{14}C yrs BP with a cluster of values around zero as representative of a ΔR value for the region of around zero, with the frequent excursions to negative values being driven by the incursion of younger, less depleted Atlantic water during relatively rapid, local events. This interpretation was made using the mean values and the associated error on the mean that produce precise ΔR measurements that can appear significantly different from one another using the previous method (Chapter 5). The standard error on the mean represents how precisely the population mean value is known, but if a statement about a future (hypothetical ΔR value) calculated from this population is to be made, then a measure of the variability within that population (which would be the standard deviation) must be included. The use of the standard error for predicted values (Equation 6.1) is recommended in order to represent the true variability inherent in ΔR calculations from a multiple paired sample approach: The standard error for predicted values gives a measure

of how well individual predictions could be made in the future (Livingstone, 1999) and is based on the spread of data from the sample population (Hartigan and Wigdor, 1989), incorporating the standard deviation on the spread of data, as well as the error on the mean.

$$\sigma = \sqrt{(x^2 + y^2)}$$

Equation 6.1: Standard error for predicted values where x = the error on the weighted mean and y = the standard deviation on the ΔR values.

Table 6.5 shows the standard error for predicted values for each context and when published alongside the histograms and mean ΔR values from Figures 6.1 – 6.13, provides a comprehensive picture of the variability inherent within the calculation of ΔR values. This in turn provides a more accurate assessment of the range within which future ΔR values derived from samples recovered from the same site and context would lie.

Site	Weighted mean ΔR value (^{14}C yrs BP)	Standard error for predicted values (^{14}C yrs BP)
Gallowgate Middle School	-59	49
16 - 18 Netherkirkgate	-98	44
Arbroath Abbey	22	45
Horse Cross	12	32
Kirkgate 400	-8	54
Kirkgate, 413	8	51
St Leonard's school	-172	49
Archerfield, 90	-33	43
Archerfield, 142	-130	48
Scottish Seabird Centre 1226	39	48
Scottish Seabird Centre 1287	-21	47
Castle Park 0341	4	44
Castle Park 3017	1	38

Table 6.5: Weighted mean ΔR values for each site alongside the standard error for predicted values

6.3.1 Comparison of previous and new methods

In order to compare the results produced using the new method with those produced using the method described in Chapter 5, the two datasets were plotted against one another in

Figure 6.14.

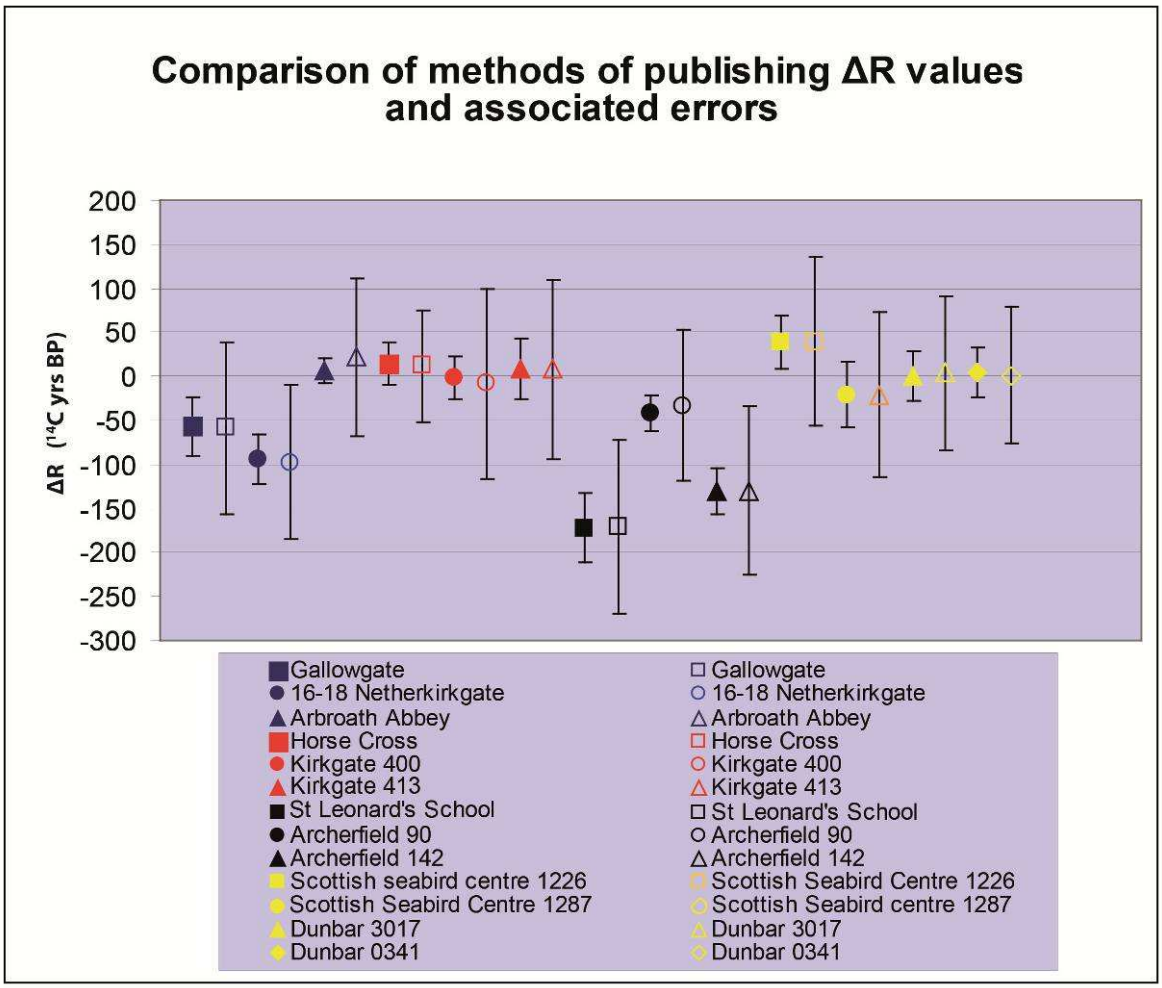

Figure 6.14: Comparison of ΔR values showing error on the mean (filled symbols) (Chapter 5 and Russell et al., 2010) and standard error for predicted values (empty symbols)

(All errors are presented at 2σ)

It can be observed that when using the error on the mean, not all mean ΔR values overlap, even at 2 σ and therefore the values could be interpreted as significantly different. However, using the standard error for predicted values results in a small overlap at 2σ, suggesting that these values are indistinguishable at this level of confidence. In order to investigate this theory, all 13 ΔR values calculated using the new method were χ^2-tested using the standard error for predicted values producing a result of (t = 22.5: $\chi^2_{:0.05}$ = 21.0). This shows that all 13 contexts are not statistically indistinguishable from one another, however it was noted that the very negative ΔR of -172 from St Leonard's school made a large contribution to the T-statistic and upon excluding this value, produced a χ^2-test result of (t = 13.4: $\chi^2_{:0.05}$ = 19.7). This means that 12 out of the 13 contexts produce ΔR values

where the error on the value is larger than the variablitiy within the group and therefore could justify the generation of a mean value for this dataset. When these 12 contexts (excluding St Leonard's School) are combined they produce a weighted mean ΔR value of -19 ^{14}C yrs ± 1 standard error for predicted values of 52 ^{14}C yrs. Using the old method, all 13 contexts fail the χ^2-test, producing a result of (t = 224: $\chi^2_{:0.05}$ = 21.0) and 5 out of the 13 contexts would need to be excluded in order for the remaining 8 contexts to pass the χ^2-test and be considered statistically indistinguishable.

.

Using a much larger error alongside the weighted mean ΔR value, such as the standard error for predicted values may not be desirable, but offers a more realistic estimate of the range in which future calculations of ΔR values for these sites may lie. Using the standard error for predicted values better represents the true variability inherent within the ΔR calculation itself as well as providing better information on the prediction and comparability of future values. This is important when considering that ΔR values are often used as proxy indicators for specific ocean ^{14}C activity and shifts in oceanic regimes that may force such a change (e.g. Kennett et al., 1997; Kovanen and Easterbrook, 2002). If the variability shown by the multiple paired sample approach for statistically indistinguishable ^{14}C ages is considered alongside the use of the larger standard error for predicted values at 2 σ when comparing mean ΔR values, (or MRE values), considerable changes in the significance of reservoir offsets, both temporally and spatially may be apparent. This may be of importance to studies using MRE variability as a proxy for oceanographic changes that have identified large scale and rapid fluctuations in ΔR or MRE values over relatively short timescales in various regions (Burr et al., 2009; Fontugne et al., 2004). Using a larger error term such as the standard error for predicted values may result in an increased overlap between ΔR values, meaning that the values are no longer significantly different and therefore conclusions on oceanic or climatic proxies cannot be drawn. This may lead to the reinterpretation of currently available ΔR values for global ocean waters.

6.4 Conclusions

The errors on the measurements of ^{14}C data used in the calculation of ΔR values must be realistic and based on replicate measurements of "in house" standards or a similar regime.

This study recommends using multiple paired samples as the best approach when determining ΔR values, (a) because each group of marine and terrestrial samples is subjected to a χ^2 test to demonstrate that they are contemporary and this will give confidence that the samples used to calculate ΔR are from secure contexts and that the terrestrial and marine samples are therefore contemporary in age and (b) because this will give the best indication of the likely variability in ΔR values that could be expected from the context. Publishing the full dataset of pairings used to calculate ΔR and/ or using histograms can help give a better representation of the variability inherent in the calculation and the level of refinement realistically achievable. Of course, a mean ΔR value and an associated error are required when calibrating unknown samples. In such situations the weighted mean should be used, and the most reliable error is the standard error for predicted values which encompasses both the standard deviation of the distribution of ΔR values as well as the associated error on the mean. Using this error is the only method which fully assesses the prediction of where future ΔR values from a similar site and temporal/geographical location are likely to lie. By standardising publication methods, ΔR values can be used more accurately by all, and appropriate conclusions can be drawn of what significant shifts in ΔR may or may not signify. The study has not dealt with the topic of the marine model uncertainty which in itself would deserve a separate discussion. This does not however weaken the argument concerning the presentation of the ΔR variability. Using this methodology, a mean ΔR of -19 ± 52 ^{14}C years is suggested for the North Sea coast of Scotland throughout the entire Medieval period.

CHAPTER 7

COMPARISON OF ΔR VALUES DERIVED FROM *PATELLA VULGATA* (LIMPET) SHELL CARBONATE AND *GADUS MORHUA* (ATLANTIC COD) BONE COLLAGEN

7.1 Comparison of fish bone and mollusc shell for ΔR calculations

The majority of this thesis, as well as a number of other recent studies of the UK coastal environment (Ascough et al., 2004, 2005, 2006, 2007a, 2007b, 2009; Butler et al., 2009; Harkness, 1983; Russell et al., 2010; Russell et al., 2011b), have assessed the ^{14}C marine reservoir effect (MRE) for several periods throughout the Holocene via quantification of ΔR values derived using marine mollusc shells. Fish bone is rarely used as the marine sample for ΔR calculations, and the importance of being able to use this material as a reliable dating tool is evident when considering the boom in the British fish trade during the first millennium AD, the so-called 'fish event horizon' (Barrett et al., 2004), and the corresponding volume of fish remains that appear in the archaeological record from this time. The final focus of this thesis compares ΔR values already derived from barley grain (*Hordeum* sp) and limpet shell (*Patella vulgata*) with new ΔR values calculated from the same grain and new samples of fish bone from North Sea cod (*Gadus morhua*).

Molluscs are most frequently selected as the material of choice for ΔR calculations as they are relatively sedentary organisms that precipitate their shell carbonate in relative equilibrium with the ambient seawater (Epstein et al., 1953). Archaeological research has also shown that most mollusc shells are processed by man close to the place of collection, as a result of the large weight of the shell relative to that of the edible soft tissue (Meehan, 1982; Waselkov, 1987). Mollusc shells can therefore be taken as a reliable indicator of local coastal conditions around the site from which they were collected. Conversely, fish are much more mobile, increasing the possibility of carbon uptake from a wider geographical area. Given the volume of fish bone and mollusc shell found together in coastal archaeological deposits and the total lack of comparative ΔR values, it was deemed important to investigate whether fish remains can be considered to be as representative of local MRE values as shellfish. A well documented period of fish trade increase in Britain

from the 1st millennium AD onwards, (Barrett et al., 2004, 2008), highlights the importance of this resource in the national archaeological assemblages. ΔR values were calculated for cod bones from two sites in north east Scotland; Quoygrew in Orkney and Robert's Haven in Caithness (Figure 2.2). Site information is detailed in Chapter 2.3. Data generated from the ΔR calculations on fish bone were compared to mollusc-derived ΔR data (from Ascough et al., 2009) for the same sites and contexts. The ΔR values and errors for mollusc shell published by Ascough et al., (2009) were recalculated in accordance with the methodology outlined in Chapter 6 (Russell et al., 2011b).

7.2 Sample material

The fish bones from both sites are representative of North Sea cod populations (James Barrett, pers. comm.) (also see Figure 7.1). North Sea cod are stocks of Atlantic Cod (*Gadus morhua)* which are not generally migratory and can be found within 100 km of their spawning grounds (Wright et al., 2006). Diet can be varied although benthic feeding on sessile crustaceans always remains a major component, even in older specimens where pisciverous and cannibalistic behaviour is often evident (Barrett et al., 2008; Du Buit, 1995). Evidence of the fish remains being the result of local subsistence activities and not as the result of international trade was primarily derived from previous stable isotope work defining Orkney and the north east of Scotland as a producer rather than consumer region (Barrett et al., 2008). This is particularly important when using fish remains of this age, given the boom in the British fish trade from the first millennium onwards, known as the "fish event horizon" (Barrett and Richards, 2004; Barrett et al., 2004). Therefore, it can be confidently implied that the fish bones which were dated are unlikely to be imported goods and are therefore 'local' to within 100 km of the site which they represent. Their demersal feeding (i.e. bottom feeding) habits should represent the consumption of sessile benthic crustaceans within the area travelled. The fish bone was not subject to biological age determination before analysis due to the fragmentary and disarticulated nature of the bone material present in the burial environment. The assemblage could therefore range from juvenile fish to adults, the latter of which can have a lifespan in excess of 20 years (Muus and Dahlstrom, 1974).

7.2.1 Fish bone analysis

Stable isotope ($\delta^{13}C$ and $\delta^{15}N$) analyses of the fish bone samples were undertaken using a Costech Elemental Analyser (EA) interfaced to a Fisher Scientific Delta V Plus continuous flow isotope ratio mass spectrometer. Gelatin was used as the primary internal standard, alanine as the secondary standard (Tavares et al., 2009). Stable isotope ratios were expressed in delta (δ) notation (Craig, 1957) as per mille (‰) deviations from the international standards (VPDB; Vienna Pee Dee Belemnite for $\delta^{13}C$, and AIR (atmospheric nitrogen) for $\delta^{15}N$). Measurement precisions (1σ) on $\delta^{15}N$ and $\delta^{13}C$ are estimated to be 0.3‰ and 0.2 ‰, respectively, based on repeats of the internal laboratory gelatin standard over the long term. Each run is normalized with respect to gelatin, which is then normalized to the international standards. It is acknowledged that no lipid extraction was performed on the fish bone prior to stable isotope analysis as it was considered that the likelihood of considerable lipid preservation in our archaeological samples was low (Liden et al., 1995). Even if a high lipid content was present, a small shift in $\delta^{13}C$ values would have little effect on the ^{14}C determinations after correction for fractionation and the ΔR values which are calculated from the ^{14}C ages.

^{14}C ages for the fish bones were determined according to the methodology in Chapter 3 (Table 7.1). Again, these ages were subject to χ^2 statistical testing in order to prove that they were contemporaneous samples, before being used to calculate ΔR. The χ^2-test results for the fish bone are shown in table 7.3. By using every possible pairing, typically 16 estimates of ΔR were calculated for each context for both mollusc shell and fish bone. In accordance with the protocol outlined by Russell et al. (2011b), all data from the ΔR calculations were depicted using histograms (Figure 7.2). These were produced using Minitab® (Version 16), and show the spread of data for all possible pairings of ΔR. A weighted mean was then calculated to give a single representative value for each context and reported alongside the standard error for predicted values (Table 7.4). As described in Chapter 6, the standard error for predicted values incorporates the standard deviation on the spread of ΔR values and the error on the weighted mean itself (Russell et al., 2011b). A weighted mean terrestrial age was also determined for each context and then calibrated using OxCal 4.1 (Bronk Ramsey, 2009; Reimer, 2009) to produce a calendar age range for the context (Table 7.5).

7.3 Results

Site/Context	Terrestrial			Mollusc shell			Fish bone		
	Sample I.D.	Age BP ± 1σ	$\delta^{13}C$ (‰)	Sample I.D.	Age BP ± 1σ	$\delta^{13}C$ (‰)	Sample I.D.	Age BP ± 1σ	$\delta^{13}C$ (‰)
RH 3004	SUERC-254	655 ± 50	-23.3	SUERC-258	1105 ± 60	1.3	SUERC-24553	1187 ± 30	-14.4
	SUERC-255	665 ± 50	-23.2	SUERC-259	1125 ± 55	2.3	SUERC-24554	1115 ± 30	-13.8
	SUERC-256	650 ± 50	-21.8	SUERC-260	1020 ± 50	1.2	SUERC-24555	1157 ± 30	-13.6
	SUERC-257	610 ± 50	-25.1	SUERC-261	1080 ± 50	1.7	SUERC-24556	1167 ± 30	-13.4
RH 3019	SUERC-243	910 ± 45	-23.6	SUERC-247	1210 ± 45	0.6	SUERC-24560	1229 ± 30	-14.3
	SUERC-244	855 ± 45	-24.9	SUERC-248	1175 ± 45	1.6	SUERC-24561	1280 ± 30	-12.4
	SUERC-245	855 ± 50	-27.0	SUERC-249	1220 ± 50	1.2	SUERC-24562	1270 ± 30	-13.2
	SUERC-246	920 ± 50	-25.0	SUERC-253	1200 ± 50	0.5	SUERC-24563	1315 ± 30	-13.1
QG A004	SUERC-3149	980 ± 40	-23.8	SUERC-3152	1235 ± 40	1.2	SUERC-24564	1251 ± 30	-12.6
	SUERC-3142	875 ± 35	-24.7	SUERC-3156	1200 ± 35	1.9	SUERC-24565	1230 ± 30	-14.0
	SUERC-3150	960 ± 40	-24.7	SUERC-3157	1195 ± 35	1.8	SUERC-24566	1181 ± 30	-13.9
	SUERC-3151	925 ± 40	-24.1	SUERC-3159	1210 ± 35	1.1	SUERC-24570	1210 ± 30	-13.3
QG A023	AA-52329	875 ± 45	-24.0	SUERC-3162/4109*	1258 ± 35	1.7/0.0	SUERC-24571	1287± 30	-12.0
	AA-52330	835 ± 40	-24.1	SUERC-4110	1175 ± 35	1.7	SUERC-24572	1283 ± 30	-12.7
	AA-52331	835 ± 40	-22.0	SUERC-3166/4111*	1233 ± 35	1.2/1.1	SUERC-24573	1246 ± 30	-13.0
	AA-52332	945 ± 55	-22.4	SUERC-4112	1210 ± 30	0.2	SUERC-24574	1256 ± 30	-13.8
	SUERC-3160	940 ± 35	-22.7						
	SUERC-3161	940 ± 35	-24.5						

* Indicates samples where multiple measurements have been made on one shell. The weighted mean is given as the age

Table 7.1: ^{14}C and $\delta^{13}C$ measurements for each sample

All ^{14}C ages and $\delta^{13}C$ results relative to VPDB ± 0.1‰ from CO_2 sub-samples measured on a VG SIRA 10 are given in Table 7.1. The measured $\delta^{13}C$ values of the terrestrial grain samples (-27.0 to -21.8 ‰) fall within the typical range for C3 plant material (DeNiro and Epstein, 1978). Previous work on North Sea cod populations has demonstrated that distinct groupings of fish stocks exhibit particular isotopic signals (Barrett et al., 2008, 2011). Stable isotope values ($\delta^{13}C$ and $\delta^{15}N$) of cod bone measured within this study (Table 7.2) are in agreement with values for cod from the northern North Sea area (Barrett et al., 2008, 2011) (Figure 7.1).

SUERC Lab Code	**Site / Context**	**$\delta^{13}C$ ± 0.2 ‰**	**$\delta^{15}N$ ± 0.3 ‰**
24553	RH 3004	-14.7	13.5
24554		-14.1	15.3
24555		-13.7	13.7
24556		-13.4	13.9
Mean ± 1σ		-14.0 ± 0.6	14.1± 0.8
24560	RH 3019	-14.4	15.0
24561		-12.5	13.1
24562		-13.3	15.3
24563		-13.3	14.0
Mean ± 1σ		-13.4 ± 0.8	14.4 ± 1.0
24564	QG A004	-12.9	13.9
24565		-14.3	13.7
24566		-14.2	14.9
24570		-13.7	13.7
Mean ± 1σ		-13.8 ± 0.6	14.1 ± 0.6
24571	QG A023	-12.4	14.2
24572		-13.0	13.6
24573		-13.4	13.1
24574		-13.0	13.8
Mean ± 1σ		-13.0 ± 0.4	13.7 ± 0.5
Overall Mean ± 1σ		**-13.5 ± 0.7**	**14.0 ± 0.7**

Table 7.2: Stable isotope data and associated errors from sampled fish bone (continuous flow)

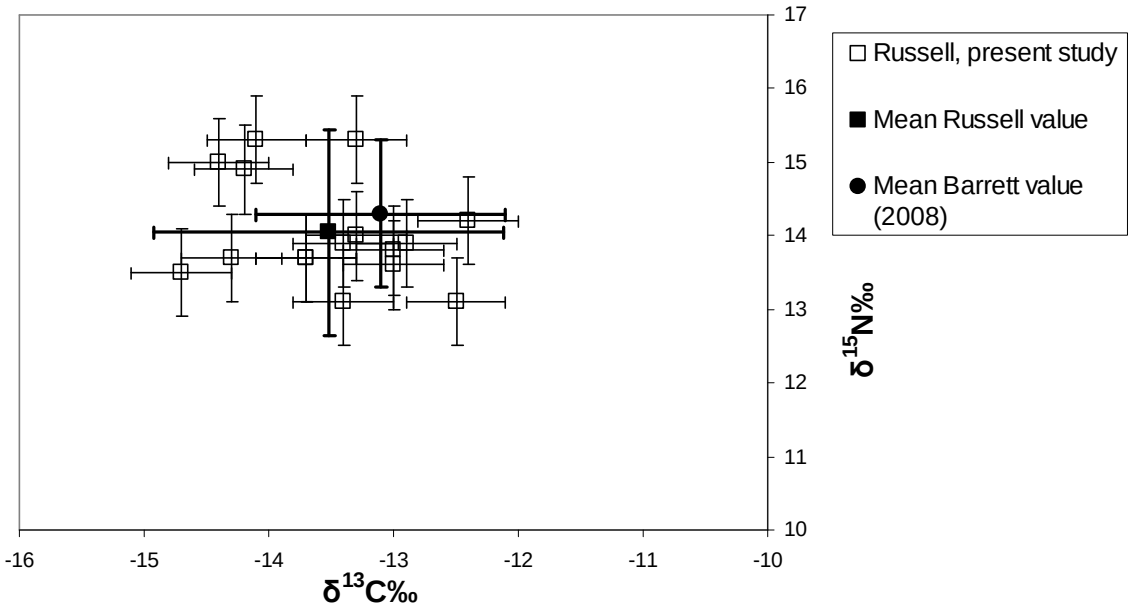

Figure 7.1: Comparison of fish bone $\delta^{13}C$ and $\delta^{15}N$ values from the present study, with mean data for the North Sea region from Barrett et al., (2008)

(All data at ± two standard deviations)

Site	Fish bone χ^2 T-statistic	Critical 95% acceptance value
RH 3004	3.08	7.81
RH 3019	4.16	7.81
QG 004	2.96	7.81
QG A023	1.34	7.81

Table 7.3: χ^2 results from the fish bone from each of the four contexts

In all cases the T – statistic is smaller than the 95% critical acceptance value meaning all four contexts pass the χ^2 test.

The ^{14}C ages for each context all passed the χ^2 test, giving confidence that each group of samples is internally coherent, contemporary, and can therefore be used to calculate ΔR. The distribution of ΔR values produced for each context is illustrated in Figure 7.2. The wide range of ΔR values for each context was then reduced to a weighted mean ΔR ± 1 standard error for predicted values for fish bone and shell in each context (Table 7.4).

Considerable overlap in ΔR values is evident between the values for fish bone and the values for shell, although in each case, the mean ΔR value for the fish bone is greater (Table 7.4). It should also be noted that the offsets between fish bone and mollusc-based ΔR values are smaller for samples from Quoygrew than from Robert's Haven (Table 7.4).

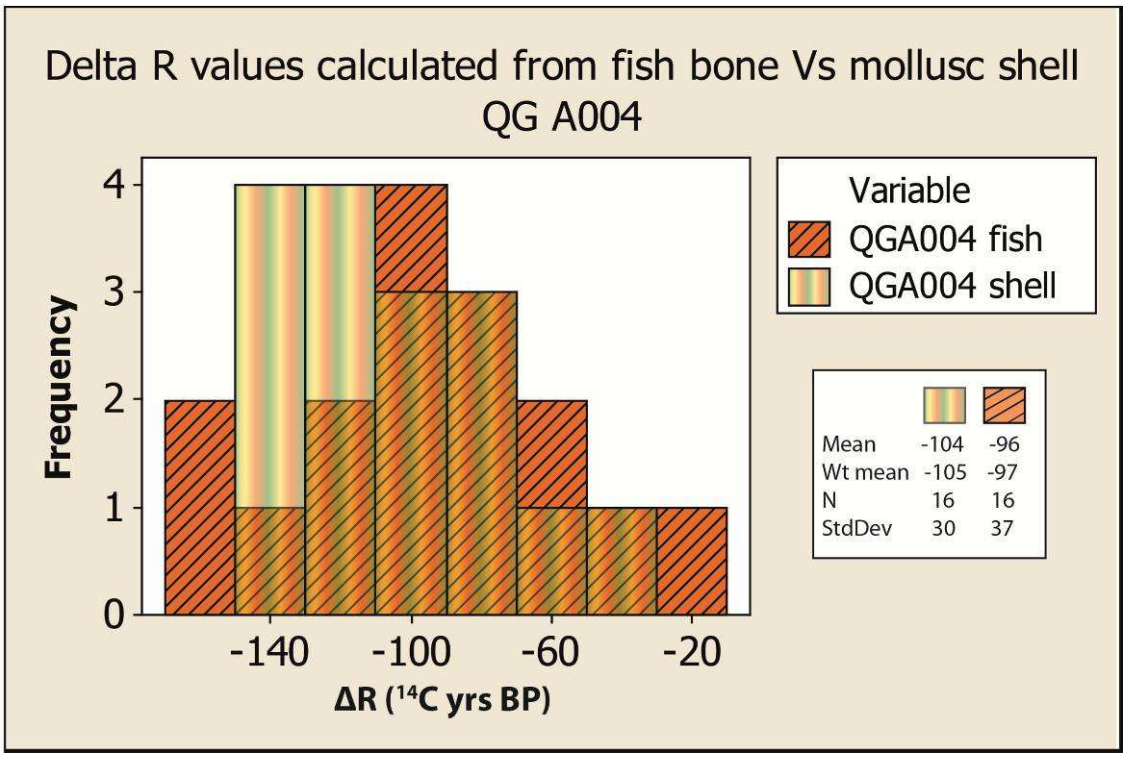

Figure 7.2(a): Comparison of calculated ΔR values for shell and fish for QG A004

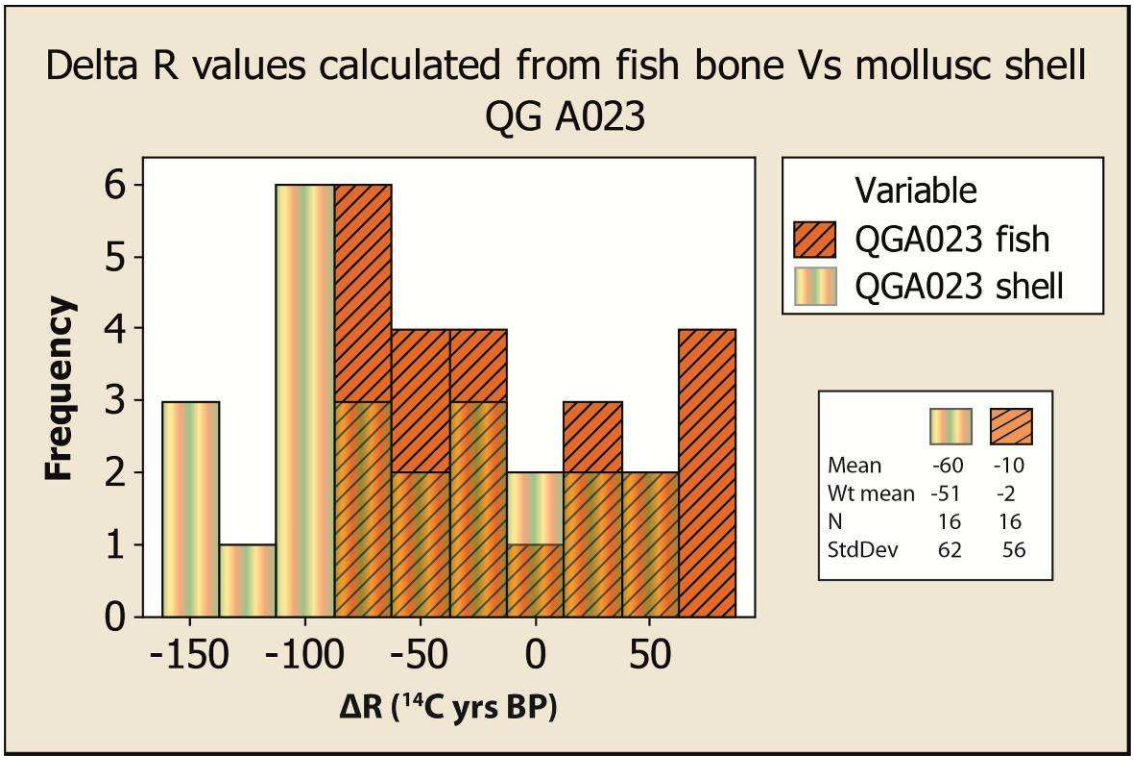

Figure 7.2(b): Comparison of calculated ΔR values for shell and fish for QG A023

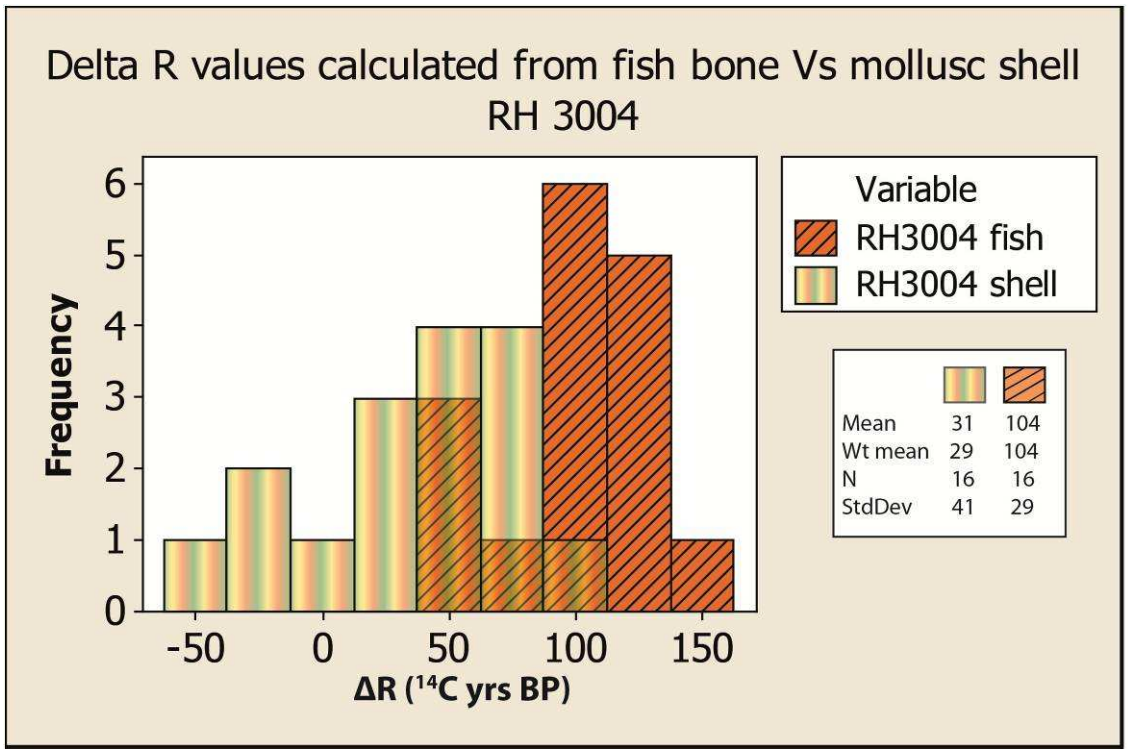

Figure 7.2(c): Comparison of calculated ΔR values for shell and fish for RH 3004

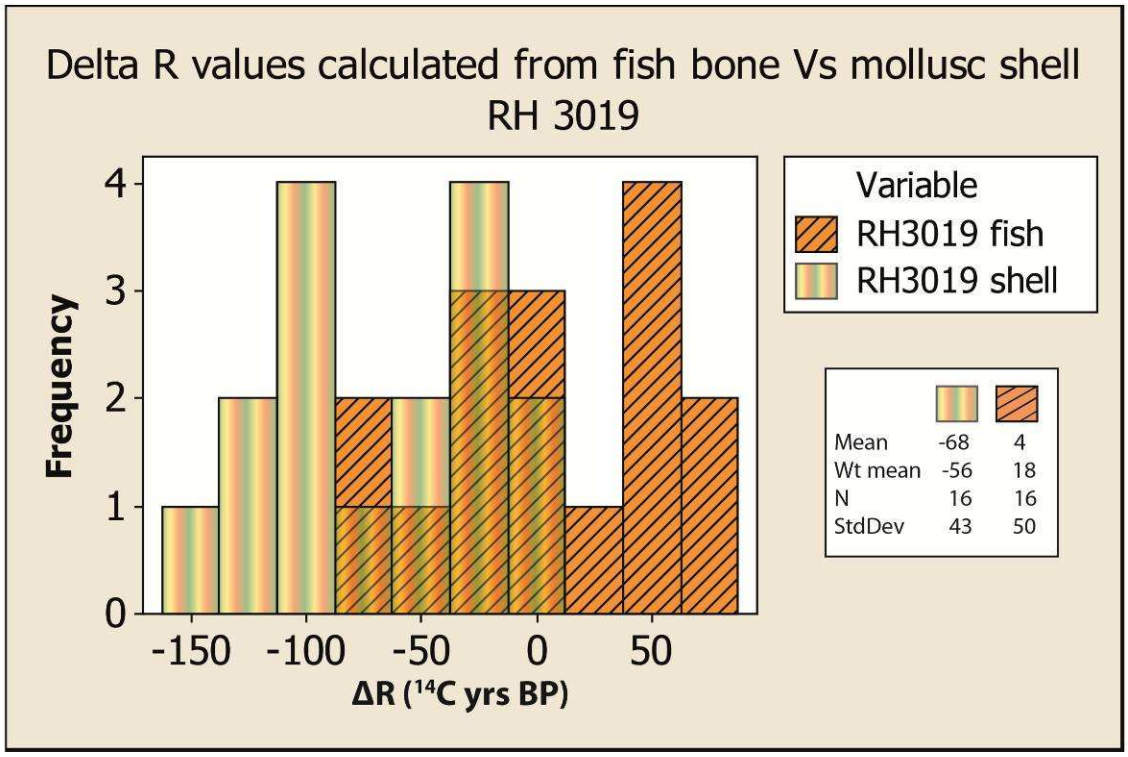

Figure 7.2(d): Comparison of calculated ΔR values for shell and fish for RH 3019

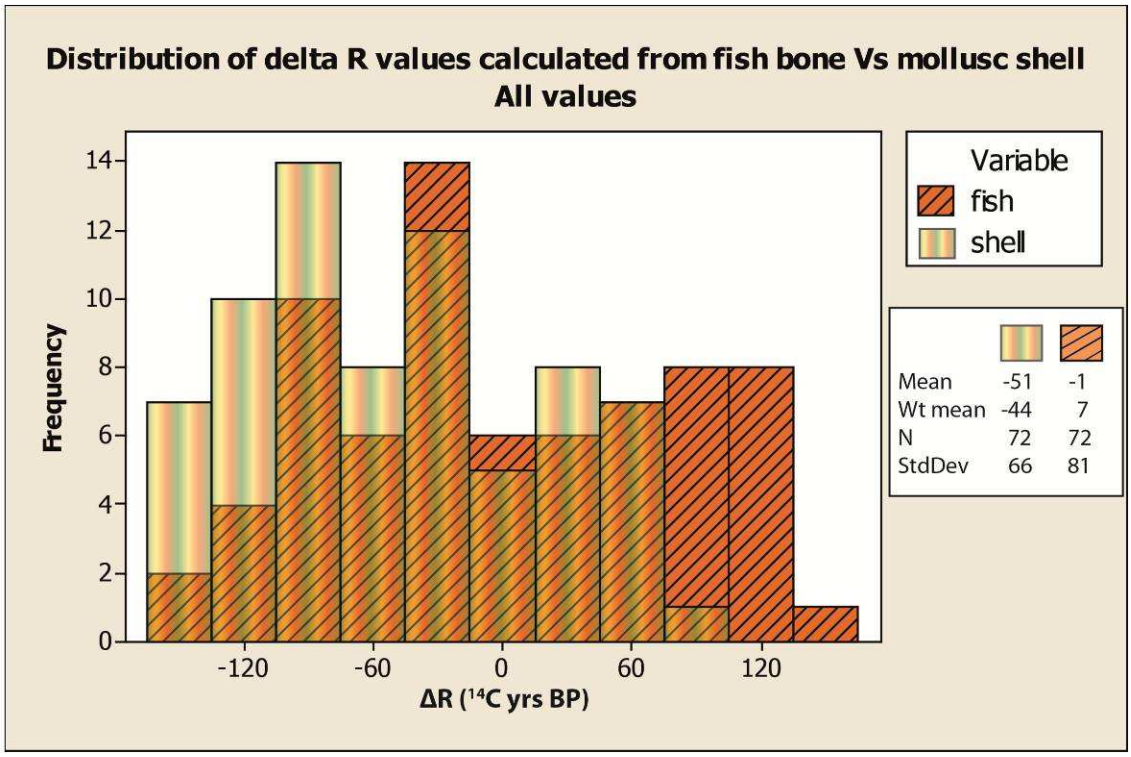

Figure 7.3: Comparison of calculated ΔR values for marine mollusc shell and fish bone using combined values from all 4 contexts

Site	ΔR shell (^{14}C yrs BP)	ΔR fish bone (^{14}C yrs BP)
RH 3004	29 ± 45	104 ± 35
RH 3019	-56 ± 46	18 ± 52
QG A004	-105 ± 35	-97 ± 41
QG A023	-51 ± 63	-2 ± 57

Table 7.4: Summary of weighted mean values ± 1 standard error for predicted values

(Mollusc shell ΔR values are recalculated from raw data from Ascough et al., (2009) using the method outlined in Chapter 6 (Russell et al., 2011b))

Context	Weighted mean terrestrial age (BP)	Calibrated age range 2σ (AD)
RH 3004	645 ± 25	1283 - 1395
RH 3019	885 ± 24	1045 - 1219
QG A004	931 ± 24	1030 - 1161
QG A023	896 ± 22	1043 - 1213

Table 7.5: Weighted mean terrestrial ages from each context calibrated with OxCal 4.17 (Bronk Ramsey, 2009) and the Intcal09 atmospheric dataset (Reimer et al., 2009) to a calendar age range after recalibration of original data from Ascough et al., (2009)

The weighted mean terrestrial ^{14}C ages derived for each context and the calibrated age ranges (Table 7.4) show that the dates fall within the period of increased British fish trade around the 1st millennium AD (Barrett et al., 2004; Barrett and Richards, 2004; Milner et al., 2007).

7.4 Interpretations

It can be observed from Figure 7.2 and Table 7.4 that in all 4 contexts there is an increase in ΔR value and therefore an increased MRE when using mean values for fish bone compared to mollusc shell. However, when using the standard error for predicted values to represent the variability within the data, the differences between the ΔR values are not significant at 2σ. Also, 7 out of the 8 ΔR values are not significantly different from one another at 2σ (Figure 7.4).

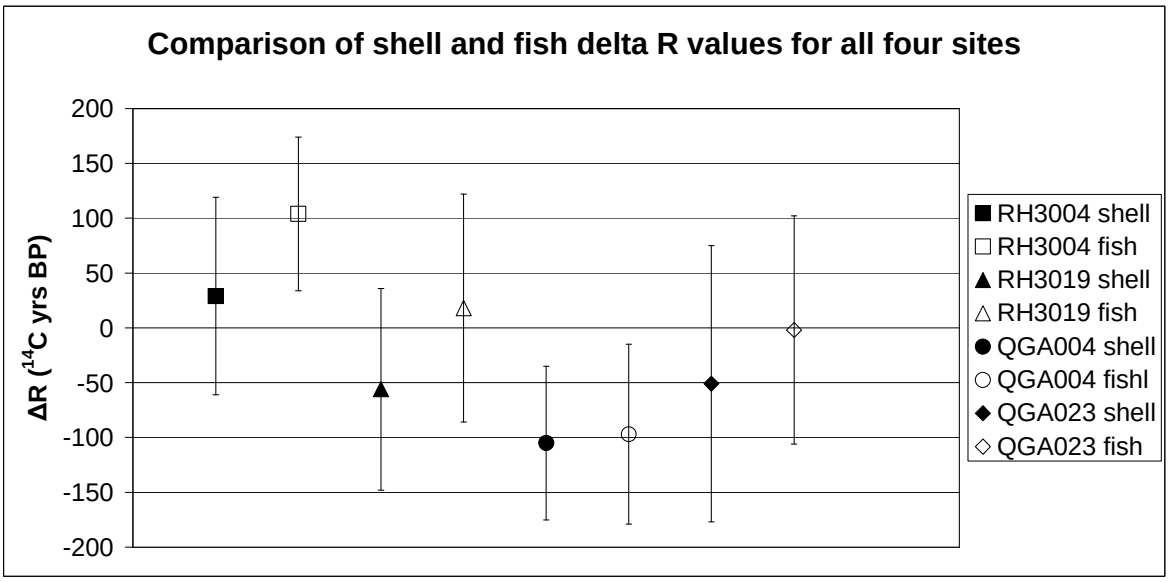

Figure 7.4: Comparison of mollusc shell and fish bone ΔR values showing overlap between 7 out of the 8 values at 2σ

Variations in ΔR values for shell and fish bone collagen from the 4 individual contexts and in the combined data from Figure 7.4 were examined with reference to geographical location, diet and the biological age of the fish compared to the shells. The slightly larger ΔR offset at Robert's Haven compared with Quoygrew is unlikely to be due to geographically-related differences in the ^{14}C content of the water as similar Atlantic-derived water masses are present at both sites (Turrell et al., 1992). It is possible that the biological age of the fish in the Robert's Haven contexts was greater than those at Quoygrew; however it is difficult to substantiate this point, given the lack of information on the age or size of the fish. The potential age range of the cod (in excess of 20 years) when compared to the molluscs (5 years) is more likely to contribute to the small (and insignificant) offset shown between fish bone and mollusc shell, giving cod higher ΔR values than shell.

Dietary differences between the species may result in different sources of carbon (and hence differences in ^{14}C content) in each sample type. However, it is important to note that the $\delta^{13}C$ and $\delta^{15}N$ values (Table 7.2, Figure 7.1) are indistinguishable between sites (albeit from small data sets), and dietary differences do not explain the larger offset between fish bone and shell ^{14}C ages at Robert's Haven compared to Quoygrew. ^{14}C dating of marine shell involves the analysis of the inorganic fraction of the shell, which is formed mainly from the DIC in the surrounding water (Gillikin et al., 2006; McConnaughey et al., 1997). A small (ca.10%) contribution to the shell carbonate is provided via respiration and

metabolic contributions (McConnaughey et al., 1997; Kennedy et al., 2001; Lorrain et al., 2004; Gillikin et al., 2005), although this percentage is subject to variations between species and environments (Gillikin et al., 2005, 2006). The feeding habitat of different mollusc species therefore has the potential to influence the carbon metabolised for shell production. Some studies (e.g. Claassen, 1998) have shown that the ingestion of 'old carbon' from rocks such as limestone can lead to the production of an erroneously old ^{14}C age, particularly when measuring the shells of gastropods, which tend to be mainly deposit feeders on sedimentary materials (Kesler, 1983). However, in areas where carbonaceous geology is absent, the difference in species diet has not been shown to be an influencing factor in shell carbon content (Ascough et al., 2005a.). The shells used in this study were exclusively limpet (*Patella vulgata)* which, although belonging to the class gastropoda, were not collected from areas with a carbonate rich geology and therefore were considered to be representative of coastal water DIC at the time.

The fish analysed in this study were all North Sea cod, a generally non-migratory stock of Atlantic Cod (*Gadus morhua),* which has well documented benthic feeding habits. In general, dietary studies have concluded that cod diet shows greatest variability during the younger stages of life, whilst moving from a pelagic diet based on zooplankton to benthic prey e.g. crustaceans, and eventually to pisciverous habits (Du Buit, 1995; Nielsen and Andersen, 2001; Sherwood et al., 2007). An increase in trophic level of prey was in line with an increase in fish length (equated with age), for most of the dietary studies, however, for Atlantic cod, large crustaceans dominate the diet of even the largest individuals which seemingly prefer not to progress to a mainly pisciverous diet as observed for other cod species (Du Buit, 1995; Nielsen and Andersen, 2001). Therefore, the MRE as determined for North Sea cod collagen may be fully representative of the open benthic ocean rather than the mixed dietary contributions from pisciverous behaviour. It would appear that comparing North Sea cod values with mollusc shells may act as a proxy for the carbon content of the open benthic ocean compared to surface coastal water as measured in shell carbonate. This may indicate that the open benthic ocean has a slightly increased MRE when compared to coastal waters. It is however important to note that this difference in ΔR between shell and fish bone, is not significant at 2σ.

RH3019, QGA004 and QGA023 provide similar calendar age ranges around the first millennium AD, during the fish event horizon. The mean ΔR results for both shell and fish

bone from these three contexts were proven by χ^2 testing to be indistinguishable from one another (t = 5.8: $\chi^2_{:0.05}$ = 11.1) and so could be combined to provide a weighted mean ΔR value of -63 ^{14}C yrs BP and a standard error for predicted values of ± 53 ^{14}C yrs. This mean ΔR value is representative of marine material from either mollusc shell or fish bone during the first millennium AD from the far north of Scotland.

7.5 Conclusions

Direct comparison of ΔR values based on ^{14}C measurements made on fish bone and mollusc shell reveals a trend of increased values in fish bone. However, these differences are not statistically significant at 2σ using the standard error for predicted values. This suggests that fish bone can be used reliably for radiocarbon dating in place of mollusc shell in the absence of terrestrial material, if an appropriate ΔR value and error are used in the calibration. It would appear that for the North Sea, cod bone may be likely to produce slightly higher ΔR values than mollusc shell, possibly owing to differences in the open benthic ocean ^{14}C composition when compared to coastal waters. However, provided that the ΔR for the region is well known from previous studies and used alongside an appropriate error term such as the standard error for predicted values, it should be appropriate to use ΔR values calculated on mollusc shell when dating North Sea cod collagen. The publication of the full dataset, at least in histogram form, and the use of the standard error for predicted values avoid underestimating the reproducibility of ΔR values for either mollusc shell or fish bone.

CHAPTER 8

CONCLUSIONS AND RECOMMENDATIONS FOR FURTHER STUDY

The purpose of this thesis was to investigate spatial and temporal variability in the Marine Radiocarbon Reservoir Effect (MRE) for the North Sea coast of Scotland throughout the Holocene. By investigating this variability in the MRE through changes in ΔR**,** a number of conclusions and recommendations for further study can be drawn, focusing upon methodological approaches to the publication of future ΔR values and their associated errors. Specific findings from the methodology that has been developed for this thesis have been drawn in Chapters 6 and 7, but a concise summary of all of the conclusions from this study is presented here together with recommendations for future work.

8.1 Summary of thesis conclusions

- The multiple paired sample approach is the only method that demonstrates the inherent variability in the ΔR calculation, and therefore is recommended for all cases of future ΔR calculations where possible. The variability inherent within the calculation can be attributed to: 1) the contemporeity of the terrestrial and marine samples used in the ΔR calculation, 2) the generation of the sample ^{14}C ages and their associated errors, 3) the modelled marine ^{14}C ages used in ΔR calculation and the uncertainty arising from the use of a relatively simple marine model to generate these, and 4) the actual calculation of the ΔR value, and the number of ^{14}C ages used in its calculation. Conclusions or inferences drawn from single paired samples (and the associated errors) are unlikely to fully demonstrate the possible variability within the ΔR calculation and can lead to interpretations based on 'false' variability that is a function of the calculation, not as a result of actual changes in ^{14}C activity within various global carbon reservoirs. This is discussed in more detail in Section 8.2.

- Where a multiple paired sample approach is employed, every effort should be made to avoid rounding the data before chi-squared testing and ΔR calculations. Rounding may affect the statistical results/treatment of the data and therefore should be avoided in order to ensure that the published data are as unaltered as possible (see Chapter 6.2). It is acknowledged that the raw data may not be

available to all researchers but where it is, every effort should be made to follow this method of best practice.

- Once ΔR values have been calculated from multiple paired samples, all of the data should be made available for publication in order to show the distribution of the multiple calculated ΔR values. Using histograms succinctly displays all of the data, rather than overwhelming tables of multiple ΔR values for each context.

- It is recommended that mean ΔR values should be published alongside the histograms for calibrations on marine derived carbon. When using these mean values, an appropriate error to quote is the standard error for predicted values. The standard error for predicted values incorporates both the standard deviation on the dataset as well as the error on the mean and gives a more representative estimate of where ΔR values from a similar site and time period may lie.

- For the sites studied in this thesis, 12 out of the 13 mean ΔR values produced in Chapter 6 from mollusc shell (and contemporaneous, short-lived terrestrial samples) are indistinguishable from one another when χ^2-tested using the standard error for predicted values ($t = 13.4$: $\chi^2_{:0.05} = 19.7$). St Leonard's School is the only site which failed the χ^2-test as, when this ΔR value was included, the test statistic for the dataset is $t = 22.5$: $\chi^2_{:0.05} = 21.0$. The weighted mean ΔR value for the 12 sites that pass the χ^2-test is -19 ± 52 ^{14}C years. This value encompasses sites ranging from Aberdeen in the north to East Lothian in the south (c130 km) and spans a temporal range from 443 – 1449AD.

- After comparing fish bone and shell ΔR values, it was found that although North Sea cod produce a slightly higher ΔR than mollusc shell, this offset is not significant using the standard error for predicted values. North Sea cod can therefore be reliably dated using ΔR values calculated on mollusc shell from a similar region. Three of the 4 contexts used in the fish bone study (Chapter 7) passed the χ^2-test (excluding Robert's Haven 3004). Using the 3 contexts that pass the χ^2-test, a combined ΔR from the fish bone values produced for this thesis and the recalculated mollusc shell values from Ascough et al.'s (2009) data gives a mean ΔR value for the period around the first millenium AD of -63 ± 53 ^{14}C years.

This value is valid for North Sea cod and/or mollusc shell from northern Scotland and the Orkney Islands.

- If all of the data discussed in this thesis are combined (Chapter 6 and 7), and the weighted mean ΔR values produced from the 21 contexts included in this study are χ^2-tested, only 2 contexts from the entire dataset fail the χ^2-test. The results for the entire dataset are (t = 33.9: $\chi^2_{:0.05}$ = 31.4). However, if the two contexts which contribute highly to the T-value are excluded, (St Leonard's school and Robert's Haven 3004 (fish bone)), all of the remaining ΔR values pass the χ^2-test (t = 24.7: $\chi^2_{:0.05}$ = 28.9). If these values are combined to give a weighted mean for the entire dataset, they produce a ΔR of -29 ± 51 ^{14}C years which is in good agreement with Reimer et al., (2002) who quote a value of -33 ± 93 ^{14}C years for the area encompassing western Ireland, Scotland and the Orkney Islands during the mid to late Holocene (4185 – 368 BP). The mean value derived for this thesis is also in good agreement with that determined by Cage et al., (2006) of -26 ± 14 ^{14}C years on samples dating back to 1850 AD from fjordic and coastal waters in north-west Scotland.

- The data produced in this thesis are comparable with those from Ascough et al., (2004) for their study of the Middle Iron Age where ΔR= -79 ± 17 for the west coast of Scotland, even though the studies focus on different temporal periods on opposite Scottish coasts. Interpreting the Medieval value of ΔR= -29 ± 51 produced for this thesis alongside the Iron Age value of ΔR= -79 ± 17 would suggest that although the east coast shows a slightly higher ΔR value and therefore increased MRE, the two are not significantly different at this level of confidence.

8.2 Applications of the findings from this thesis/further work

- Comparing the mean ΔR of -29 ± 51 ^{14}C years produced in this thesis with that derived by Reimer et al., (2002), Cage et al., (2006) or Ascough et al., (2004) can only be justified if the presence of definitive temporal or spatial associations in ΔR values are considered to be absent or indistinguishable at the level of confidence at which the ΔR values are reported. This is the case for Reimer et al., (2002) where confidence in a

time dependency for ΔR was lacking and thus justified the publication of a mean ΔR value ± the standard deviation on the dataset. A similar case is presented for this thesis whereby spatial or temporal patterning in the data appears to be absent and therefore justifies the publication of a mean value for the dataset ± one standard error for predicted values.

- Comparing the values from the study by Ascough et al., (2004) with those produced from this thesis cannot draw any firm conclusions at this level of confidence as both studies are concerned with temporally and spatially different study areas. In order for the values from the east and west coast of Scotland to be compared directly, further work on either Medieval samples from the west coast, or Iron Age samples from the east coast would be necessary to determine whether the small (yet insignificant) offset is consistent for temporal or spatial variations throughout the latter half of the Holocene.

- By employing the multiple paired sample approach and the resultant mean ΔR's alongside the standard error for predicted values, the inherent variability within the calculation of ΔR from sets of statistically indistinguishable dates is highlighted. This variability is partly derived from the uncertainties inherent within the box model which is used to model equivalent marine ages from dates based on terrestrial material. Investigation of the uncertainties in the model was outwith the scope of this study but is certainly an area for further research that has been highlighted by this thesis and the publications derived from it (Russell et al., 2011b).

- The major application of the conclusions from this thesis focuses on situations where interpretations are drawn from single pairs of radiocarbon dates used to calculate ΔR, and then infer that large apparent shifts in ΔR are as a result of large-scale oceanographic or climatic changes. This study has shown that combining multiple pairs of radiocarbon dates that are statistically indistinguishable in a matrix-style approach can produce variability in the subsequent ΔR values of up to 198 ^{14}C years as shown at Arbroath Abbey. This variability of 198 ^{14}C years represents uncertainties inherent within the production and calculation of ΔR values – not as a result of oceanographic/climatic changes influencing the ^{14}C activity of the local surface waters. The identification of the ΔR calculation method itself as a potential source of

variability is only highlighted through the multiple paired sample approach, and therefore studies using single paired samples interpret this inherent variability as the result of significant changes in oceanic ^{14}C activity. This variability demonstrated in the calculation of ΔR values from the multiple paired sample approach can be used to explain cases of intra-shell ΔR variability such as that described by Jones et al., (2007). Jones et al., (2007) document intra-shell variability in ΔR of up to 216 ^{14}C years, which they try to interpret in relation to el Niño events but fail to provide any definitive explanation. If pairs of statistically indistinguishable ^{14}C dates can produce ΔR values that range up to 198 ^{14}C years (Arbroath Abbey), it is therefore not inconceivable that variations of up to 216 ^{14}C years could represent similar variability within the calculation of ΔR values and not variability in ^{14}C activity in relation to oceanographic or climatic changes. Caution should therefore be placed on interpretations drawn from single pairs of dates used to calculate ΔR as any variability of up to c. 200 ^{14}C years may be inherent within the calculation method and therefore not representative of oceanographic/climatic changes influencing local ^{14}C activity in surface waters.

This thesis has produced new methods of interpreting and presenting ΔR values and their associated errors for publication alongside recommending best practice statistical treatment of the data used in ΔR calculations. In addition, 21 new mean ΔR values have been calculated for the North Sea coast of Scotland alongside a new regional mean value valid for the Medieval period. Previous MRE research in this area has been limited and so this thesis has contributed significantly to the understanding of the North Sea MRE and the spatial and temporal variations throughout the Holocene in the UK coastal environment.

APPENDIX A

The selection protocol for the samples was extremely strict in order to minimise the possibility of dating unsuitable samples for ΔR calculations. Unsuitable samples were those which were not of the same age due to post depositional disturbance and therefore did not constitute contemporary marine and terrestrial material. For ΔR calculations to provide accurate and precise results, all samples must be contemporary in order to evaluate the offset between terrestrial and marine material. Three of the sites chosen for this study appeared at first to meet the site selection criteria upon consultation with the site excavators and should therefore have produced suitable sample material. Unfortunately, due to circumstances beyond our control, the samples were not contemporary and therefore not suitable for use in ΔR calculation. The three sites that proved unsuitable for study were Whitegate, Portmahommack and Fife Ness.

A.1 Whitegate, Caithness

Sample material was provided during ongoing excavations at Whitegate by AOC archaeology. Marine material was plentiful, resulting in the selection of 4 limpet (*Patella vulgata*) shells, however, terrestrial material was not as available, meaning only a minimum number of 2 individuals could be identified from a cattle tibia, a cattle ulna, a cattle metapodial and a sheep pelvis. The resultant dates (Table A1) showed that while the marine material formed a contemporary group of material, the terrestrial samples formed a suite of dates so widely spread that they did not pass the χ^2 test. The terrestrial material could not be considered a contemporary group of samples and therefore the site could not be used in the study.

A.2 Portmahommack, Tarbat

Sample material was provided from Portmahommack by Field Archaeology Specialists (FAS) during the Tarbat Discovery Programme. Four winkle shells (*Littorina littorea*) and 4 charred grains identified as barley (*Hordeum* sp) were supplied as sample material. Only 3 of the marine samples passed the χ^2 test for contemporeity and 3 out of the 4 grain samples produced $\delta^{13}C$ values around -15‰ as opposed to the expected values for barley around -23 to -25‰. $\delta^{13}C$ values in the range of -15‰ are normally indicative of plants

following a C4 pathway as opposed to a C3 pathway as followed by barley. Therefore, the grains may have been incorrectly identified. The variations in $\delta^{13}C$ between the individuals were small, however, the dates for the 4 grain samples were vastly different, spanning a range of 672 ^{14}C years and thus not comprising a group of contemporary material (Table A2).

A.3 Fife Ness, Crail, Fife

Samples were provided by Fife Museums from the site at Fife Ness. The samples provided were 4 winkle shells (*Littorina littorea*), 3 hazelnut shells (*Corylus avellana)* and 1 oak (*Quercus*) acorn. The site codes on the terrestrial and marine samples were different from one another, but this was assumed to be an administrative error and the samples were dated for study. Unfortunately the error was not clerical, but down to sample selection error on the part of the museum; the marine samples were 7,500 ^{14}C years younger than the terrestrial material (Table A3). The terrestrial material with the site code CGC96 was from excavations at the Mesolithic site on Crail Golf course. The marine material however was not from Crail Golf Course, but from neighbouring excavations of the Medieval Crail Middle Drain (code CMG96). The samples were therefore not contemporary and rejected as unsuitable for this study.

Whitegate

Context: 515 **Standard deviation on batch QA:** 13 ^{14}C yr								
	Sample lab code	**Sample Type**	**δ^{13}C (± 1‰)**	**Age BP (Unrounded)**	**Error 1σ (Unrounded)**	**Unrounded error (Batch limited)**	**Age BP (Rounded)**	**Error 1σ (Rounded)**
Terrestrial	SUERC - 20279	Cattle tibia	-22.1	1317	30	30	1315	30
	SUERC - 20280	Cattle ulna	-25.9	1299	30	30	1300	30
	SUERC - 20285	Cattle metapodial	-22.6	1439	30	30	1440	30
	SUERC - 20370	Sheep pelvis	-20.6	1425	30	30	1425	30
Marine	SUERC - 20286	Limpet (*Patella vulgata*)	1.6	1624	30	30	1625	30
	SUERC - 20287	Limpet (*Patella vulgata*)	1.7	1606	25	25	1605	30
	SUERC - 20288	Limpet (*Patella vulgata*)	0.6	1650	30	30	1650	30
	SUERC - 20289	Limpet (*Patella vulgata*)	1.5	1608	25	25	1610	30

Table A1: Results of ^{14}C and δ^{13}C measurements on samples from Whitegate, Caithness

Portmahommack

Context: 1886 **Standard deviation on batch QA:** 32 ^{14}C yr								
	Sample lab code	**Sample Type**	**δ^{13}C (± 1‰)**	**Age BP (Unrounded)**	**Error 1σ (Unrounded)**	**Unrounded error (Batch limited)**	**Age BP (Rounded)**	**Error 1σ (Rounded)**
Terrestrial	SUERC - 19698	Barley (*Hordeum* sp.)	-15.3	1417	30	32	1415	35
	SUERC - 19699	Barley (*Hordeum* sp.)	-14.9	1560	30	32	1560	35
	SUERC - 19700	Barley (*Hordeum* sp.)	-23.4	890	30	32	890	35
	SUERC - 19701	Barley (*Hordeum* sp.)	-13.5	1562	30	32	1560	35
Marine	SUERC - 19691	Winkle (*Littorina littorea*)	1.8	1947	30	32	1945	35
	SUERC - 19695	Winkle (*Littorina littorea*)	0.2	1680	30	32	1680	35
	SUERC - 19696	Winkle (*Littorina littorea*)	2.5	1623	30	32	1625	35
	SUERC - 19697	Winkle (*Littorina littorea*)	0.9	1657	30	32	1655	35

Table A2: Results of ^{14}C and δ^{13}C measurements on samples from Portmahommack, Tarbat

Fife Ness, Fife

Context: F40 **Standard deviation on batch QA:** 45 ^{14}C yr.								
	Sample lab code	**Sample Type**	**δ^{13}C (± 1‰)**	**Age BP (Unrounded)**	**Error 1σ (Unrounded)**	**Unrounded error (Batch limited)**	**Age BP (Rounded)**	**Error 1σ (Rounded)**
Terrestrial	SUERC - 21611	Hazelnut (*Corylus avellana)*	-26.0	8667	35	45	8665	45
	SUERC - 21612	Hazelnut (*Corylus avellana)*	-	-	-	-	-	-
	SUERC – 21613	Oak (*Quercus*)	-	-	-	-	-	-
	SUERC – 21614	Hazelnut (*Corylus avellana)*	-	-	-	-	-	-
Marine	SUERC – 21604	Winkle (*Littorina littorea*)	1.4	1130	35	45	1130	45
	SUERC – 21605	Winkle (*Littorina littorea*)	1.5	998	35	45	1000	45
	SUERC – 21606	Winkle (*Littorina littorea*)	0.5	1136	35	45	1135	45
	SUERC – 21610	Winkle (*Littorina littorea*)	1.3	1133	35	45	1135	45

Table A3: Results of ^{14}C and δ^{13}C measurements on samples from Fife Ness, Fife

REFERENCES

Addyman Associates. 2007. *Evaluation and watching brief at Anchor Green, North Berwick.* Unpublished data.

Aitken M. J. 1990. *Science-based dating in archaeology*. Longman Archaeology series. Longman Group, England.

Alley R. B., Meese D. A., Shuman C. A., Gow A. J., Taylor K. C., Grootes P. M., White J. W. C., Ram M., Waddington E. D., Mayewski P. A. and Zielinski G. A. 1993. Abrupt increase in Greenland snow accumulation at the end of the Younger Dryas event. *Nature* **362**, 527-529.

Alley R. B., Mayewski P. A., Sowers T., Taylor K. C., and Clark P. U. 1997. Holocene climatic instability - A prominent, widespread event 8200 yr ago. *Geology* **25**, 483-486.

Alley, R.B. 2000. The Younger Dryas cold interval as viewed from central Greenland. *Quaternary Science Reviews* **19**, 213-226.

Alley, R. 2004. GISP2 Ice Core Temperature and Accumulation Data. *IGBP PAGES/World Data Center for Paleoclimatology Data Contribution Series 2004-013*. Boulder, Colorado: NOAA/NGDC Paleoclimatology Program

Ambers J. C. 1987. Identification of the use of marine plant material as animal fodder by stable isotope ratios. In Mook W.G. and Waterbolk H.T., editors, *PACT 29 Proceedings of the second international symposium on 14C and archaeology (11I.7),* Strasbourg, France: Council of Europe, 251-258.

Ascough P. L., Cook G. T., Dugmore A. J., Barber J., Higney E., and Scott E. M. 2004. Holocene variations in the Scottish marine radiocarbon reservoir effect. *Radiocarbon* **46** (2), 611-620.

Ascough P. L., Cook G. T. and Dugmore A. J. 2005a. Methodological approaches to determining the marine radiocarbon reservoir effect. *Progress in Physical Geography* **29**, 532-547.

Ascough P. L., Cook G. T., Dugmore A. J., Scott E. M. and Freeman S. P. H. T. 2005b Influence of mollusc species on marine DELTA R determinations. *Radiocarbon* **47** (3), 433-440.

Ascough P. L., Cook G. T., Church M. J., Dugmore A. J., Arge S. V. and McGovern T. H. 2006. Variability in North Atlantic marine radiocarbon reservoir effects at c.1000 AD. *The Holocene* **16** (1), 131-136.

Ascough P. L., Cook G. T., Dugmore A. J. and Scott E. M. 2007a. The North Atlantic Marine Reservoir Effect in the Early Holocene: Implications for Defining and Understanding MRE Values. *Nuclear Instruments and Methods in Physics B* **259** (1), 438-447.

Ascough P. L., Cook G. T., Church M. J., Dugmore A. J., McGovern T. G., Dunbar E., Einarsson Á., Friðriksson A. and Gestsdóttir H. 2007b. Reservoirs and Radiocarbon: ^{14}C

dating problems in Myvatnssveit, Northern Iceland. *Radiocarbon* **49** (2), 947-961.

Ascough P. L., Cook G. T. and Dugmore A. J. 2009. North Atlantic Marine ^{14}C Reservoir Effects: implications for late-Holocene chronological studies. *Quaternary Geochronology* **4** (3), 171-180.

Ashmore P. J. 1999. Radiocarbon dating: avoiding errors by avoiding mixed samples. *Antiquity* **73**, 124-30.

Austin W.E.N., Cage A.G., and Scourse J.D. 2006. Mid-latitude shelf seas: a NW European perspective on the seasonal dynamics of temperature, salinity and oxygen isotopes. *The Holocene* **16** (7), 937-947.

Balasse M., Tresset A. and Ambrose S. H. 2005. Stable isotope evidence ($\delta^{13}C$, $\delta^{18}O$) for winter feeding on seaweed by Neolithic sheep of Scotland. *Journal of Zoology* **270** (1), 170-176.

Barber D. C., Dyke A., Hillaire-Marcel C., Jennings A. E., Andrews J. T., Kerwin M. W., Bilodeau G., McNeely R., Southon J., Morehead M. D., and Gagnon J. M. 1999. Forcing of the cold event of 8,200 years ago by catastrophic drainage of Laurentide lakes. *Nature* **400**, 344-348.

Bard E., Arnold M., Hamelin B., Tisnerat-Laborde N., and Cabioch G. 1998. Radiocarbon calibration by means of mass spectrometric $^{230}Th/^{234}U$ and ^{14}C ages of corals. An updated database including samples from Barbados, Mururoa and Tahiti. *Radiocarbon* **40** (3), 1085-1092.

Bard E., Rostek F. and Ménot-Combes G. 2004. Radiocarbon calibration beyond 20,000 ^{14}C yr B.P. by means of planktonic foraminifera of the Iberian Margin. *Quaternary Research* **61** (2), 204–14.

Barrett J. H. and Richards M. P. 2004. Identity, gender, religion and economy: New isotope and radiocarbon evidence for marine resource identification in Early Historic Orkney, Scotland, UK. *European Journey of Archaeology* **7**, 249-271.

Barrett J. H., Locker A. M. and Roberts C. M. 2004. The origins of intensive marine fishing in medieval Europe: the English evidence. *Proceedings of the Royal Society of London Series B -Biological Sciences* **271** (1556), 2417-2421.

Barrett J. H., Johnstone C., Harland J., Van Neer W., Ervynck A., Makowiecki D., Heinrich D., Hufthammer A. K., Enghoff I. B., Amundsen C., Christiansen J. S., Jones A. K. G., Locker A., Hamilton-Dyer S., Jonsson L., Lougas L., Roberts C. and Richards M**.** 2008. Detecting the medieval cod trade: a new method and first results**.** *Journal of Archaeological Science* **35 (**4), 850-861.

Barrett J. H., Orton D., Johnstone C., Harland J., Van Neer W., Ervynck A., Roberts C., Locker A., Amundsen C., Bodker Enghoff I., Hamilton-Dyer S., Heinrich D., Hufthammer A. K., Jones A. K. G., Jonsson L., Makowiecki D., Pope P., O'Connell T. C., De Roo T., Richards M. 2011. Interpreting the expansion of sea fishing in medieval Europe using stable isotope analysis of archaeological cod bones. *Journal of Archaeological Science* **38** (7), 1516-1524.

Bartlett R. 1993. *The Making of Europe. Conquest, colonization and cultural change 950-1350.* Princeton N.J. Princeton University Press.

Barton T. 2008. *Kirkgate, Perth, Perth and Kinross (Perth parish), watching brief*. Cathedral Communications Limited, Wiltshire, England.

Beck J. W., Hewitt L., Burr G. S., Loret J., and Hochstetter F. T. 2003. *Mata Ki Te Rangi: Eyes Towards the Heavens in Easter Island* (ed. J Loret and J T Tanacredi), Kluwever Academic/Plenum Publishers, New York.

Bell W. T. and Ogilvie A. E. J. 1978. Weather compilations as a source of data for the reconstruction of European climate during the medieval period. *Climatic Change* **1**, 331-348.

Bemis B. E., Spero H. J., Bijma J. and Lee D. 1998. Re-evaluation of the oxygen isotopic composition of planktonic foraminifera: Experimental results and revised paleotemperature equations. *Paleoceanography* **13**, 150-160.

Bersch M., Yashayaev I., Koltermann K.P. 2007. Recent changes of the thermohaline circulation in the subpolar North Atlantic. *Ocean Dynamics* **57** (3), 223-235.

Birks C. J. A. and Koç N. 2002. A high resolution diatom record of late Quaternary sea surface temperatures and oceanographic conditions from the Eastern Norwegian Sea. *Boreas* **31**, 323-341.

Bjorck S., Hjort C., Ingolfsson O., and Skog G. 1991. Radiocarbon dates from the Antarctic peninsula region - problems and potential. In: Lowe, J. J. (ed.). *Radiocarbon Dating: Recent Applications and Future Potential, Quaternary Proceedings* **1**, 55-65. Quaternary Research Association, Cambridge.

Björck S., Koç N., and Goran S. 2003. Consistently large reservoir ages in the Norwegian Sea during the last deglaciation. *Quaternary Science Reviews* **22**, 429-435.

Blockley S. P. E., Housley R. A. 2009. Calibration commentary. *Radiocarbon* **51** (1), 287-90.

Bowman G. M. and Harvey N. 1983. Radiocarbon dating marine shells in South Australia. *Australian Archaeology* **17**, 113 -123.

Bradley R. S. 1985. *Quaternary Paleoclimatology: Methods of Paleoclimatic Reconstruction*. Allen & Unwin; Boston.

Broecker W. S., Peteet D., Rind D. 1985. Does the ocean-atmosphere system have more than one stable mode of operation? *Nature* **315**, 21-25.

Broecker W. 1987. The great ocean conveyor. *Natural History Magazine* **97**, 74-82.

Broecker W. S., Klas M,. Clark E., Bonani G., Ivy S., and Wolfli W. 1991. The influence of $CaCO_3$ dissolution on core top radiocarbon ages for deep sea sediments. *Paleoceanography* 6 (5), 593-608.

Bronk Ramsey C. 1994. Analysis of Chronological Information and Radiocarbon

Calibration: The Program OxCal. *Archaeological Computing Newsletter* **41**, 11-16.

Bronk Ramsey C. 1995. Radiocarbon Calibration and Analysis of Stratigraphy: The OxCal Program. *Radiocarbon* **37** (2), 425-430.

Bronk Ramsey C., Buck C. E., Manning S. W., Reimer P., and Van Der Plicht H. 2006. Developments in radiocarbon calibration for archaeology. *Antiquity* **80** (310), 783–98.

Bronk Ramsey C. 2009. Bayesian analysis of radiocarbon dates. *Radiocarbon* **51** (1), 337-360.

Bruns M., Levin I., Munnich K. O., Hubberten H., and Fillipakis S. 1980. Regional sources of volcanic carbon dioxide and their influence on ^{14}C content of present-day plant material. *Radiocarbon* **22** (2), 532-536.

Buchanan D. L. and Corcoran B. 1959. Sealed tube combustions for the determination of carbon-13 and total carbon. *Analytical Chemistry* **31**, 1635-1637.

Buck C. E. and Blackwell P. G. 2004. Formal statistical models for estimating radiocarbon calibration curves. *Radiocarbon* **46** (3), 1093–102.

Burr G. S., Beck J. W., Corrège T., Cabioch G., Taylor F. W., Donahue D. J. 2009. Modern and Pleistocene reservoir ages inferred from South Pacific corals. *Radiocarbon* **51** (1), 319-335.

Butler P. G., Scourse J. D. Richardson C. A., Wanamaker A. D., Bryant C. L. and Bennell J. D. 2009. Continuous marine radiocarbon reservoir calibration and the ^{13}C Suess effect in the Irish Sea: Results from the first multi-centennial shell-based marine master chronology. *Earth and Planetary Science Letters* **279**, 230-241.

Cachart R. 2000. Arbroath Abbey (Arbroath & St Vigeans parish), medieval monastic. SUAT Evaluation. *Discovery and Excavation Scotland* **1**, 12.

Cage A. G., Heinemeier J. and Austin, W. E. N. 2006. Marine radiocarbon reservoir ages in Scottish coastal and fjordic waters. *Radiocarbon* **48** (1), 31-43.

Cameron A. S. 1992. 16-18 Netherkirkgate, Aberdeen (Aberdeen parish): medieval buildings and pits. *Discovery Excavation Scotland*, 35.

Cameron A. S. and Stones J. A. 2001. Aberdeen: An In-Depth View of the City's Past. Edinburgh: *Society of Antiquaries of Scotland, Monograph Series* **19**, 271-275.

Campin J. M, Fichefet T., Duplessy J. C. 1999. Problems with using radiocarbon to infer ocean ventilation rates for past and present climates. *Earth and Planetary Science Letters* **165**, 17-24.

Chisholm B. S., Nelson D. E., Schwarcz H. P. 1982. Stable carbon ratios as a measure of marine versus terrestrial protein in ancient diets. *Science* **216**, 1131-1132.

Classen C. 1998. *Shells*. Cambridge University Press, Cambridge.

Clilverd M., Clarke E., Rishbeth H., Clark T.and Ulich T. 2003. Solar activity levels in 2100. *Astronomy & Geophysics* **44** (5), 5.20-5.22.

Clilverd M., Clarke E., Clark T., Rishbeth H. and Ulich T. 2004. …and a reply. *Astronomy & Geophysics* **45** (2), 2.6 -2.7.

Cook G. T., Bonsall C., Hedges R. E. M., McSweeney K., Boronean V. and Pettitt P. B. 2001. A freshwater diet-derived ^{14}C reservoir effect at the stone age sites in the Iron Gates Gorge. *Radiocarbon* **43** (2A), 453-460.

Coplen T. B. 1994. Reporting of stable hydrogen, carbon and oxygen isotope abundances. *Pure and Applied Chemistry* **66**, 273-76.

Cox A. 2007. Excavations at the Horse Cross, Perth. *Tayside and Fife Archaeological Journal* **13,** 197-198.

Craig H. 1953. The geochemistry of the stable carbon isotopes. *Geochimica et Cosmochimica Acta* **3**, 53-92.

Craig H. 1957a. The Natural Distribution of Radiocarbon and the Exchange Time of Carbon Dioxide Between Atmosphere and Sea. *Tellus* **9**, 1-17.

Craig H. 1957b. Isotopic Standards for Carbon and Oxygen and Correction Factors for Mass- Spectrometric Analysis of Carbon Dioxide. *Geochimica et Cosmochimica Acta* **12**, 133-149.

Damon P. E., Lerman J. C. and Long A. 1978. Temporal fluctuations of atmospheric ^{14}C: Causal factors and implications. *Annual Review of Earth and Planetary Science* **6**, 457-494.

Dansgaard W., Johnsen S. J., Clausen H. B., Dahl-Jensen D., Gundestrup N. S., Hammer C. U., Hvidberg C. S., Steffensen J. P., Sveinbjornsdottir A. E., Jouzel J. and Bond G. 1993. Evidence for general instability of past climate from a 250-kyr ice-core record. *Nature* **364**, 218-220.

Deevey E. S., Gross M. S., Hutchinson G. E., and Kraybill H. L. 1954. The natural c14 contents of materials from hard-water lakes. *Proceedings of National Academy of Science* U S A **40** (5), 285–288.

De Jong A. F. M. and Mook W. G. 1982. An anomalous Suess effect above Europe. *Nature* **298,** 641-644.

DeNiro M. J. and Epstein S. 1978. Influence of diet on the distribution of carbon isotopes in animals. *Geochimica et Cosmochimica Acta* **42**, 495-506.

de Vries H. and Barendsen G. W. 1952. A new technique for the measurement of age by radiocarbon. *Physica* **18**, 652.

Dickson R. R., Meinke J., Malmberg S. A. and Lee A. J. 1988. The 'Great Salinity Anomaly' in the northern North Atlantic 1968 – 1982. *Progress in Oceanography* **20** (2), 103-151.

Donahue D. J., Linick T. W. and Jull A. J. T. 1990. Isotope ratio and background corrections for accelerator mass spectrometry radio carbon measurements. *Radiocarbon* **32** (2), 135-142.

Du Buit M. H. 1995. Food and feeding of cod (*Gadus-morhua*) in the Celtic Sea. *Fisheries Research* **22 (**3-4), 227-241.

Dutta K., Bhushan R. and Somayajulu B. L .K. 2001. ΔR correction values for the Northern Indian Ocean. *Radiocarbon* **43** (2A), 483-488.

Dutta K. 2008. Marine ^{14}C Reservoir Age and Suess Effect in the Indian Ocean. *Earth Science India*, **I** (III), 175-188.

Eiríksson J., Larsen G., Knudsen K. L., Heinemeier J. and Símonarson L. A. 2004. Marine reservoir age variability and water mass distribution in the Iceland Sea. *Quaternary Science Reviews* **23**, 2247-2268.

Elmore D. and Phillips F. M. 1987. Accelerator Mass Spectrometry for Measurement of Long-Lived Radioisotopes. *Science* **236**, 543-550.

Epstein S. Buchsbaum R. Lowenstam H. and Urey H. C. 1953. Revised carbonate water isotopic temperature scale. *Geological Society of America Bulletin* **64**, 1315-1326.

Fairbanks R. G., Mortlock R. A., Chiu T. C., Cao L., Kaplan A., Guilderson T. P, Fairbanks T. W., Bloom A. L., Grootes P. M. and Nadeau M. J. 2005. Radiocarbon calibration curve spanning 0 to 50,000 years BP based on paired 230Th/ 234U/238U and 14C dates on pristine corals. *Quaternary Science Reviews* **24** (16–17), 1781–96.

Fifield L. K. 1999. Accelerator mass spectrometry and its applications. *Reports on Progress in Physics* **62**, 1223-1274.

Finkel R. C. and Suter M. 1993. AMS in the Earth sciences: Techniques and applications In Hyman M and Rowe M. W. (eds.) *Advances in Analytic Geochemistry*. Greenwich, Connecticut, JAI Press **1**, 1-114.

Fontugne, M., Carré M., Bentaleb I., Julien M. and Lavallée D. 2004. Radiocarbon reservoir age variations in the South Peruvian upwelling during the Holocene. *Radiocarbon* **46** (2), 531-537.

Forman S. L. and Polyak L. 1997. Radiocarbon content of pre-bomb marine mollusks and variations in the 14C reservoir age for coastal areas of the Barents and Kara seas, Russia. *Geophysical Research Letters* **24**, 885-888.

Freeman S. P. H. T., Dougans A. B., McHargue L., Wilcken K .M., Xu S. 2008. Performance of the new single stage accelerator mass spectrometer at the SUERC. *Nuclear Instruments and Methods in Physics Research* B **266,** 2225-2228.

Freeman S. P. H. T., Cook G. T., Dougans A. B., Naysmith P., Wilcken K. M., Xu S. 2010. Improved SSAMS performance. *Nuclear Instruments and Methods in Physics Research* B **268,** 715-717.

Friedrich M., Lucke A. and Hanisch S. 2004a. Late Glacial environmental and climatic changes from synchronized terrestrial archives of Central Europe: the Network PROSIMUL. *PAGES News* **12** (2), 27-29.

Friedrich M., Remmele S., Kromer B., Hofmann J., Spurk M., Kaiser K. F., Orcel C. and Küppers M. 2004b. The 12,460-year Hohenheim oak and pine tree-ring chronology from Central Europe—a unique annual record for radiocarbon calibration and paleoenvironment reconstructions. *Radiocarbon* **46** (3), 1111–1122.

Funder S. 1982. 14C-dating of samples collected during the 1979 expedition to North Greenland. *The Geological Survey of Greenland Report* **110**, 9-13.

Gaudinski J. B., Trumbore S. E., Davidson E. A. and Zheng S. 2000. Soil carbon cycling in a temperate forest: radiocarbon-based estimates of residence times, sequestration rates and partitioning of fluxes. *Biogeochemistry* **51,** 33-69.

Gillikin D. P., De Ridder F., Ulens H., Elskens M., Keppens E., Baeyens W. and Dehairs F. 2005. Assessing the reproducibility and reliability of estuarine bivalve shells (*Saxidomus giganteus*) for sea surface temperature reconstruction: implications for paleoclimate studies. *Palaeogeography Palaeoclimatology Palaeoecology* **228**, 70–85.

Gillikin D. P., Dehairs F., Lorrain A., Steenmans D., Baeyens W. and Andre´ L. 2006. Barium uptake into the shells of the common mussel (*Mytilus edulis*) and the potential for estuarine paleo-chemistry reconstruction. *Geochimica et Cosmochimica Acta* **70**, 395–407.

Gillikin, D. P., Lorrain, A., Meng, L., and Dehairs, F. 2007. A large metabolic carbon contribution to the [delta]13C record in marine aragonitic bivalve shells. *Geochimica et Cosmochimica Acta* **71**, 2936-2946.

Godwin H. 1951. Comments on radiocarbon dating for samples from the British Isles, *American Journal of Science* **249,** 301-307.

Godwin H. 1962. Half-life of Radiocarbon. *Nature* **195**, 984.

Gomez E. A., Borel C. M., Aguirre M. L. and Martinez D. E. 2008. Radiocarbon reservoir ages and hardwater effect for the northeastern coastal waters of Argentina. *Radiocarbon* **50** (1), 119-129.

Gordon J. E. and Harkness D. D. 1992. Magnitude and geographic variation of the radiocarbon content in Antarctic marine life: Implications for reservoir corrections in radiocarbon dating. *Quaternary Science Reviews* **11** (7-8), 697-708.

Gosse J. C. and Phillips F. M. 2001. Terrestrial in situ cosmogenic nuclides: theory and application. *Quaternary Science Reviews* **20**, 1475-1560.

Gulliksen S. and Scott E. M. 1995. Report on TIRI. *Radiocarbon* **37** (2), 820-821.

Haflidason H., Sejrup H. P., Kristensen D. K. and Johnsen S. 1995. Coupled response of the late glacial climatic shifts of northwest Europe reflected in Greenland ice cores: Evidence from the Northern North Sea. *Geology* **23** (12), 1059-1062.

Hakkinen S. and Rhines P. B. 2009. Shifting surface currents in the northern North

Atlantic Ocean. *Journal of Geophysical Research-Oceans* **114**.

Harkness, D. D. 1979. Radiocarbon dates from Antarctica. *British Antarctic Survey Bulletin* **41**, 43-59.

Harkness D. D. 1983. The extent of the natural ^{14}C deficiency in the coastal environment of the United Kingdom. *Journal of the European Study Group on Physical, Chemical and Mathematical Techniques Applied to Archaeology* **8** (IV.9), 351-364.

Hartigan J. A. and Wigdor A. K. (eds). 1989. *Fairness in employment testing: validity generalization, minority issues and the general aptitude test battery.* By National Research Council (U.S.), Committee on the General Aptitude Test Battery and commission on behavioural and social sciences and education. National Academy Press. Washington, 179.

Heier-Nielsen S., Heinemeir J., Nielsen H. L. and Rud N. 1995. Recent reservoir ages for Danish fjords and marine waters. *Radiocarbon* **37** (3), 875-882.

Hesshaimer V., Heimann M. and Levin I. 1994. Radiocarbon evidence for a smaller oceanic carbon dioxide sink than previously believed. *Nature* **370**, 201-203.

Hoyt J. B. 1973. *Man and the earth.* 3rd edition. Prentice-Hall. Englewood Cliffs, N.J.

Hughen K. A., Baillie M. G. L., Bard E., Beck J. W., Bertrand C. J. H., Blackwell P. G. Buck C. E., Burr G. S., Cutler K. B., Damon P. E., Edwards R. L., Fairbanks R. G., Friedrich M., Guilderson T. P., Kromer B., McCormac G., Manning S., Bronk Ramsey C., Reimer P. J., Reimer R. W., Remmele S., Southon J. R., Stuiver M., Talamo S., Taylor F. W., van der Plicht J. and Weyenmeyer C. E. 2004. MARINE04 Marine radiocarbon age calibration, 0-26 cal kyr BP. *Radiocarbon* **46** (3), 1059-1086.

Hut G. 1987. *Consultants group meeting on stable isotope reference samples for geochemical and hydrological investigations, report to the director general*. International Atomic Energy Agency, Vienna.

Imbrie J. and Imbrie K. P. 1979. *Ice Ages: Solving the Mystery*. Macmillan; London.

Ingram B. L. and Southon J. R. 1996. Reservoir ages in Eastern Pacific coastal and estuarine waters. *Radiocarbon* **38**, 573-582.

Jarumayan G. A. and Sadili M. V. 2003. *The Changing Earth.* Katha Publishing Co. Inc. Quezon City. Luzon. Phillipines.

Jones D. S. and Quitmyer I. R. 1996. Marking Time with Bivalve Shells: Oxygen Isotopes and Season of Annual Increment Formation. *Palaios*. **11** (4), 340-346.

Jones K. B., Hodgkins G. W. L., Dettman D. L., Andrus, C. F. T., Nelson, A. and Etayo-Cadavid, M. F. 2007. Seasonal variations in Peruvian marine reservoir age from pre-bomb *Argopecten purpuratus* shell carbonate, *Radiocarbon* **49** (2), 877-888.

Keith M. L., Anderson G. M. and Eichler R. 1964. Carbon and oxygen isotope composition of mollusk shells from marine and fresh-water environments. *Geochimica et Cosmochimica Acta* **28**, 1757-1786.

Kennedy H., Richardson C. A., Duarte C. M., Kennedy D. P. 2001. Oxygen and carbon stable isotopic profiles of the fan mussel, *Pinna nobilis*, and reconstruction of sea surface temperatures in the Mediterranean. *Marine Biology* **139**, 1115-1124.

Kennett D. J., Ingram L., Erlandson J. M. and Walker P. 1997. Evidence for temporal fluctuations in Marine Radiocarbon Reservoir Ages in the Santa Barbara Channel, Southern California. *Journal of Archaeological Science* **24**, 1051-1059.

Kesler D. H. 1983. Variation in cellulose activity in *Physa heterostropha* (Gastropoda) and other species of gastropods in a New England pond. *The American Midland Naturalist* **109**, 280–288.

Klitgaard-Kristensen D., Sejrup H. P., Haflidason H., Johnsen S. and Spurk M. 1998. The short cold period 8,200 years ago documented in oxygen isotope records of precipitation in Europe and Greenland. *Journal of Quaternary Sciences* **13**, 165-169.

Kong G. S. and Lee C. W. 2005. Marine reservoir corrections (ΔR) for southern coastal waters of Korea. *The Sea, Journal of the Korean Society of Oceanography* **10** (2), 124-128.

Kovanen D. J. and Easterbrook D. J. 2002. Paleodeviations of radiocarbon marine reservoir values for the northeast Pacific. *Geology* **30**(3), 243-246.

Lewis C. A., Reimer P. J., Reimer R. W. 2008. Marine Reservoir corrections: St Helena, South Atlantic Ocean. *Radiocarbon* **50** (2), 275-280.

Levin I., Kromer B., Wagenbach D. and Münnich K. O. 1987. Carbon isotope measurements of atmospheric CO_2 at a coastal station in Antarctica. *Tellus B* **39B**, 89–95.

Levin I., Schuchard J., Kromer B., Münnich K. O. 1989. The continental European Suess effect. *Radiocarbon* **31**(3), 431–40.

Levin I. and Hesshaimer V. 2000. Radiocarbon – a unique tracer of global carbon cycle dynamics. *Radiocarbon* **42** (1), 69-80.

Libby W. F. 1946. Atmospheric Helium Three and Radiocarbon from Cosmic Radiation. *Physical Review* **69**, 671-672.

Libby W. F., Anderson E. C. and Arnold J. R. 1949. Age Determination by Radiocarbon Content: World-Wide Assay of Natural Radiocarbon. *Science* **109**, 227-228.

Liden, K., Takahashi, C. and Nelson, D. E. 1995. The Effects of Lipids in Stable Carbon Isotope Analysis and the Effects of NaOH Treatment on the Composition of Extracted Bone Collagen. *Journal of Archaeological Science* **22**(2), 321-326

Livingstone, D. 1999. *A practical guide to scientific data analysis*. Wiley. West Sussex. p158

Longin R. 1971. New method of collagen extraction for radiocarbon dating. *Nature* **230,** 241-242.

Lorrain A., Paulet Y. M., Chauvaud L., Dunbar R., Mucciarone D. and Fontugne M. 2004. $\delta^{13}C$ variation in scallop shells: increasing metabolic carbon contribution with body size? *Geochimica et Cosmochimica Acta* **68**, 3509–3519.

Lowe D. C. and Judd W. J. 1987. Graphite target preparation for radiocarbon dating by accelerator mass spectrometry. *Nuclear Instruments and Methods in Physics Research Section B* **28** (1), 113-116.

Lyons M. G., Balls P. W., Turrell W. R. 1993. A preliminary study of the relative importance of riverine nutrient inputs to the Scottish North Sea Coastal Zone. *Marine Pollution Bulletin* **26** (11), 20-28.

Mangerud J. 1972. Radiocarbon dating of marine shells, including a discussion of apparent age of recent shells from Norway. *Boreas* **1**, 143-172.

Mangerud J. and Gulliksen S. 1975. Apparent Radiocarbon ages of recent marine shells from Norway, Spitsbergen and Arctic Canada. *Quaternary Review* **5**, 263-273.

Masarik J. and Beer J. 1999. Simulation of particle fluxes and cosmogenic nuclide production in the Earth's atmosphere. *Journal of Geophysical Research* **104**, 12,009-12,111.

Masuda K., Nagaya K., Miyahara H., Muraki Y., and Nakamura T. 2009. Cosmogenic Radiocarbon and the Solar Activity. *Journal of the Physical Society of Japan* **78,** 1-6.

Mayewski P. A. and White F. 2002. *The Ice Chronicles.* University Press of New England.

McConnaughey T. A., Burdett J., Whelan J. F. and Paull, C. K. 1997. Carbon isotopes in biological carbonates: respiration and photosynthesis. *Geochimica et Cosmochimica Acta* **61**, 611–622.

McCormac F. G, Hogg A. G, Blackwell P. G, Buck C, Higham T. F. G, and Reimer P. J. 2004. SHCAL04 Southern hemisphere calibration, 0-11.0 cal kyr BP. *Radiocarbon* **46** (3), 1087-1092.

McNeely R., Dyke A. S., and Southon J. R. 2006. Canadian marine reservoir ages, preliminary data assessment, Open File 5049, pp. 3. *Geological Survey Canada*.

McNichol A. P, Jull A. J. T and Burr G. S. 2001. Converting AMS data to radiocarbon values: Considerations and conventions. *Radiocarbon* **43** (2A), 313-320.

Meehan B. 1982. *Shell bed to shell midden*. Australian Institute of Aboriginal Studies. Canberra. p117.

Mellars P. 2006a. Archaeology: progress and pitfalls in radiocarbon dating (reply). *Nature* **443** (7108), E4.

Mellars P. 2006b. A new radiocarbon revolution and the dispersal of modern humans in Eurasia, *Nature*, **439** (7079), 931–5.

Merlivat L. and Memery L. 1983. Gas exchange across an air-water interface:

Experimental results and modelling of bubble contribution to transfer. *Journal of Geophysical Research* **88** (C1), 707-724.

Middleton R. 1983. A versatile high intensity negative ion source: *Nuclear Instruments and Methods in Physics Research* **214**, 139–150.

Milankovitch, M. 1930. Mathematische klimalehre und astronomische theorie der Klimaschwankugen. In: Köppen, W. and Geiger, R., (Eds.) 1930. *Handbuch der Klimatologie*, Gebrüder Borntraeger, Berlin, 1–176.

Mills G. A. and Urey H. C. 1940. The kinetics of isotopic exchange between carbon dioxide, bicarbonate ion, carbonate ion and water. *Journal of the American Chemical Society* **62**, 1019–1026.

Milner N., Barrett J.H. and Welsh J. 2007. Marine Resource intensification in Viking Age Europe: the molluscan evidence from Quoygrew, Orkney. *Journal of Archaeological Science* **34**, 1461-1472.

Mook W. G., Bommerson J. C., Staverman W. H. 1974. Carbon isotope fractionation between dissolved bicarbonate and gaseous carbon dioxide. *Earth and Planetary Science Letters* **22** (2), 169-176.

Muus B. J. and Dahlström P. 1974. *Collins Guide to the Sea Fishes of Britain and North-Western Europe*. Collins, London, UK, 244.

Muzikar P., Elmore D. and Granger D. E. 2003. Accelerator mass spectrometry in geologic research. *Geological Society of America Bulletin*, **115** (6), 643-654.

Nadal De Masi M. A. 1999. Prehistoric hunter-gatherer mobility on the southern Brazilian coast: Santa Catarina Island. *Unpublished PhD dissertation*. Stanford University, 186.

Naysmith P., Cook G. T., Freeman S. P. H. T., Scott E. M., Anderson R., Xu S., Dunbar E., Muir G. K. P., Dougans A., Wilcken K., Schnabel C., Russell N., Ascough P L., Maden C. 2010. 14C AMS at SUERC: Improving QA Data with the 5MV Tandem and 250kV SSAMS. *Radiocarbon* **52** (2), 263-271.

Nicholson, R. 1974. *Scotland:The Later Middle Ages.* Edinburgh

Nielsen J. R. and Andersen M. 2001. Feeding habits and density patterns of Greenland cod (*Gadus ogac*) (Richardson 1836) at West Greenland compared to those of the coexisting Atlantic cod, *Gadus morhua L. Journal of Northwest Atlantic Fishery Science* **29**, 1–22.

Nydal R., and Lövseth K. 1970. Prospective Decrease in Atmospheric Radiocarbon. *Journal of Geophysical Research* **75** (12), 2271–2278.

Nydal R. and Lovseth K. 1996. Carbon-14 measurement in atmospheric CO_2 from Northern and Southern Hemisphere sites. 1962-1993. *ORNL/CDIAC-93, NDP-05.* Carbon Dioxide Information Analysis Center –World DataCenter-A for Atmospheric Trace Gases OakRidge National Laboratory, Tennessee. Available online at http://gcmd.nasa.gov/records/GCMD_CDIAC_NDP057.html (last visited 19/06/2011)

Oeschger H., Siegenthaler U., Schotterer U. and Gugelmann A. 1975. A box diffusion model to study the carbon dioxide exchange in nature. *Tellus* **27**, 168-192.

O'Leary, M. H. 1981. Carbon isotope fractionation in plants. *Phytochemistry* **20**, 553-567.

O'Leary M.H. 1988. Carbon isotopes in photosynthesis. Fractionation techniques may reveal new aspects of carbon dynamics in plants. *BioScience* **38**, 328-336.

Olsson I. U. 1970. Radiocarbon variations and absolute chronology. In Proceedings of the Twelfth Nobel Symposium held at the Institute of Physics at Uppsala University. Nobel Symposium No. 12. *Nature* **231**, 270.

OSPAR Commission. 2000. *Quality Status Report 2000*. London: OSPAR Comission, 108.

Otlet R. L., Fulker M. J. and Walker A. J. 1992. Environmental impact of atmospheric carbon-14 emissions resulting from the nuclear energy cycle. In: Taylor R. E., Long A. and Kra R. S. (Eds) *Radiocarbon After Four Decades, An Interdisciplinary Perspective* Springer, New York.

Pandow, M., MacKay, C., and Wolfgang, R. 1960. The reaction of atomic carbon with oxygen: Significance for the natural radio-carbon cycle. *Journal of Inorganic Nuclear Chemistry* **14**, 153–158.

Pearson G. W. 1987. How to cope with calibration. *Antiquity* **61**, 98-103.

Pearson G. W. and Stuiver M. 1993. High-precision bidecadal calibration of the radiocarbon time scale 500-2500 BC. *Radiocarbon* **35** (1), 25-33.

Perry D. R. 2000. Castle Park, Dunbar: two thousand years on a fortified headland, *Society of Antiquaries of Scotland Monograph series 16.* Edinburgh. Held at RCAHMS D.7.13.DUN.

Peterson, B. J. and B. Fry. 1987. Stable isotopes in ecosystem studies. *Annual Review of Ecology and Systematics* **18**, 293–320.

Post D. M. 2002. Using stable isotopes to estimate trophic position: models, methods, and assumptions. *Ecology* **83**, 703–718.

Rakowski A. Z., Kuc T., Nakamura T. and Pazdur A. 2005. Radiocarbon Concentration In Urban Area. *Geochronometria* **24**, 63-68.

Reimer P. J., McCormac F. G., Moore J., McCormick F. and Murray E. V. 2002. Marine radiocarbon reservoir corrections for the mid- to late Holocene in the eastern subpolar North Atlantic. *The Holocene* **12** (2), 129-135.

Reimer P. J., Baillie M. G. L., Bard E., Bayliss A., Beck J. W., Bertrand C. J. H., Blackwell P. G., Buck C. E., Burr G. S., Cutler K. B., Damon P. E., Edwards R. L., Fairbanks R. G. Friedrich M., Guilderson T. P., Hogg A. G., Hughen K. A., Kromer B., McCormac G., Manning S., Bronk Ramsey C., Reimer R. W., Remmele S., Southon J. R.,

Stuiver M, Talamo S., Taylor F. W., van der Plicht J. and Weyhenmeyer C. E. 2004. INTCAL04 Terrestrial radiocarbon age calibration, 0-26 cal kyr BP. *Radiocarbon* **46** (3), 1029-1058.

Reimer P. J., Baillie M. G. L., Bard E., Bayliss A., Beck J. W., Blackwell P. G., Bronk Ramsey C., Buck C. E., Burr G. S., Edwards R. L., Friedrich M., Grootes P. M., Guilderson T. P., Hajdas I., Heaton T. J., Hogg A. G., Hughen K. A., Kaiser K. F., Kromer B., McCormac F. G., Manning S. W., Reimer R. W., Richards D. A., Southon J. R., Talamo S., Turney C. S. M., van der Plicht J. and Weyhenmeyer C. E. 2009. IntCal09 and Marine09 Radiocarbon Age Calibration Curves, 0–50,000 Years cal BP. *Radiocarbon* **51** (4), 1111-1150.

Reiter P. 2000. From Shakespeare to Defoe: Malaria in England in the Little Ice Age. *Emerging infectious diseases* **6** (1).

Rounick J. S. and Winterbourn M. J. 1986. Stable Carbon Isotopes and Carbon Flow in Ecosystems. *BioScience* **36** (3), 171-177.

Ruddiman W. F., Sancetta C. D. and McIntyre, A. 1977. Glacial/Interglacial response rate of subpolar North Atlantic waters to climate change: the record in oceanic sediments. *Philosophical Transactions of the Royal Society of London B* **280**, 119-142.

Ruddiman W. F and McIntyre A. 1981. The North Atlantic Ocean during the last deglaciation. *Palaeoceanography, Palaeoclimatology, Palaeoecology* **35**, 145-214.

Russell N., Cook G. T., Ascough P. L. and Dugmore A. J. 2010. Spatial variation in the Marine Radiocarbon Reservoir Effect throughout the Scottish Post-Roman to Late Medieval period: North Sea values (500 – 1350BP.) *Radiocarbon* **52** (3), 1166-1182.

Russell N., Cook G. T., Ascough P. L., Barrett J. H. and Dugmore A. J. 2011a. Species specific marine radiocarbon reservoir effect: a comparison of ΔR values between *Patella vulgata* (limpet) shell carbonate and *Gadus morhua* (Atlantic cod) bone collagen. *Journal of Archaeological Science* **38** (5), 1008-1015.

Russell N., Cook G. T., Ascough P. L., Scott, E. M. and Dugmore A. J. 2011b. Examining the inherent variability in ΔR: New methods of presenting ΔR values and implications for MRE studies. *Radiocarbon* **53**(2), 277-288.

Schaub M., Buntgen U., Kaiser K. F., Kromer B., Talamo S., Andersen K. K. and Rasmussen S. O. 2008a. Late glacial environmental variability from Swiss tree rings. *Quaternary Science Reviews* **27** (1-2), 29-41.

Schaub M., Kaiser K. F., Frank D. C., Buntgen U., Kromer B. and Talamo S. 2008b. Environmental change during the Allerød and Younger Dryas reconstructed from Swiss tree-ring data. *Boreas* **37** (1), 74-86.

Schiffer M. B. 1986. Radiocarbon dating and the "old wood" problem: The case of the Hohokam chronology. *Journal of Archaeological Science* **13** (1), 13-30.

Schimel D. 1995. Terrestrial ecosystems and the carbon cycle. *Global Change Biology* **1**, 77-91.

Schoeninger, M. J., DeNiro, M. J. 1984. Nitrogen and carbon isotopic composition of bone collagen from marine and terrestrial animals. *Geochimica et Cosmochimca Acta* **48**, 625- 639.

Scott E. M. 2003. The Third International Radiocarbon Intercomparison (TIRI) and The Fourth International Radiocarbon Intercomparison (FIRI), 1990-2002. Results, Analyses and Conclusions. *Radiocarbon* **45** (2), 135-408.

Scott E. M., Cook G. T., Naysmith P., Bryant C. and O'Donnell D. 2007. A report on Phase 1 of the 5th International Radiocarbon Intercomparison (VIRI). *Radiocarbon* **49** (2), 409-26.

Scott E. M., Cook G. T. and Naysmith P. 2010a. A Report on Phase 2 of the Fifth International Radiocarbon Intercomparison (VIRI). *Radiocarbon* **52** (3), 846-858.

Scott E. M., Cook G. T. and Naysmith P. 2010b. The Fifth International Radiocarbon Intercomparison (VIRI): An Assessment of Laboratory Performance in Stage 3. *Radiocarbon* **52** (3) 859-865.

Shackleton N. 1973. Oxygen isotope analysis as a means of determining season of occupation of prehistoric midden sites. *Archaeometry* **15** (1), 133-141.

Sherwood G. D., Rideout R. M., Fudge S. B. and Rose G. A. 2007**.** Influence of diet on growth, condition and reproductive capacity in Newfoundland and Labrador cod (*Gadus morhua*): Insights from stable carbon isotopes (δ^{13}C). *Deep-Sea Research Part II: Topical Studies in Oceanography* **54** (23-26), 2794-2809.

Simpson I. A. and Barrett J. H. 1996. Interpretation of midden formation processes at Robert's Haven, Caithness, Scotland using thin section micromorphology. *Journal of Archaeological Science* **23**, 543-556.

Catherine Smith pers. comm.

Soares, A. M. M. and Alveirinho J. M. D. 2006. Coastal upwelling and radiocarbon evidence for temporal fluctuations in ocean reservoir effect off Portugal during the Holocene. *Radiocarbon* **48** (1), 45-60.

Soares, A. M. M. and Alveirinho J. M. D. 2007. Reservoir Effect of Coastal Waters off Western and Northwestern Galicia. *Radiocarbon* **49** (2), 925-936.

Soares A. M. M. and Martins J. M. M. 2010. Radiocarbon dating of marine samples from Gulf of Cadiz: The reservoir effect. *Quaternary International* **221** (1-2), 9-12.

Southon J., Kashgarian M., Fontugne M., Metivier B. and Yim W. W. S. 2002. Marine reservoir corrections for the Indian Ocean and Southeast Asia. *Radiocarbon* **44** (1), 167-180.

Stocker T. F and Wright D. G. 1996. Rapid changes in ocean circulation and atmospheric radiocarbon. *Paleoceanography* **11**, 773-796.

Stuiver M. and Suess H.E. 1966. On the relationship between radiocarbon dates and true

ages. *Radiocarbon* **8**, 534-540.

Stuiver M. and Polach H. 1977. Discussion: Reporting of ^{14}C data. *Radiocarbon* **19** (3), 355-363.

Stuiver M. 1983. International agreements and the use of the new oxalic acid standard, *Radiocarbon* **25** (2), 793-795.

Stuiver M. and Braziunas T. F. 1993. Modelling atmospheric ^{14}C influences and ^{14}C ages of marine samples to 10,000 BC. *Radiocarbon* **35** (1), 137-189.

Stuiver M. and Reimer P. J. 1993. Extended 14C database and revised CALIB radiocarbon calibration program. *Radiocarbon* **35** (1), 215-230.

Stuiver M., Braziunas T. F., Grootes P. M. and Zielinski, G. A. 1997. Is there evidence for solar forcing of climate in the GISP2 oxygen isotope record? *Quaternary Research* **48,** 259-266.

Stuiver M., Reimer P. J., Bard E., Beck W., Burr G. S., Hughen K. A., Kromer B., McCormac G., Van der Plicht J. and Spurk M. 1998a. INTCAL98 Radiocarbon age calibration, 24,000-0 cal BP. *Radiocarbon* **40** (3), 1041-1083.

Stuiver M., Reimer P. J. and Braziunas T. F. 1998b. High-precision radiocarbon age calibration for terrestrial and marine samples. *Radiocarbon* **40** (3), 1127-1151.

Stuiver M., Reimer P. J. and Reimer R. W. 2005. CALIB 5.0. [WWW program and documentation] [Online]. Available from: http://radiocarbon.pa.qub.ac.uk/calib/

Suess H. E. 1955. Radiocarbon Concentration in Modern Wood. *Science* **120**, 415-417.

Suess, H. E. 1965. Secular variations of the cosmic ray-produced carbon-14 in the atmosphere and their interpretations. *Journal of Geophysical Research* **70**, 5937-5950.

Suess H. E. 1979. A calibration table for conventional radiocarbon dates. In Berger R, and Suess H. E. (eds.). *Radiocarbon Dating. Proceedings of the 9th International Radiocarbon Conference.* University of California Press, Berkeley, 777-785.

Sulerzhitzky L. D. 1971. Radiocarbon dating of volcanoes**.** *Bulletin of Volcanology* **35** (1), 85-94.

Svendsen E., Sætre R. and Mork M. 1991. Features of the northern North Sea circulation. *Continental Shelf Research* **11** (5), 493-508.

Taylor R. E. and Berger R. 1967. Radiocarbon content of marine shells from the Pacific coasts of Central and South America. *Science* **158**, 1180-1182.

Tavares P.C., McGill R., Newton J., Pereira E., Duarte A. and Furness R.W. 2009. Relationships between carbon sources, trophic level and mercury exposure in generalist shorebirds revealed by stable isotope ratios in chicks. *Waterbirds* **32**, 311–321.

Thomas, D. H. 2008. Native American Landscapes Of St. Catherines Island, Georgia II. The Data. *Anthropological papers of the American Museum of Natural History* **88** (2),

343-831.

Thurman H. V. 1990. *Essentials of Oceanography*. Prentice Hall, London.

Tobias S., Weiss N. and Beer J. 2004. Long-term prediction of solar activity – a discussion… *Astronomy & Geophysics* **45** (2), 2.6.

Tuniz C., Bird J. R., Fink D. and Herzog G. F. 1998. *Accelerator mass spectrometry: ultrasensitive analysis for global science*. CRC Press LLC.

Turney C. S. M., Roberts R. G., Jacobs Z. 2006. Archaeology: progress and pitfalls in radiocarbon dating. *Nature* **443** (7108), E3.

Turrell W. R. 1992. New hypotheses concerning the circulation of the northern North Sea and its relation to North Sea fish stock recruitment. *ICES Journal of Marine Science* **49** (1), 107-23.

Turrell W.R., Henderson E. W. R., Slesser G., Payne R., Adams R. D. 1992. Seasonal changes in the circulation of the northern North Sea. *Continental Shelf Research* **12** (2-3), 257-86.

Vandeputte K., Moens L., Dams R. 1996. Improved sealed-tube combustion of organic samples to CO_2 for stable carbon isotope analysis, radiocarbon dating and percent carbon determinations. *Analytical Letters* **29** (15)**,** 2761-2773.

Van der Merwe N. J. 1989. Natural variation in 13C concentration and its effect on environmental reconstruction using 13C/12C ratios in animal bones. In: Price TD, (Editor). *The Chemistry of Prehistoric Human Bone*. Cambridge: Cambridge University Press, 105-25.

Vogel J. S., Southon J. R. and Nelson D. E. 1987. Catalyst and binder effects in the use of filamentous graphite for AMS. *Nuclear Instruments and Methods in Physics Research Section B* **29**, 50-56.

Waelbroeck C., Duplessy J. C., Michel E., Labeyrie L., Paillard D. and Dupratt J. 2001. The timing of the last deglaciation in North Atlantic climate records. *Nature* **412**, 724-727.

Wang Y. J., Cheng H., Edwards R. L., An Z. S., Wu J. Y., Shen C. C. and Dorale J. A. 2001. A high-resolution absolute dated Late Pleistocene monsoon record from Hulu Cave, China. *Science* **294** (5550), 2345-2348.

Ward G. K. and Wilson S. R. 1978. Procedures for comparing and combining radiocarbon age determinations: A critique. *Archaeometry* **20**, 19-31.

Waselkov G. A. 1987. Shellfish gathering and shell midden archaeology. *Advances in Archaeological Method and Theory* **10**, 93-210.

Weisler M., Hua Q. and Zhao J. 2009. Late Holocene C marine reservoir corrections for Hawaii derived from U-series dated archaeological coral. *Radiocarbon*, **51** (3), 955-968.

Winther N. G, Johannessen J. A. 2006. North Sea circulation: Atlantic inflow and its destination. *Journal of Geophysical Research*. **111**, 1-12.

Wright P. J., Neat F. C., Gibb F. M., Gibb I. M. and Thordarson H. 2006. Evidence for metapopulation structuring in cod from the west of Scotland and North Sea. *Journal of Fish Biology* **69**, 181-199.

Wüst G. 1935. Die stratosphare. *Wissenschaftiliche Ergebnisse der Deutschen Atlantischen Expedition "Meteor"* **6**, 109-288.

Wüst G. and Defant A. 1936. *Atlas zur schichtung und zirkulation des Atlantischen Ozeans. Schnitte und karten von temperatur, salzgehalt und dichte.* Verlag von Walter de Gruyter Co., Berlin

Wyrtki K. 1961. The thermohaline circulation in relation to the general circulation in the oceans. *Deep Sea Research* **8** (1), 39-64.

Yamazaki T. and Oda H. 2002. Orbital Influence on Earth's Magnetic Field: 100,000-Year Periodicity in Inclination. *Science* **295** (5564), 2435 – 3438.

Yoneda M., Tanaka A., Shibata Y., Morita M., Uzawa K., Hirota M., Uchida M. 2002. Radiocarbon Marine Reservoir Effect in Human Remains from the Kitakogane Site, Hokkaido, Japan. *Journal of Archaeological Science*, **29** (5), 529-536.

WEB REFERENCES

14 CHRONO Marine Reservoir database: http://intcal.qub.ac.uk/marine/.

CEFAS: http://www.cefas.co.uk/

Eurosites: http://outreach.eurosites.info/outreach/DeepOceans/station.php?id=1

Geological Map Data © NERC 20. http://edina.ac.uk/digimap/

Planet for life: http://planetforlife.com/gwarm/globclimate.html

SEPA: http://www.sepa.org.uk.